

**Hydraulic and Thermal Studies on High Temperature
Superconducting (HTS) Cables for Large Scale Power
Applications**

A

Thesis

Submitted to



For the award of

DOCTOR OF PHILOSOPHY (Ph.D)

in

Mechanical Engineering

By

Mohit Kalsia

11617335

Supervised By

Dr. Raja Sekhar Dondapati

(17715)

FACULTY OF TECHNOLOGY AND SCIENCES

LOVELY PROFESSIONAL UNIVERSITY

PUNJAB

2019

DECLARATION

I, Mohit Kalsia, declare that this thesis, submitted in fulfillment of the requirements for the award of Doctor of Philosophy, in the School of Mechanical Engineering, Lovely Professional University, Punjab, is entirely my own work unless otherwise referenced or acknowledged.

Mohit Kalsia

October 2019

CERTIFICATE

I certify that **Mohit Kalsia** bearing Regd. Number **11617335** has prepared his thesis entitled “**Hydraulic and Thermal Studies on High Temperature Superconducting (HTS) Cables for Large Scale Power Applications**” for the award of Ph.D degree of Lovely Professional University, under my guidance. He has carried out the work at the School of Mechanical Engineering, Lovely Professional University.

Dr. Raja Sekhar Dondapati

Associate Professor,

School of Mechanical Engineering,

Lovely Professional University, Phagwara, Punjab, India,

Date:

ABSTRACT

High temperature superconducting (HTS) cables cooled with liquid nitrogen (LN₂) have been found to be a most promising alternative to conventional cables for meeting the ever-rising energy demand across the world. The heat accommodated by the LN₂ flowing in HTS cable has various major sources such as A.C losses in the superconductor, dielectric losses in dielectric material, and heat influx through the cryogenic enclosure wall from ambient temperature. Thus, in order to operate long length HTS cables, the thermal and hydraulic analysis of LN₂ flowing in the HTS cable is essential. However, the LN₂ flow is more complex when flowing through stainless steel corrugated pipes with counter-flow cooling arrangement. In this thesis, counter-flow cooling (single-sided cooling with internal coolant return flow) system is considered for the analysis to reduce the highest temperature in the HTS cable. The explicit contributions of the thesis comprise:

To investigate the A.C losses due to self and external field and dielectric losses in the HTS cables to be used in power transmission application.

To examine the pressure drop, friction factor and pumping power needed to circulate the cryogen through counter-flow cooled HTS cable.

To investigate the effect of heat flux (heat-in-leak losses), heat generation (A.C and dielectric losses) and the effect of inlet temperature of coolant on the pressure drop and heat transfer rate.

To investigate the effect of various corrugation topologies (rectangular, circular and triangular) on pressure drop and heat transfer rate of LN₂ in HTS cable.

Development of friction factor correlation applicable to flow through corrugated pipe and optimization of the mass flow rate of LN₂ flowing through the HTS cable using entropy generation minimization (EGM) technique.

An exhaustive literature review with special prominence on A.C loss, dielectric loss, thermal analysis, hydraulic analysis and entropy generation for the HTS cable is presented in this thesis. The key reason for considering counter flow cooling HTS cable is due to effective use of cooling power. Moreover, counter flow cooling

arrangement makes the highest temperature of the cable probably less and space saving due to the coolant returns within the cable itself instead of distinct return pipe. A few of the widely used analytical approach to investigate the temperature profiles in the HTS cable and existing computational techniques for the thermohydraulic analysis and entropy generation are reviewed and discussed in detail.

The temperature distribution profiles along the counter flow cooled HTS cable has been solved and programmed using MATLAB for the modeled HTS cable in this thesis. The temperature profiles are obtained using energy balance equations, in purpose of thermal analysis of the HTS cable. The obtained temperature profiles are further used to investigate the influence of various volumetric flow rates and heat loss (A.C. loss and exterior heat load) on liquid nitrogen (LN2) in the HTS cable.

In addition, the thermohydraulic analysis of the HTS cable using computational fluid dynamics (CFD) approach has been also investigated and demonstrated in the thesis. The thermohydraulic analysis includes the influence of various heat flux (heat-in-leak losses), heat generation (A.C and dielectric losses), corrugation topologies (rectangular, circular and triangular) and coolant inlet temperature on the pressure drop and heat transfer in the HTS cable. The 2-D axisymmetric model of HTS cable with counter flow cooling system is considered by changing the corrugation shapes for Reynolds number ranging from 3.0×10^4 to 6.0×10^4 . The two-equation turbulence model k-epsilon ($k - \varepsilon$) is used to analyze the thermohydraulic behavior of LN2, where the thermophysical properties of LN2 are considered to be temperature dependent. Finite volume method is adapted to solve the governing equations (continuity, momentum and energy) using Semi-Implicit Pressure Linked Equations (SIMPLE) scheme with turbulence model and enhanced wall treatment.

It is also observed that the fluid flow, pressure drop and heat transfer across the long length cold dielectric counter cooled High Temperature Superconducting (HTS) cables are significantly influenced by the different corrugation topologies. Further, results reveal that the various corrugation topologies (rectangular, circular and triangular) have significant effect on heat transfer and pressure drop analysis. The corrugated pipes with different topologies exhibit different friction factors due to the

variations in the contact of wall surfaces with the LN₂. Moreover, the calculated friction factors and pressure drop for all the three corrugation topologies are compared with the experimental results available in the literature. Consequently, the calculated friction factor and pressure drop for the present work (employing counter flow through corrugated pipes placed centrally as well as externally) are found to be significant larger than the (annulus flow through centrally placed smooth pipe enveloped by a corrugated pipe) parallel flow HTS system. The large pressure drop in the considered model of counter flow cooling system is due to the turbulence occurred in both the inner corrugated pipe and outer corrugated pipe of HTS cable. The main reason for the high friction factor in the HTS cable, is due to the combined effect of LN₂ interaction with the walls of inner corrugated pipe and outer (annular) corrugated pipe simultaneously. Moreover, the distribution of the velocity, temperature and turbulent kinetic energy (TKE) of liquid nitrogen (LN₂) in the HTS cable are also estimated and presented in this thesis. Later, the amount of entropy generation (E.G) in the HTS cable due to thermal and velocity gradients are also estimated and presented in the thesis. Furthermore, the effect of heat flux, heat generation and various corrugation topologies on the entropy generation rate is also calculated and discussed.

Finally, the thermohydraulic analysis of HTS cable was done using analytical and computational techniques in order to accurately predict the maximum temperature of LN₂, Nusselt number, cooling capacity, friction factor and pumping power required to flow the LN₂. These studies will assist to the many manufacturing industries in manufacturing their HTS cables.

ACKNOWLEDGEMENTS

I am extremely thankful for the invaluable assistance of many people who have contributed to this research work presented in the thesis, even though you are not personally mentioned here.

This Ph.D. thesis involves the results of three years and two months of comprehensive research, which has been carried out at Applied Superconductivity Laboratory, Lovely Professional University Punjab. I would like to express my sincere gratitude to my supervisor, Dr. Raja Sekhar Dondapati, for his supervision, advice, guidance and financial support during the first day of this research. Moreover, I am thankful for giving me such an extraordinary experiences throughout the work. I am truly very fortunate to have the opportunity to work with him. I found his guidance to be extremely valuable and priceless. Special thanks are given to Mrs. Preeti Rao Usurumarti for invaluable discussions and advice on theoretical and computational concepts of turbulence modelling and flow through non-uniform diameter pipes. Additionally, I thank Dr. Priti Kalsia Soni for the generous help and suggestions she gave for the mathematical modelling part of the thesis. I also would like to thank Assistant Professor Mr. Gaurav Vyas for his continuous assistance in the research work. I would like to show my gratitude to the entire family of Lovely Professional University for providing me with a suitable research atmosphere to carry out my work in proper time. I would like to thank the Division of Research and Development and School of Mechanical Engineering for all the support and encouragement throughout the research work. I am also very thankful to the friends, fellow researchers and lab members, Mr. Rajesh Kumar Gadekula, Mr. Uppada Venkat and Mr. Rahul Aggarwal for their constructive assistance throughout the research work.

I am also very much grateful to my parents, Mrs. Sheela Devi and Mr. Om Parkash, and all my sisters and brothers for their love, moral support and care that they have shown during the course of my study. The love, patience, understanding and support of my fiancée Dr. Shivika Arya was also of great help in completing my study on time.

Last but not least, I thank God for sailing me through all the rough and tough times during this research work.

CONTENTS

DECLARATION.....	i
CERTIFICATE.....	ii
ACKNOWLEDGEMENTS	vi
1 INTRODUCTION	1
1.1 Thesis Background `	1
1.2 Research Motivation	2
1.3 The contribution of the thesis.....	3
1.4 Introduction to Superconductivity	6
1.4.1 Zero Resistivity in superconductors.....	7
1.4.2 Diamagnetism in superconductors	9
1.4.3 Type I superconductors	10
1.4.4 Type II superconductors	11
1.5 High Temperature Superconducting Cables	12
2 LITERATURE REVIEW	17
2.1 Literature Review on AC Losses and Dielectric Losses	17
2.2 Literature Review on Hydraulic Studies	26
2.3 Literature Review on Thermal Studies	33
2.4 Literature Review on Entropy Generation	38
2.5 Research Gaps.....	40
2.6 Objectives	41
3 MATHEMATICAL AND COMPUTATIONAL MODELING OF HTS CABLES.....	43
3.1 Analytical Modeling	43
3.2 Analytical Solution Procedure	45
3.2.1 Axial Temperature Profile for Inner Region.....	47
3.2.2 Axial Temperature Profile for Annular Region	50
3.3 Computational Modeling	52
3.3.1 Boundary Conditions.....	57
3.3.2 Computational modeling for various corrugation topologies of HTS cable.....	58
3.3.3 Boundary Conditions for various corrugation topologies of HTS cable	61
3.4 Governing Equations	62
4 HYDRAULIC ANALYSIS OF HTS CABLE	65

4.1	Grid Independence Study.....	65
4.2	Validation.....	70
4.2.1	Various corrugation topology	71
4.3	Velocity Distribution in HTS Cables	74
4.3.1	Effect of Heat Flux on Velocity Distribution	74
4.3.2	Effect of A.C Loss on Velocity Distribution.....	76
4.3.3	Effect of LN2 temperature on Velocity Distribution	77
4.4	Pressure Drop in HTS Cables	78
4.4.1	Effect of Heat Flux on Pressure Drop	78
4.4.2	Effect of A.C Loss on Pressure Drop.....	80
4.4.3	Effect of LN2 temperature on Pressure Drop.....	82
4.5	Pumping Power through HTS Cables	83
4.5.1	Effect of Heat Flux on Pumping Power	83
4.5.2	Effect of A.C Loss on Pumping Power.....	85
4.5.3	Effect of LN2 temperature on Pumping Power.....	87
4.6	Friction Factors in HTS Cables.....	88
4.6.1	Effect of Heat Flux on Friction Factor.....	88
4.6.2	Effect of A.C Loss on Friction Factor	90
4.6.3	Effect of LN2 temperature on Friction Factor.....	92
4.6.4	Correlation for Friction Factor applicable to Flow through Corrugated Pipe	93
4.7	Summary and Conclusions	94
5	THERMAL ANALYSIS OF HTS CABLE.....	97
5.1	Validation.....	97
5.2	Temperature Distribution in HTS Cables	98
5.2.1	Axial Temperature Distribution.....	98
5.2.2	Effect of flow rates on temperature profiles of LN ₂	98
5.2.3	Effect of heat flux on temperature profiles of LN ₂	100
5.2.4	Comparison of temperature profiles of LN ₂ with SCN.....	102
5.3	Nusselt Numbers in HTS Cables	103
5.3.1	Effect of Heat Flux on Nusselt Numbers.....	104
5.3.2	Effect of A.C Loss on Nusselt Numbers	105
5.3.3	Effect of LN2 temperature on Nusselt Number	107
5.4	Cooling Capacity	108
5.4.1	Effect of Heat Flux on Cooling Capacity.....	108
5.4.2	Effect of A.C Loss on Cooling Capacity.....	110
5.4.3	Effect of LN2 temperature on Cooling Capacity	112
5.5	Summary and Conclusions	113

6	ENTROPY GENERATION IN HTS CABLE	115
6.1	Effect of Heat flux on Entropy Generation.....	116
6.1.1	<i>Entropy Generation due to Thermal Gradients</i>	<i>119</i>
6.1.2	<i>Entropy Generation due to Velocity Gradients</i>	<i>121</i>
6.2	Effect of A.C losses on Entropy Generation in the HTS Cable	123
6.2.1	<i>Entropy Generation due to Thermal Gradients</i>	<i>126</i>
6.2.2	<i>Entropy Generation due to Velocity Gradients</i>	<i>128</i>
6.3	Summary and Conclusions	130
7	CONCLUSIONS AND FUTURE SCOPE	133
7.1	Conclusions.....	133
7.2	Future Scope	134

List of Tables

Table 1-1 Overview of commercially available superconducting wires. MTS-Middle Temperature Superconductor [1]	8
Table 1-2 List of Type I superconductors	11
Table 1-3 List of Type II superconductors	11
Table 1-4 HTS cable project around the world.....	14
Table 3-1 Parameters for conceptual design of HTS cable.....	45
Table 3-2 parameters for conceptual design of HTS cable.....	55
Table 3-3 compared approximate entry lengths at various Reynolds numbers	55
Table 3-4 Parameters for conceptual design of HTS cable.....	58
Table 4-1 Number of nodes for respective element size of circular corrugation shape	66
Table 4-2 Number of nodes for respective element size of rectangular corrugation shape.....	67
Table 4-3 Number of nodes for respective element size of triangular corrugation shape	69
Table 4-4 Correlation for friction factors at various heat flux and A.C loss in circular corrugation shape HTS cable	93
Table 4-5 Correlation for friction factors at various heat flux and A.C loss in rectangular corrugation shape HTS cable	93
Table 4-6 Correlation for friction factors at various heat flux and A.C loss in triangular corrugation shape HTS cable.....	93
Table 4-7 Comparison of hydraulic characteristics with various corrugations	95
Table 5-1 Feasibility of HTS cable cooling with defined lengths	102
Table 5-2 Comparison of thermal characteristics with various corrugations	114

List of Figures

Figure 1.1 The critical boundary of superconductivity.....	6
Figure 1.2 Typical behavior of normal conductor insulator and superconductor.....	7
Figure 1.3 History of development of superconductors [2].....	9
Figure 1.4 The Meissner effect	9
Figure 1.5 (a) Type I superconductor at applied field H_c (b) Type II superconductor	12
Figure 1.6 Single phase cold dielectric HTS cable	13
Figure 1.7 Comparison between conventional copper cables and HTS cables, [Data Source: Long Island Power Authority (LIPA)].....	15
Figure 3.1 (a) Modelled single-phase cold dielectric HTS cable (b) schematic of HTS cable with no cryocooler at end (c) schematic of HTS cable with cryocooler at end	44
Figure 3.2 Phase diagram for operating range and boiling curve of liquid nitrogen ...	45
Figure 3.3 (a) Schematic of fluid and solid domains of HTS cable (b) heat balancing within control volume	46
Figure 3.4 Schematic of overall thermal conductance in HTS cable.....	47
Figure 3.5 Heat balancing in the inner region of HTS cable	47
Figure 3.6 Heat balancing in the annular region of HTS cable	50
Figure 3.7 (a) Flow chart of thermohydraulic analysis of HTS cable (b) Schematic of Counter flow arrangement	53
Figure 3.8 Schematic representation of single-phase co-axial superconducting cable system.....	54
Figure 3.9 (a) 2-D Axisymmetric view of counter flow cold dielectric HTS cable and (b) a view of typical Mesh	56
Figure 3.10 Schematic and structural parameters of 2-D axisymmetric HTS cable with various corrugation shapes (a) rectangular (b) circular (c) triangular	60
Figure 3.11 Typical mesh of 2-D axisymmetric HTS cable with various corrugation shapes (a) rectangular (b) circular (c) triangular.....	61
Figure 4.1 Typical mesh view for circulation corrugation with different element sizes: (a) 0.70mm (b) 0.64mm (c) 0.58mm (d) 0.52mm.....	66
Figure 4.2 Pressure drop for various element sizes in the HTS cable with circular corrugation	67
Figure 4.3 Typical mesh view for rectangular corrugation with different element sizes: (a) 1.0mm (b) 0.8mm (c) 0.6mm (d) 0.4mm.....	68
Figure 4.4 Pressure drop for various element sizes in the HTS cable with rectangular corrugation	68

Figure 4.5 Typical mesh view for triangular corrugation with different element sizes: (a) 1.0mm (b) 0.9mm (c) 0.7mm (d) 0.5mm.....	69
Figure 4.6 Pressure drop for various element sizes in the HTS cable with triangular corrugation	70
Figure 4.7 Comparison of various turbulence models available with CFD in the estimation of (a) friction factor at different Reynolds number (b) Nusselt number at different Reynolds number	71
Figure 4.8 Validation of friction factor from present investigation with those of existing correlations [101] and result obtained by Sasaki et al.....	72
Figure 4.9 Validation of obtained pressure drop (present work) with experimental results performed by Mukoyama S et al. and calculated results by O Maruyama et al. [50].....	73
Figure 4.10 Validation of friction factor from present investigation with experimental results obtained by Li et al. [49]	73
Figure 4.11 Validation of obtained pressure drop (present work) with experimental and simulation results performed by Li et al. [49].....	74
Figure 4.12 Effect of heat flux on radial velocity distribution with all three corrugation topologies at constant heat flux of 6 W/m ² with	75
Figure 4.13 Velocity distribution in the circular corrugated steel pipe with a flow rate of 25 L/min and constant heat flux of 6 W/m ² at (a) at 0.15m and (b) at 0.49m from inlet.....	75
Figure 4.14 Effect of A.C loss on radial velocity distribution with all three corrugation topologies at constant heat generation of 800 W/m ³	76
Figure 4.15 Velocity distribution in the circular corrugated steel pipe with a flow rate of 25 L/min and constant heat generation of 800 W/m ³ (a) at 0.15m and (b) at 0.49m from inlet	77
Figure 4.16 Effect of coolant inlet temperature on velocity distribution with heat flux of 4 W/m ² and heat generation of 800W/m ³ at 0.150m at the inlet.....	78
Figure 4.17 Effect of heat flux on pressure drop at constant heat generation of 800 W/m ³ with rectangular corrugation	79
Figure 4.18 Effect of heat flux on pressure drop at constant heat generation of 800 W/m ³ with circular corrugation	80
Figure 4.19 Effect of heat flux on pressure drop at constant heat generation of 800 W/m ³ with triangular corrugation.....	80
Figure 4.20 Effect of A.C loss on pressure drop at constant heat flux of 6 W/m ² with rectangular corrugation	81
Figure 4.21 Effect of A.C loss on pressure drop at constant heat flux of 6 W/m ² with circular corrugation	81
Figure 4.22 Effect of A.C loss on pressure drop at constant heat flux of 6 W/m ² with triangular corrugation.....	82

Figure 4.23 Effect of coolant inlet temperature on pressure drop at heat flux of 4 W/m ² and heat generation of 800W/m ³	83
Figure 4.24 Effect of heat flux on pumping power at constant heat generation of 800 W/m ³ with rectangular corrugation.....	84
Figure 4.25 Effect of heat flux on pumping power at constant heat generation of 800 W/m ³ with circular corrugation.....	84
Figure 4.26 Effect of heat flux on pumping power at constant heat generation of 800 W/m ³ with triangular corrugation.....	85
Figure 4.27 Effect of A.C loss on pumping power at constant heat flux of 6 W/m ² with rectangular corrugation.....	86
Figure 4.28 Effect of A.C loss on pumping power at constant heat flux of 6 W/m ² with circular corrugation.....	86
Figure 4.29 Effect of A.C loss on pumping power at constant heat flux of 6 W/m ² with triangular corrugation.....	87
Figure 4.30 Effect of coolant inlet temperature on pumping power at heat flux of 4 W/m ² and heat generation of 800W/m ³	88
Figure 4.31 Effect of heat flux on friction factor at constant heat generation of 800 W/m ³ with rectangular corrugation.....	89
Figure 4.32 Effect of heat flux on friction factor at constant heat generation of 800 W/m ³ with circular corrugation.....	89
Figure 4.33 Effect of heat flux on friction factor at constant heat generation of 800 W/m ³ with rectangular corrugation.....	90
Figure 4.34 Effect of A.C loss on friction factor at constant heat flux of 6 W/m ² with rectangular corrugation.....	91
Figure 4.35 Effect of A.C loss on friction factor at constant heat flux of 6 W/m ² with circular corrugation.....	91
Figure 4.36 Effect of A.C loss on friction factor at constant heat flux of 6 W/m ² with triangular corrugation.....	92
Figure 4.37 Effect of coolant inlet temperature on friction factor at heat flux of 4 W/m ² and heat generation of 800W/m ³	92
Figure 5.1 Comparison of temperature difference between outlet and inlet of LN2 in counter flow HTS cable (present work) with that of LN2 estimated by Dondapati et al. [102] and with the experimental results performed by Ivanov et al. [103].....	97
Figure 5.2 Temperature distribution along the cable at varying volumetric flow: a) with an additional cryocooler at right end of the cable, b) no cryocooler at right end of the cable.....	99
Figure 5.3 Comparison of temperature distribution along the cable at different volumetric flow with a cryocooler at end and without cryocooler a) at 20L/min, b) at 25 L/min, c) at 30 L/min, d) at 35 L/min.....	100

Figure 5.4 Temperature distribution along the cable at different heat loads with constant volumetric flow: a) at 20 L/min, b) at 25 L/min, c) at 30 L/min, d) at 35 L/min.....	101
Figure 5.5 Temperature distribution along the cable at different volumetric flow with constant heat loads: a) at 2.3 W/m, b) at 2.4 W/m, c) at 2.5 W/m, d) at 2.6 W/m.....	101
Figure 5.6 Comparison of temperature distribution of LN ₂ and SCN along the cable at varying volumetric flow a) at 20L/min, b) at 25 L/min, c) at 30 L/min, d) at 35 L/min	103
Figure 5.7 Effect of heat flux on Nusselt number at constant heat generation of 800 W/m ³ with rectangular corrugation	104
Figure 5.8 Effect of heat flux on Nusselt number at constant heat generation of 800 W/m ³ with circular corrugation	105
Figure 5.9 Effect of heat flux on Nusselt number at constant heat generation of 800 W/m ³ with triangular corrugation.....	105
Figure 5.10 Effect of A.C loss on Nusselt number at constant heat flux of 6 W/m ² with rectangular corrugation	106
Figure 5.11 Effect of A.C loss on Nusselt number at constant heat flux of 6 W/m ² with circular corrugation	106
Figure 5.12 Effect of A.C loss on Nusselt number at constant heat flux of 6 W/m ² with triangular corrugation.....	107
Figure 5.13 Effect of coolant inlet temperature on Nusselt number at heat flux of 4 W/m ² and heat generation of 800W/m ³	108
Figure 5.14 Effect of heat flux on cooling capacity at constant heat generation of 800 W/m ³ with rectangular corrugation	109
Figure 5.15 Effect of heat flux on cooling capacity at constant heat generation of 800 W/m ³ with circular corrugation	109
Figure 5.16 Effect of heat flux on cooling capacity at constant heat generation of 800 W/m ³ with triangular corrugation.....	110
Figure 5.17 Effect of A.C loss on cooling capacity at constant heat flux of 6 W/m ² with rectangular corrugation	111
Figure 5.18 Effect of A.C loss on cooling capacity at constant heat flux of 6 W/m ² with circular corrugation	111
Figure 5.19 Effect of A.C loss on cooling capacity at constant heat flux of 6 W/m ² with triangular corrugation.....	112
Figure 5.20 Effect of coolant inlet temperature on cooling capacity at heat flux of 4 W/m ² and heat generation of 800W/m ³	113
Figure 6.1 Entropy generation in a system consisting of thermodynamics, fluid mechanics and heat transfer	116

Figure 6.2 Effect of heat flux of 4 W/m ² on total entropy generation at constant heat generation of 800 W/m ³ with all three corrugations (rectangular, circular and triangular)	117
Figure 6.3 Effect of heat flux of 6 W/m ² on total entropy generation at constant heat generation of 800 W/m ³ with all three corrugations (rectangular, circular and triangular)	117
Figure 6.4 Effect of heat flux of 8 W/m ² on total entropy generation at constant heat generation of 800 W/m ³ with all three corrugations (rectangular, circular and triangular)	118
Figure 6.5 Effect of heat flux of 10 W/m ² on total entropy generation at constant heat generation of 800 W/m ³ with all three corrugations (rectangular, circular and triangular)	118
Figure 6.6 Effect of heat flux of 4 W/m ² on entropy generation due to thermal gradients at constant heat generation of 800 W/m ³ with all three corrugations (rectangular, circular and triangular)	119
Figure 6.7 Effect of heat flux of 6 W/m ² on entropy generation due to thermal gradients at constant heat generation of 800 W/m ³ with all three corrugations (rectangular, circular and triangular)	120
Figure 6.8 Effect of heat flux of 8 W/m ² on entropy generation due to thermal gradients at constant heat generation of 800 W/m ³ with all three corrugations (rectangular, circular and triangular)	120
Figure 6.9 Effect of heat flux of 10 W/m ² on entropy generation due to thermal gradients at constant heat generation of 800 W/m ³ with all three corrugations (rectangular, circular and triangular)	121
Figure 6.10 Effect of heat flux of 4 W/m ² on entropy generation due to velocity gradients at constant heat generation of 800 W/m ³ with all three corrugations (rectangular, circular and triangular)	122
Figure 6.11 Effect of heat flux of 6 W/m ² on entropy generation due to velocity gradients at constant heat generation of 800 W/m ³ with all three corrugations (rectangular, circular and triangular)	122
Figure 6.12 Effect of heat flux of 8 W/m ² on entropy generation due to velocity gradients at constant heat generation of 800 W/m ³ with all three corrugations (rectangular, circular and triangular)	123
Figure 6.13 Effect of heat flux of 10 W/m ² on entropy generation due to velocity gradients at constant heat generation of 800 W/m ³ with all three corrugations (rectangular, circular and triangular)	123
Figure 6.14 Effect of A.C loss of 1 W/m on total entropy generation at constant heat flux of 6 W/m ² with all three corrugations (rectangular, circular and triangular).....	124
Figure 6.15 Effect of A.C loss of 1.5 W/m on total entropy generation at constant heat flux of 6 W/m ² with all three corrugations (rectangular, circular and triangular).....	125

Figure 6.16 Effect of A.C loss of 2 W/m on total entropy generation at constant heat flux of 6 W/m ² with all three corrugations (rectangular, circular and triangular).....	125
Figure 6.17 Effect of A.C loss of 2.5 W/m on total entropy generation at constant heat flux of 6 W/m ² with all three corrugations (rectangular, circular and triangular).....	126
Figure 6.18 Effect of A.C loss of 1 W/m on entropy generation due to thermal gradients at constant heat flux of 6 W/m ² with all three corrugations (rectangular, circular and triangular)	127
Figure 6.19 Effect of A.C loss of 1.5 W/m on entropy generation due to thermal gradients at constant heat flux of 6 W/m ² with all three corrugations (rectangular, circular and triangular)	127
Figure 6.20 Effect of A.C loss of 2 W/m on entropy generation due to thermal gradients at constant heat flux of 6 W/m ² with all three corrugations (rectangular, circular and triangular)	128
Figure 6.21 Effect of A.C loss of 2.5 W/m on entropy generation due to thermal gradients at constant heat flux of 6 W/m ² with all three corrugations (rectangular, circular and triangular)	128
Figure 6.22 Effect of A.C loss of 1 W/m on entropy generation due to velocity gradients at constant heat flux of 6 W/m ² with all three corrugations (rectangular, circular and triangular)	129
Figure 6.23 Effect of A.C loss of 1.5 W/m on entropy generation due to velocity gradients at constant heat flux of 6 W/m ² with all three corrugations (rectangular, circular and triangular)	129
Figure 6.24 Effect of A.C loss of 2 W/m on entropy generation due to velocity gradients at constant heat flux of 6 W/m ² with all three corrugations (rectangular, circular and triangular)	130
Figure 6.25 Effect of A.C loss of 2.5 W/m on entropy generation due to velocity gradients at constant heat flux of 6 W/m ² with all three corrugations (rectangular, circular and triangular)	130

1 INTRODUCTION

This chapter demonstrates the detailed introduction of the research work presented in the thesis along with the background, research challenges and motivation. The research work dedicates the thermohydraulic investigation of high temperature superconducting cables used for large scale power applications. Therefore, the background of superconductivity and HTS cables are discussed. Moreover, the challenges occurred during operation of HTS cable and their solutions are also contributed in this chapter.

1.1 Thesis Background`

Conventional power grids around the world in recent days, facing serious challenges resulting from rapidly increase in the consumption of electricity. The basic services of social life such as manufacturing plants, refineries, online transactions, railways, hospitals and stock exchange markets are highly depend on the electricity. It is predicted that the demand of electrical energy will be approximately double by 2050. Electrical energy plays a significant role for the economic development of every country. However, the enormous amount of electric energy is being lost during generation, storage and transmission processes in the conventional power grids. In addition, about 20% to 30% of the produced electricity is lost only in distribution and transmission through the grids to the end users. One of the major issues for the distribution and transmission losses is due the resistance offered by the conventional copper and aluminum power cables. Moreover, few other challenges such as right-off-way, environmental hazards (Icing and wind storms) and overhead hanging are still unsolved. Sometimes, the conventional power grids fail to distribute and transmit persistently rising demand of electricity. Thereby, frequent blackouts around the world can be seen due to the failure of conventional power grids during the period of highest demand of electricity. In July, 2012 two massive blackouts hit India due to the disturbances faced on the power transmission lines in the grids. In many of the developing countries, majority of the electricity is being produced by burning of fossil

fuels such as coal, oil and gas which further leads to the environmental pollution. The biggest environmental challenge in the world is global warming, which is caused by greenhouse gases (GHG) emission such as carbon dioxide (CO₂), methane (CH₄), nitrous oxide (NO₂) and chlorofluorocarbons (CFCs). Moreover, the main source of GHG emissions is the burning of fossil fuels (coal, oil and gas) by the power grids for the production of electricity.

The reasons behind the issues discussed above are ever-rising demand of electricity, massive consumption of electricity and inefficient infrastructures of conventional power grids. Hence, an efficient electric transmission system is required in order to prevent future power blackouts and to conquer other discussed challenges.

1.2 Research Motivation

Due to the rapid increase in the power demand, need arises to help the society in terms of providing energy security and fulfilling the energy demand by introducing new and advanced technology. One of the promising solutions to deal with such complex issues is to replace the conventional conductors with the High Temperature Superconducting (HTS) power cables. A numerous types of superconductors are now commercially in trading for the HTS applications in research and industries. The most commonly used superconductors are Yttrium Barium Copper Oxide (YBCO) and Barium Strontium Calcium Cooper Oxide (BSCCO) having critical temperatures (T_c) of 92K and 110K respectively. In order to reduce the cooling cost of superconductors, the critical temperature of those high temperature superconductors has to be upgraded up to room temperature. Hence, HTS cables with YBCO materials are now becoming promising to the grids as compared to the conventional copper cables. The key benefits of superconducting power cable over conventional copper cable are as follows:

- The HTS cables can carry about five times more electric current than that of conventional copper cables which further contributes in meeting the increased power demand.
- The HTS cables replace the overhead transmission in the event of environmental hazards eliminate the need of installation of conventional cables.
- Due to lower losses in HTS cables, the overall efficiency of the entire system increases than that with conventional copper cables.

- The capital cost can be massively reduced using HTS cables, due to the higher current carrying capability at lower transmission voltages, which enables reduction in the electricity cost.
- It is now possible and easy to install HTS cables in the limited underground space, owing to the compact structure of HTS cable in underground conduits.

One of the other advantages of HTS cable is the reduced compatible size with capability to carry the same power as by conventional power cable. This compact size cable can be placed underground for large power transmission in the cities where additional digging space is limited and enables the cost reduction of overall system. Since, these HTS cables are thermally insulated and independent of geographical conditions, it is more suitable to install these HTS cables for larger power transmission than with conventional power cables. Although the large power can be transmitted through these HTS cables by installing into the power grids, an additional mechanical power must be needed to cool the superconductors down to their critical temperature. Therefore, the overall losses saved in HTS cable is counter balanced by the cooling system which shows the cost effectiveness of the entire cooling system. Hence, an inexpensive and cost-effective solution for robust large scale transmission by introducing the HTS cables is provided.

1.3 The contribution of the thesis

High temperature superconducting (HTS) cables cooled with liquid nitrogen (LN₂) have been found to be most promising alternative to conventional cables for meeting the ever-rising energy demand across the world. Thus, in order to operate HTS cables in the power grids for the efficient distribution and transmission of power, the present thesis addresses various results pertaining to different challenges encountered by the operation of HTS cables.

Firstly, the A.C losses due to self-field and external field in the HTS cable are studied considering the properties of 2G HTS tape. Since the performance of HTS cable is influenced by the electrical heat dissipation due to A.C losses in the HTS tape, the magnitude of A.C losses per unit length (W/m) in the cable are calculated. Further, the losses due to the polarization of insulator/dielectric called as dielectric losses are estimated. In other words, the calculation of A.C losses and dielectric losses are an

important factors in determining the performance of HTS cable. Hence, a reliable analytical methodology including Norris equation was adapted to estimate the self-field A.C losses in the HTS cable. The solution using both the equations are implemented in MATLAB code to obtain the A.C losses and dielectric in HTS cable. The electrical heat dissipation due to A.C losses and dielectric losses (W/m) are considered as the heat generation (W/m³) in the superconducting tapes for the further analysis.

Secondly, the other major issue such as heat-in-leak from the ambient to the wall enclosure of HTS cable is also considered for the further analysis. The heat-in-leak (W/m) is assumed and later converted into wall heat flux (W/m²) for the thermohydraulic analysis of HTS cable. Therefore, the combined effect of heat generation (W/m³) and wall heat flux (W/m²) on the hydraulic and thermal performance of HTS cable is studied. The hydraulic analysis consists of various investigations such as estimation of friction factor, pressure drop, pumping power and velocity distribution in the HTS cable. Further, the thermal analysis consists of the estimating Nusselt number, cooling capacity and temperature distribution in the HTS cable. Moreover, the effect of various corrugation topologies (rectangular, circular and triangular) on the thermohydraulic performance of HTS cable are also investigated.

Later, a computational model has been developed to investigate the thermal and hydraulic performance of HTS cable. Finite volume method is adapted to solve the governing equations (continuity, momentum and energy) using Semi-Implicit Pressure Linked Equations (SIMPLE) scheme with $k-\varepsilon$ turbulence model and enhanced wall treatment. The 2-D axisymmetric model of HTS cable with counter flow cooling system is considered by changing the corrugation shapes for Reynolds number ranging from 3.0×10^4 to 6.0×10^4 . Robust boundary conditions are chosen to simulate the counter flow cooling HTS cable system.

Finally, the results on thermohydraulic performance from computational investigations in counter flow HTS cable turn out to be interesting to understand the effective and efficient design. Further utilizing the developed cable model, various losses, flow characteristics and heat transfer rate are analyzed and compared with the experimental results available in the literature. Hence, a novel counter cooled HTS cable is developed considering the detailed configurations.

The explicit contributions of the thesis are as follows:

Chapter 2 presents an exhaustive literature review on estimation of A.C losses, dielectric losses, hydraulic, thermal and entropy generation for the HTS cable. This literature review helped in identifying the possible research gaps and to frame objectives of the present work in accordance with the identified research gaps. The recent development of the HTS cable for large scale power application is also outlined and discussed in detail.

Chapter 3 contains the mathematical and computational modeling along with the analytical solution of temperature distribution of LN₂ in HTS cable. Mathematical and computational models are developed and discussed in order to estimate the behavior of LN₂ under the influence of corrugation geometry, heat-in-leak (W/m^2) and heat generation (W/m^3).

Chapter 4 investigates the hydraulic issues such as pressure drop, friction factor and pumping power required to circulate the cryogen in the counter-flow cooled HTS cable. Moreover, the effect of heat flux (heat-in-leak losses), heat generation (A.C and dielectric losses), effect of inlet temperature of coolant and various corrugation topologies on the hydraulic performance of HTS cable are also investigated.

Chapter 5 dedicated to address the thermal issues such as Nusselt number, cooling capacity and temperature distribution in the counter-flow cooled HTS cable. Moreover, the effect of heat flux (heat-in-leak losses), heat generation (A.C and dielectric losses), effect of inlet temperature of coolant and various corrugation topologies on the thermal performance of HTS cable are also investigated.

Chapter 6 presents the entropy generation due to the thermal and velocity gradients in the counter-flow cooled HTS cable. The effect of heat flux (heat-in-leak losses) and heat generation (A.C and dielectric losses) and various topologies on the entropy generation due to the thermal and velocity gradients are also discussed.

Chapter 7 summarizes the research work with recommendations on operating conditions of HTS Cable for economic and safe operation. The feasible future scope for the designing the long length counter cooled HTS power cable are also discussed.

1.4 Introduction to Superconductivity

The superconductivity phenomenon was first observed in metals by Kamerlingh-Onnes in 1911. It was indeed a remarkable discovery, which states the phenomenon of losing resistivity and expulsion of magnetic field, when cooled to a certain temperature (below critical temperature, T_c).

In order to maintain the superconductivity, a material must be in the region defined by the three inter-linked boundaries such as critical current (I_c), critical temperature (T_c) and critical magnetic field (H_c) as shown in Figure 1.1. These three inter-linked boundaries are called critical boundaries for a superconducting material. A material can lose its superconductivity if beyond any of these critical boundaries. The critical values of a superconducting material will be chosen based on the application of the HTS.

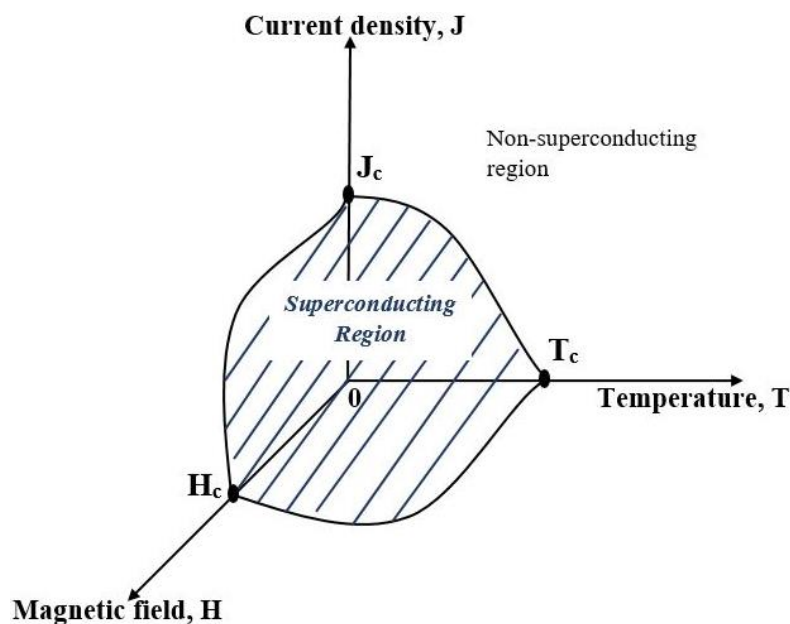


Figure 1.1 The critical boundary of superconductivity

1.4.1 Zero Resistivity in superconductors

The electrical resistance in a superconductor abruptly falls to zero when cooled below its critical temperature, this phenomenon is known as zero resistivity in the superconductors. Figure 1.2 indicates the variation of resistance with temperature of typical normal conductor, insulator and superconductor. With decrease in the temperature, the resistance of insulators will increase. Whereas, a decreasing value up to an extent can be seen for normal conductors. However, resistance would be exactly zero at the critical temperature (T_c) for a superconductor. In this figure, Mercury (Hg)

was taken into consideration having critical temperature nearer to 4K, and after investigating several metals, mercury was found to be the first superconductor at a temperature of 4.2K. Moreover, few other metals such as Lead (Pb) and Tin (Sn) were added later to the list of superconductors. After the discovery of superconductivity with T_c of 4.2 K in mercury (Hg) in 1911 by H. K. Onnes, were brought later up to 7 K in lead (Pb) and tin (Sn). Niobium (Nb) in 1930 with a critical temperature of 9.2 K remained the highest T_c found in the material.

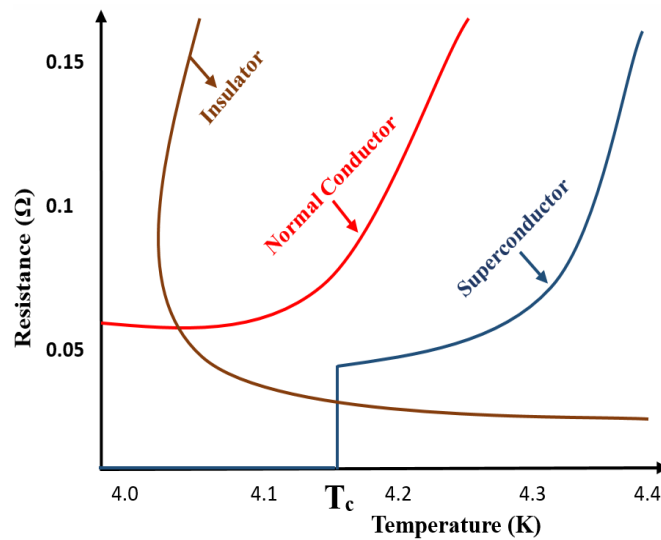
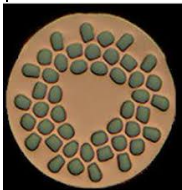

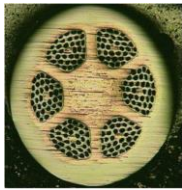
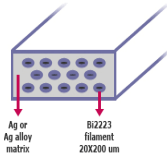
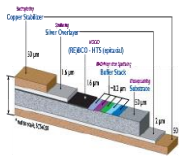


Figure 1.2 Typical behavior of normal conductor insulator and superconductor

According to the critical temperature (T_c) values, the superconductors can be classified into two key groups such as low temperature superconductors (LTS) and high temperature superconductors (HTS). The LTS group was invented previously to the HTS group. The blue dots represent the discovery of metals and alloys whereas the red dots signify the discovery of higher T_c cuprates in their respective years. The highest critical temperature of LTS group is approximately measured as 30K. The main examples of LTS group are Nb_3Sn and $NbTi$. The low temperature superconductor materials are widely used in clinical magnetic resonance imaging (MRI), ultra-high field device called nuclear magnetic resonance (NMR), and particle accelerators such as large hadron collider (LHC). Due to the less critical current density of low T_c superconductors, a gradual development of superconductor technology with higher current density has been taken up since 1960. However, the discovery of HTS group came into the existence in the year of 1986. The structure of HTS group is found to be more complicated than that of LTS group which results in the higher production cost.

The lowest critical temperature of HTS group materials begin from approximately 50K. The most promising superconductor for numerous HTS applications are BSCCO and YBCO with critical temperature of 110K and 92K respectively. The HTS materials are nowadays used in many applications such as generators, transformers, motors, fault current limiters, power storage, power transmission, fusion reactors and magnetic levitation devices. The development of the critical temperature of the superconductors over the years are shown in Figure 1.3. Moreover, the commonly used and commercially available superconducting wires with several key features are presented in the Table 1-1.

Table 1-1 Overview of commercially available superconducting wires. MTS-Middle Temperature Superconductor [1]

	NbTi	Nb ₃ Sn	MgB ₂	BSCCO	YBCO
Wire					
T _c (K)	9	18	39	110	90
LN2 Compatible	No	No	No	Yes	Yes
Group	LTS	LTS	MTS	HTS	HTS
Flexibility	Yes	No	Yes	Yes	Yes
Cost	Low	Low	Low	High	High

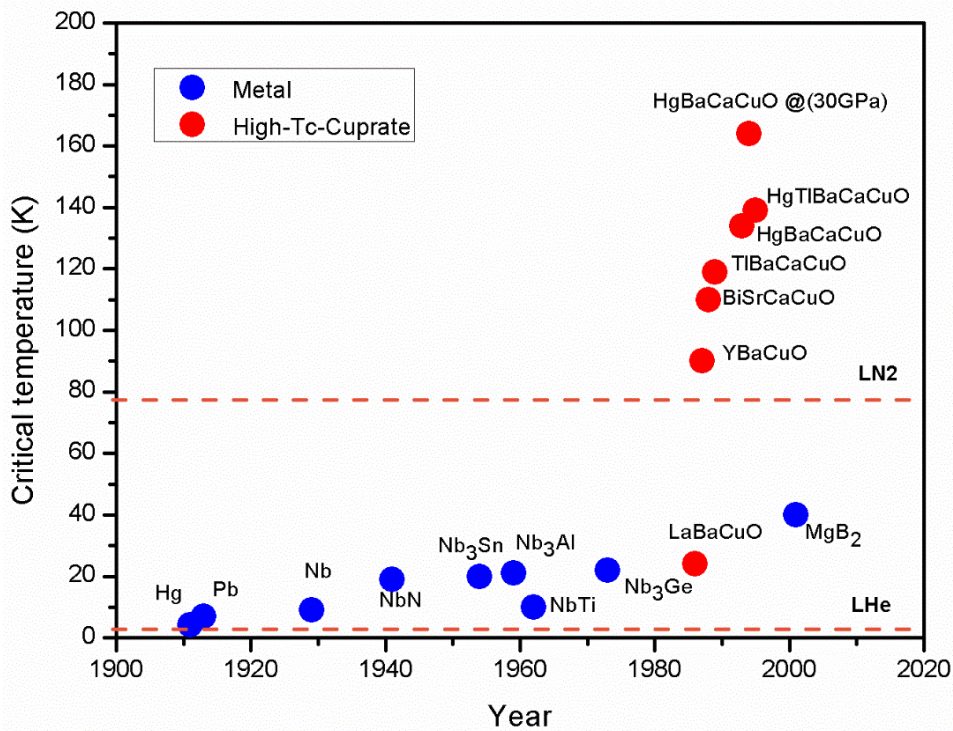


Figure 1.3 History of development of superconductors [2]

1.4.2 Diamagnetism in superconductors

Perfect diamagnetism in superconductors is one another discovery by German Physicists Walther Meissner and Robert Ochsenfeld in 1933. The theory, perfect diamagnetism, reveals that the flux expelled from the superconductor if cooled below its critical temperature. This phenomenon is called as the Meissner effect.

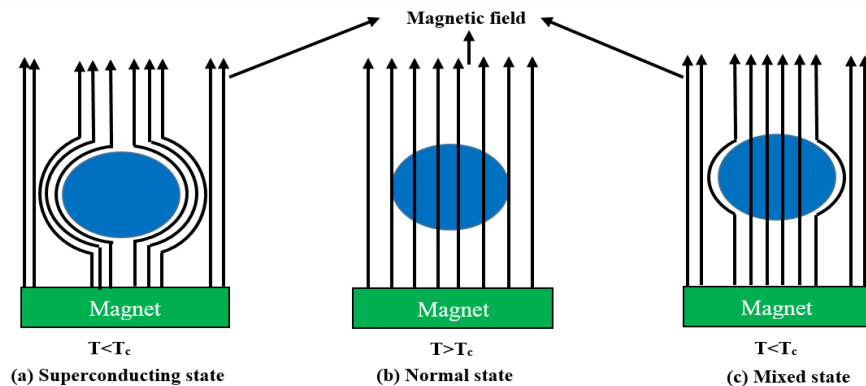


Figure 1.4 The Meissner effect

Figure 1.4 (a) shows the behavior of a material placed in a magnetic field at the temperature below its critical temperature. The blue oval shaped geometry indicates the material and vertical black color arrows represent the magnetic field produced through

the magnet (green color box). In a superconducting state the magnetic field expels when a material is placed in the magnetic field at $T < T_c$. On the other hand, the normal state can be observed when a material is placed under magnetic field at $T > T_c$, as represented in Figure 1.4 (b). Whereas, a mixed state can also be seen under the magnetic field at $T < T_c$, as shown in Figure 1.4 (c). Superconductors have the ability to exhibit superconducting state, normal state and mix state depending upon the external applied magnetic field (H). According to Nicholas Gerbis, the categorization of superconductors on the basis of critical magnetic field (H_c) can be done as follows.

1.4.3 Type I superconductors

In Type I superconductors, current flows only on the surface and superconductivity vanishes in the presence of magnetic field at a well-defined critical field (H_c) as shown in Figure 1.5 (a) Type I superconductor at applied field H_c (b) Type II superconductor (a). Type I superconductors obey the Meissner effect. In other words, Type I superconductor switches sharply from Meissner state (M_s) to normal state (N_s) at a particular applied magnetic field. Due to the easy process of losing their own superconductivity, the superconductors are also known as soft superconductors. Few examples of Type I superconductors are Hg, Al and Sn as shown in Table 1-2. The technological potential of these developed superconductors for generation of magnetic field, was unexpectedly less.

Table 1-2 List of Type I superconductors

Type I superconductors			
Name	T_c (K)	Name	T_c (K)
Lead (Pb)	7.196	Zinc (Zn)	0.85
Lanthanum (La)	4.88	Osmium (Os)	0.66
Tantalum (Ta)	4.47	Zirconium (Zr)	0.61
Mercury (Hg)	4.15	Americium (Am)	0.60
Tin (Sn)	3.72	Cadmium (Cd)	0.517
Indium (In)	3.41	Ruthenium (Ru)	0.49
Palladium (Pd)	3.3	Titanium (Ti)	0.40
Chromium (Cr)	3	Uranium (U)	0.20
Thallium (Tl)	2.38	Hafnium (Hf)	0.128
Rhenium (Re)	1.697	Iridium (Ir)	0.1125
Protactinium (Pa)	1.40	Beryllium (Be)	0.023
Thorium (Th)	1.38	Tungsten (W)	0.0154
Aluminum (Al)	1.175	Platinum (Pt)	0.0019
Gallium (Ga)	1.083	Lithium (Li)	0.0004
Molybdenum (Mo)	0.915	Rhodium (Rh)	0.000325

1.4.4 Type II superconductors

Type II superconductor switches from the Meissner state (M_s) to a mixed state with partial vortex penetration (S_v) of magnetic flux, at a critical field, H_{c1} . Thereafter, it exhibits to normal state, with full flux penetration at an upper critical field, H_{c2} as shown in Figure 1.5 (a) Type I superconductor at applied field H_c (b) Type II superconductor (b). The typical examples of Type II superconductors are Nb_3Sn and $NbTi$ as shown in Table 1-3.

Table 1-3 List of Type II superconductors

Type II superconductors	
Name	T_c (K)
$HgBa_2Ca_2Cu_3O_8$	133-135
$HgBa_2Ca_3Cu_4O_{10+}$	125-126
$HgBa_2CuO_{4+}$	94-98
$Tl_2Ba_2Ca_2Cu_3O_{10}$	127-128
$Tl_2Ba_2CuO_6$	95
$Bi_2Sr_2Ca_2Cu_3O_{10}$	110
$YBa_2Cu_3O_7$	90
Zn_3MgO_4	152

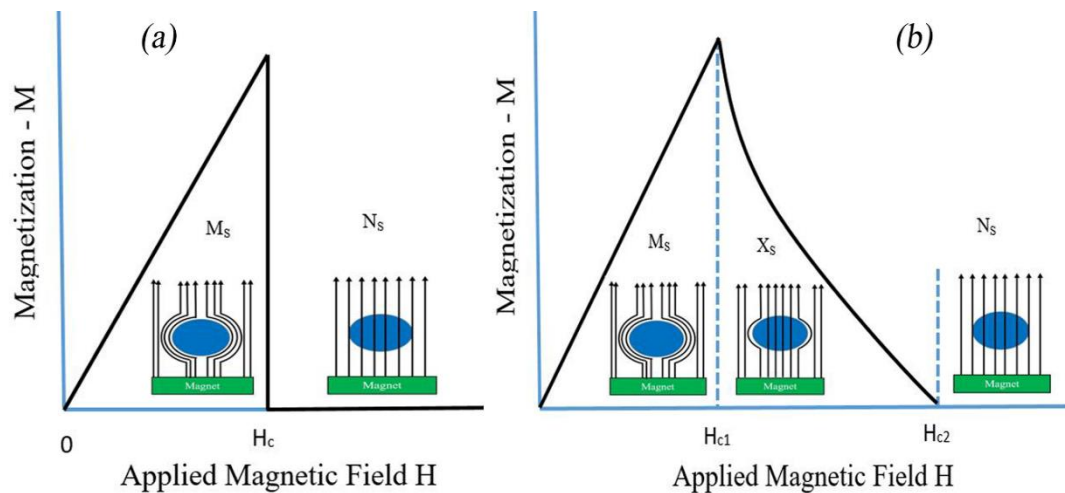


Figure 1.5 (a) Type I superconductor at applied field H_c (b) Type II superconductor

1.5 High Temperature Superconducting Cables

The high temperature superconducting (HTS) cables are generally classified into two categories such as warm dielectric (WD) HTS cable and cold dielectric (CD) HTS cable. The categorization of HTS cables is based on the cooling of their insulations. When the insulation of HTS cable is placed at room temperature, the cable known as warm dielectric (WD). On the other hand, the insulation of HTS cable is placed at cryogenic temperature, the cable called as cold dielectric (CD). The insulation material used in the WD and CD cables are cross-linked polyethylene (XLPE) and polypropylene laminated paper (PPLP) respectively. Due to the interesting properties such as withstanding a high breakdown voltage in LN₂ environment, the PPLP is used as an insulating material for the CD HTS cables. A typical view of single phase cold dielectric HTS cable is shown in Figure 1.6.

The functions of each component of single phase CD HTS cable are as follows:

Corrugated pipe (Former): stainless steel corrugated pipe is used as former to ensure the flexibility to the entire cable system and cryogenic-environment compatibility with higher heat transfer properties.

HTS tapes: spirally wound on the former in the cable structure and main source of carrying large current.

Dielectric: Poly propylene laminated paper (PPLP) is used as an insulating layer in CD HTS cable which can withstand high-voltage breakdown.

Cryogenic fluid: LN2 is used as coolant to maintain the superconductivity and to accommodate the heat generated through losses in HTS tapes and dielectric.

Inner and outer cryostat walls: in order to maintain the vacuum and to prevent the heat-in-leaks from the environment.

Cable shield: the outermost component wrapped over the outer wall of the cryostat used as a super insulation to prevent the thermal leakages.

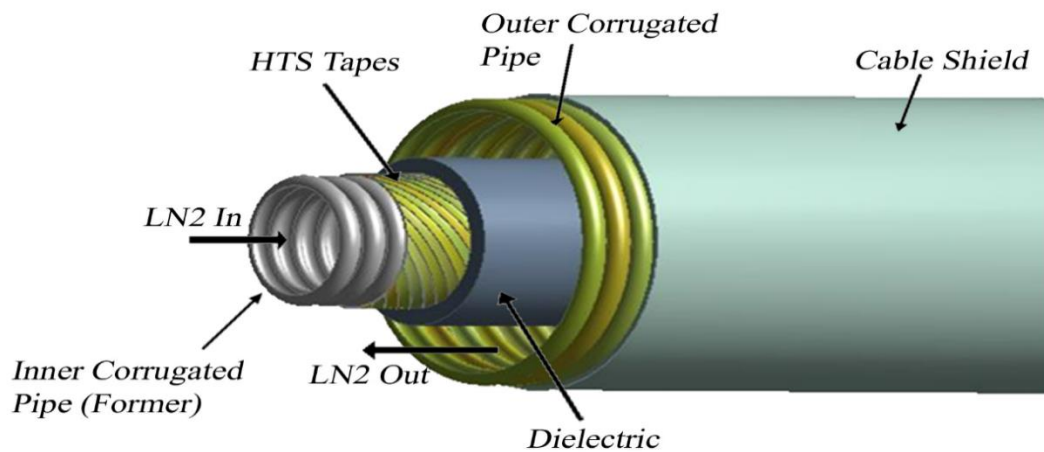


Figure 1.6 Single phase cold dielectric HTS cable

Further, the cooling system of HTS cables comprise several components such as cooling station, HTS cable termination and stainless steel cryostat along with LN2 feed pipes. The LN2 flows through the inner region of cable and returns from the same cable annular region which makes a cable loop to provide efficient cooling. In order to maintain the flow rate and pressure of LN2, a circulation pump is used in the circulating loop. The circulation loop cooling system can be divided into two parts such as open loop and closed loop. The open loop cooling system has an advantage of working with long length HTS cable. However, mostly closed loop circulating cooling systems are implemented with short length HTS cable used in ships, submarine and aircrafts.

The development of HTS power cables in large scale power applications was triggered after the discovery of high temperature superconductors in 1987. Physical prototype HTS cable with a length of 7m and current of 1000A was firstly carried out by Sumitomo Electric Industries in 1993 in Japan. Later, in 2004 the HTS cable length of

33m with cable rating of 35kV/2kA was developed and implemented in power grid by Innopower Superconductor Cable Co. Ltd as shown in n Table 1-4.

Table 1-4. Many other manufacturers have shown their interest in manufacturing the HTS cables of different lengths and rating for the large scale power applications. Finally, the longest HTS cable so far in the world was successfully implemented into the power grid in the Germany with a length of 1km. The HTS cable projects initiated by various manufacturers around the world are summarized in Table 1-4.

Table 1-4 HTS cable project around the world.

Manufacturing Company	Cable Rating	Cable Length (m)	HTS Tape	Year	Location/country
Innopower	35kV/2kA	33	Bi2223	2004	Yunnan/China
Furukawa	77kV/1kA	500	Bi2223	2004	Yokosuka/Japan
Sumitomo	34.5kV/800A	350	Bi2223	2006	Albany/U.S
Sumitomo	29kV/1.25kA	100	Bi2223	2006	Gochang/Korea
LS cable	29kV/1.26kA	100	Bi2223	2007	Gochang/Korea
Nexans	38kV/1.8kA	30	YBCO	2007	Hannover/Germany
Nexans	10kV/1kA	30	YBCO	2008	Madrid/Spain
Nexans	138kV/1.8kA	600	Bi2223	2008	Long Island/U.S
Sumitomo	10kV/3kA/DC	15	Bi2223	2010	Chubu U./Japan
LS cable	154kV/1GVA	100	YBCO	2011	Gochang/Korea
LS cable	22.9kV/50MVA	400	YBCO	2011	Seoul/Korea
Sumitomo	66kV/5kA	15	YBCO	2012	TEPCO/Japan
Sumitomo	66kV/200MVA	15	Bi2223	2013	Yokohama/Japan
Nexans	10kV/40MVA	1000	Bi2223	2013	Essen/Germany

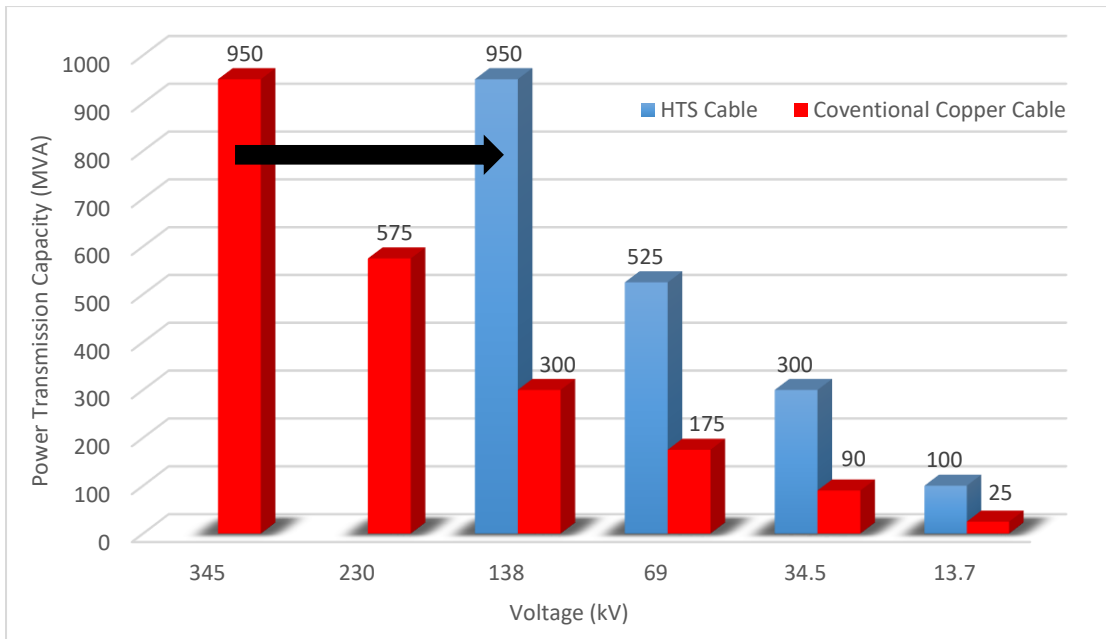


Figure 1.7 Comparison between conventional copper cables and HTS cables, [Data Source: Long Island Power Authority (LIPA)]

Figure 1.7 illustrates the comparison between conventional copper power cables and HTS power cables with power transmission capability (MVA) and voltages (kV). It can be observed that if 345 kV is needed to transport 950 MVA power for a conventional copper cable, equivalently, only 138 kV is needed to transmit same amount of power for HTS cable.

The HTS cable no longer needs higher voltages to transport higher powers due to the very low impedance and low resistive losses. Moreover, superconducting material costs much more than the conventional conductor commercially available in the market. However, the overall cost (construction, installation and maintenance) of the HTS cable system are cheaper than that of conventional cable system due to the achievability of more than five times power transmission capability with barely any losses even through the existing underground cable conduits space. Hence, the huge investment and losses can be saved by installing HTS cables instead of conventional copper cable into the power grids.

2 LITERATURE REVIEW

This chapter involves a comprehensive literature review on the various aspects of HTS cable. The aspects of HTS cable include estimation of A.C losses, dielectric losses, hydraulic, thermal and entropy generation which results in the designing of the HTS cable. The literature review on each aspect has been discussed below. Further, after doing an exhaustive review of literature on every aspect of HTS cable, few research gaps are also identified in this chapter. Finally, the objectives of the thesis are framed considering all the identified research gaps from the literature review.

2.1 Literature Review on AC Losses and Dielectric Losses

Wesche et al. [3] reported the design of superconducting power cables along with the losses occurred in the cable. Moreover, the 500 MW/110 kV rating superconducting power cable with warm dielectrics design found to be reasonable. The superconducting power cable comprises the main sources of losses are A.C loss, thermal loss and dielectric loss. Considering the cable conductor cost and causing losses, an operating temperature below 60 Kelvin was found to be optimal for Bi-2223 tapes. The low-cost Bi-2212 with an operating temperature ranges from 45 Kelvin to 50 Kelvin could be a substitute to the Bi-2223. Evidently, it was also observed that for the low conductor cost, the superconducting cables could be an economically alternative with conventional power cable techniques. Three phase 500 MW superconducting cable was reported to be feasible in loss reduction as compared to the conventional copper cables.

Demko et al. [4] discussed the AC Loss and thermal considerations for HTS Power cable systems. AC losses and thermal losses were estimated for parallel flow and counter flow cooling arrangements in HTS cable. The HTS cable temperature increases at lower flow rates which reduces the cable critical current and contribute higher AC losses. For a given length and flow rate in the counter flow HTS cable, the A.C losses were found to be lesser. Whereas, the temperature and pressure drop in the counter flow cable were reported higher than the parallel flow arrangement. In counter flow arrangement of HTS cable, the maximum cable system temperature was found to be significant higher than

that of LN2 return temperature. Whereas, In parallel flow arrangement, the maximum cable temperature was reported significant lesser to the return temperature of LN2.

Noji et al. [5] reported the AC loss analysis of high temperature superconducting cable with rating of 114 MVA. The AC loss analysis for single phase HTS cable was carried out using Electric circuit (EC) method. Norris equation was used to estimate the hysteresis losses due to self-field in the resistive part of HTS tape. A.C. losses in single phase HTS cable were investigated by considering the self-field, axial field and the circumferential field analysis of the HTS tape. On validating the axial magnetic fields (B_{am}) and circumferential magnetic fields (B_{cm}), the circumferential magnetic fields were found to be more dominating in the applied fields. Moreover, the circumferential magnetic fields in the electrical shielding was found to be significant low compared with B_{cm} in the conductor. In the electrical shielding, the layer losses comprise of self-field loss and circumferential field hysteresis losses.

Yagi et al. [6] reported the AC Losses in superconducting cable by calorimetric method. Moreover, the development of HTS conductors with low AC losses were also investigated and presented. A HTS cable with low A.C losses of 1 W/m at 3 kA_{rms} for 66/67 kV was developed by Furukawa with collaboration of Super-ACE project. Electric and Calorimetric method were developed and used to estimate the A.C. losses. It was reported from the paper that winding pitches and twisted filaments optimization in the HTS tapes produce an AC loss of 1W/m. Accuracy of AC losses in a 3 m HTS conductor was found to be 0.09 W/m with a distance of 2 meter and a mass flow rate of 0.5 kg/min. Keeping insulation in the inner and outer pipe of the cable system, eliminates the induced losses and reduces the eddy current losses. AC losses using uniform current distribution (UCD model) were found larger as compared to the electric and calorimetric method.

Noji et al. [7] reported the AC loss in a high temperature superconducting cable using calorimetric method. Electric Circuit method was used to calculate AC losses in HTS cable produced by Furukawa Electric Industries Ltd (FEI). AC losses on HTS cable was measured using Calorimetric method. Moreover, the measured AC losses were

compared with those of calculated AC losses and shown good agreement between the results. The losses due to the self-field (W_{self}) was reported dominating as compared to that of total losses (W_{total}) in the cable.

Noji [8] discussed the AC losses of 500 meters long HTS power cable in Super-ACE project. The AC loss using electric circuit (EC) model for a 500 meters HTS power cable in Super-Ace project were estimated. The total loss of 1.29 W/m in the superconducting cable model was also reported. Moreover, the total loss consists of self-field loss (W_{self}) with 0.89 W/m, exterior heat load (W_{ext}) with 0.32 W/m, ohmic losses (W_{ohmic}) of 0.06 W/m and 0.02 W/m of eddy current losses (W_{eddy}). On comparing with CRIEPI, the calculated AC loss was found to be 0.5 W/m for the superconductor material and superconducting shield as the hysteresis losses, and 0.8 W/m for the copper former as the eddy current losses. Using the field test data of Ag/Bi-2223, 500 meters HTS cable as reference, FEI were designed a five kilometers long length HTS cable. The AC losses in single phase conductor and three-in-one conductor were estimated 0.4 W/m and 1.0 W/m respectively.

Famakinwa et al. [9] analysed eddy current losses in HTS tapes - Self field analysis using 3D finite element method. 3D finite element method (FEM) tool of Ansoft Maxwell 3D was used to investigate eddy current losses in twisted filament Bi-2223 HTS tapes. Twisted filament in rectangular and circular tape models were used to calculate eddy current losses. The lesser eddy current losses can be found in the circular tape model of same twist pitch and same volume than rectangular model. Also, the eddy current losses were found to be inversely proportional to square of the twist pitch of filament. The eddy current losses were reported significantly constant for the calculated frequency.

Famakinwa et al. [10] analyzed eddy current losses of HTS tapes- external field analysis using 3D finite element method (FEM). Using 3D finite element method (FEM) software, the eddy current losses in two twisted filaments Bi-2223 HTS tapes placed in external A.C. magnetic field were evaluated. Applying magnetic field perpendicular to the wide side of rectangular tape model, the highest eddy current loss in the matrix of two twisted filaments were found. In the transverse direction of magnetic field, longer filament twist pitch models were found to be the cause of higher eddy current losses.

Whereas, shorter filament twist pitch experienced higher eddy current losses in longitudinal magnetic field. The eddy current losses will increase on rising the applied external magnetic field, matrix conductivity and frequency. The eddy current losses can be reduced only when the uniform external magnetic field found to be perpendicular to both circular and rectangular HTS tape models.

AC loss characteristics of YBCO tapes in external AC magnetic fields were investigated by Ogawa et al. [11]. A.C losses in the YBCO HTS tape placed in an external A.C. magnetic field were calculated. Calorimetric method was used to evaluate dependency of A.C losses on the angle between direction of external field and face of the HTS tape. The experiment was conducted at temperature of 77 Kelvin. It was found from the study that normal component of applied magnetic field to the HTS tape surface contributes the higher A.C losses. However, the A.C. losses can be reduced by applying the external magnetic field parallel to the HTS tape face. The simple arrangement was shown in the article to measure the A.C losses by electric method and calorimetric method.

AC losses in one meter long HTS cable was investigated by Wen et al. [12]. An experimental method known as electric method was adopted to estimate the A.C losses in 1 meter long HTS cable. It was reported that the A.C losses in the cable are found to be 0.22 watts at operating alternating current of 600 A_{rms} and frequency of 50 Hz. The HTS cable losses depend upon current and that can be expressed by power law perfectly. Moreover, the A.C. losses in the cable were found to be linear function of the frequency used to transport the current as shown below. The linear A.C losses show that the A.C losses in the HTS cable were mainly due to hysteresis losses.

AC Losses of Prototype HTS Transmission Cables were estimated by Lue et al. [13]. The A.C loss measurements of five HTS cable prototypes jointly designed by Southwire Company and Oak Ridge National Laboratory (ORNL) were reported. Calorimetric and Electric methods were used to investigate the A.C losses in the HTS cable. The computed A.C. losses using both the methods were validated with each other and Dresner theoretical approach. A.C losses below and above the critical currents can be calculated using Dresner's theory as reported in the paper. The HTS cables with more number of HTS tape layers won't reduce the A.C loss at low currents. Thus, a cable

with lesser layer was desirable. Tight winding of the HTS tapes used to manufacture the HTS cable contribute lesser A.C losses.

The various losses in the HTS cables were investigated by Oestergaard et al. [14]. Different losses induced in HTS cables were conductor A.C losses, thermal leaks, dielectric losses, hydraulic losses, pumping losses, losses in joints and termination. Most important loss elements in a superconducting cable system were reported as thermal insulation and cooling machine efficiency. Using room temperature dielectric (RTD) design HTS cables, the total energy losses at production units can be reduced by 40%. At the low load factor of the HTS cable, the minimal energy savings were possible. The losses in the RTD design HTS cable at 450 MVA, 132 kV were found to be 25% of the losses in the conventional cables of same rating.

Ryu et al. [15] reported the AC losses of five meters long BSCCO HTS cables with shield. AC losses for 22.9kV/50MVA multi-layered conductor and shield HTS cable were measured. It was reported from the results that, measured AC loss from the current lead to the shield (shield-lead) found to be constant with varying I_c . However, the measured loss from the lead to the conductor (conductor-lead) was significantly dependent on transport period. The heat transfer from the ambient to the coolant and vice versa was difficult due to the thick insulation around the conductor. As I_c high, the conductor's temperature rises in the cable with increase in transport period which leads to the significant increase in the measured AC loss from the conductor-lead. The measured AC loss in current-lead was dominating about 1.5 times than that of shield-lead for transport period of few cycles.

Vysotsky [16] discussed the AC loss of five meter long 2G HTS power cable using wires with NiW substrates. An American Superconductor second generation (2G) high temperature superconducting (HTS) tapes produced with the MOD/RABiTS process were used to construct a 5 meter HTS cable model. The HTS cable model comprised of two spirally counter-wound layers of brass-laminated tapes and NiW as a substrate material of these tapes. AC losses in this cable model were measured and analyzed by use of digital measurements of current and voltage. At the operating current of $0.5I_c$, the AC loss measurements were found to be in the range of few tenths of W/m. A few

tests such as critical current measurement, current distribution measurement over layers and joint resistance were performed on the cable model.

The simulations of HTS cable for current applications have carried out by Grilli et al. [17] using finite element method (FEM). The cable model comprises of four conductor layers and each layer composed of twenty number of tapes. The total critical current carried by the cable is about 4 kA. The AC losses as a function of transport current and the magnetic field distribution have carried out numerically and later compared with electric model of HTS cable. In order to evaluate the influence of contact resistance with various values on the repartition of the I_{rms} , the values were implanted in the electric model of the cable.

HTS Tape Characteristics Measurements with other Parallel HTS Tapes were carried out by Joo et al. [18]. In order to improvise the AC loss properties of BSCCO and YBCO tapes, the I_c and I_{rms} losses of these tapes with paralleled magnetic material (Ni tape) and/or diamagnetic material (BSCCO tape) were investigated experimentally. With paralleled Ni tape, the critical currents of HTS tapes decreased slightly and an increment was marked in transport current losses. However, with paralleled BSCCO tape, the I_c and I_{rms} losses of HTS tapes were not improved more than single HTS tape. Both of current losses such as transport and critical current were effected by intervention of the neighboring magnetic material to an HTS tape. In order to estimate the transport current loss Norris equation was used. If the substrate material magnetism was removed further, the AC loss of YBCO tape found to be decreasing.

In this study the AC loss characteristics of assembled conductor of multiple HTS tapes in polygonal arrangement were studied by Fukui et al. [19] numerically with high aspect ratio. To examine the AC loss in HTS tape in polygonal arrangement a numerical model was developed in this work. The dependencies of polygonal conductor on the geometrical configuration of the AC loss characteristics such as number of tapes and gaps were verified. It was found from the numerical results that, when YBCO tapes with high aspect ratio is used, the tape width will be lower than 3.5 mm. the gap between the tapes in polygonal arrangement should also be carefully adjusted.

In this present study AC losses, nature and effect of self-field in Bi-2223/Ag tape and pancake coils in terms of critical current were discussed by Alamgir et al. [20]. It was reported in the work that average perpendicular component of self-field directed oppositely at the two halves of tape-width. Towards the end of tape, self-field orientation increases considerably. However, throughout the tape width for tape and single-turn coil the resultant field amplitude remains almost unchanged. Whereas, both amplitude and orientation of self-field increases toward the end of the tape for multi-turn coil. In order to develop HTS magnet or to design HTS magnet this investigation of DC and AC behavior in HTS tape and coil would be useful.

AC losses were measured using electrical transport method by means of a lock in amplifier by Daney et al. [21]. It was found that the net azimuthal component of current in the conductor is nearly zero because of the layers were helically wound, the alternative layers wrapped with the alternative pitch. Multiple HTS tapes were arranged in a single layer to form HTS cable. Based on the current flow, the hysteresis losses produced were reported to be decreased. If the current flow is in the opposite direction, hysteresis losses are canceling out and almost becoming zero in the single layer arrangement.

Xiao et al. [22] discussed about BSCCO multifilament tapes, LN₂ high voltage insulation, a flexible cryostat, terminations and LN₂ cooling system used in the Coaxial conductors of 2223 HTS cables. Moreover, superconducting cable needs tape with high critical current, uniformity in critical current, flexible mechanical properties and long length determined by the cable core length. The losses in the cables were reported as dielectric loss in the insulation, thermal loss of the cryostat and ac loss of the conductor and shield.

Politano et al. [23] discussed the phenomenon of transition from the conventional lines to superconductivity lines. It was reported that 110 kV/1 GVA transalpine line can replace a 380 kV overhead lines and 30 km/600 MVA lines. Cold dielectric insulation was used only for the DC operated cable. The main aspect for direct current was flux jumping and high frequency ripples.

The dielectric measurements were tested with different structures and aging by Sumereder et al. [24]. It was reported from the paper that LN₂ exhibit excellent dielectric properties when used as a coolant. In order to achieve a long time stability of the dielectric characteristics for electrical insulation system should be sealed hermetically.

The losses involved in the HTS cable are thermal losses due to heat-in-leaks and AC losses due to internal heat generation were reported by Koh et al. [25]. The rise in temperature at the outlet of the cable shows good vacuum conditions. Cooling capacity was sufficient for HTS Cable with the defined ratings.

Electrical and mechanical properties of PPLP in LN₂ at 77K were discussed by Kimura et al. [26]. For electrical breakdown characteristics and mechanical characteristics, PPLP was reported as an excellent material. The mechanical properties of PPLP such as elastic modulus yield and fracture strength increased at 77K as compared with those at 300K.

The mechanical strength, critical current and AC losses were investigated by Mukoyama et al. [27] during manufacturing of the Hastelloy based YBCO and BSCCO tapes. It was found from the results that YBCO tapes have higher strength than BSCCO conductors. Capability to withstand for the over-current was found to be high for YBCO as compared to that of BSSCO.

The tape arrangement and the direction of current behavior on the AC losses were discussed by Li et al. [28]. Various arrangements were made for three models of the HTS tape. Moreover, the AC losses were measured for three different coils placed with a gap of 14mm. The self-field losses were observed higher in this arrangement of HTS tapes. The measured AC loss for the conductor was found in good agreement with the numerical method and Monoblock method at critical current of ($I_c=1830$ A). Whereas, the measured AC loss for shield used in the cable was significantly large than the results obtained from the numerical method.

Three various types of insulation conductors were discussed by Mukoyama et al. [29]. It was reported that various insulation conductors had good electrical properties to withstand voltage and $\tan\delta$. AC loss and electrical insulation of the cable were investigated in this study. AC loss of 0.49 W/m at 3 kV rms was achieved using HTS tapes of width 2.25 mm, when the critical current of the HTS conductor was observed over to 7 kA.

Zubko et al. [30] investigated that, tape over the tape and tape between the gap arrangements can be made in 2G HTS conductors between inner and outer layers to study AC losses. It was reported that the HTS cables were manufactured using 2G HTS wires. The AC losses in the cable due to the heat generated by HTS tapes and substrate losses were reported due to weak magnetic fields contributed at very small currents. While hysteresis losses were found to be dominating at the higher currents.

Fetisov et al [31] found that in 1G HTS cable, the superconducting losses were dominating compared to the coated conductors with magnetic substrate losses at lower transport currents. AC losses due to parallel and perpendicular magnetic fields in the cables by different mechanisms were taken into account. Because of the higher critical current density of the HTS layer in 2G HTS cables reduce the surface conductor hysteresis losses and these losses were increased by small gaps between the cables.

A.C. losses and dielectric losses in the HTS cable using calorimetric method for smart grid applications were reviewed by Kalsia et al. [32]. A.C. losses were found to be 0.1 W/m to 10W/m with operating current (I_{rms}) of 1100 A at various frequencies. It was also reported that A.C. losses can also be reduced using methods such as narrow filament diameter by twisting the filaments and introducing barrier between filaments for minimizing the coupling.

Maruyama et al. [33] investigated that thermal characteristics of the cables under over-current. Moreover, the optimum cable design and AC losses were also examined in the study. HTS cable development was for transmitting higher currents at lower voltages and to reduced AC losses with protection under over current and electrical insulation.

2D finite element model based on the H formulation was studied by Ainslie et al. [34]. The AC losses were increased due to the flow of transport current at the central region of the HTS tape. Further, higher flux density in the localized area and material magnetic strength were found to be increased which results in higher penetration of fluxes. It was concluded from the study that in order to reduce the AC losses in the whole HTS cable system, the HTS tapes should be manufactured using non-magnetic substrate.

The simulations which are time variant under fixed boundaries was studied with coupling of magnetic and electrical fields by Zhou et al [35]. It was observed that in the thermal analysis, HTS cable had a high temperature when compared with the YBCO shield because of the convection heat transfer between conductor and the tape.

3D finite element method of dynamic modeling was analyzed by He et al. [36]. The protection system for the action time by the variation in the relay for the safety was observed from the study. The marginal changes during the fault on the adiabatic model was also investigated at the adiabatic condition to check the safeness of the HTS cable.

Self-field analysis for BSCCO and YBCO tapes were obtained by Vyas et al. [37] using approximating Norris equation. It was reported from the results that A.C losses increase with increase in the transport current, and decreases with critical current and voltage. It was also reported that when the frequency rises, the self-field losses in the HTS cable found to be increasing.

2.2 Literature Review on Hydraulic Studies

In order to design an efficient HTS power cable, Fuchino et al. [38] investigated the hydraulic behavior of sub cooled LN₂ flowing in the cable. An experimental comparison between smooth and corrugated pipe of 10 meters length was done for different mass flow rates to estimate the friction factor and pressure drop. Liquid helium was used as a coolant in the inner three phase coaxial cables while liquid nitrogen was used as a coolant in the corrugated geometry. The thermal conductivity of dielectric material was found ten times larger at nitrogen temperature as compared to that of liquid helium. Friction factor was found to be an important parameter in designing of the HTS cable. The measured friction factor for heat exchanger type counter cooling structure and other empirical formula were compared and presented in this work.

A computational investigation on hydraulic analysis of HTS cable former with LN2 as a coolant was performed by Lee et al. [39]. The stainless steel former material was used to ensure the flexibility to the cable structure. The effect of variable parameters such as pitch (p), depth (e) and diameter (D) of former on hydraulic behavior of LN2 in cable former were investigated and presented. The parameters ratios such as (p/e) and (e/D) were assumed to be in range of 1-15 and 0.039-0.118 respectively. Pressure drop was proportional to the depth of the former, as reported in the previous researches. The (p/e) ratio less than 5 for the corrugation geometry was found the flexible corrugated pipe for the cable former. The maximum pressure drop was found at the range of (p/e)=5 to 10.

Koh et al. [40] performed a test of HTS cable cooling system based on LN2 forced flow. The operating range for the test was expected in between 65 kelvin to 80 kelvin with a subcooler heat exchanger to cool down the HTS cable temperature. Heat transfer and pressure drop between inner flow regime and outer flow regime in the corrugated pipes were calculated for the test. Due to the addition of valve for LN2 circulation in the HTS cable, the pressure drop was found greater for the whole cable system. It was also reported that subcooler heat exchanger, ventilation and vacuum pump system need to be remodified. Also, the pressure drop was measured for three different coolant such as water, LN2 and air in the cable former. The pressure drop using LN2 in the cable former was found to be greater than that of air flowing in former and smaller than that of water flow.

Hydraulic analysis on two different types superconducting power transmission lines (SC PT) with LN2 flowing in straight channels were performed and presented by Sasaki et al. [41]. The two different cables such as single phase DC-SC PT and three phase AC-SC PT were modeled and analyzed. Velocity distribution, pressure drop and pumping power of the LN2 were also investigated in both types of superconducting power lines. The heat generated in DC cable was reported to be zero due to the zero electric resistance and heat flux from ambient was considered 1.0 W/m. Whereas, AC loss and exterior heat flux of 3 W/m were considered for the AC superconducting cable. The flow velocities for DC and AC type cables were considered to be 0.10 and 0.25 m/s respectively. The pressure drop and pumping power of the DC-SC PT system cable

were reported lower as compared to the AC-SC PT cable. The pressure drop in single phase DC-SC PT cable for the velocities of 0.1 m/s, 0.3 m/s and 0.5 m/s were estimated 22 Pa, 170 Pa and 430 Pa respectively. However, the pressure drop in three phase AC-SC PT cable for the velocities of 0.1 m/s, 0.3 m/s and 0.5 m/s were estimated 46 Pa, 340 Pa and 840 Pa respectively.

LN₂ flow through corrugated and bellow pipes in DC superconducting power transmission (SC PT) cable of 1 meter long was computationally investigated by [42]. The new way of flow of LN₂ such as combination of corrugated/bellow pipes with straight pipes was proposed in this work. Moreover, the hydraulic characteristics such as pressure drop and velocity profiles of LN₂ in corrugated and bellow pipes were also discussed. Reynolds Average Navier-Stokes (RANS) equations were used to obtain the desired results. The pressure drop per unit length (Pa/m) of LN₂ in bellows were found lesser than that of corrugated pipes. The pressure drop per unit length of LN₂ in corrugated and bellows sections was respectively 3.7 and 2.6 times than that in straight (non-corrugated) section. Due to the less pressure drop, the bellows were preferred and proposed instead of corrugated pipes for the DC superconducting power transmission line.

The effect of natural circulation of the coolant by thermosiphon effect in the HTS cable cooling system with subcooled LN₂ was observed by Ivanov et al [43]. An experimentation on 200 meters DC HTS cable at Chubu University was carried out using thermosiphon effect. Moreover, Pumping power for forced LN₂ circulation and heat loads were reported smaller using thermosiphon effect in the HTS cables. It was evident that heat load due to intrusions were reduced and the power required for pumping also reduced. This method is advantageous in decreasing the pressure drop. The effect of the bypass between terminations joints of the cable were also investigated through this paper. The pressure drop for theoretical designed model and experimentally measured thermosiphon model were validated and found in satisfactory agreement.

Pumping power of LN₂ new circulation system in 200 meters HTS DC cable was experimentally investigated at Chubu University by Ivanov et al. [44]. Bi-2223 HTS tapes were used for the HTS DC cable manufactured by the Sumitomo Electric

Industries, Ltd. The designed cooling system for HTS DC cable was predicted to be a unique system than other systems [43]. Peltier element was used in the current leads to reduce the heat transfer process. Moreover, the smooth cryopipes were undertaken despite of corrugated pipes to reduce the friction and pressure drop in the designed cable. The whole experimental setup was divided into two main parts such as horizontal and vertical arrangements. Smooth cryopipe with HTS cable and termination joints were included in the horizontal arrangement. However, heat exchanger subcooler, LN2 tanks, circulation pump, and flow meter were associated with vertical arrangement of the setup. 5m level difference of LN2 circulation loop contributed less pumping power and driving force due to densities difference in cold and hot LN2.

The circulation of liquid nitrogen through cryopipe in the HTS cable was investigated using computational fluid dynamics (CFD) method by Sasaki et al. [45]. The combination of straight and corrugated pipes were proposed as cryopipes in the present work. Moreover, the effect of decentering of the HTS cable with different physical dimensions in the cryopipes were investigated. The effect of centering of the cable in cryopipes could be investigated using empirical formulas however, the decentering of cable could be investigated. Limited length of computational domain was considered due to the computer capability. Friction factor correlation was also developed in the corrugated cryopipe with the HTS cable. Lesser pressure drop was found in case of decentering of the HTS cable in the cryopipe as compared to that of centering of the cable. The required volumetric flow rate and pumping power to circulate LN2 in 10 kilometers of length was found to be 19 L/min and 10watts respectively. The pressure drop in the whole system was found as 23 kPa with cable/cryopipe diameter of 40/80 mm.

A theoretical method of inline cooling system for long length HTS cable with feasibility test was proposed by Zajackowski et al. [46]. The inline cooling method was proposed for the infinite length HTS ccable. The pressure distribution profiles and cooling power required to run a cryocooler were investigated. The proposed inline cooling method with counter flow consists of cryounits (cryocooler and pumps) at certain location on HTS cable line. According to the inline cooling method, the LN2 can either pass through the cryounit to other section of cable or return through the cryounit to the same

section of cable. It was found that 1 kW cryocooler needed every 400 meters with existing cable parameters and proposed inline cooling method. This cable length could be increased every 1000 meters with same cooler capacity of 1 kW using heat load reduction.

The effect of corrugation pitch on the heat transfer analysis of a warm dielectric HTS cable at the Reynolds numbers range from 14000 to 22000 was investigated by Dondapati et al. [47]. The major sources for losses in the cable were reported as the A.C. loss due to the superconductors and heat-in-leak from the ambient temperature to raise the temperature in the cable. The pressure drop and pumping power required to flow the cryogen in the HTS cable were evaluated. Both BSCCO and YBCO HTS tapes were used for the analysis and the thermophysical properties of cryogen (LN₂) were undertaken as temperature dependent. Consequently, the pressure drop found to be increasing with increase in the corrugation pitch at constant corrugation depth. Moreover, the variation in the pressure drop was because of the turbulent flow in LN₂ which caused fluctuations in the fluid flow. These fluctuations in the corrugated pipe further contributed higher shear stress at the walls. It was also observed that the cooling capacity of the coolant decreases with the increase in corrugation pitch.

Pressure drop modelling in the HTS three phase concentric power cable was investigated by Shabagin et al. [48]. The differential equation model was used to describe thermohydraulic performance of concentric three phase HTS cable. The longest installed HTS cable named Ampacity project cable in the world was considered as the reference. Firstly, A.C losses in the HTS cable were calculated analytically later the axial and radial temperature profiles were analyzed using the same analytical model. Thereafter, the hydraulic modelling was also carried out. Cooling capacity at various mass flow rates were investigated for the existing cable design. The pressure drop for the both inner flow region and annular flow region was calculated using Darcy Wiesbach equation. The assumption made for the cable corrugation (Corrugation pitch/diameter) was less than 0.2 which makes the corrugated pipes in the cable similar to the smooth pipes.

Pressure drop and friction factor comparison of LN₂ in the corrugated pipe with smooth pipe for the application of 5 meter HTS power cable were investigated by Li et al. [49].

This hydraulic analysis were carried out using experimentation performed on cable and the computer simulation. The LN2 annular flow through centrally placed smooth pipe enveloped in corrugated pipe was conducted experimentally and then validated with the simulated results performed using CFD. Moreover, the effect of corrugation pitch and corrugation depth were also evaluated and compared with that of smooth pipe. The pressure drop was following an increasing trend with the flow rate of LN2 in the corrugated and smooth pipes. Moreover, the pressure drop was found to be decreased for the increasing corrugation pitches at constant corrugation depth. The pressure drop was increasing with the increase in the corrugation depth at constant corrugation pitch.

Fluid characteristics such as pressure drop, friction factor and velocity distribution of LN2 flowing in HTS cable were investigated using CFD method by Maruyama et al. [50]. A 275 kV/3 kA high-voltage (HV) M-PACC project manufactured HTS cable was considered for the analysis. The HTS cable was placed eccentrically to the center of cryostat pipe and LN2 flow occurred through annulus of that spiral corrugated cryostat pipe. As a result, the calculated pressure drop in the annular corrugated pipe was found almost 17 times larger as compared to that of straight pipe. The calculated pressured drop for the eccentric position of the cable core was found to be 143 Pa/m which shows the four-fifth of the pressure drop of centrally positioned cable. The large pressure drop was due to the shrinkage and expansion of the LN2 flowing through the annular corrugated pipe. The calculated pressure drop was later compared with measured results of the cable developed in NEDO project.

The effect of spirally inserted cables on the hydraulic behavior of LN2 in helical corrugated pipes at Reynolds number ranges from 1000 to 10000 were computationally investigated by Zuo et al. [51]. Three spirally inserted cables of diameter 5 mm each and four straight cables of diameter 8 mm each were placed in 40 mm diameter corrugated pipe. The 3 D models were created for the analysis and single phase simulations were performed using CFX solver with an inlet temperature of 70K. The pressure drop in the corrugated pipes was found larger that in smooth pipes. It was also reported that with the insertion of straight cables in the helical corrugated pipe, the friction factor will increase. Moreover, with the insertion of spiral cables, the friction

factor was further increased by 15.2%. In addition, the size and twist pitches of the cable also affects the friction factor and pressure drop in the corrugated pipe.

The hydraulic analysis of long length three phase coaxial HTS cable for several kilometers was carried out using computer simulations by Lee et al. [52]. By considering the pressure drop and heat loss analysis, the required specifications of refrigeration system could be determined. A HTS cable with the power capability of 23 kV/60 MVA was considered for the analysis and to be used as interconnection cable in power grids. The analysis carried the annulus flow of turbulent LN2 between outer corrugated pipe and cable core placed centrally. The boundary conditions for the CFD analysis such as inlet mass flow rate and temperature were considered as 0.51 kg/s and 70 K respectively. The computed pressure drop in the center cable core and offset cable core was found as 199 Pa/m and 192 Pa/m respectively. The thermohydraulic analysis would be applied to installation of the three phase HTS power cable of length 3 kilometers.

Hydraulic analysis of sub-cooled LN2 flowing through concentric annulus corrugated cryostat of HTS cable was carried out using CFD by Das et al. [53]. The friction factor and velocity distribution profiles for turbulent flow of LN2 within the cable cryostat were also presented. Moreover the effect of corrugation pitches and depths on the friction factors between LN2 and the corrugated wall surface, pressure drop and respective pumping powers were also investigated. With the various combinations of corrugation pitches and depths, the nine different corrugated cryostat geometries were considered for the analysis. The length of the modeled fluid domain for the analysis was considered as 800 mm including entrance length, fully developed turbulent flow length and outlet length. The uniform heat load from the ambient to the outer wall of the corrugated cryostat was considered in range of 0.4 W/m to 1.4 W/m. finally, it was reported from the results that smaller pitch and depth ratios (<0.5) were preferred for lesser friction factor in the annulus flow.

2.3 Literature Review on Thermal Studies

While operating with alternating current (A.C), HTS cables experience various thermal losses such as AC loss in the superconductor, dielectric loss in dielectric material, and heat influx through the cryogenic enclosure wall from ambient temperature. These

thermal losses contribute overall temperature rise in the HTS cable. If the maximum temperature in the HTS cable exceeds to the critical temperature of the superconductor, the cable behaves same as the conventional cable. Thus, in order to operate long length HTS cables, the efficient cooling arrangement is required which can maintain the critical temperature of superconductor. In this regard, many researchers have discussed their own HTS cooling systems with single flow cooling system and counter flow cooling system. The feasibility of these cooling systems has been experimentally, numerically and computationally proved. The enormous amount of literature review has been done on the thermal issues in the HTS cables.

Fuchino et al. [54] proposed the counter flow cooling method for superconducting power cables. The mathematical model with heat balance equations was used to analyze the temperature behavior of LN₂ in HTS cable with counter flow arrangement. The pressure drop and the conduction through other solid parts such as former and the HTS tapes were neglected. Also, the influence of thermal conductance of dielectric placed between coolant streams were considered and investigated. The temperature distribution profiles of LN₂ at various mass flow rates and thermal conductivity were obtained. It was reported from the results that the maximum temperature in the HTS cable exceeds superconductor critical temperature at large thermal conductance of dielectric material polypropylene laminated paper (PPLP).

The characteristics of counter flow cooling arrangement with LN₂ in the superconducting power cables were discussed by Furuse et al. [55]. A 100 meters long duplex-counter-flow tube with LN₂ was experimentally tested to obtain the temperature distribution in that counter flow arrangement of HTS cable. The experimentally measured temperature distribution profiles were validated with the mathematical model proposed by [54]. Both the measured and calculated temperature profiles in the HTS cable were agreed for the inner flow region but not for the annular flow. Therefore, in order to calculate the accurate temperature profile in the annular tube, adiabatic coolant expansion and pressure distribution in the annular tube must be considered. Moreover, the relation between oscillation period due to cooling test and tube length were also discussed.

The heat transfer analysis in the HTS cable former of realistic dimensions with full of LN2 was performed numerically by Lee et al. [39]. Stainless steel corrugated pipes were used as the former of HTS cable in order to provide the flexibility to the whole cable structure. The effect of variable parameters such as pitch (p), depth (e) and diameter (D) of former on heat transfer behavior was investigated and presented. Where ratios (p/e) and (e/D) were assumed to be in range of 1-15 and 0.039-0.118 respectively. Heat transfer was proportional to the depth of the former, reported in the earlier research. However, the effect of pitch was found to be different and heat transfer in terms of Nusselt number found to be maximum at the range of (p/e)=5 to 10. After analyzing the effect of various pitches, depths and diameters on heat transfer of LN2 in cable former, the temperature difference between HTS tape and LN2 was found less than 0.1 degree Celsius ($^{\circ}\text{C}$) at nusselt number of greater than 150.

Furuse et al. [56] investigated the different structures of HTS cables with counter flow cooling arrangement. The effect of thermal conductivity of dielectric material was investigated and reported that a great thickness of PPLP is required to reduce the heat transfer between counter flow regions. Thereby, the temperature distribution profiles were investigated for the three different proposed design of HTS cables. The various conceptual designs of HTS cable were: (a) three-core cold dielectric (b) three-core warm dielectric (c) concentric HTS cable. Eventually, it was concluded that Concentric HTS cable with counter flow arrangement was found to be most effective due to its compact design.

Demko et al. [57] analyzed a 2000 meters long LN2 cooled concentric tri-axial HTS cable system. The radial and axial temperature distribution profiles with two various cooling arrangements were also investigated. The AC losses in all the three layers of HTS tapes were considered for the calculations. The temperature rise in the cable was found very low when LN2 was flowing in inner region flow through former as well as through annular corrugated pipe. Whereas, the temperature gradients were higher, when LN2 flow took place through annular corrugated pipe only. Moreover, sufficient cooling was observed even when LN2 flow through annular corrugated pipe only. These results introduced the feasibility of long-length HTS cables using the existing parameters.

Conduction cooling arrangement of a long HTS power cable was proposed by Posada et al. [58]. The proposed concept eliminates the usage of cryogenic fluid LN2 flow inside the HTS cable. The conduction cooling was achieved in the three different proposed designs by incorporating a copper layer in the thermal insulation of the cable. The detailed heat transfer analysis was carried out for various case studies using finite element method tool called FEMLAB. The refrigeration load needed for the BSCCO HTS tapes conduction cooling was found to be five times lower than that of liquid hydrogen as coolant flowing inside the HTS cable.

Triaxial three phase concentric counter cooled HTS cable design for the thermohydraulic response to over-current faults was presented by Demko et al. [59]. The second generation (2G) stainless steel-stabilized HTS tape was used for the analysis of 1000 meters long cable. Counter flow cooling design was proposed to be energy efficient cooling due to its compact size. Moreover, the main benefit of counter flow cooling was reported that it avoids the separate cooling pipe for return flow. The recovery time was also discussed for after a fault detected in the cable. Stable recovery can be achieved in reasonable time with the availability of efficient refrigeration system.

The counter flow cooling arrangement with gravity fed LN2 circulation in a HTS cable was presented by Ivanov et al. [60]. An attempt was made in order to circulate the LN2 using thermal siphon effect due to density difference and avoiding the circulation pump. An investigation was done on the feasibility of proposed cooling scheme using counter flow arrangement with a length of 500 meters. A significant temperature rise in the cable than critical temperature of superconductor was found in case of high inclination position of subcooling siphon. Whereas, the nitrogen gas condensed in the outer channel due to high heat flux from outer flow to inner flow occurred in case of slightly inclination of subcooled siphon. The condensation in the outer pipe causes the circulation loss. Therefore, counter flow thermosiphon was reported as the promising method to enhance the performance of short length HTS cables.

The concept of inline cooling in the long length HTS power cable using counter flow arrangement was introduced by Zajaczkowski et al. [46]. Analytically proposed the concept of inline cooling system to achieve the cables of infinite length, where an

infinite long HTS cable was divided into several sections consist of cryo-coolers. In case of inline cooling the cryogenic coolant in the inner corrugated pipe can either pass through cryo-cooler from one section to another called as pass mode. Whereas, returning of cryogen to annulus region of the same cable was reported as loop mode. The temperature distribution profiles of LN2 were obtained using no cryocooler and with cryocooler at right end of the HTS cable. Moreover the axial temperature distribution profiles were also obtained using inline cooling method. After every 1000 meters length of HTS cable, placing of cryocooler was proposed in the analysis.

Thermal modelling of direct current (DC) operated HTS cable with helium cooling was presented by Souza et al. [61]. A numerical method called volume element model (VEM) was used to solve the formulated mathematical model for HTS cable. The VE model deals with the modes of heat transfer such as conduction, convection and radiation in the vacuum channel and numerically obtained temperature distribution profiles in the HTS cable. The temperature and pressure dependent thermophysical properties (ρ , C_p , C_v) of helium coolant was considered for the analysis. The model was reported as the useful tool for activities such as designing, simulations and optimization of the DC operated HTS cables.

In order to analyze the thermal behavior of HTS cable, the three dimensional (3-D) FEM model was presented by He et al. [36]. The method was developed to obtain action time of relay protection in the cable. The various dynamic thermal characteristics of HTS cable under different operating conditions were also investigated. Improper cooling system and fault current were reported as the major causes for quenching/overheating in the cable. The transient radial temperature distribution in the HTS cable for 600 seconds was presented in the analysis. 3-D adiabatic and heat transfer models were compared and analyzed at time of 600 seconds. It was reported that 3-D adiabatic model was reported as the reasonable method to confirm the action time of relay protection system.

The heat transfer analysis between terminal joint and the LN2 in the high voltage (HV) cable was carried out using computer simulations by Maruyama et al. [62]. The flow condition in the termination vessel of M-PACC project HTS cable was considered to be natural convection, forced convection and static condition flow. Almost all the heat

intrusion occurred into the LN2 in natural convection case. Moreover, the volumetric flow of LN2 was found to be large which results high heat transfer coefficient. The rise of temperature of LN2 in the inner pipe caused increase in the temperature of superconductor which further devoted the increase in A.C losses in the cable. In order to increase the heat inflow from termination joint to LN2 in the vessel, the outer surface area of termination joint was expected.

Long length of one kilometer HTS cable cryogenic cooling system as a new concept was proposed and investigated by Chang et al. [63]. A range of thermodynamic arrangements were investigated on standard and modified Claude cycles. LN2 was considered as a part of closed loop in the studied Claude cycles. In order to evaluate the FOM (figure of merit) and feasibility of cooling system, four various thermodynamic cycles were analyzed and optimized following a process simulator (Aspen HYSYS). As a result, the modified dual pressure cycle cooled using expander stream was recommended among all the modified cycles for the efficient cooling of long length HTS cable.

3 D temperature distribution profiles using a differential equation model for concentric three phase HTS power cable of 10 kV were investigated by Shabagin et al. [48]. The radial and axial temperature distribution profiles were presented based on the derived differential equations system. The one kilometer long Ampacity project HTS power cable was used as reference and this cable was reported as the world's longest installed cable so far. A.C losses in the superconducting phase and thermal losses from the external ambient environment were considered for the temperature distribution profiles. Installing another cryocooler at the right end of the HTS cable, the maximum cable length was found to be doubled. Moreover, the HTS cable length could be increased using the eutectic mixture of N_2/O_2 as subcooled liquid coolant.

Thermal analysis of various cooling designs of three phase co-axial HTS cable were investigated using finite element method (FEM) by Lee et al. [64]. The maximum temperatures of the proposed case I and case II cryogenic cooling systems were found 73.6 kelvin at the middle of the HTS cable. However, the temperature at the outlet of the proposed cooling system case III was found to be 70.9 kelvin with the LN2 inlet temperature of 68 kelvin. Therefore, case III with return pipe mechanism in the HTS

cable along with LN2 as coolant was found to be most suitable method for more than one kilometer long HTS cables. The center pipe inlet temperature and the separate return pipe inlet temperature were found minimum due to the thermal insulation done on the each pipes.

2.4 Literature Review on Entropy Generation

Sahin et al. [65] presented a method used to determine the optimized duct shape for minimal losses with a range of low Reynolds number at constant heat flux. The method used to optimize the duct shape is a second-law comparison of irreversibility. The various duct shapes such as circular, square, equilaterally triangular, rectangular with an aspect ratio of 1/2, and sinusoidal with an aspect ratio of $\sqrt{3}/2$ are used at the heat flux of 250 to 1000 W/m². Heat flux significantly affects both pumping power and entropy generation of the various shaped ducts with a length of 1 meter. It was observed from the results that as the heat flux arose the entropy generation also rises. However, pumping power per unit heat-transfer rate reduces with increase in the heat flux. Finally, the circular duct was found to be best in terms of low entropy generation and less pumping power.

Sahin et al. [66] investigated the influence of inconstant viscosity in a laminar flow through a duct on entropy generation minimization and pumping power at constant wall heat flux. The viscosity of the fluid was considered as temperature dependent for the analytical investigation of entropy generation. Along the axial length of the duct, the ratio of pumping power to the heat flux reduces and the entropy generation increases for the viscous fluids. In order to minimize both the losses such as entropy generation and pumping power, an optimized duct length was obtained. It was observed that the entropy generation due to the viscous friction dominates at low heat fluxes. Hence, variable viscosity with temperature dependence was found as key issue to be considered in the estimation of entropy generation.

Ratts et al. [67] presented an entropy generation minimization (EGM) technique to optimize laminar and turbulent flow at constant heat flux. An optimal Reynolds number for laminar and turbulent flow was obtained by fixing the mass flow rates and total heat transfer rate. The optimal Reynolds number and minimal entropy generation were also obtained and compared for various cross sections such as square, equilateral

triangle, and rectangle with aspect ratios of two and eight. The rectangular shape ducts with aspect ratio of eight was found optimal duct with smallest Reynolds number, lesser entropy generation and the smallest length.

Ko et al. [68] analyzed entropy generation of a steady, laminar and fully developed fluid flowing through a helical coil with constant and uniform heat flux. Moreover, the effect of optimal design parameters such as Reynolds number, ratio of coil-tube radius and coil pitch on the entropy generation were also investigated. The Reynolds number ranges from 100 to 1000 and the coil pitch had a range of 0.01 to 0.3 for the analysis. Minimum entropy generation was found at the Reynolds number optimal range from 2271 to 4277 and coil pitch from 0.17 to 0.3. The irreversibility of the system was found to be less at these values of Re and coil pitches, which shows that the entire system would be optimized. The results would help in designing the heat exchangers and selecting the optimum design parameters.

Dondapati et al. [69] reported the entropy generation minimization method in the cable-in-conduit conductors using CFD method with supercritical helium as the coolant. The application of the work was considered as the optimum cooling of fusion grade magnets. Entropy generation in fluid flow system occurs due to fluid flow with friction, heat transfer due to finite temperature difference and mixing of fluids. In the case of cold dielectric type of HTS cables the probability of mixing of coolants flowing through different channels was found to be worth negligible. The first term in the entropy generation equation presented in the work represented the entropy generation due to thermal gradients and the other term showed entropy generation due to velocity gradients. These temperature and velocity gradients were obtained from computer simulations used to estimate the entropy generation. The investigation could be useful in minimizing entropy generation and to find the optimum mass flow rates at which higher heat transfer rate could be obtained with lower pumping power.

2.5 Research Gaps

Referring to the literature review, enormous amount of work has been done on the investigation of thermohydraulic behavior of HTS cable. The performance of warm dielectric HTS cable is inferior to cold dielectric HTS cable. Further, the AC losses in the cold dielectric cable are reported to be lower due to nullification of magnetic fields

due to the twist pitches chosen for different layers of HTS Tapes. Moreover, the triaxial HTS cables enveloped in three different cryostats contribute higher pressure drop and results in higher pumping power. Hence, Co-axial cold dielectric cable is preferable to be used in power grid as reported by the researchers. Moreover, several studies on cooling mechanism (thermal) and flow system (hydraulic) in corrugated pipe HTS cables have been carried out and published so far. The HTS cable system has different cooling arrangements such as single flow cooling and counter flow cooling systems. A massive research using analytical, experimental and computational approach has been performed on the warm and cold dielectric HTS cable using single flow cooling system. However, computational and experimental work for thermohydraulic investigation of the (single-sided cooling with internal coolant return flow) counter cooled cold dielectric HTS cable have not yet been reported.

Hence, the present work is focused at addressing the thermohydraulic issues of counter cooled cold dielectric HTS cable using computational method. Moreover, the combined effect of A.C losses (W/m) and heat fluxes (W/m^2) on the thermohydraulic performance of counter cooled HTS cable was also presented in this study. In addition, the effect of corrugation topologies (rectangular, circular and triangular) and coolant (LN₂) inlet temperatures on the thermohydraulic performance of counter cooled HTS cable was also illustrated. Finally, the entropy generation due to velocity gradients and thermal gradients was also investigated in the HTS cable.

2.6 Objectives

The specific objectives of the research work are:

- To investigate the hydraulic characteristics such as friction factor, pressure drop and pumping power in HTS cable.
- To investigate the thermal characteristics such as heat transfer rate, Nusselt number and cooling capacity in HTS cable.
- To investigate the entropy generation in the HTS cable.

3 MATHEMATICAL AND COMPUTATIONAL MODELING OF HTS CABLES

In the previous chapter, relevant review of literature on the hydraulic and thermal issues in the HTS cables is presented. In the present chapter, mathematical and computational models are developed and discussed in order to estimate the behavior of LN2 under the influence of corrugation geometry, heat-in-leak (W/m^2) and heat generation (W/m^3). Firstly, the analytical and computational model for the HTS cable with circular corrugations are presented. Also, the solution for the temperature distribution profiles of LN2 in counter cooled HTS cable are obtained assuming one dimensional (1-D) model. In addition, the boundary conditions and governing equations used to investigate the fluid flow are discussed and presented in this chapter.

3.1 Analytical Modeling

The conceptual design of single phase cold dielectric HTS cable to be used in the present analysis is shown in Figure 3.1 (a). This HTS cable consists of many important parts such as inner corrugated pipe (former), HTS tapes, dielectric and outer corrugated pipe along cryostat-pipe and cable shield. The HTS cable is cooled by liquid nitrogen at 65 K and 3 bar, which is pumped through the inner corrugated pipe of the cable, and returns from the outer corrugated pipe (annular region). The layer consisting of HTS tapes and dielectric material made of polypropylene laminated paper (PPLP) is known as conductor layer. HTS tapes are arranged on a corrugated pipe to transmit large capacity current and dielectric material on the same axis for electrical insulation. The conductor single phase is surrounded by two concentric corrugated pipes known as cryostat with vacuum (10^{-3} to 10^{-5} mbar) in order to reduce the exterior heat from ambient. The exterior heat in flux (Q_e) due to ambient temperature on the outer corrugated pipe of HTS cable is also shown in Figure 3.1 (a). In the design of HTS cable for the effective cooling, the coolant (LN2) must remain in the liquid state during its normal operation. If the temperature exceeds to its boiling point (77 K at 1 bar), the liquid nitrogen becomes a gas and thereby the cooling efficiency is reduced. Liquid nitrogen solidifies (<65 K at 1 bar) and challenging to transport through corrugated

pipes in the HTS cable. The boiling of liquid nitrogen can only be avoided by increasing operating pressure of the cable higher than ambient pressure (1 bar). Figure 3.1 (b-c) shows the overview of counter-flow arrangement of LN2 in HTS cable along the length (L). In this section we will use the analytical model to investigate the temperature profile of LN2 with an additional cryocooler at right end and without cryocooler. The steady-state energy balance equations [6], [46] are solved using boundary conditions of with cryocooler and without cryocooler at the right end of the HTS cable. The temperature difference between the inner region flow and annular region flow, due to the presence of cryocooler at the far end, is an extra factor in the boundary condition of model. The conceptual design parameters of single phase HTS cable considered for the present analysis are compiled in Table 3-1. Moreover, the operating range of LN2 and the boiling curve as a function of temperature and pressure are shown in Figure 3.2. In order to achieve maximum possible HTS cable length for cooling, the pressure drop and the maximum temperature rise must be kept within the defined operating range.

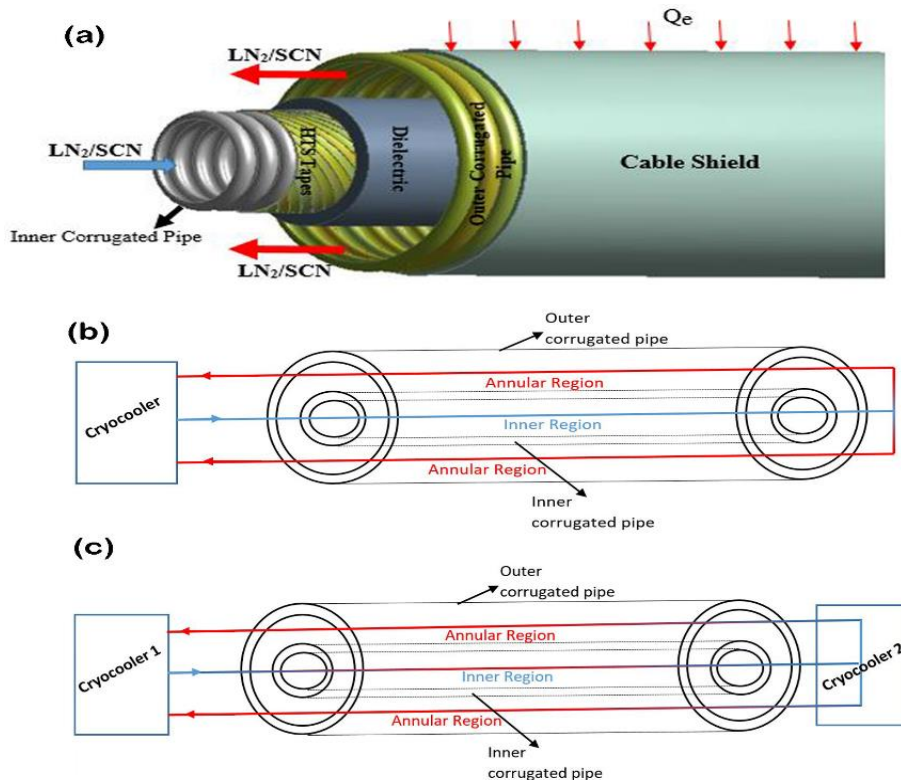


Figure 3.1 (a) Modelled single-phase cold dielectric HTS cable (b) schematic of HTS cable with no cryocooler at end (c) schematic of HTS cable with cryocooler at end

Table 3-1 Parameters for conceptual design of HTS cable

<i>Parameters</i>	<i>Values</i>
Inner radius of former, r_1 (mm)	18
Outer radius of cable core, r_2 (mm)	24
Heat from ambient/exterior, Q_e (W/m)	0.9-1.2
Heat from HTS tapes/A.C loss, Q_{AC} (W/m)	1.4
Inlet temperature, T_o (K)	65
Inlet Pressure, P_1 (bar)	2
Volumetric flow, m (L/min)	20-35
Length of cable, L (m)	1500-3000

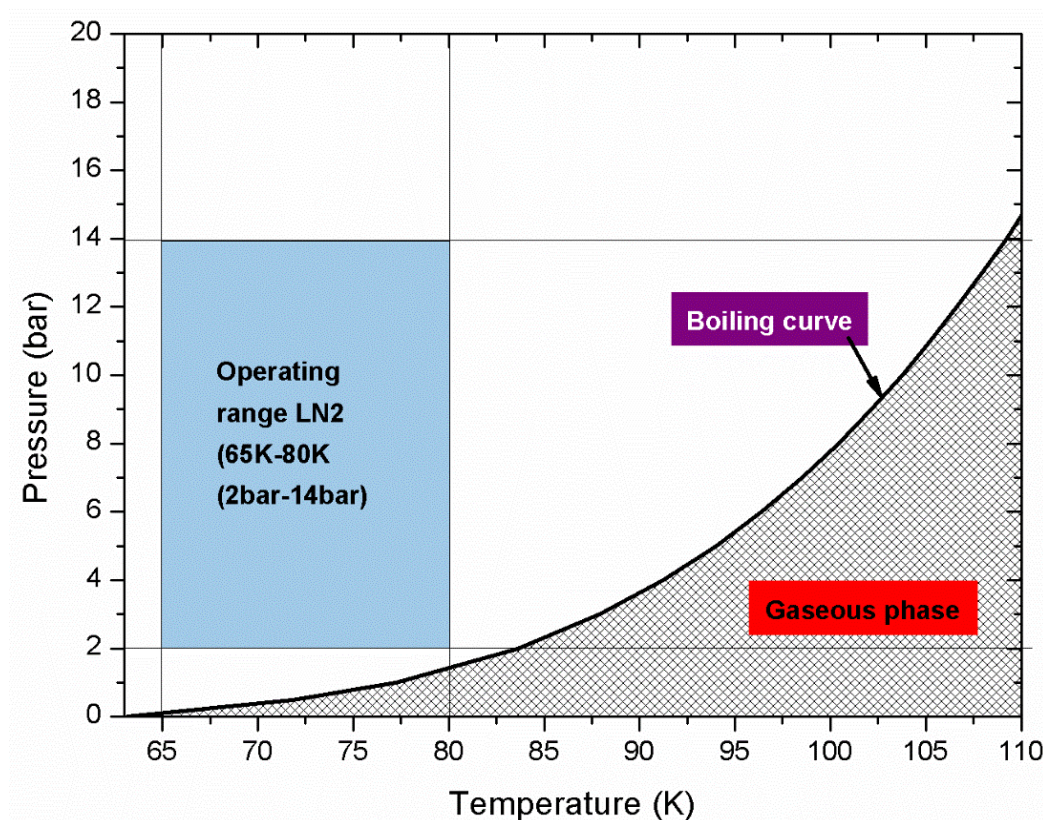


Figure 3.2 Phase diagram for operating range and boiling curve of liquid nitrogen

3.2 Analytical Solution Procedure

After developing a conceptual model of a counter cooled HTS cable system, it is important to develop a mathematical model that will allow estimating the quantitative behavior of the system. Therefore, this section demonstrates the derivation of equations used to attain temperature distribution profiles in the simplified model of cold-dielectric counter flow cooling HTS cable. The temperature of the LN2 in the inner region is calculated by energy balance of the fluid flow in an infinite small flow element

$$mc_p \frac{dT_1}{dx}$$

where m is the mass flow rate and c_p the specific heat capacity of the LN2 flowing through the cable. Q_{AC} and $q(x)$ are the heat input sources for the inner region as shown in the Figure 3.3. Q_{AC} is the heat dissipated by alternating current passed through HTS tapes and assumed to be dispersed equally in both the regions and the heat flow from the annular region to inner region due to temperature difference is represented as $q(x)$. Moreover, the conduction through stainless steel corrugated pipe and pressure drop across the cable is neglected in the present work.

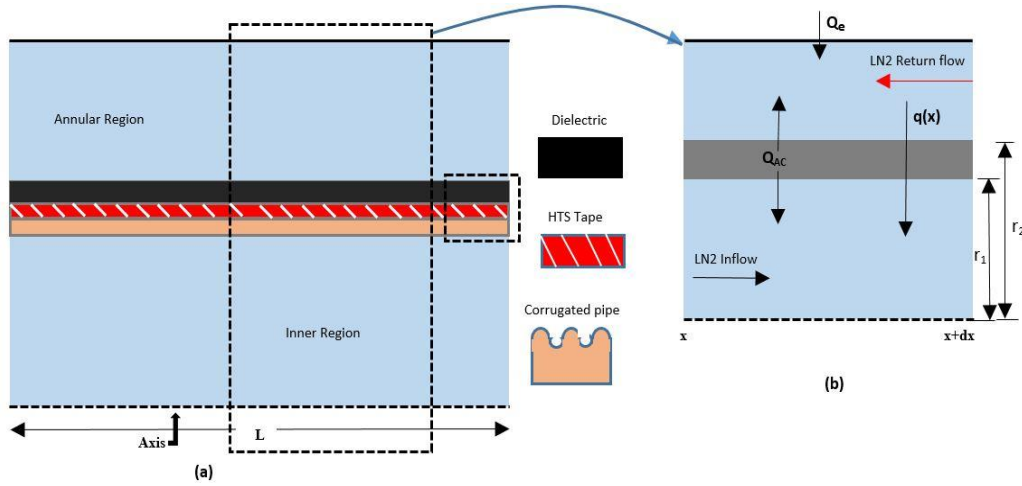


Figure 3.3 (a) Schematic of fluid and solid domains of HTS cable (b) heat balancing within control volume

Now, the energy balance equation for the inner region and annular region for steady-state conditions may be written as:

$$mc_p \frac{dT_1}{dx} = q(x) + \frac{Q_{AC}}{2} \quad (1)$$

$$mc_p \frac{dT_2}{dx} = -q(x) + \frac{Q_{AC}}{2} + Q_e \quad (2)$$

The heat flow from the annular region to inner region due to temperature difference is represented as $q(x)$ and defined below.

$$q(x) = 2\pi k [T_2(x) - T_1(x)] \quad (3)$$

where k is assumed to be linear thermal conductance between the regions.

$$k = 1 / \left[1 / h_1 r_1 + \ln(r_2 / r_1) / \lambda + 1 / h_2 r_2 \right] \quad (4)$$

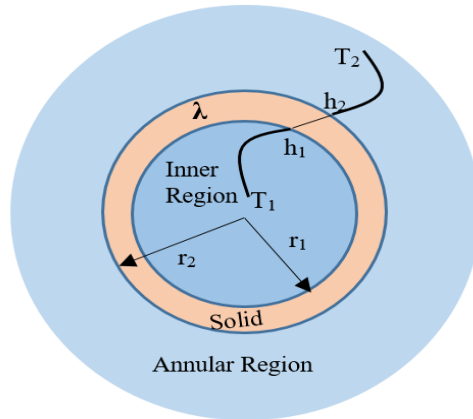


Figure 3.4 Schematic of overall thermal conductance in HTS cable

Here h_1 and h_2 are the heat transfer coefficients between corrugated walls and the LN2 flowing through different regions. The radii r_1 and r_2 are the radius of inner corrugated pipe and the outer radius of dielectric material as shown in Figure 3.4. The thermal conductivity of dielectric (λ) is assumed to be 0.005 W/mK. The resistance between wall and flow regions $(1/h_1r)(1/h_2r_2)$ is very small as compared to dielectric resistance, therefore it can be neglected for the present analysis.

The boundary conditions for solving the equations are as:

$$x = 0, \quad T_1(0) = T_0$$

$$x = L, \quad T_1(L) = T_2(L)$$

3.2.1 Axial Temperature Profile for Inner Region

In order to investigate the temperature distribution of liquid nitrogen in the inner region of HTS cable, the heat balancing in the 1-D model is represented in Figure 3.5.

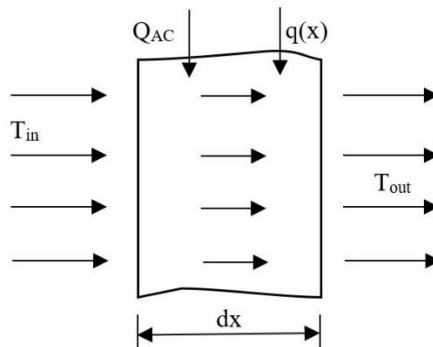


Figure 3.5 Heat balancing in the inner region of HTS cable

To investigate the temperature distribution of liquid nitrogen in HTS cable for Inner region.

Considering first heat balance equation (1)

$$mc_p \frac{dT_1}{dx} = q(x) + \frac{Q_{AC}}{2} \quad (5)$$

and from equation (3), $q(x) = 2\pi k [T_2(x) - T_1(x)]$

Substituting $q(x)$ in equation (5), we have

$$mc_p \frac{dT_1}{dx} = 2\pi k [T_2(x) - T_1(x)] + \frac{Q_{AC}}{2} \quad (6)$$

Here we assume a linear temperature gradients across the infinitely small tube element to investigate the temperature profile in the cable. Therefore, it is necessary to involve a general heat conduction equation to evaluate temperature gradient in x -direction under steady condition which further leads to investigate the temperature profile in the cable.

In order to find out the temperature distribution in the HTS cable for both the flows ($t_2(x)$, $t_1(x)$), the assumed one-dimensional steady-state heat conduction equation is:

$$\frac{\partial^2 t}{\partial x^2} = 0 \quad (7)$$

On integrating the above equation, we have

$$t = C_1 x + C_2 \quad (8)$$

Now using the boundary conditions shown in the figure

At $x = x_1$, $t = t_1$ and $x = x_2$, $t = t_2$

Substituting the boundary conditions in Eq. (8)

$$t_1 = C_1 x_1 + C_2$$

$$t_2 = C_1 x_2 + C_2$$

Now, the solution of these equations gives

$$C_1 = \frac{t_1 - t_2}{x_1 - x_2} \quad \text{and} \quad C_2 = t_1 - \left(\frac{t_1 - t_2}{x_1 - x_2} \right) x_1$$

First substitute the t_1 , t_2 and later C_1 , C_2 in Eq. (8)

$$mc_p \frac{dT_1}{dx} = 2\pi k (C_1 x_2 + C_2) - 2\pi k (C_1 x_1 + C_2) + \frac{Q_{AC}}{2} \quad (9)$$

After Expanding 1st term on the right hand side of Eq. (9)

$$mc_p \frac{dT_1}{dx} = \left[2\pi k \left(\frac{t_1 - t_2}{x_1 - x_2} \right) x_2 + 2\pi k t_1 - 2\pi k \left(\frac{t_1 - t_2}{x_1 - x_2} \right) x_1 \right] - 2\pi k (C_1 x_1 + C_2) + \frac{Q_{AC}}{2}$$

After Expanding 2nd term on the right hand side of Eq. (9), and rearranging, we obtain

$$\frac{dT_1}{dx} = \left[-\frac{2\pi k}{mc_p} \left(\frac{t_1 - t_2}{x_2 - x_1} \right) x_2 + \frac{2\pi k}{mc_p} \left(\frac{t_1 - t_2}{x_2 - x_1} \right) x_1 + \frac{Q_{AC}}{2mc_p} \right] \quad (10)$$

Integrate both the sides to get $T_1(x)$

$$T_1(x) = \left[\left(-\frac{2\pi k}{mc_p} \left(\frac{t_1 - t_2}{x_2 - x_1} \right) x_2 \right) x_1 + \frac{2\pi k}{mc_p} \left(\frac{t_1 - t_2}{x_2 - x_1} \right) \frac{x_1^2}{2} + \frac{Q_{AC}}{2mc_p} x_1 + C \right] \quad (11)$$

Now substitute the boundary conditions in the Eq. (11)

$$x = 0, \quad T_1(0) = T_0 \quad (i)$$

$$x = L, \quad T_1(L) = T_2(L) \quad (ii)$$

After substituting boundary condition (i) in Eq. (11)

$$T_1(0) = 0 + 0 + 0 + C \Rightarrow C = T_0$$

Therefore, substituting C again in Eq. (11), we obtain

$$T_1(x) = \left[\left(-\frac{2\pi k}{mc_p} \left(\frac{t_1 - t_2}{x_2 - x_1} \right) x_2 \right) x_1 + \frac{2\pi k}{mc_p} \left(\frac{t_1 - t_2}{x_2 - x_1} \right) \frac{x_1^2}{2} + \frac{Q_{AC}}{2mc_p} x_1 + T_0 \right] \quad (12)$$

Substitute boundary condition (ii) in Eq. (12), we obtain

$$T_1(l) = \left[\left(-\frac{2\pi k}{mc_p} \left(\frac{t_1 - t_2}{x_2 - x_1} \right) l \right) x_1 + \frac{2\pi k}{mc_p} \left(\frac{t_1 - t_2}{x_2 - x_1} \right) \frac{x_1^2}{2} + \frac{Q_{AC}}{2mc_p} x_1 + T_0 \right] \quad (13)$$

$$\left(\frac{t_1 - t_2}{x_2 - x_1} \right) = \left(\frac{Q_{AC} + Q_e}{mc_p} \right) \quad (\text{Assumed})$$

Therefore the final equation will be

$$T_1(x) = \frac{1}{mc_p} \left(2\pi k \left(\frac{Q_{AC} + Q_e}{mc_p} \right) l + \frac{Q_{AC}}{2} \right) x - \frac{\pi k}{m^2 c_p^2} (Q_{AC} + Q_e) x^2 + T_0 \quad (14)$$

3.2.2 Axial Temperature Profile for Annular Region

In order to investigate the temperature distribution of liquid nitrogen in the annular region of HTS cable, the heat balancing in the 1-D model is represented in Figure 3.6.

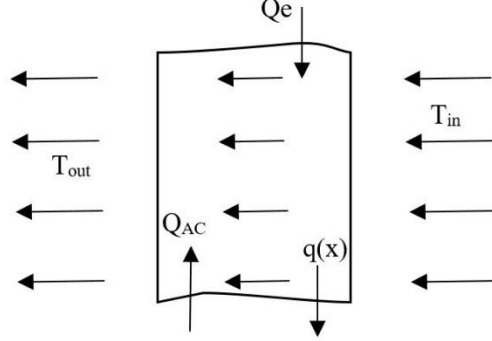


Figure 3.6 Heat balancing in the annular region of HTS cable

To investigate the temperature distribution of liquid nitrogen in HTS cable for annular regions.

Considering second heat balance equation (2), we have

$$mc_p \frac{dT_2}{dx} = -q(x) + \frac{Q_{AC}}{2} + Q_e$$

$$q(x) = 2\pi k [T_2(x) - T_1(x)]$$

Substituting the $q(x)$ in heat balance equation (2), we have

$$mc_p \frac{dT_2}{dx} = -2\pi k [T_2(x) - T_1(x)] + \frac{Q_{AC}}{2} + Q_e \quad (15)$$

The general steady-state heat conduction is used again to obtain the temperature gradient for annular region and then substituting t_1 , t_2 and C_1 , C_2 in the Eq. (15).

$$t_1 = C_1 x_1 + C_2$$

$$t_2 = C_1 x_2 + C_2$$

$$C_1 = \frac{t_1 - t_2}{x_1 - x_2} \quad \text{and} \quad C_2 = t_1 - \left(\frac{t_1 - t_2}{x_1 - x_2} \right) x_1$$

First put the t_1 and t_2 and later C_1 and C_2 in Eq. (15)

$$mc_p \frac{dT_2}{dx} = -2\pi k (C_1 x_2 + C_2) + 2\pi k (C_1 x_1 + C_2) + \frac{Q_{AC}}{2} + Q_e$$

After expanding the C_1 and C_2 , we have the rearranged equation as

$$mc_p \frac{dT_2}{dx} = \left[-2\pi k \left(\frac{t_1 - t_2}{x_1 - x_2} \right) x_2 + 2\pi k \left(\frac{t_1 - t_2}{x_1 - x_2} \right) x_1 + \frac{Q_{AC}}{2} + Q_e \right] \quad (16)$$

$$\frac{dT_2}{dx} = \left[\frac{-2\pi k \left(\frac{t_1 - t_2}{x_1 - x_2} \right) x_2}{mc_p} + \frac{2\pi k \left(\frac{t_1 - t_2}{x_1 - x_2} \right) x_1}{mc_p} + \frac{Q_{AC}}{2mc_p} + \frac{Q_e}{mc_p} \right] \quad (17)$$

Integrate the Eq. (17) on both sides to obtain temperature distribution as

$$T_2(x) = \left[\frac{2\pi k \left(\frac{t_1 - t_2}{x_2 - x_1} \right) x_2^2}{mc_p} + \left(-\frac{2\pi k \left(\frac{t_1 - t_2}{x_2 - x_1} \right) x_1}{mc_p} \right) x_2 + \frac{Q_{AC}}{2mc_p} x_2 + \frac{Q_e}{mc_p} x_2 + C \right] \quad (18)$$

Now use the boundary condition

$$T_2(0) = [0 + 0 + 0 + 0 + C] \Rightarrow T_2(0) = C$$

Since, $T_2(0)$ is the outlet temperature of return flow (Annular region) therefore it must be greater than ($T_0 = 65$ K).

We can also write, $T_2(0) = T_0 + dt$

$$\text{where, } dt = \left(\frac{Q_{AC} + Q_e}{mc_p} \right) x_1$$

Now solving for C , we have

$$C = T_0 + \left(\frac{Q_{AC} + Q_e}{mc_p} \right) x_1$$

Substitute C in Eq. (18)

$$T_2(x) = \left[\frac{2\pi k \left(\frac{t_1 - t_2}{x_2 - x_1} \right) x_2^2}{mc_p} + \left(-\frac{2\pi k \left(\frac{t_1 - t_2}{x_2 - x_1} \right) x_1}{mc_p} \right) x_2 + \frac{Q_{AC}}{2mc_p} x_2 + \frac{Q_e}{mc_p} x_2 + T_0 + \left(\frac{Q_{AC} + Q_e}{mc_p} \right) x_1 \right] \quad (19)$$

Use the boundary condition (ii) in the above equation (19), we have

$$T_2(l) = \left[\frac{2\pi k \left(\frac{t_1 - t_2}{x_2 - x_1} \right) x_2^2}{mc_p} + \left(-\frac{2\pi k \left(\frac{t_1 - t_2}{x_2 - x_1} \right) l}{mc_p} \right) x_2 + \frac{Q_{AC}}{2mc_p} x_2 + \frac{Q_e}{mc_p} x_2 + T_0 + \left(\frac{Q_{AC} + Q_e}{mc_p} \right) l \right]$$

$$\left(\frac{t_1 - t_2}{x_2 - x_1} \right) = \left(\frac{Q_{AC} + Q_e}{mc_p} \right) \quad (\text{Assumed})$$

Therefore the temperature distribution function can be written as

$$T_2(x) = \left[-\frac{\pi k}{m^2 c_p^2} (Q_{AC} + Q_e) x^2 + \frac{1}{mc_p} \left(2\pi k \left(\frac{Q_{AC} + Q_e}{mc_p} \right) l + \frac{Q_{AC}}{2} + Q_e \right) x + T_0 + \left(\frac{Q_{AC} + Q_e}{mc_p} \right) l \right] \quad (20)$$

3.3 Computational Modeling

The solution process of computational method used for thermohydraulic analysis of HTS cable is shown in Figure 3.7 (a). The method involves the creation of geometry, mesh (grid) and few significant solver settings to obtain the desired results. Referring the method, geometries with various corrugation shapes are modelled using ANSYS Design Modeler with physical parameters as discussed in Table 3-2. The modelled HTS cable with various corrugation topologies are further meshed using ANSYS Meshing and the mesh size varies for each of geometry depending upon the wall corrugation surface. The meshed geometries are further exported to the ANSYS Fluent in order to define boundary conditions, material properties, turbulence model and pressure-velocity coupling scheme. The solver will stop the calculation once the solution criteria for the continuity, x, y and z velocities, the kinetic energy k, and the dissipation of energy ϵ is satisfied. The mesh geometries are refined for the grid independent analysis to achieve more accurate results. Using post-processing tool of the ANSYS Fluent, the required results for the defined model can be retrieved.

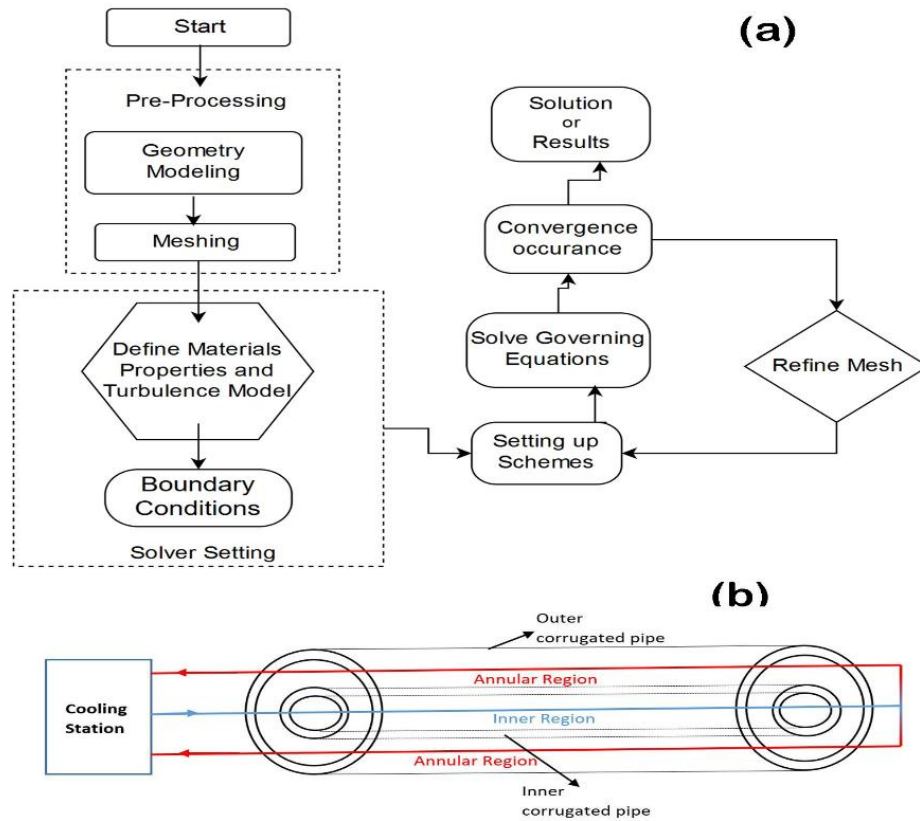


Figure 3.7 (a) Flow chart of thermohydraulic analysis of HTS cable (b) Schematic of Counter flow arrangement

The schematic representation of superconducting cable is shown in the Figure 3.8. In this configuration, cooling is supplied by cryo-cooler at one-end of the HTS cable to the other end. LN₂ circulated through inner corrugated pipe (inner region) of HTS cable to the far end. After reaching to the other end of the HTS cable, LN₂ will face the other cryo-cooler and returns through outer corrugated pipe (annular region). This system of counter flow cooling of superconducting cables is called as loop mode [46]. The loop mode separates the infinite long HTS cable into several sections in order to make the maintenance easy. The cryo-cooler is used to reset the temperature, thus the temperature at inlet of every section will be equal on both ends.

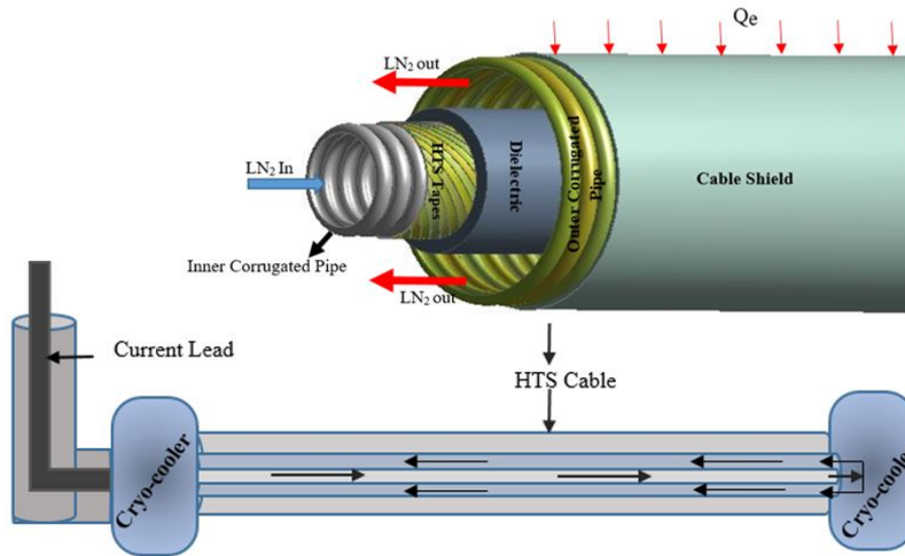


Figure 3.8 Schematic representation of single-phase co-axial superconducting cable system

Moreover, conceptual design of single phase coaxial cold dielectric HTS cable is also shown in Figure 3.8. The HTS cable comprises of inner corrugated pipe, HTS tapes, Dielectric, and outer corrugated pipe with cable shield. The yttrium barium copper oxide (YBCO) HTS tapes having critical temperature of 90 K are wound on inner corrugated pipe to carry the large amount of electric current. Poly propylene laminated paper (PPLP) is used as the dielectric material in HTS cable due to its high dielectric strength. The HTS cable is surrounded by two concentric corrugated pipe including outer corrugated pipe and above which make the cryostat in order to reduce the exterior heat load. All such parameters for the conceptual design of single phase coaxial cold dielectric HTS cable are compiled in Table 3-2

Table 3-2 parameters for conceptual design of HTS cable

Parameters	Details
Diameter of Inner region (mm)	40
Diameter of Annular region (mm)	35
Thickness of corrugated pipe, g (mm)	2
Corrugation pitch, p (mm)	8
Corrugation depth, s (mm)	4
Heat Flux from ambient/exterior, Q_e (W/m ²)	4-10
Heat from HTS tapes/A.C loss, Q_{AC} (W/m)	1-2.5
Inlet temperature, T_o (K)	65
Inlet Pressure, P_1 (bar)	2
Volumetric flow, V (L/min)	20-35

Table 3-3 compared approximate entry lengths at various Reynolds numbers

Reynolds Number	32450	40563	48675	56788
Entry Length (m)	0.99	1.03	1.06	1.09

There are many analytical and experimental studies reported on counter flow cooling system in the HTS cables. In case of computational investigation on thermal and hydraulic analysis of HTS cables, finite volume method (FVM) is mostly preferred due to the accuracy. Two dimensional (2-D) model of HTS cable having length of 0.5 meter with counter flow cooling system is designed and meshed (see Figure 3.9) using ANSYS software of CFD package. The present study involves the effect of exterior heat flux of (4-10 W/m²) and A.C. losses of (1-1.25 W/m) on pressure drop and heat transfer, encountered on the outer corrugated wall of the HTS model.

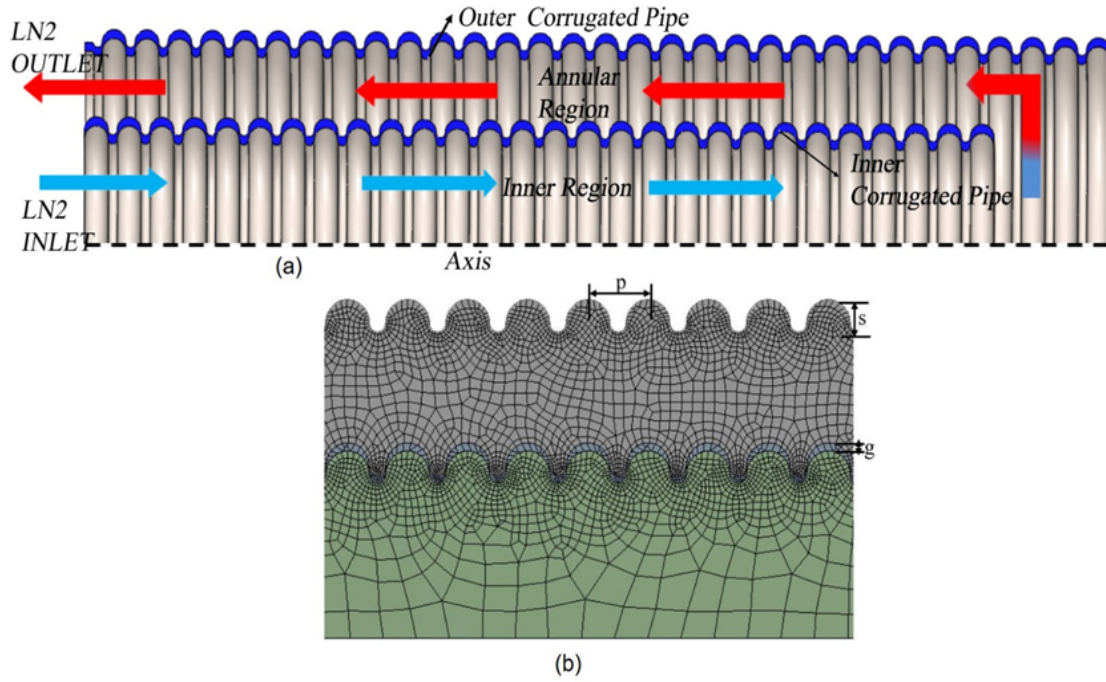


Figure 3.9 (a) 2-D Axisymmetric view of counter flow cold dielectric HTS cable and (b) a view of typical Mesh

The HTS tapes and dielectric thickness is neglected in the present simulation for the simplicity of computational domain. Hence, the heat generated (W/m^3) in the HTS tapes due to electrical dissipation power is assumed to be uniform in the inner corrugated pipe for the present analysis and estimated using (21),

$$\omega = \frac{Q_{AC}}{A_{SC}} \quad (21)$$

where, ω is the heat generated by power dissipation in HTS phase (W/m^3). Q_{AC} is known as the AC losses in superconducting phase (W/m) and A_{SC} is the cross-sectional area of the HTS phase (W/m^2).

The pressure drop in the HTS cable is investigated using post-processing module of ANSYS- FLUENT. These values of pressure drop are further used to determine the friction factor (f) at different flow rates using (22).

$$f = \frac{2\Delta p \times D_h}{\rho l v^2} \quad (22)$$

where Δp = Pressure Drop, l = length of HTS cable, D_h = Hydraulic Diameter, ρ = Density of LN_2 and v = average velocity of flow in the corrugated pipe.

In order to flow the LN2 through inner corrugated pipe and outer corrugated in the HTS cable, pump is required and the power of pump is calculated using (23).

$$W = \Delta p \cdot Q \quad (23)$$

where $Q = A \times v$ is the volume flow rate (m^3/s) and A is the cross-sectional area of the corrugated pipe (m^2).

The location of the fully developed flow from the inlet and for the turbulent flow in a pipe can be calculated using (24) as [70]

$$L_{entry} = 4.4 \times D \times \text{Re}^{1/6} \quad (24)$$

where Re = Reynolds number

3.3.1 Boundary Conditions

The HTS cable cooling system is arranged in such a way that at the inlet, LN2 flows (65 K and 3 bar) in the inner corrugated pipe to accommodate the heat generated by the HTS tapes and exit from the outer corrugated pipe. The HTS cable of length 0.5 meter comprised of inner fluid domain (inner region) and outer fluid domain (annulus region), separated by a corrugated pipe (solid) of thickness 2mm. The inlet of the LN2 fluid domain is allocated as mass flow inlet (kg/s) matching with the experiments on HTS cables performed by Fuchino et al. [54], whereas, the outlet boundary condition is assigned as outflow. The heat loss (W/m) in the HTS tapes due to electrical dissipation power is transformed in heat generation (see Eq.21) and assumed to be uniform in the inner corrugated pipe for the present analysis. Heat-in-Leak encountered on the cable shield due to the ambient temperature is assumed to be equally imposed on the outer corrugated wall of the computational model in the boundary conditions.

No slip boundary condition is imposed on the walls of corrugated pipe surfaces. A pressure based, laminar/k-epsilon realizable turbulent model, incompressible, steady state solver is used in the simulation. However, the thermophysical properties of LN2 are considered to be temperature dependent for the present analysis. The solver uses SIMPLE algorithm for pressure and velocity coupling

3.3.2 Computational modeling for various corrugation topologies of HTS cable

The single phase coaxial cold dielectric HTS cable using (single-sided cooling with internal coolant return flow) counter flow cooling was proposed in our previous study with circular corrugations [71]. In the present model the various corrugation topologies [72]–[78] were chosen to investigate the thermal and hydraulic performance of LN2. Figure 3.7 (b) depicts the counter flow cooling arrangement in which liquid nitrogen (LN2) is used to cool the HTS cable, which is circulated through inner corrugated pipe (inner region) and exits from the annular outer corrugated pipe (annular region). The HTS cable comprises of inner corrugated pipe, HTS tapes, Dielectric material, and outer corrugated pipe with cable shield. HTS tape comprises of different layers of solid materials such as silver/copper (protective layer), YBCO (superconducting layer), buffer layer and metal substrate with total thickness of ≤ 0.2 mm. Polypropylene laminated paper (PPLP) is commonly used as an insulation material for superconducting device applications with an advantage of low dielectric losses. The corrugated pipes used in the HTS cable are mainly of stainless steel (SS) material with cryogenic compatible grades such SS316L. Figure 3.10 shows the 2-D axisymmetric model of HTS cable with various corrugation topologies (rectangular, circular and triangular) having a computational length of 504 mm with their respective mesh shown in Figure 3.11. The physical parameters such as inner corrugated pipe of 40mm in diameter and an annular outer corrugated pipe with diameter of 37.5mm is considered for the present work. The thickness of HTS tape and dielectric material (solid domain) is $< 1\%$ of the diameter of corrugated pipe as can be seen in Table 3-4.

Table 3-4 Parameters for conceptual design of HTS cable

Parameters	Details
Diameter of Inner region (mm)	40
Equivalent Diameter of Annular region (mm)	37.5
Thickness of corrugated pipe, g (mm)	1
Thickness of HTS tape (mm)	0.02
Thickness of Dielectric material (mm)	0.1
Corrugation pitch, p (mm)	8
Corrugation depth, s (mm)	4
Heat Flux from ambient/exterior, Q_e (W/m ²)	4-10
Heat from HTS tapes/A.C loss, Q_{AC} (W/m)	1-2.5
Inlet temperature, T_o (K)	65
Inlet Pressure, P_1 (bar)	2
Volumetric flow, V (L/min)	20-35

Therefore, due to the lesser thickness of HTS tape and dielectric material than fluid domain, the thickness of HTS tapes and dielectric material is worth neglecting for the present CFD analysis. During operation with alternating current (A.C), the HTS tapes cause electrical power dissipation (W/m) that indicates an internal heat source (W/m^3). Therefore, the effect of heat generation (W/m^3) in the HTS tapes due to electrical dissipation power is considered and assumed to be equal in the inner corrugated pipe of 1 mm thickness for the present analysis. Moreover, the exterior heat-in-leak (W/m) from the ambient temperature on the outer corrugated pipe is converted into heat flux (W/m^2) and worth considered for the analysis. The present study involves the effect of heat-in-leak of (4-10 W/m^2) and A.C. losses of (1-2.25 W/m) on pressure drop and heat transfer analysis of the HTS model. The heat generated (W/m^3) in the HTS tapes due to electrical dissipation power can be estimated using equation 1. The analytical process of estimating flow characteristics such as pressure drop, friction factor and pumping power in the HTS cable is discussed by Kalsia et al. [71].

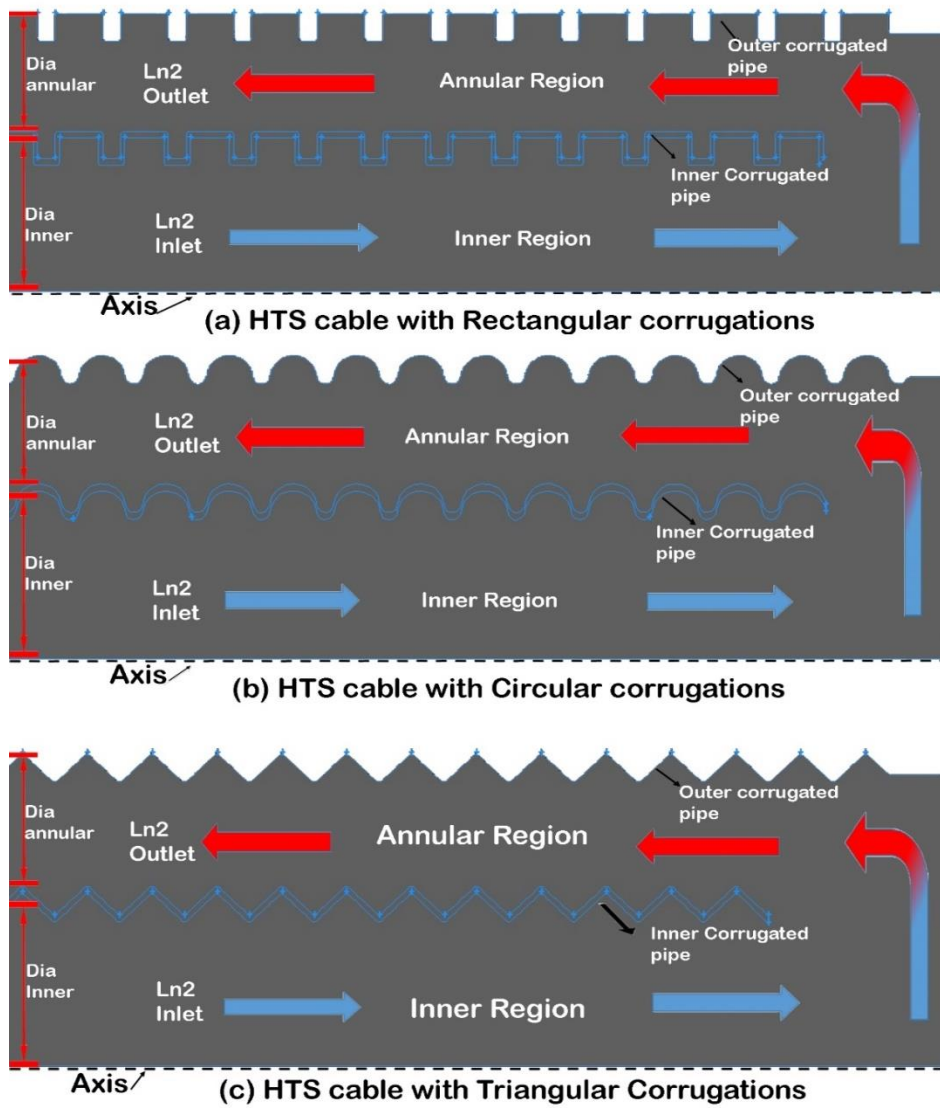
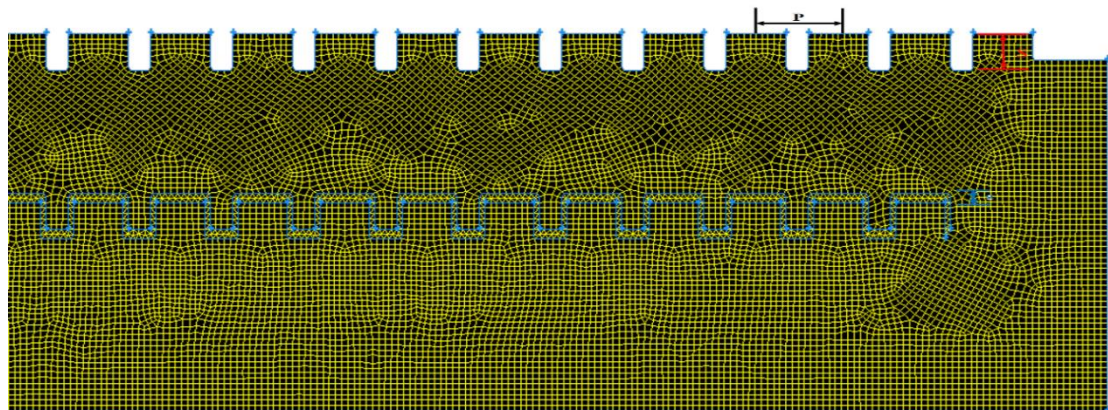
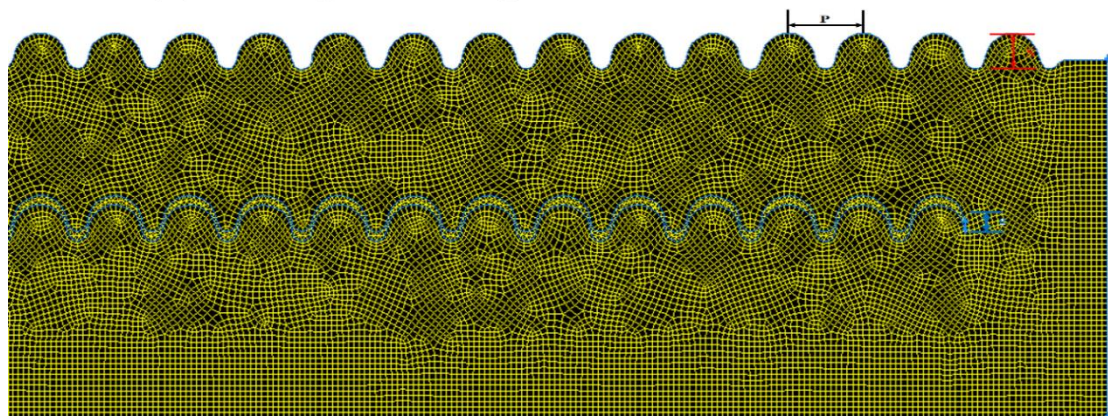


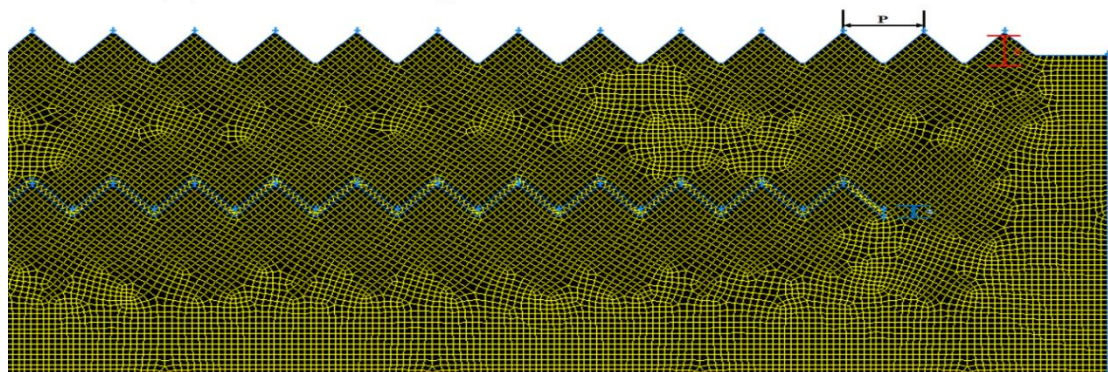
Figure 3.10 Schematic and structural parameters of 2-D axisymmetric HTS cable with various corrugation shapes
 (a) rectangular (b) circular (c) triangular



(a) Rectangular corrugations with mesh size:0.6mm



(b) Circular corrugations with mesh size:0.58mm



(c) Triangular corrugations with mesh size:0.7mm

Figure 3.11 Typical mesh of 2-D axisymmetric HTS cable with various corrugation shapes (a) rectangular (b) circular (c) triangular

3.3.3 *Boundary Conditions for various corrugation topologies of HTS cable*

The boundary conditions of counter cooled HTS cable with various corrugation shapes are discussed below.

- a) Steady state and incompressible flow of LN2 with the temperature dependent thermophysical properties is considered for the analysis.

- b) The LN2 inlet conditions such as inlet temperature of 65K, inlet mass flow rate ranges from 20L/min to 35L/min [54], the turbulence intensity of $I = 5\%$ and the hydraulic diameter of 40 mm are considered for the present analysis.
- c) The outlet boundary is assigned as outflow, a turbulence intensity of $I = 5\%$ and the hydraulic diameter of 37.5mm.
- d) Inner corrugated pipe (solid) of thickness 1mm is considered as heat source and allocated as heat generation of $(396 \text{ W/m}^3 \text{ to } 986 \text{ W/m}^3)$ corresponding to the A.C. losses.
- e) The wall boundary condition at outer corrugated wall is assigned as heat flux of $(4 \text{ W/m}^2 - 10 \text{ W/m}^2)$. No slip boundary condition is imposed on the walls of corrugated pipe surfaces.
- f) The k-epsilon turbulent model with enhanced wall treatment and pressure based solver is used in the simulation. The solver uses SIMPLE algorithm for pressure and velocity coupling

3.4 Governing Equations

In order to solve the small fluctuations of physical properties such as pressure and velocity which causes instability and makes the fluid turbulent, the proposed averaged equations are presented in this section. The velocity and the pressure fields were acquired from the numerical solution of the mass momentum and energy conservation equations under incompressible and steady-state conditions, in the domain of the finite volume CFD approach. Since flow is turbulent in all cases due to the corrugations, the simulations are obtained using general Reynolds averaged Navier-Stokes (RANS) equations [71].

The time-averaged conservation of mass for 2-D flow can be written as:

$$\frac{\partial \bar{u}}{\partial x} + \frac{\partial \bar{v}}{\partial y} = 0 \quad (25)$$

where, u is the momentary velocity component, \bar{u} is the time-averaged velocity and u' is the fluctuating velocity.

The time-averaged conservation of momentum equations are as follows:

X-momentum

$$\rho \left(\frac{\partial \bar{u}}{\partial t} + \bar{u} \frac{\partial \bar{u}}{\partial x} + \bar{v} \frac{\partial \bar{u}}{\partial y} \right) = F_x - \frac{\partial \bar{p}}{\partial x} + \mu \nabla^2 \bar{u} - \rho \left(\frac{\partial \overline{u'u'}}{\partial x} + \frac{\partial \overline{u'v'}}{\partial y} \right) \quad (26)$$

Y-momentum

$$\rho \left(\frac{\partial \bar{v}}{\partial t} + \bar{u} \frac{\partial \bar{v}}{\partial x} + \bar{v} \frac{\partial \bar{v}}{\partial y} \right) = F_y - \frac{\partial \bar{p}}{\partial y} + \mu \nabla^2 \bar{v} - \rho \left(\frac{\partial \overline{u'v'}}{\partial x} + \frac{\partial \overline{v'v'}}{\partial y} \right) \quad (27)$$

Where, $\nabla^2 \bar{u} = \left(\frac{\partial^2 \bar{u}}{\partial x^2} + \frac{\partial^2 \bar{u}}{\partial y^2} + \frac{\partial^2 \bar{u}}{\partial z^2} \right)$ and $\nabla^2 \bar{v} = \left(\frac{\partial^2 \bar{v}}{\partial x^2} + \frac{\partial^2 \bar{v}}{\partial y^2} + \frac{\partial^2 \bar{v}}{\partial z^2} \right)$

$\rho \left(\frac{\partial \overline{u_i u_j}}{\partial x_j} \right)$ is termed as Reynolds stress or turbulent shear stress and $\left(\mu \frac{\partial u_i}{\partial x_j} - \rho \overline{u_i u_j} \right)$ is

known as total shear stress τ_{ij} .

F_x , F_y and F_z are the body forces, which are neglected for the present simulations

The time-averaged energy equation can be written as:

$$\rho C_p \left[\bar{u} \frac{\partial \bar{T}}{\partial x} + \bar{v} \frac{\partial \bar{T}}{\partial y} \right] = \frac{\partial}{\partial x} \left[k \frac{\partial \bar{T}}{\partial x} - \rho C_p \overline{u'T'} \right] + \frac{\partial}{\partial y} \left[k \frac{\partial \bar{T}}{\partial y} - \rho C_p \overline{v'T'} \right] \quad (28)$$

Turbulence equations

Turbulence equations are used to describe the mean flow characteristics for turbulence in the flow. The first transported variable in the flow is turbulence kinetic energy (k) and the other variable is the rate of dissipation of turbulence energy (ϵ).

Turbulence kinetic energy equation

$$\rho \frac{\partial k}{\partial t} + \rho U_j \frac{\partial k}{\partial x_j} = \sigma_{ij} \frac{\partial U_i}{\partial x_j} - \rho \epsilon + \frac{\partial}{\partial x_j} \left[\left(\mu + \frac{\mu_T}{\sigma_k} \right) \frac{\partial k}{\partial x_j} \right] \quad (29)$$

The unsteady and advection term on the left side of turbulence kinetic energy equation represents the rate of change of k following a fluid particle in a mean flow.

$\sigma_{ij} \frac{\partial U_i}{\partial x_j}$ is the production of turbulent kinetic energy which represents the rate at which k is transferred from mean flow to the fluctuations (turbulence flow).

$\mu \frac{\partial k}{\partial x_j}$ is known as molecular diffusion which represents the diffusion of k by fluid's molecular transport process.

σ_k is known as closure coefficient and μ_T represents the turbulent (eddy) viscosity.

$$\text{where, } \mu_T = \rho C_\mu \frac{k^2}{\varepsilon}$$

Turbulence dissipation energy

The rate at which turbulent kinetic energy k is converted into the thermal internal energy

$$\rho \frac{\partial \varepsilon}{\partial t} + \rho U_j \frac{\partial \varepsilon}{\partial x_j} = C_{\varepsilon 1} \frac{\varepsilon}{k} \sigma_{ij} \frac{\partial U_i}{\partial x_j} - C_{\varepsilon 2} \rho \frac{\varepsilon^2}{k} + \frac{\partial}{\partial x_j} \left[\left(\mu + \frac{\mu_T}{\sigma_\varepsilon} \right) \frac{\partial \varepsilon}{\partial x_j} \right] \quad (30)$$

$C_{\varepsilon 1}$, $C_{\varepsilon 2}$, C_μ , σ_k and σ_ε are the constants which are derived empirically or by data fitting of the turbulent flows.

$$C_{\varepsilon 1}=1.44, C_{\varepsilon 2}=1.92, C_\mu=0.09, \sigma_k=1.0, \sigma_\varepsilon=1.3$$

Entropy Generation

The volumetric rate of entropy generation [69], S''' (W/m³ K) in HTS cable can be calculated using the sum of equations (31) and (32). The calculation of total entropy generation involves the estimation of velocity and temperature gradients at all locations in the flow channel.

$$S'''_{frictional\ source} = \frac{\mu}{T_{ref}} \left[2 \left(\left(\frac{\partial \bar{u}}{\partial x} \right)^2 + \left(\frac{\partial \bar{v}}{\partial y} \right)^2 + \left(\frac{\partial \bar{w}}{\partial z} \right)^2 \right) + \left(\frac{\partial \bar{u}}{\partial y} + \frac{\partial \bar{v}}{\partial x} \right)^2 + \left(\frac{\partial \bar{u}}{\partial z} + \frac{\partial \bar{w}}{\partial x} \right)^2 + \left(\frac{\partial \bar{v}}{\partial z} + \frac{\partial \bar{w}}{\partial y} \right)^2 \right] \quad (31)$$

$$S'''_{Thermal\ source} = \frac{k}{T_{ref}^2} \left[\left(\frac{\partial \bar{T}}{\partial x} \right)^2 + \left(\frac{\partial \bar{T}}{\partial y} \right)^2 + \left(\frac{\partial \bar{T}}{\partial z} \right)^2 \right] \quad (32)$$


4 HYDRAULIC ANALYSIS OF HTS CABLE

In the previous chapter, mathematical and computational modeling are presented along with the temperature distribution of LN₂ in HTS cable. This chapter discusses the results obtained from the development of computational model presented in chapter 3. Further results pertaining to grid independence study are presented in order to ascertain the accuracy of the computational model. In addition, the computational results obtained from the present study are validated with the experimental results available from the literature. At first, the velocity distribution in HTS cable is presented along with the effect of corrugation geometry [79]–[85], heat flux and heat generation on velocity of LN₂. Later, the results relevant to pressure drop across the length of the HTS cable and associated pumping power are presented. Finally, friction factor correlations are developed and presented as a function of Reynolds numbers. The thermal issues in the HTS cables will be discussed in chapter 5.

4.1 Grid Independence Study

The grid independent study is an important practice in order to reduce the effect of different mesh sizes on the computational results. Moreover, the grid independent study is performed to improve the results using successively smaller mesh sizes for the results. A typical view of mesh with different element sizes is presented in the Figure 4.1. The grid independent analysis of modeled 2-D axisymmetric HTS cable of circular corrugation with various element size such as 0.7mm, 0.64mm, 0.58mm and 0.52mm is shown in Figure 4.2. It can be concluded from the results that the pressure drop is grid independent after further refinement of the mesh with mesh size of 0.58mm. Therefore, in order to avoid long computational time and solution instability, mesh with element size of 0.58mm of circular corrugation shaped HTS cable was adopted for the further thermohydraulic analysis. The number of nodes corresponding to the element size are compiled in the Table 4-1.

Table 4-1 Number of nodes for respective element size of circular corrugation shape

Circulation corrugation		Element size (mm)	0.7	0.64	0.58	0.52
		Number of nodes		45073	53901	63508

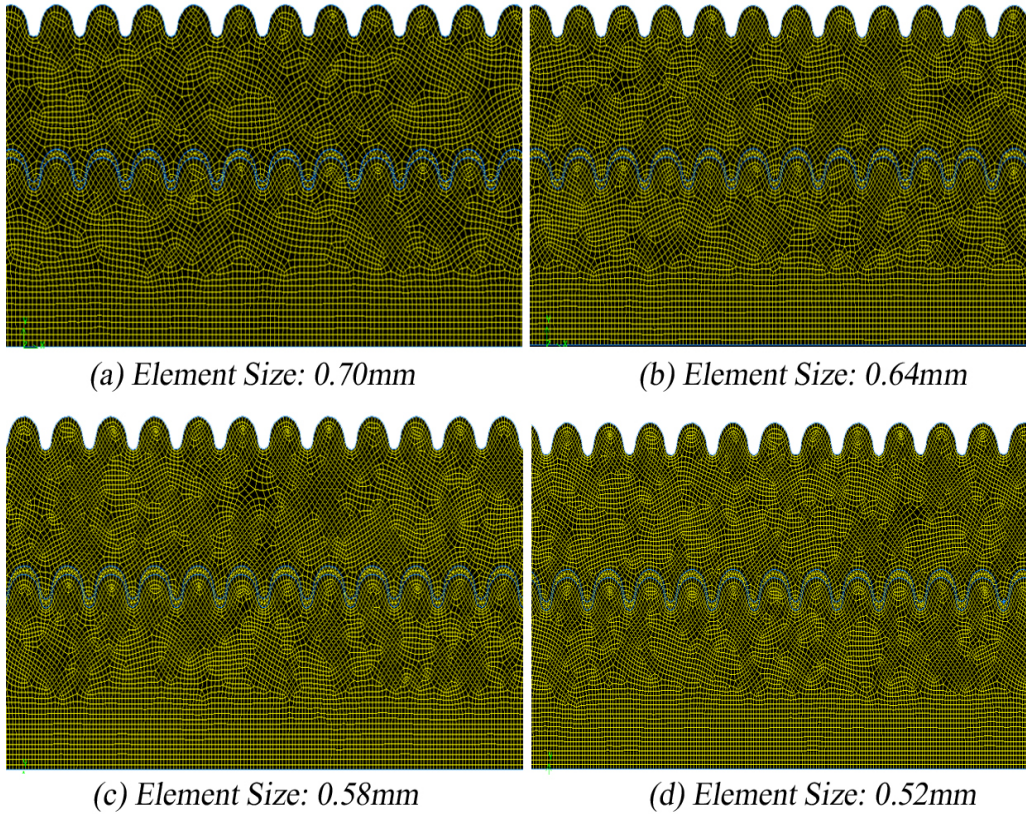


Figure 4.1 Typical mesh view for circulation corrugation with different element sizes: (a) 0.70mm (b) 0.64mm (c) 0.58mm (d) 0.52mm

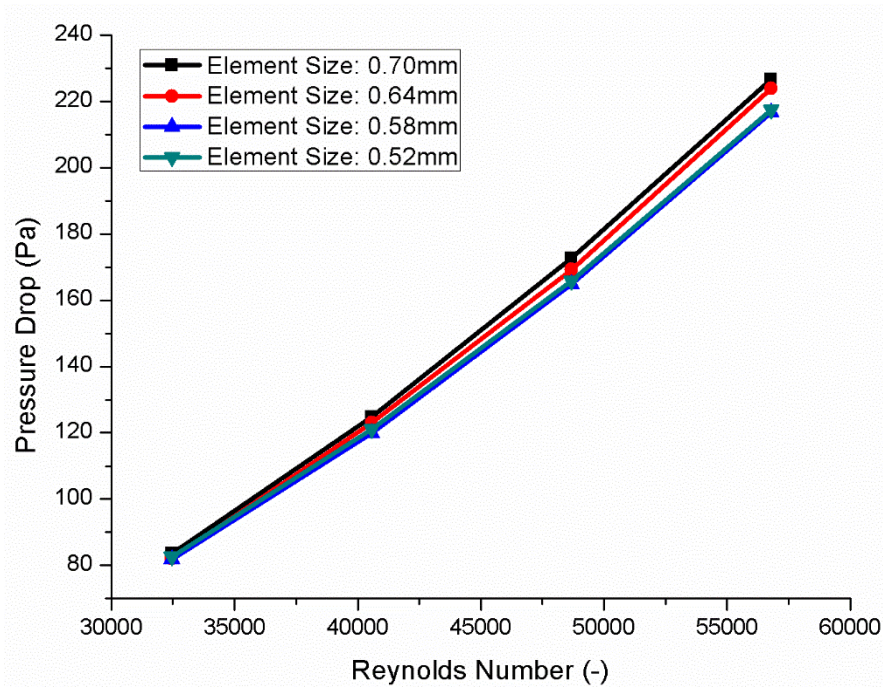
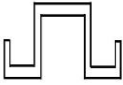


Figure 4.2 Pressure drop for various element sizes in the HTS cable with circular corrugation

In case of rectangular corrugation, typical view of mesh with different element sizes is presented in the Figure 4.3. The grid independent analysis of modeled 2-D axisymmetric HTS cable with element sizes of 1.0mm, 0.8mm, 0.6mm and 0.4mm is shown in Figure 4.4. It can be concluded from the results that the pressure drop is grid independent after further reducing the mesh element size up to 0.6mm. Therefore, in order to avoid long computational time and solution instability, mesh with element size of 0.6mm for rectangular corrugation was adopted for the further thermohydraulic analysis of HTS cable. The number of nodes corresponding to the element size for rectangular corrugation are compiled in the Table 4-2 given below.

Table 4-2 Number of nodes for respective element size of rectangular corrugation shape

Rectangular corrugation		Element size (mm)	1.0	0.8	0.6	0.4
		Number of nodes		40382	51658	60945

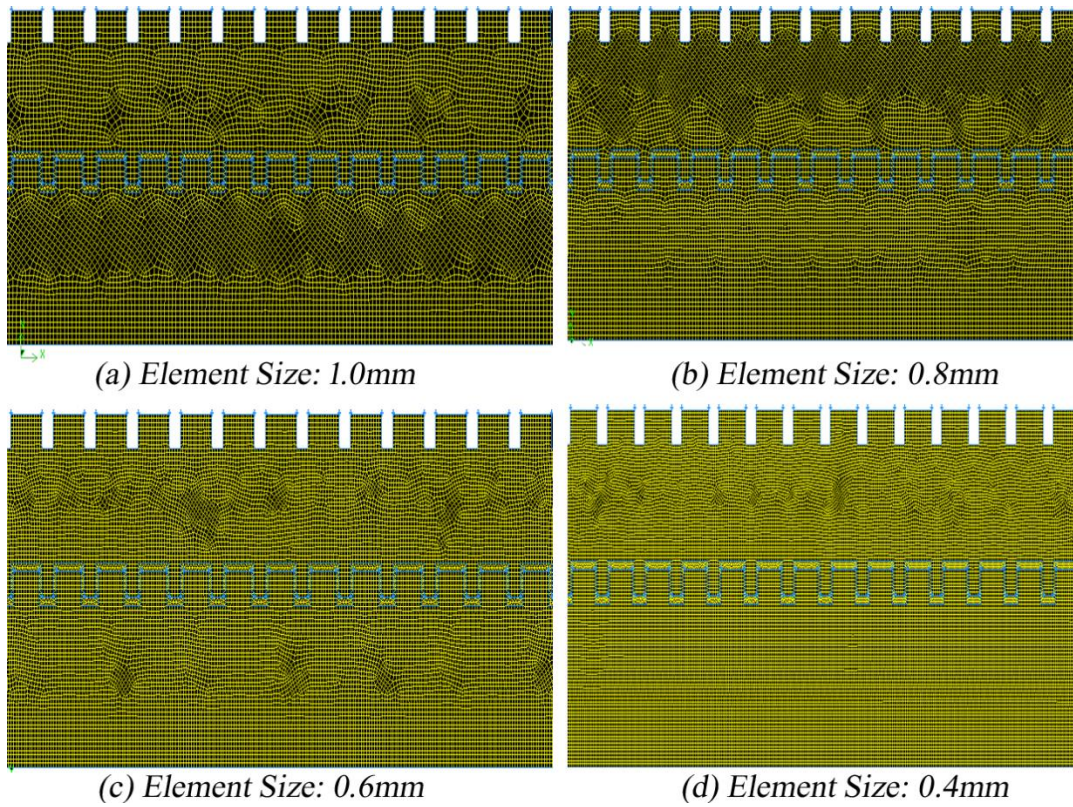


Figure 4.3 Typical mesh view for rectangular corrugation with different element sizes: (a) 1.0mm (b) 0.8mm (c) 0.6mm (d) 0.4mm

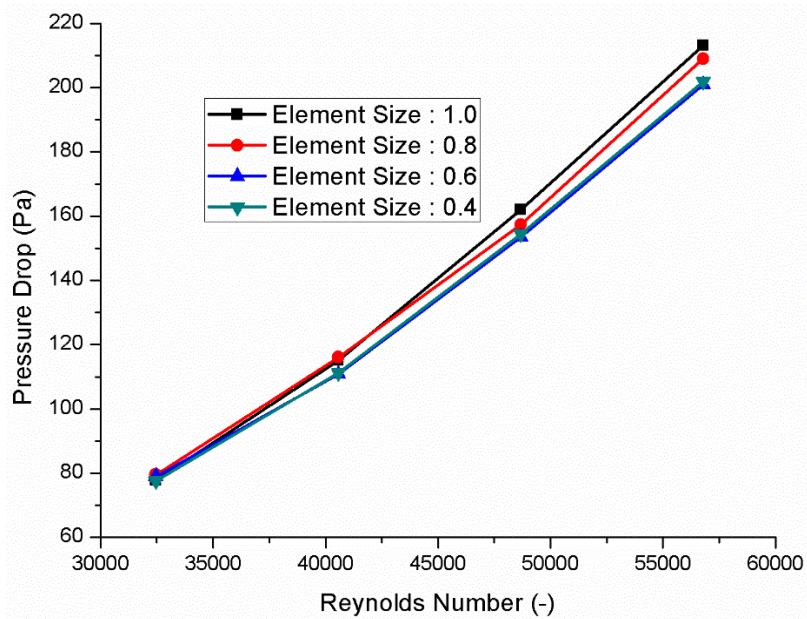



Figure 4.4 Pressure drop for various element sizes in the HTS cable with rectangular corrugation

A typical view of mesh with different element sizes for triangular shaped corrugation HTS cable is presented in the Figure 4.5. The grid independent study of modeled 2-D

axisymmetric HTS cable of triangular corrugation with element sizes of 1.0mm, 0.9mm, 0.7mm and 0.5mm is shown in Figure 4.6. It can be concluded from the results that the pressure drop is grid independent after further reducing the element size up to 0.7mm. Therefore, in order to avoid long computational time and solution instability, mesh with element size of 0.7mm for rectangular corrugation was adopted for the further thermohydraulic analysis of HTS cable. The number of nodes corresponding to the element size are gathered in the Table 4-3 given below.

Table 4-3 Number of nodes for respective element size of triangular corrugation shape

Triangular corrugation		Element size (mm)	1.0	0.9	0.7	0.5
		Number of nodes		41832	48891	56031

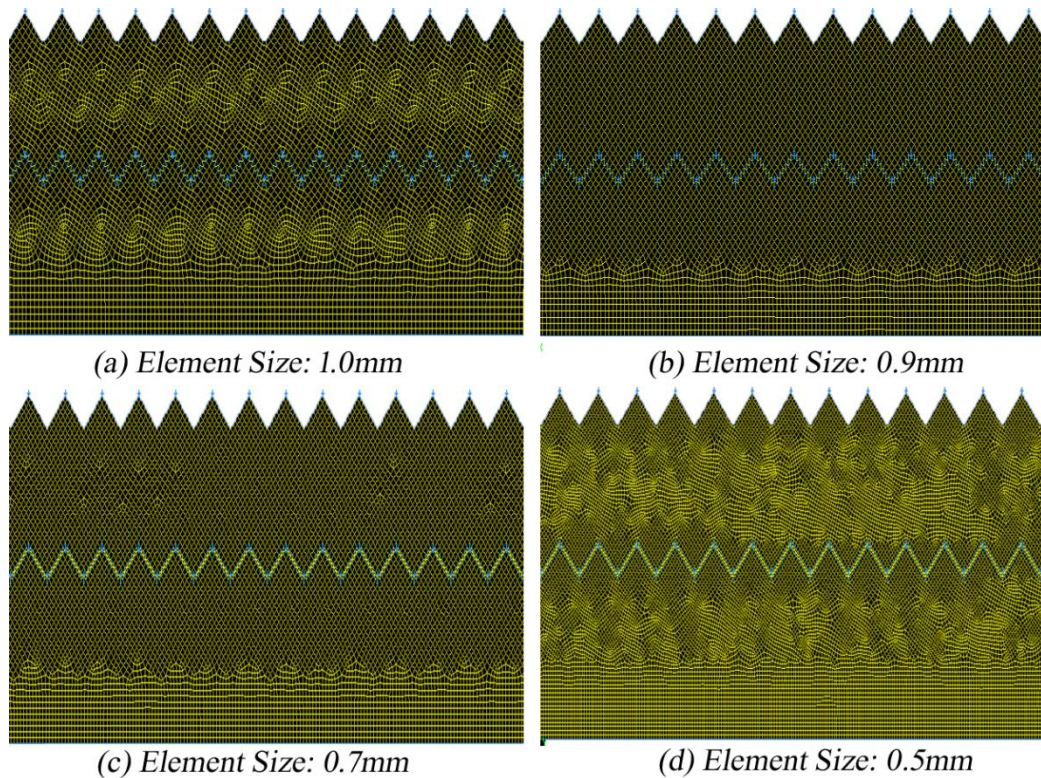


Figure 4.5 Typical mesh view for triangular corrugation with different element sizes: (a) 1.0mm (b) 0.9mm (c) 0.7mm (d) 0.5mm

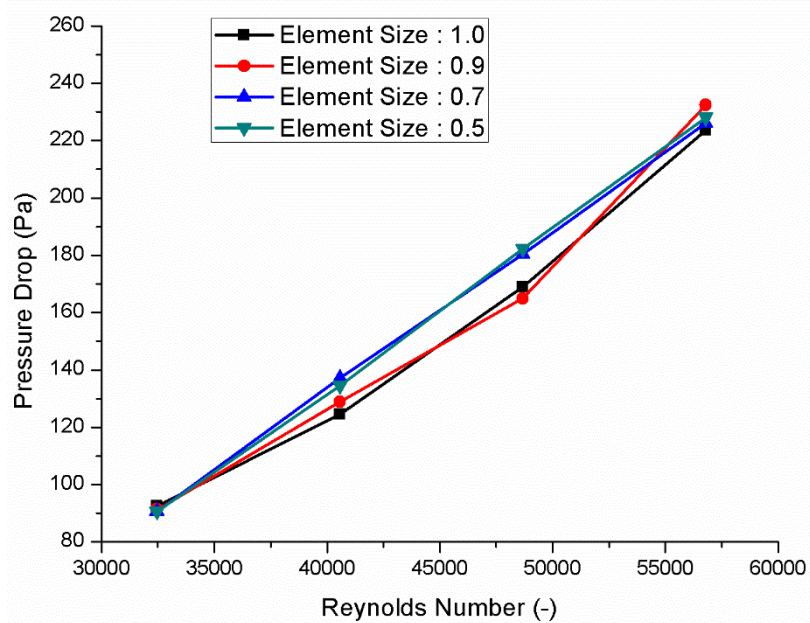


Figure 4.6 Pressure drop for various element sizes in the HTS cable with triangular corrugation

4.2 Validation

In this section, the effect of various turbulence models available with CFD package software on friction factor and Nusselt number was evaluated using computer simulations. Five popular representatives of two-equation turbulence models (RANS) were investigated as shown in Figure 4.7. The ($k-\varepsilon$) realizable turbulence model [72], [75], [76], [86]–[91] has an extra benefit of improved performance for the complex flow involving swirl/vortices/rotation, adverse pressure gradient, flow separation and recirculation. Since, the turbulent characteristics such as swirl, separation and recirculation may be expected in the LN₂ flowing through the corrugated pipes (inner and annular) due to the irregular shape of corrugations. Therefore, $k-\varepsilon$ realizable turbulence model is reported as the most suitable turbulence model to encounter such turbulent characteristics [92],[93]. Furthermore, the estimated pressure drop for the present work was verified by comparing with the experimental data available for a parallel flow HTS system, fabricated in NEDO project and numerically investigated by Maruyama et al. [50]. The result of the comparison is summarized in Figure 4.9. Analyzing the pressure drop with constant and temperature dependent thermophysical properties in counter flow cooling system of HTS cable, it was found that the pressure drop (Pa/m) in the present work (counter flow cooling system) is quite larger than the parallel flow cooling system Figure 4.11 represents the validation of pressure drop

estimated numerically for the counter flow cooling system with the experimental and calculated data available for parallel cooling system of HTS cable. It can be clearly seen from the results that pressure drop for the present work is almost ten times larger than the parallel flow cooling system (computed annular region only). The large pressure drop in the counter flow cooling system may be due to the turbulence occurred in both inner corrugated pipe and outer corrugated pipe of HTS cable.

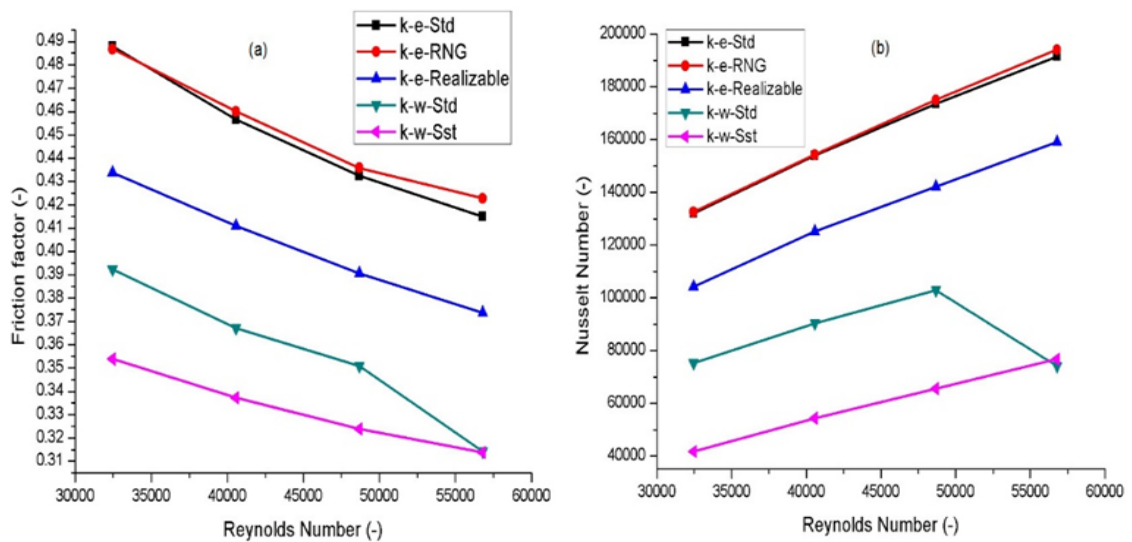


Figure 4.7 Comparison of various turbulence models available with CFD in the estimation of (a) friction factor at different Reynolds number (b) Nusselt number at different Reynolds number

4.2.1 Various corrugation topology

The results show the validation of friction factors at various Reynolds numbers computed by Sasaki et al. (annulus flow through centrally placed smooth pipe enveloped by a corrugated pipe) with the present work (employing counter flow through corrugated pipes placed centrally as well as externally) and the Colebrook-White equation for the circular rough pipes. Single flow through straight and corrugated pipe, counter flow through corrugated pipes (present work) and flow through rough circular pipes have different friction factors due to the variation in the shape of the pipe wall surfaces. Moreover, the friction factors follow the reduced trend at Reynolds numbers ranges from 5×10^3 to 30×10^3 as concluded in the Figure 4.8. So far, no correlation is established for the calculation of friction losses in the corrugated annular pipe. Therefore, the foremost reason for the high friction factor in the HTS cable of different corrugation topologies [94]–[100], is due to the combined effect of LN2

interaction with the walls of inner corrugated pipe and outer (annular) corrugated pipe simultaneously [71].

Moreover, The results obtained from the present computational investigation are validated with the experimental results computed by Li et al. [49] (annulus flow through centrally placed smooth pipe enveloped by a corrugated pipe) with the present work (employing counter flow through corrugated pipes placed centrally as well as externally). The results show that the topology of corrugation would affect the friction factors at various Reynolds numbers. Moreover, the friction factors found to be reduced at higher Reynolds numbers ranges as can be observed in the Figure 4.10.

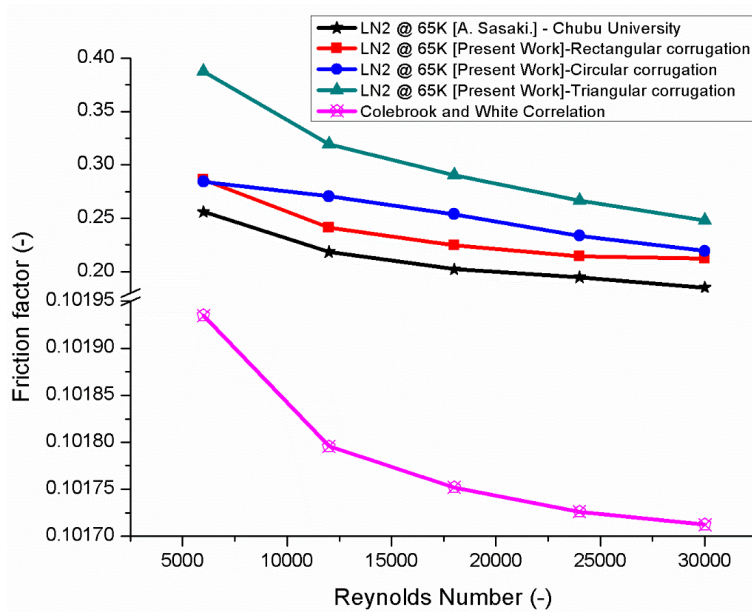


Figure 4.8 Validation of friction factor from present investigation with those of existing correlations [101] and result obtained by Sasaki et al

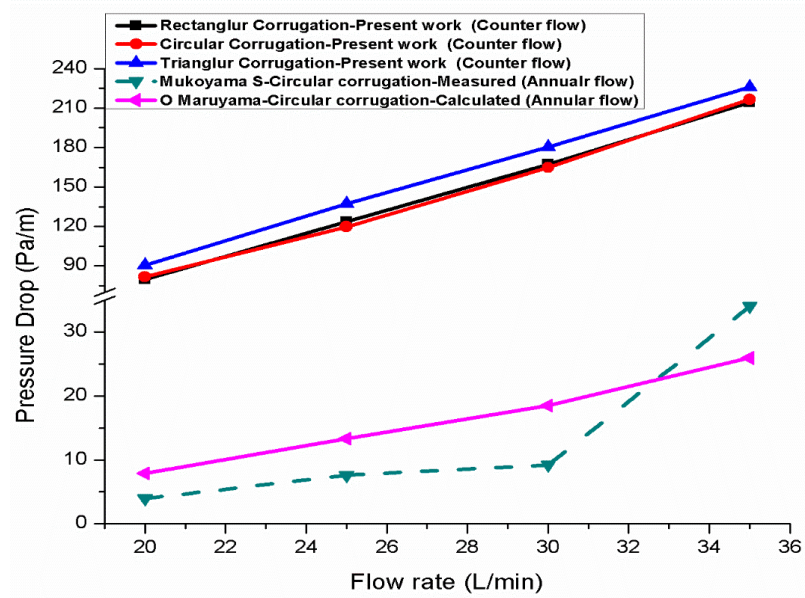


Figure 4.9 Validation of obtained pressure drop (present work) with experimental results performed by Mukoyama S et al. and calculated results by O Maruyama et al. [50]

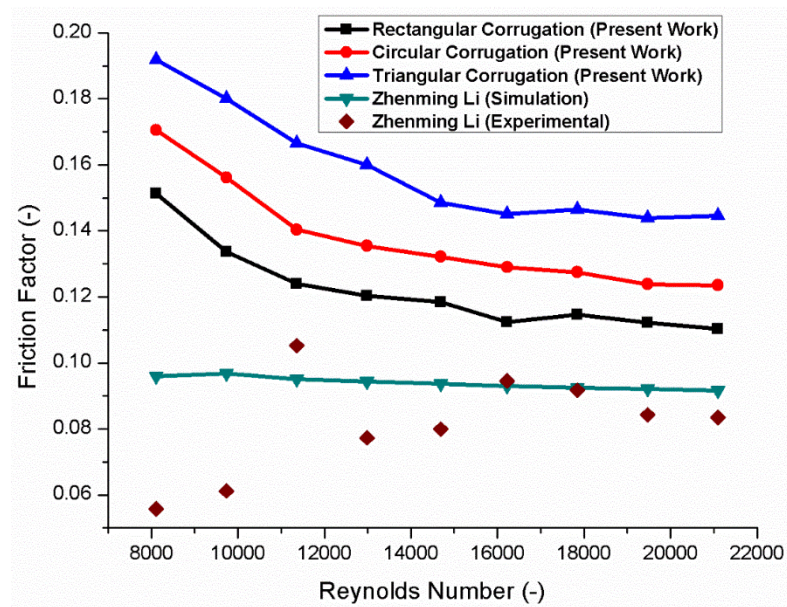


Figure 4.10 Validation of friction factor from present investigation with experimental results obtained by Li et al. [49]

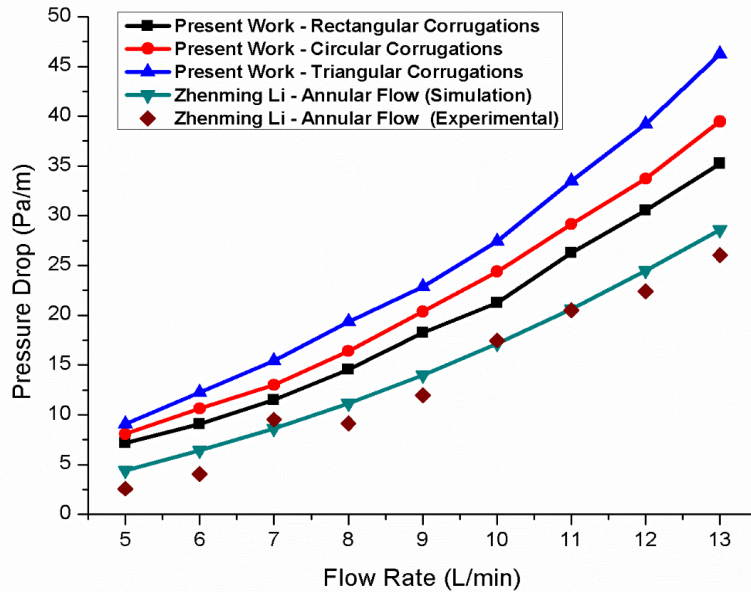


Figure 4.11 Validation of obtained pressure drop (present work) with experimental and simulation results performed by Li et al. [49]

Analyzing the pressure drop in counter cooled HTS cable of different corrugations, it was found that the pressure drop (Pa/m) in the present work (counter flow cooling system) is quite larger than the single flow cooling system. Figure 4.11 represents the validation of pressure drop estimated computationally for the counter cooled HTS cable with the experimental and calculated data available for Single (annular) flow cooling system of HTS cable. It can be clearly seen from the results that pressure drop for the present work is significantly larger than the single (annular) flow cooling system. The large pressure drop in the counter flow cooling system is due to the expected turbulent characteristics such as swirl, separation and recirculation in the LN₂ flowing through the different shaped corrugated pipes (inner and annular).

4.3 Velocity Distribution in HTS Cables

In order to investigate the velocity distribution in the HTS cable, the computational method is adopted. This section presents the combined effect of heat flux, heat generation and various corrugation topologies on the velocity distribution of LN₂ in the HTS cable. Velocity distribution of LN₂ in the HTS cable will be significantly affected due to the corrugation geometries only.

4.3.1 Effect of Heat Flux on Velocity Distribution

The velocity profiles of all three corrugation shapes in inner region and annular region at 0.150m from the inlet of the HTS cable are shown in Figure 4.12. The velocity profile

of LN2 at different locations in the circular corrugation HTS cable are shown separately in Figure 4.13 (a, b) The triangular corrugation shaped HTS cable has attained a maximum velocity of 0.44m/s at the axis of the model. The negative sign indicates the direction of flow in the annular region of the HTS cable and the maximum velocity attained in this region is 0.2m/s. It can be seen from the results that fully developed velocity profiles are not observed as also reported earlier [71]. In order to achieve the fully developed flow at inlet in the HTS cable, the domain needs to extend up to a distance called entry length. The estimated entry lengths for each Reynolds numbers are compiled in Table 3-3.

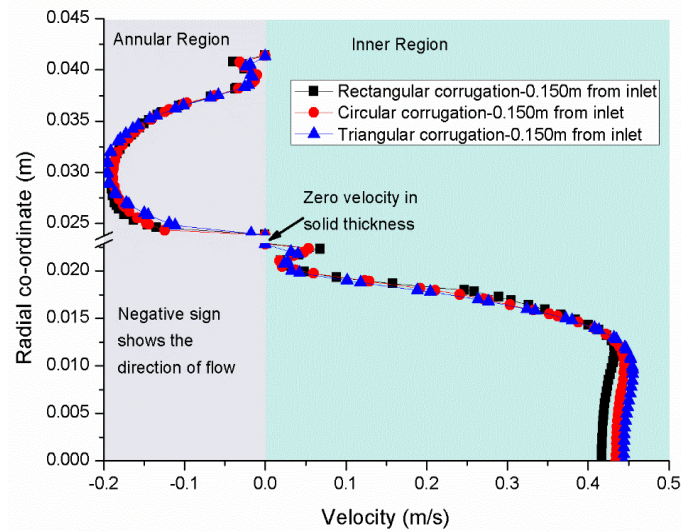


Figure 4.12 Effect of heat flux on radial velocity distribution with all three corrugation topologies at constant heat flux of 6 W/m^2 with

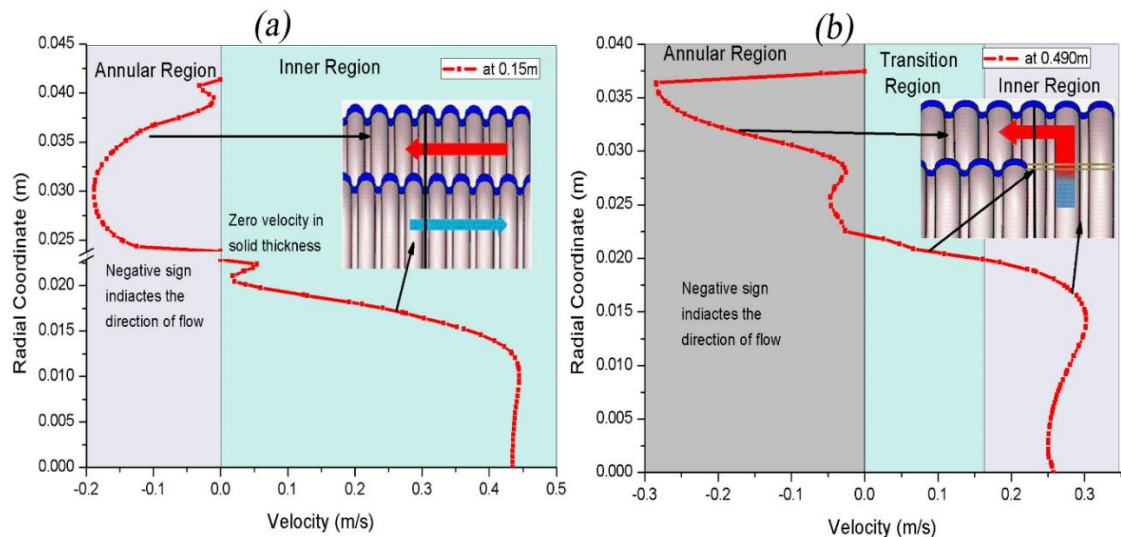


Figure 4.13 Velocity distribution in the circular corrugated steel pipe with a flow rate of 25 L/min and constant heat flux of 6 W/m^2 at (a) at 0.15m and (b) at 0.49m from inlet

4.3.2 Effect of A.C Loss on Velocity Distribution

Figure 4.14 shows the effect of various corrugation topologies and heat generation on the obtained velocity profile in the counter cooled HTS cable. Moreover, the velocity profile of LN2 at different locations in the circular corrugation HTS cable are shown separately in Figure 4.15 (a, b). It can be observed from the results that there is no significant difference between effect of heat flux and heat generation on the velocity distribution in the HTS cable. However, a significant difference between the velocities of all three corrugation topologies is observed. The maximum velocity of 0.44 m/s in the inner region of triangular corrugation shape HTS cable is observed. Therefore, the present analysis concludes that the hydraulic performance of counter cooled HTS cable is independent of heat flux or heat generation.

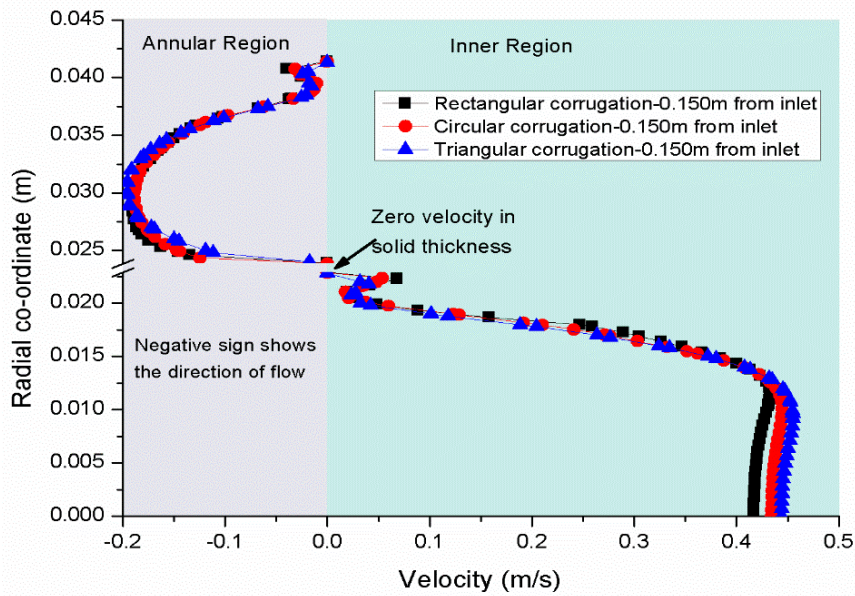


Figure 4.14 Effect of A.C loss on radial velocity distribution with all three corrugation topologies at constant heat generation of 800 W/m^3

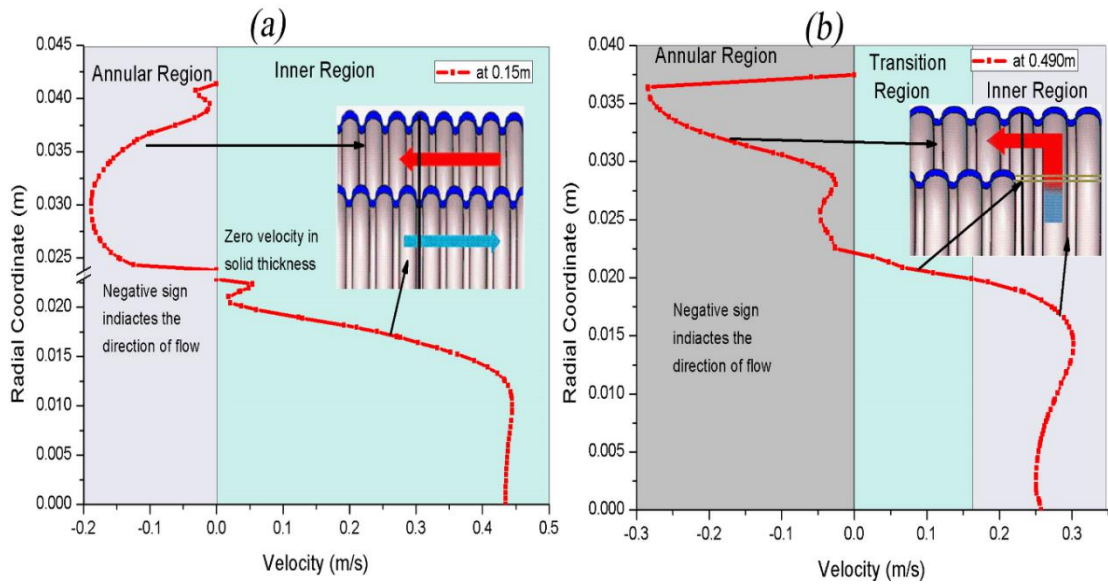


Figure 4.15 Velocity distribution in the circular corrugated steel pipe with a flow rate of 25 L/min and constant heat generation of 800 W/m^3 (a) at 0.15m and (b) at 0.49m from inlet

4.3.3 Effect of LN2 temperature on Velocity Distribution

The effect of several LN2 inlet temperatures from 65K to 70K on radial velocity distribution profile in circular corrugation shape HTS cable is discussed in Figure 4.16. The velocity profiles are obtained using computer simulations at the location of 0.15m away from the inlet with boundary conditions as heat flux of 4 W/m^2 and heat generation of 800 W/m^3 . The left side grey shaded region represents the return flow through annular region with a maximum velocity of 0.16 m/s . However, the right side cyan shaded region shows the inner flow through inner corrugated pipe with a maximum velocity of 0.43 m/s at inlet temperature of 70K. The results depicts that the fully developed velocity profiles are not observed. Therefore, in order to achieve the fully developed flow at the inlet of the modeled HTS cable domain, the domain needs to extend up to a distance called entry length. The estimated entry lengths for each Reynolds numbers are compiled in Table 3-3

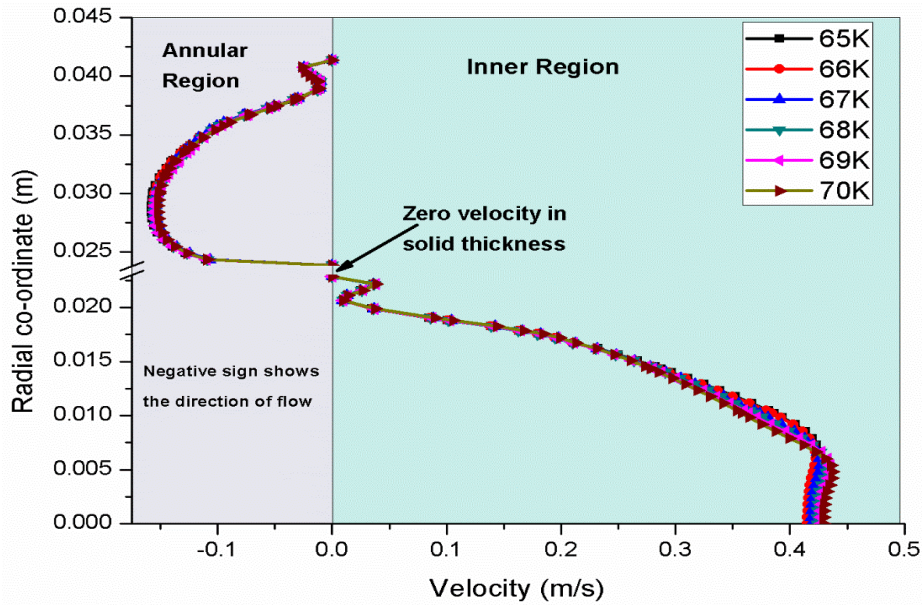


Figure 4.16 Effect of coolant inlet temperature on velocity distribution with heat flux of 4 W/m^2 and heat generation of 800 W/m^3 at 0.150 m at the inlet

4.4 Pressure Drop in HTS Cables

The method adapted to investigate the pressure drop is computational which involves, developing a computational geometry reflecting the flow domain of cryogen fluid, imposing the boundary conditions on the geometry matching with the practical conditions and obtaining the solution by solving the governing transport equations. The present research work is aimed at investigating the combined effect of cryogenic fluid, heat flux, heat generation and different corrugation geometries on pressure drop using computational fluid dynamics (CFD). Pressure drop will be significantly affected due to the turbulence in the cryogenic fluid, friction among the fluid and walls of corrugated pipes different geometries.

4.4.1 Effect of Heat Flux on Pressure Drop

The combined effect of various corrugation topologies (rectangular, circular and triangular), heat flux at constant heat generation of 800 W/m^3 on pressure drop is presented in this section. Figure 4.17, Figure 4.18 and Figure 4.19 shows that the pressure drop increases with increase in the volumetric flow of LN₂ in the HTS cable with rectangular, circular and triangular corrugation respectively. It is observed that pressure drop does not vary at various heat fluxes for each corrugation topology. However, the larger pressure drop is found in the HTS cable with triangular corrugation

corrugated pipe due to the boundary layer separation and more vortices. The value of maximum pressure drop in the triangular corrugation HTS cable is found to be 227 Pa/m at volumetric flow rate of 35L/min. The separation of boundary layer and reattachment occurs for an instance due to the continuation of upper and lower corrugations in both the regions of the HTS cable. The continuation of boundary layer separation in the corrugations increase the boundary layer thickness which leads to an additional resistance and flow reversal. An adverse pressure gradient produces vortices and eddies, results in the formation of turbulence and more pressure drop across the flow.

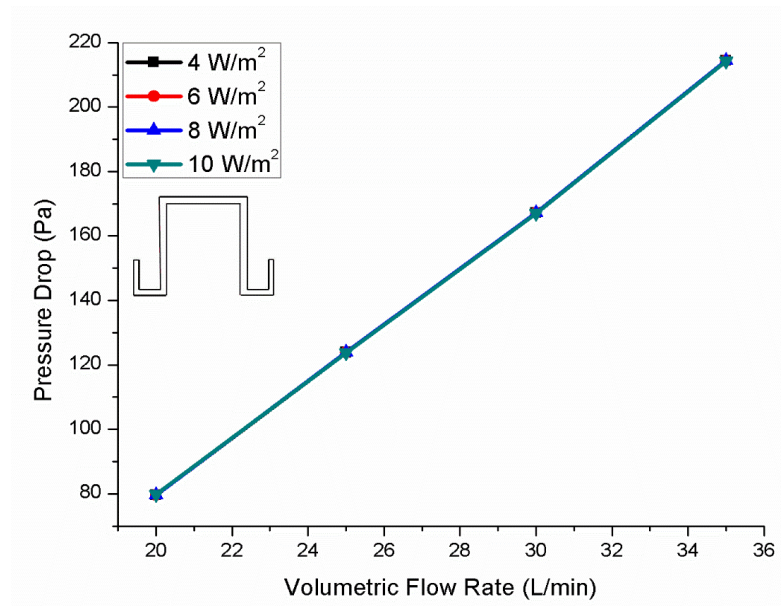


Figure 4.17 Effect of heat flux on pressure drop at constant heat generation of 800 W/m³ with rectangular corrugation

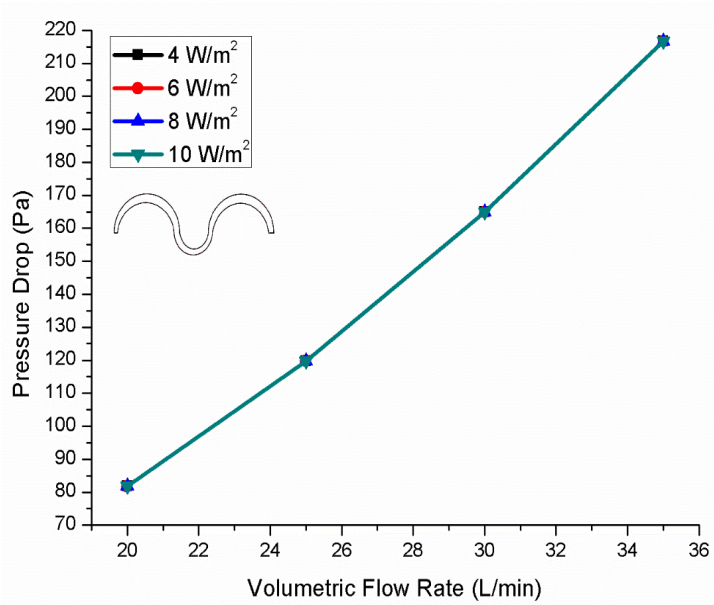


Figure 4.18 Effect of heat flux on pressure drop at constant heat generation of 800 W/m^3 with circular corrugation

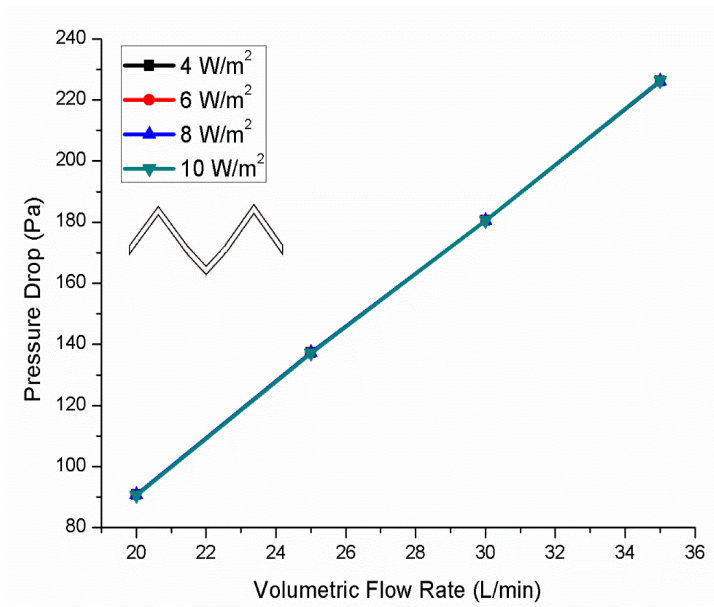


Figure 4.19 Effect of heat flux on pressure drop at constant heat generation of 800 W/m^3 with triangular corrugation

4.4.2 Effect of A.C Loss on Pressure Drop

The combined effect of various corrugation topologies (rectangular, circular and triangular), heat generation at constant heat flux of 6 W/m^2 on pressure drop is presented in Figure 4.20, Figure 4.21 and Figure 4.22. The results reveal that there is no significant difference between the effect of the heat flux and heat generation on the pressure drop of turbulent LN₂ in the HTS cable. Therefore, it is concluded that the pressure drop due

to the turbulent flow of LN2 in the counter cooled HTS cable is independent of heat flux or heat generation.

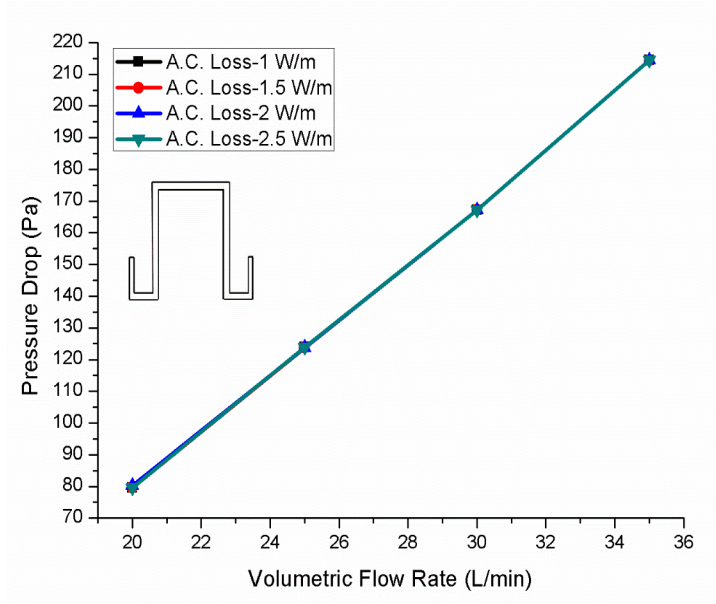


Figure 4.20 Effect of A.C loss on pressure drop at constant heat flux of 6 W/m^2 with rectangular corrugation

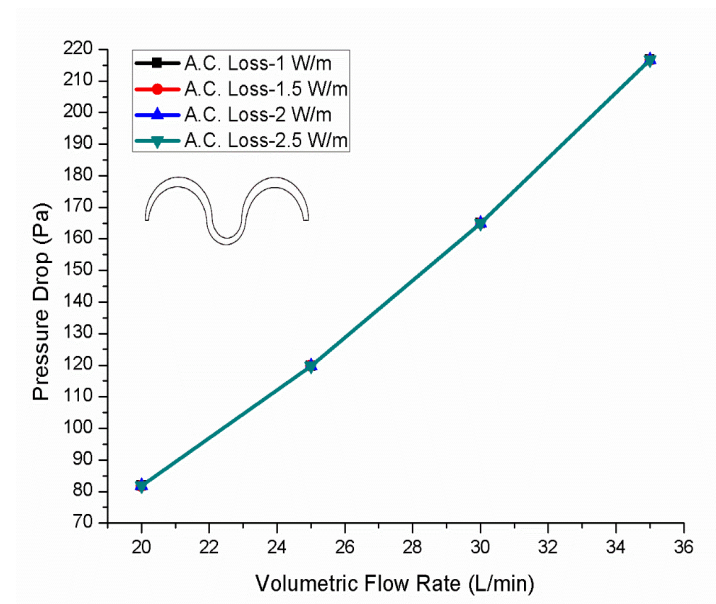


Figure 4.21 Effect of A.C loss on pressure drop at constant heat flux of 6 W/m^2 with circular corrugation

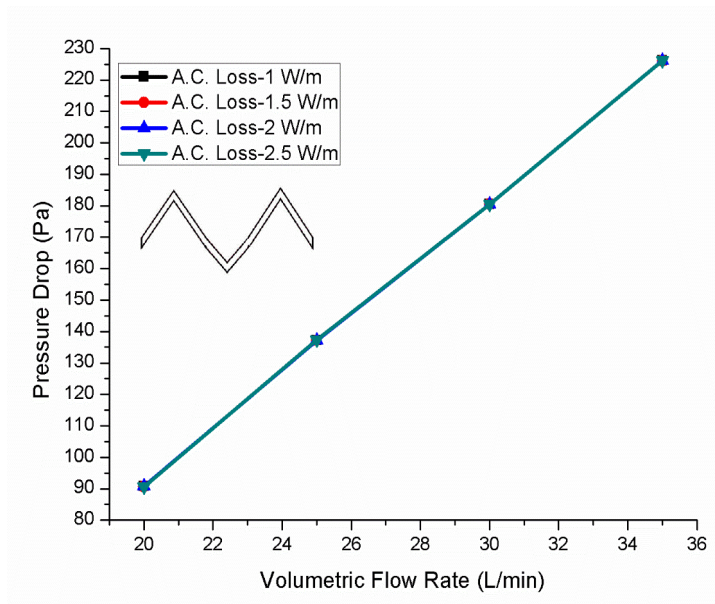


Figure 4.22 Effect of A.C loss on pressure drop at constant heat flux of 6 W/m^2 with triangular corrugation

4.4.3 Effect of LN2 temperature on Pressure Drop

The effect of LN2 inlet temperatures from 65K to 70K on the pressure drop in circular corrugation shape HTS cable is discussed in Figure 4.23. The pressure drop follows the increasing trend at different volumetric flow rates of 20L/min to 35L/min. A significant effect of varying LN2 inlet temperature on pressure drop is observed from the results. It is also observed that the pressure drop in the HTS cable reduces significantly with increase in the LN2 inlet temperature. Therefore, it is concluded that higher will be the inlet temperature of LN2, lower will be the pressure drop in the HTS cable.

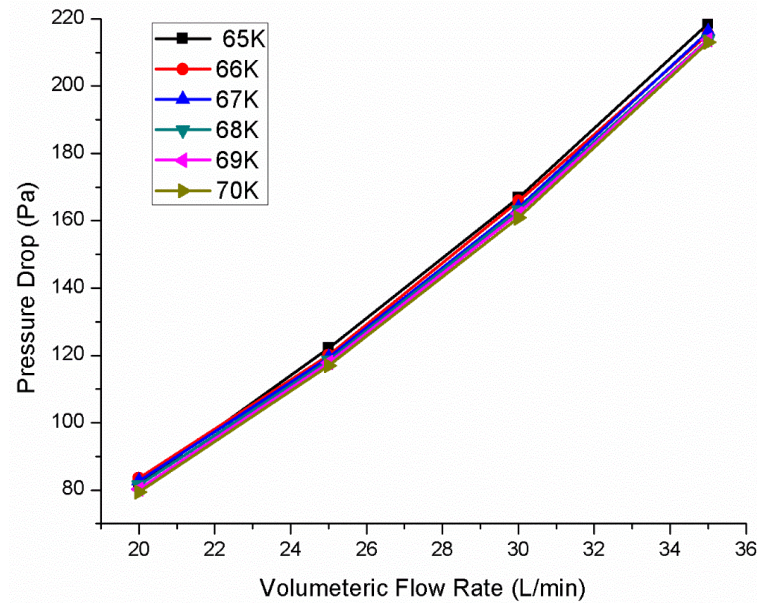


Figure 4.23 Effect of coolant inlet temperature on pressure drop at heat flux of 4 W/m^2 and heat generation of 800 W/m^3

4.5 Pumping Power through HTS Cables

In order to flow the LN2 through inner corrugated pipe and outer corrugated in the HTS cable, pump is required and the power of pump is calculated using (23). Pumping power is given in terms of pressure drop across the HTS cable and the volume flow rate of LN2. The rise in pumping power is mainly due to the friction between the LN2 and the walls of the corrugated pipe. In order to estimate the pumping power in the HTS cable, the pressure rise must be calculated accurately. The estimation of pressure drop in the HTS cable is discussed in the section 5.4.

4.5.1 Effect of Heat Flux on Pumping Power

The combined effect of various corrugation topologies (rectangular, circular and triangular), heat flux at constant heat generation of 800 W/m^3 on pumping power is presented in this section to describe the hydraulic behavior of LN2. The pumping power follows the increasing trend at various volumetric flow rates for rectangular corrugation, circular corrugation and triangular corrugation as can be seen in Figure 4.24, Figure 4.25 and Figure 4.26 respectively. It is concluded that in triangular corrugation shape counter cooled HTS cable, higher pumping power requires to circulate the liquid nitrogen as compared to rectangular and circular corrugation. Moreover, the pumping power in all the corrugation shaped HTS cable for various heat

fluxes will be quite similar at different flow rates. The highest pumping power in triangular corrugation shaped HTS cable is found to be 0.1325 W at the volumetric flow rate of 35 L/min.

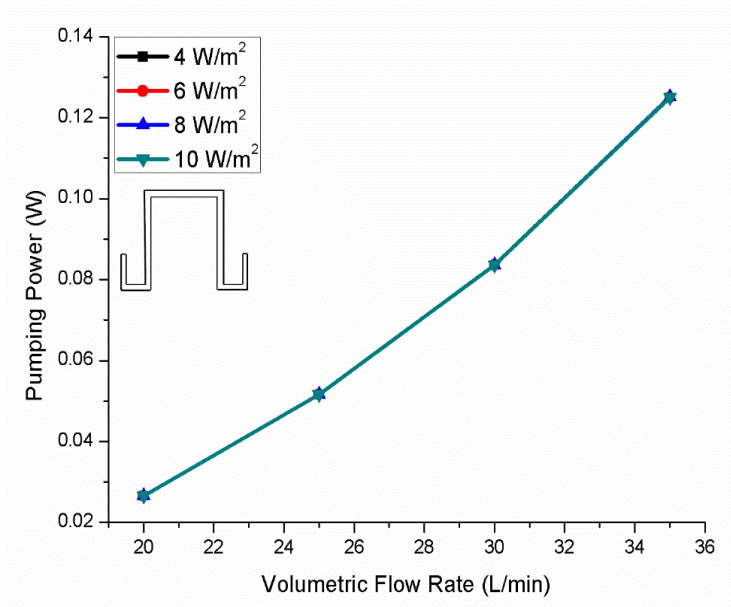


Figure 4.24 Effect of heat flux on pumping power at constant heat generation of 800 W/m³ with rectangular corrugation

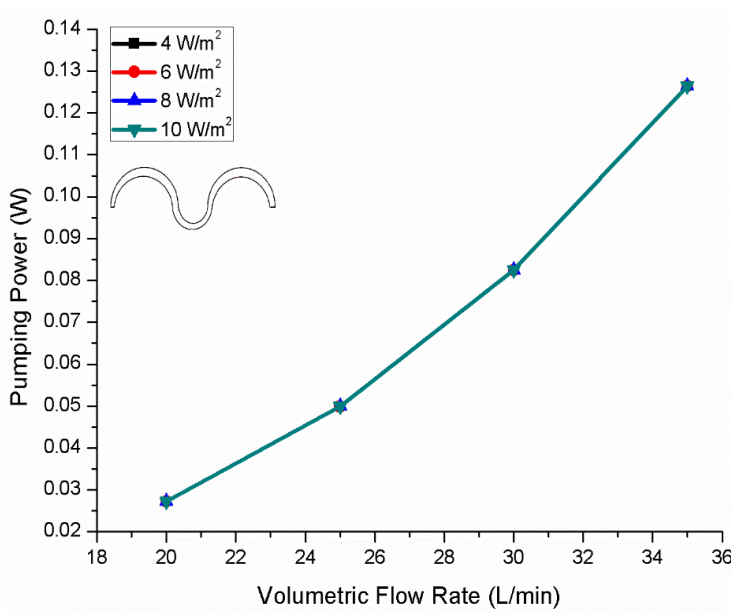


Figure 4.25 Effect of heat flux on pumping power at constant heat generation of 800 W/m³ with circular corrugation

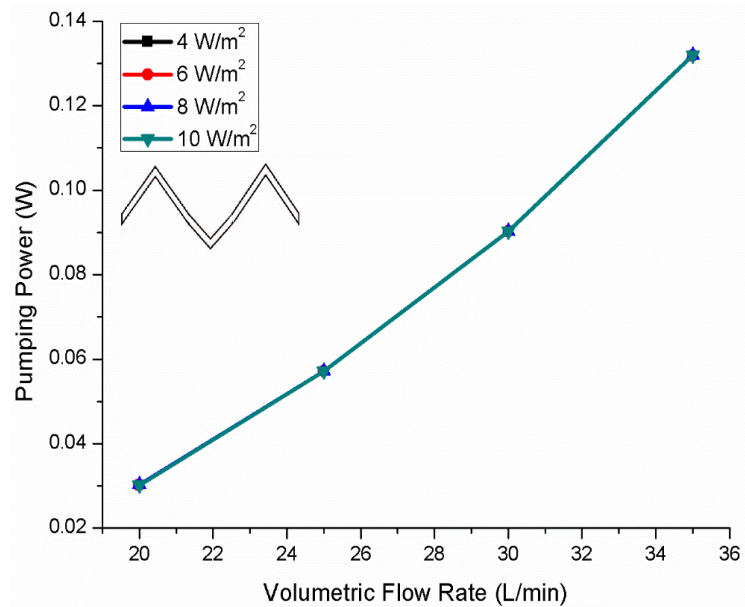


Figure 4.26 Effect of heat flux on pumping power at constant heat generation of 800 W/m^3 with triangular corrugation

4.5.2 Effect of A.C Loss on Pumping Power

The combined effect of various corrugation topologies (rectangular, circular and triangular) and heat generation at constant heat flux of 6 W/m^2 on pumping power is dedicated in Figure 4.27, Figure 4.28 and Figure 4.29. The results reveal that there is no significant difference between the effect of the heat flux and heat generation on the pumping power of turbulent LN2 in the HTS cable. Therefore, it is concluded that the pumping power due to the turbulent flow of LN2 in the counter cooled HTS cable is independent of heat flux or heat generation.

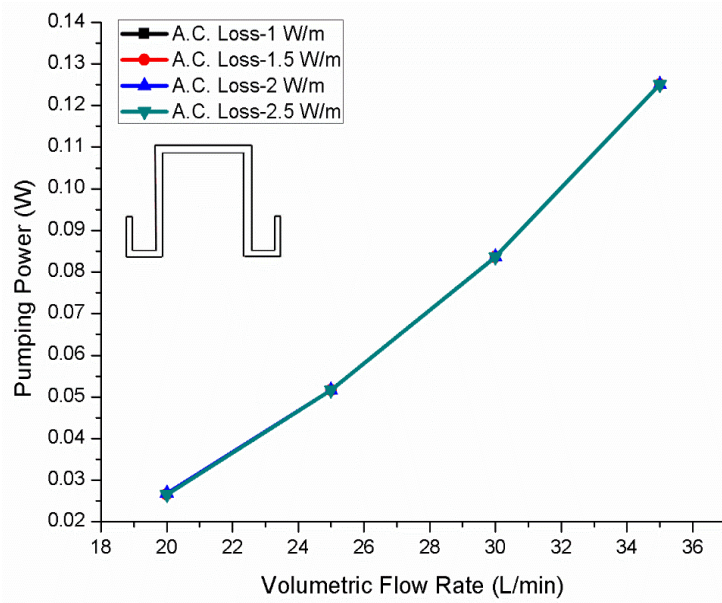


Figure 4.27 Effect of A.C loss on pumping power at constant heat flux of 6 W/m^2 with rectangular corrugation

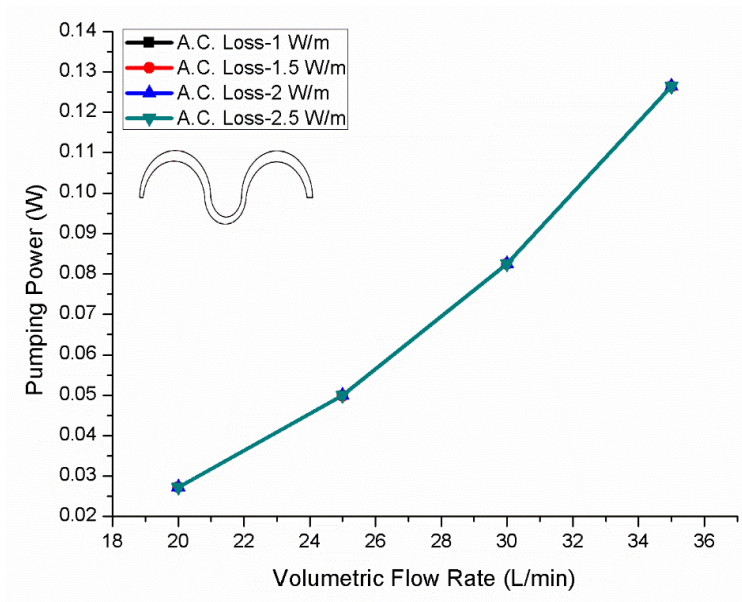


Figure 4.28 Effect of A.C loss on pumping power at constant heat flux of 6 W/m^2 with circular corrugation

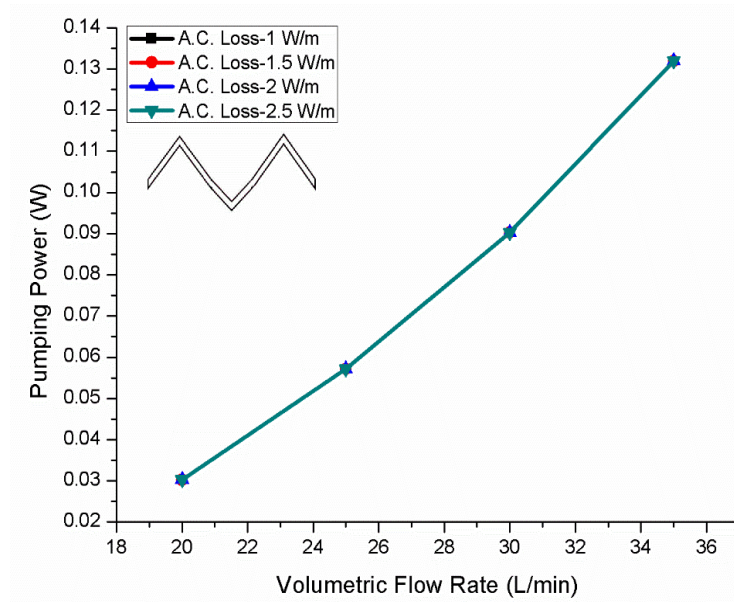


Figure 4.29 Effect of A.C loss on pumping power at constant heat flux of 6 W/m^2 with triangular corrugation

4.5.3 Effect of LN2 temperature on Pumping Power

Figure 4.30 shows the effect of LN2 inlet temperatures from 65K to 70K on the pumping power required to circulate the LN2 in circular corrugation shape HTS cable. With increase in the volumetric flow rate, the required pumping power to the HTS cable increases. However, the pumping power reduces with increase in the LN2 inlet temperature from 65K to 70K. The minimum pumping power of 0.025W is observed at the maximum inlet temperature of 70 K. Therefore, a small and significant effect of LN2 inlet temperature on pumping power is observed.

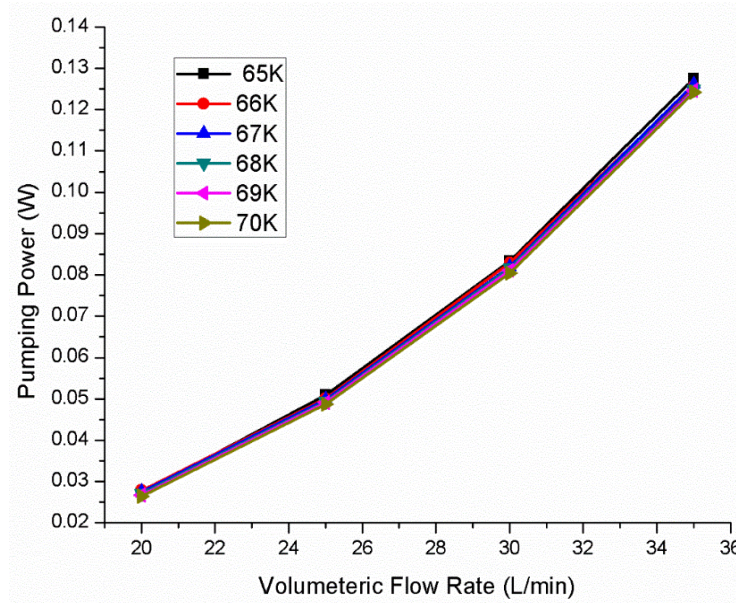


Figure 4.30 Effect of coolant inlet temperature on pumping power at heat flux of 4 W/m^2 and heat generation of 800 W/m^3

4.6 Friction Factors in HTS Cables

The combined effect of various corrugation topologies (rectangular, circular and triangular), heat flux and heat generation on friction factor is presented in this section. The friction factors are used for calculating the pressure losses in the HTS cable to describe the hydraulic behavior of LN2. Since, there is no such option of estimating the friction factor directly using computational method, thereby, the obtained value of pressure drop from CFD is substituted into eq. (24).

4.6.1 Effect of Heat Flux on Friction Factor

The pressure drop behavior in terms of friction factor in the HTS cable with various corrugation shapes for the Reynolds number range of 30,000–60,000 is displayed in Figure 4.31, Figure 4.32 and Figure 4.33. The results show that the topology of corrugation would affect the friction factors at various Reynolds numbers. Moreover, the friction factors found to be reduced at higher Reynolds numbers ranges are observed from the results. In addition, the friction factor seems quite similar at all the heat flux ranges from 4 W/m^2 to 10 W/m^2 . Consequently, it is concluded from the results that the friction factor for the triangular corrugation is significantly high as compared with the rectangular and circular corrugations. The key reason for the higher friction factor in the HTS cable of different corrugation topologies, is due to the combined effect of LN2

interaction with the walls of inner corrugated pipe and outer (annular) corrugated pipe simultaneously [71]. The maximum friction factor in the triangular shaped counter cooled HTS cable is found to be 0.2380 at Reynolds number of 32500.

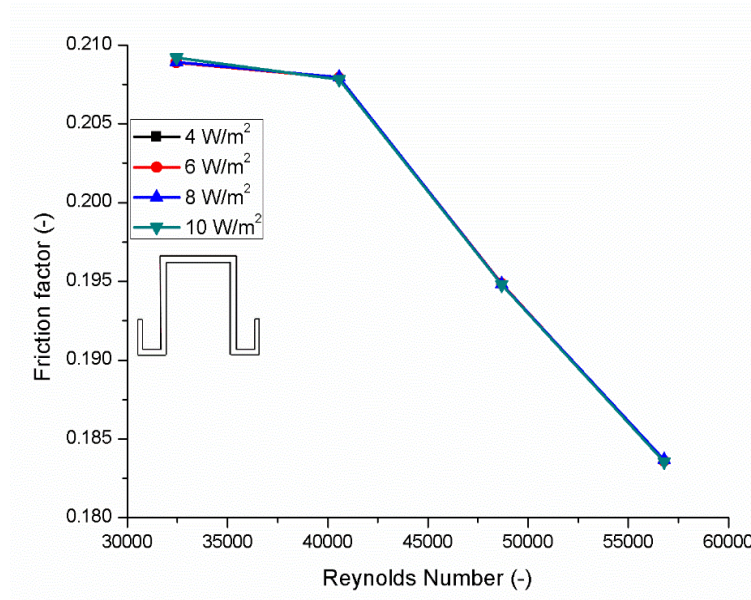


Figure 4.31 Effect of heat flux on friction factor at constant heat generation of 800 W/m^3 with rectangular corrugation

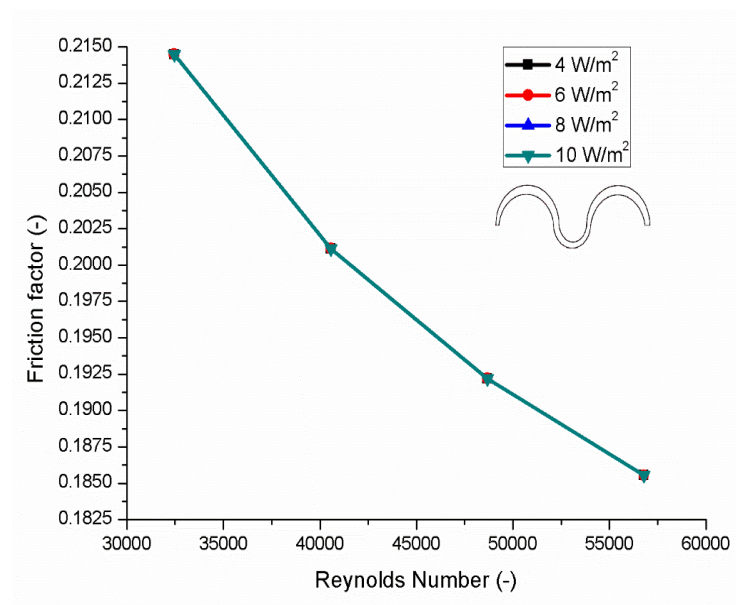


Figure 4.32 Effect of heat flux on friction factor at constant heat generation of 800 W/m^3 with circular corrugation

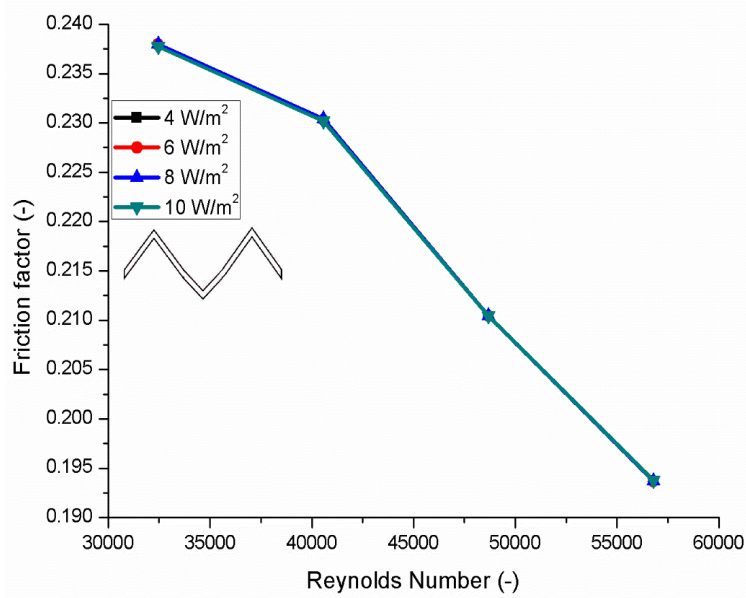


Figure 4.33 Effect of heat flux on friction factor at constant heat generation of 800 W/m^3 with rectangular corrugation

4.6.2 Effect of A.C Loss on Friction Factor

The combined effect of various corrugation topologies (rectangular, circular and triangular) and heat generation at constant heat flux of 6 W/m^2 on friction factor is dedicated in Figure 4.34, Figure 4.35 and Figure 4.36. The results reveal that there is no significant difference between the effect of the heat flux and heat generation on the friction factor of turbulent LN2 in the HTS cable. Therefore, it is concluded that the friction factor due to the turbulent flow of LN2 in the counter cooled HTS cable is independent of heat flux or heat generation.

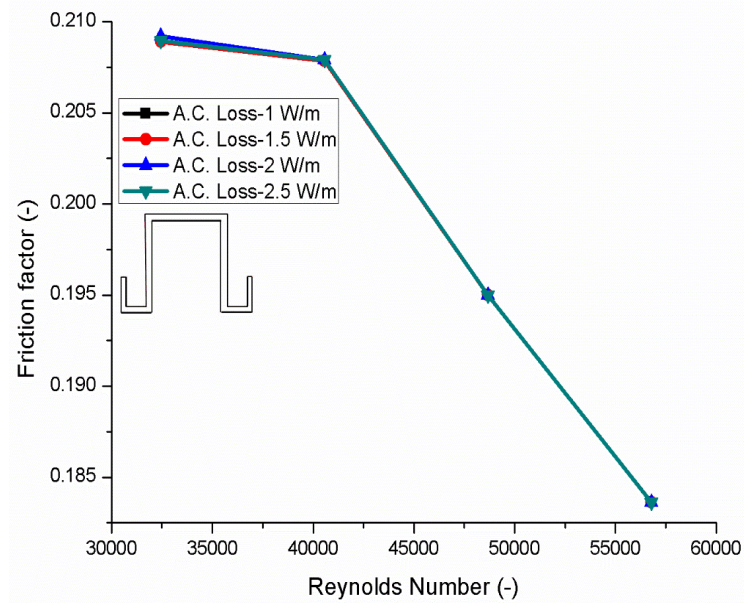


Figure 4.34 Effect of A.C loss on friction factor at constant heat flux of 6 W/m^2 with rectangular corrugation

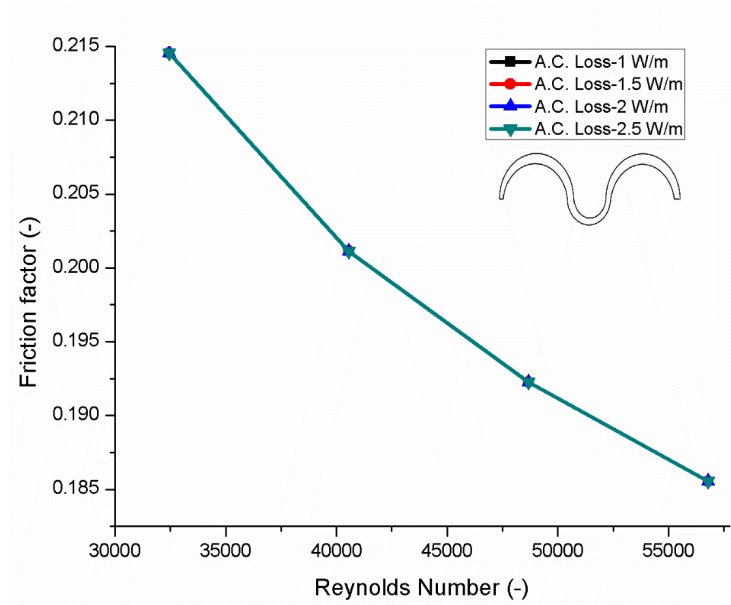


Figure 4.35 Effect of A.C loss on friction factor at constant heat flux of 6 W/m^2 with circular corrugation

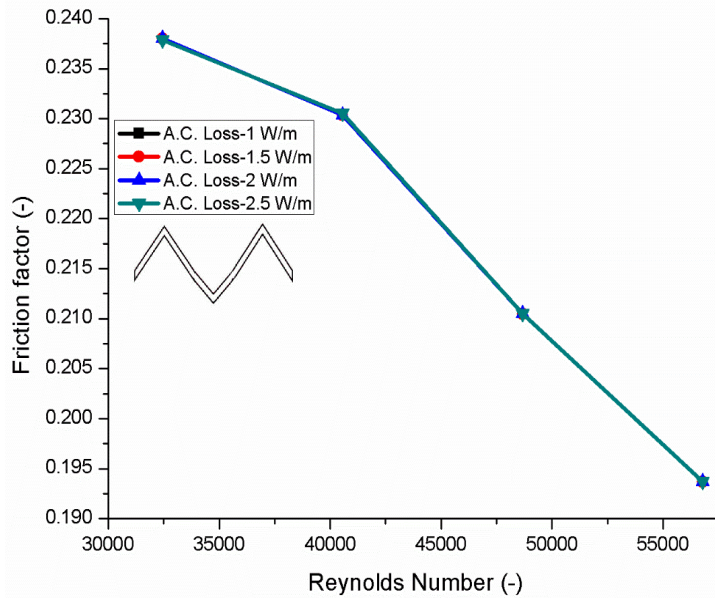


Figure 4.36 Effect of A.C loss on friction factor at constant heat flux of 6 W/m^2 with triangular corrugation

4.6.3 Effect of LN2 temperature on Friction Factor

Figure 4.37 illustrates the effect of LN2 inlet temperatures from 65K to 70K on the friction factor in the circular corrugation shape HTS cable. It can be seen from the results that friction factor reduces with increase in the Reynolds number ranges from 32500 to 57500. Similarly, it is also observed that the friction factor reduces significantly with increase in LN2 inlet temperatures from 65K to 70K. Finally, it is concluded that the hydraulic characteristics such as pressure drop, pumping power and friction factor reduce significantly with increase in the LN2 inlet temperature.

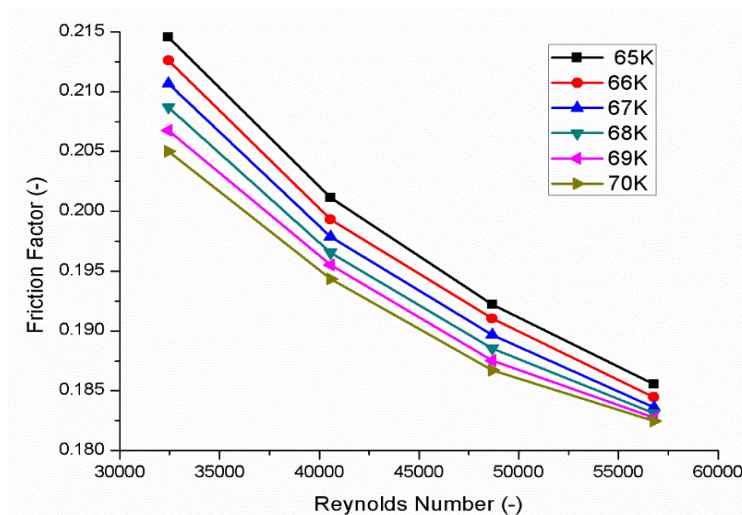


Figure 4.37 Effect of coolant inlet temperature on friction factor at heat flux of 4 W/m^2 and heat generation of 800 W/m^3

4.6.4 Correlation for Friction Factor applicable to Flow through Corrugated Pipe

In order to show the degree of relationship between Reynolds number and friction factor for various corrugation shaped HTS cable, a single correlation is obtained from the fitting of nonlinear curves and compiled in Table 4-4, Table 4-5 and Table 4-6. The correlation is computed among non-linearity scale on data for several heat fluxes and A.C losses. The novelty of the developed friction factor correlation for various corruption topologies is that minimum number of correlation coefficients are sufficient to express the correlation unlike the polynomial correlation. The accuracy of the developed friction factor correlation for various corruption topologies is found to be statistically significant as 99% as can be seen from R^2 values.

Table 4-4 Correlation for friction factors at various heat flux and A.C loss in circular corrugation shape HTS cable


		Correlation Coefficients			Correlation	R^2 Value
			a_c	b_c		
	32446<Re<56781	Heat-in-	4	3.19365	$f = a_c(Re)^{b_c}$	0.99579
		Leak	6	3.19358		0.99579
		(W/m ²)	8	3.19361		0.99579
			10	3.19343		0.99579
	A.C.	1	3.20438	-0.26053	$f = a_c(Re)^{b_c}$	0.9958
		Losses	1.5	3.20435		0.9958
		(W/m)	2	3.20435		0.9958
			2.5	3.20434		0.9958

Table 4-5 Correlation for friction factors at various heat flux and A.C loss in rectangular corrugation shape HTS cable

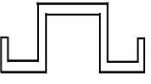

		Correlation Coefficients			Correlation	R^2 Value
			a_c	b_c		
	40500<Re<56781	Heat-in-	4	10.07498	$f = a_r(Re)^{b_r}$	0.99871
		Leak	6	10.41849		0.99897
		(W/m ²)	8	10.30139		0.99924
			10	10.31484		0.99897
	A.C.	1	10.34833	-0.3682	$f = a_r(Re)^{b_r}$	0.99895
		Losses	1.5	10.19862		0.99813
		(W/m)	2	10.28788		0.99836
			2.5	10.30811		0.99831

Table 4-6 Correlation for friction factors at various heat flux and A.C loss in triangular corrugation shape HTS cable

		Correlation Coefficients			Correlation	R^2 Value
			a_c	b_c		
	40500<Re<56781	Heat-in-	4	53.56184	$f = a_t(Re)^{b_t}$	0.99884
		Leak	6	53.22535		0.99881
		(W/m ²)	8	53.85002		0.99903
			10	51.41952		0.99888
	A.C.	1	52.94277	-0.51239	$f = a_t(Re)^{b_t}$	0.99873
		Losses	1.5	53.61333		0.99884
		(W/m)	2	53.61296		0.99884
			2.5	54.72343		0.99901

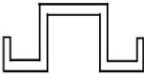


4.7 Summary and Conclusions

Firstly, in this chapter, the effect of various turbulence models available with CFD package software on friction factor and pressure drop was evaluated using computer simulations. Five popular representatives of two-equation turbulence models (RANS) were investigated. The $k-\varepsilon$ realizable turbulence model has an extra benefit of improved performance for the complex flow involving swirl/vortices/rotation, adverse pressure gradient, flow separation and recirculation. Since, the turbulent characteristics such as swirl, separation and recirculation were observed in the LN2 flowing through the corrugated pipes (inner and annular) due to the irregular shape of corrugations. Therefore, $k-\varepsilon$ realizable turbulence model is reported as the most suitable turbulence model to encounter such turbulent characteristics [92], [93].

The influence of various heat fluxes, heat generation and LN2 inlet temperature on the pressure drop was also evaluated by CFD simulations based on the solution of the RANS equations in order to describe the hydraulic behavior of LN2 with counter flow cooling system. Moreover, the hydraulic characteristics of turbulent LN2 flow in counter cooled HTS cable with various corrugation (rectangular, circular and triangular) topologies are computationally investigated. Fluid flow and pressure drop across the long length cold dielectric counter cooled High Temperature Superconducting (HTS) cables are significantly influenced by the different corrugation topologies. In addition, the velocity and pressure distribution of liquid nitrogen (LN2) in the HTS cable with various corrugations are also estimated and presented. Finite volume method is adapted to solve the governing equations (continuity, momentum and energy) using Semi-Implicit Pressure Linked Equations (SIMPLE) scheme with $k-\varepsilon$ turbulence model and enhanced wall treatment. The results reveal that the corrugation topologies (rectangular, circular and triangular) have significant effect on pressure drop. Pressure drop in the triangular corrugation shaped HTS cable is significantly larger than the circular and rectangular corrugation due to the higher intensity of the vortices appearing in the both inner and annular region as compiled in Table 4-7. The corrugated pipes with different topologies exhibit different friction factors due to the variations in the contact of wall surfaces with the LN2. Moreover, the calculated friction factors for all the three corrugation topologies are compared with the experimental

results available in the literature. In addition, the obtained friction factor for the present work is significantly larger due to the counter flow arrangement with corrugated pipes. Finally, it is concluded from the effect of LN2 inlet temperature that the hydraulic characteristics such as pressure drop, pumping power and friction factor reduce significantly with increase in the LN2 inlet temperature.

Table 4-7 Comparison of hydraulic characteristics with various corrugations

Corrugation	Pressure Drop (ΔP) (Pa/m)	Pumping Power (W)	Friction Factor (-)
	215	0.1255	0.209
	217	0.1260	0.2145
	226	0.1325	0.2380

5 THERMAL ANALYSIS OF HTS CABLE

In the previous chapter, hydraulic issues in HTS cable with turbulent flow of LN2 are discussed. In the present chapter the thermal behavior of LN2 in the HTS cable is estimated using analytical and computational methods presented in chapter 0. Further, the computational results obtained from the present study are validated with the experimental results available from the literature. In addition, the effect of flow rate and heat flux on the temperature distribution of LN2 in the HTS cable is presented and compared with that of supercritical nitrogen (SCN). Later, the results pertaining to cooling capacity and the Nusselt number in the HTS cable are presented along with the effect of corrugation geometry, heat flux and heat generation. The distribution of entropy generation due to thermal and velocity gradients in the HTS cable will be presented chapter 6.

5.1 Validation

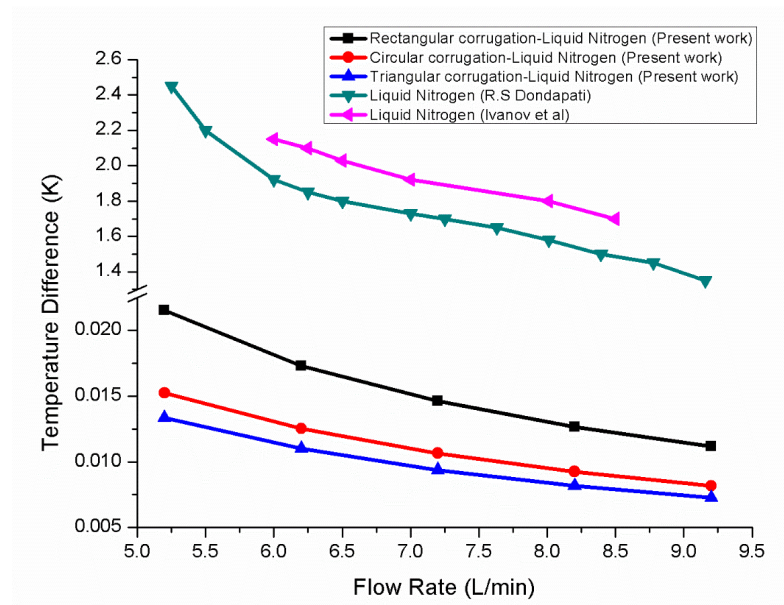


Figure 5.1 Comparison of temperature difference between outlet and inlet of LN2 in counter flow HTS cable (present work) with that of LN2 estimated by Dondapati et al. [102] and with the experimental results performed by Ivanov et al. [103]

Figure 5.1 demonstrates the comparison of temperature difference between outlet and inlet of counter flow HTS cable using LN2 estimated by Dondapati et al. [102] and that estimated by Ivanov et al. [103]. The result illustrates that the temperature difference

between outlet and inlet for LN₂ in the counter flow HTS cable of different corrugation topologies is lower than the other HTS cable system (single-way cooling). Hence, it is concluded from the results the long length counter flow HTS cables can be cooled effectively without losing the superconductivity.

5.2 Temperature Distribution in HTS Cables

In order to describe the thermal behavior of counter cooled HTS cable, the temperature distribution across the cable is necessary to investigate. The combined effect of heat flux and heat generation on the thermal behavior of the cable is studied and presented.

5.2.1 Axial Temperature Distribution

In this section the influence of various flow rates and heat losses on the axial temperature distribution profiles of LN₂ in the counter cooled HTS cable are studied. Three main sub-sections are divided to demonstrate the axial temperature distribution profiles of LN₂ along with the validation of results.

5.2.2 Effect of flow rates on temperature profiles of LN₂

This section reveals about the axial temperature distribution of liquid nitrogen along the cold dielectric HTS cable with counter flow cooling design. The solution using equation (14) and (20) is implemented in MATLAB code to obtain the temperature distribution in HTS cable for inner and annular region respectively. The temperature distributions along the cable at various volumetric flow rates (20-35 L/min) with an additional cryocooler are shown in Figure 5.2 (a). This depicts that with increase in the volumetric flow the maximum temperature in the cable decreases. The temperature of return flow in the beginning is lower than the inflow temperature at the drain which clearly express the evidence of cryocooler at right end of the cable. Similarly, the temperature distributions along the cable at various volumetric flow rates (20-35 L/min) without an additional cryocooler are shown in Figure 5.2 (b). The temperature of return flow at the beginning is equal to the inflow temperature at the drain which represents the same inflow at the right end of cable is fed to annulus return flow. In this case the maximum temperature in the cable attained 72 K at volumetric flow of 35 L/min whereas in case of no cryocooler at the end of cable the maximum temperature attained 76.5 K. The maximum temperature difference in the cable between both the cases is 4.5

K at higher volumetric flow rate. However, volumetric flow rate is also limited factor by the pressure drop conditions in the cable thereby the maximum volumetric flow becomes 35 L/min in the analysis.

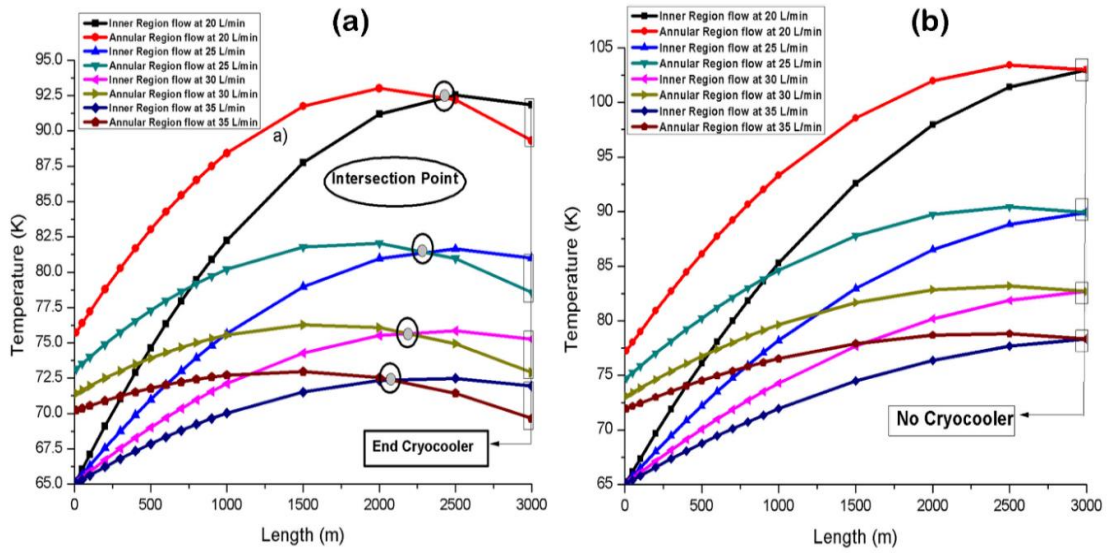


Figure 5.2 Temperature distribution along the cable at varying volumetric flow: a) with an additional cryocooler at right end of the cable, b) no cryocooler at right end of the cable

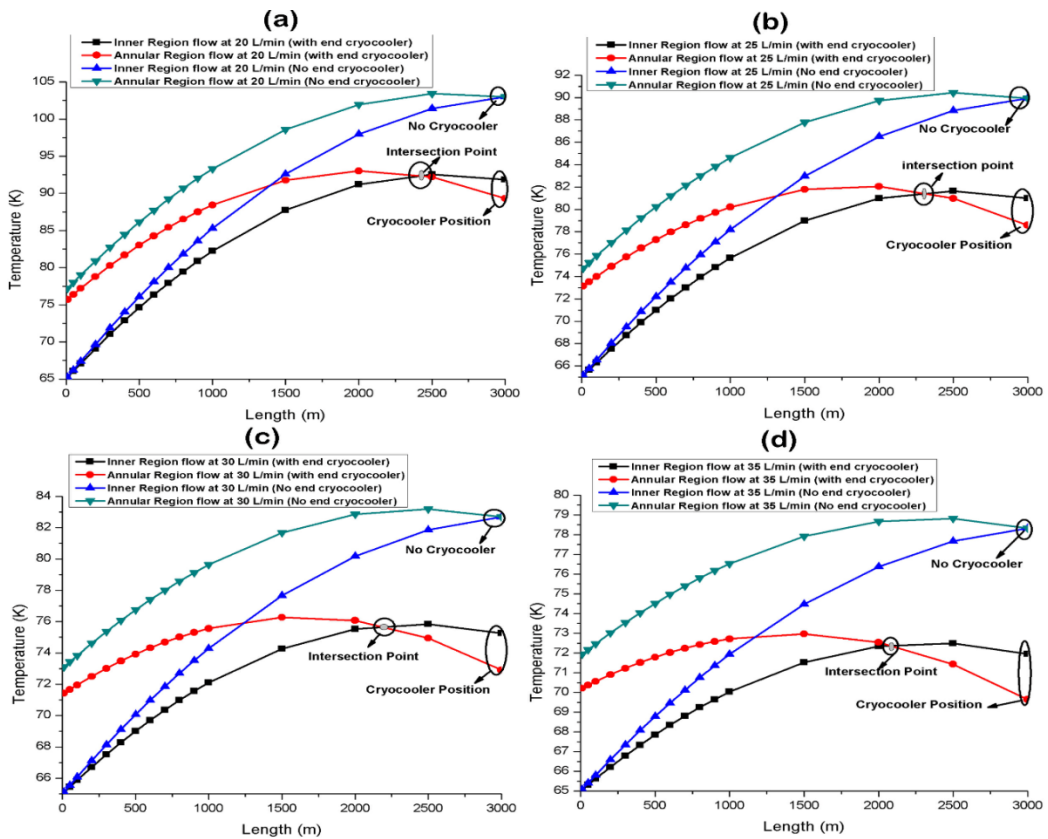


Figure 5.3 Comparison of temperature distribution along the cable at different volumetric flow with a cryocooler at end and without cryocooler a) at 20L/min, b) at 25 L/min, c) at 30 L/min, d) at 35 L/min

Comparison of temperature distributions along the cable at different volumetric flow with a cryocooler at end and that without cryocooler at the end is shown in Figure 5.3. It can be clearly seen from all the results that using cryocooler at the end of the cable reduces the maximum temperature in the cable which further avoid the boiling of LN₂ and cool the HTS cable up to long length. The inner region flow temperature will be further reduced by cryocooler at the right end of cable and the reduced temperature will be fed back to the return flow through annular region in the cable. Therefore, an intersection point forms in the results which represents the presence of cryocooler at the right end of the cable.

5.2.3 *Effect of heat flux on temperature profiles of LN₂*

Temperature distributions along the cable at various heat loads with an increment of 0.1 W/m are shown in Figure 5.4. It depicts that with increase in the heat load on the cable, the temperature distribution for go flow and return flow will increase rapidly even at the same volumetric flow. The temperature distributions at various heat loads with constant volumetric flow are shown in separate graphs. It can be concluded that high volumetric flow and low heat load on the cable reduces the maximum temperature in the cable and thus results in avoiding the boiling of LN₂.

Figure 5.5 represent the temperature distributions along the cable at different volumetric flow with constant heat loads. It can be seen clearly that the maximum temperature in the cable will reduce with increase in the volumetric flow even at constant heat load. However, volumetric flow is also a limited factor by pressure drop in the cable due to directly proportional to the square of volumetric flow. Therefore, maximum volumetric flow is taken as 35 L/min for the analysis which is suitable for the lower pressures and long length cables as well.

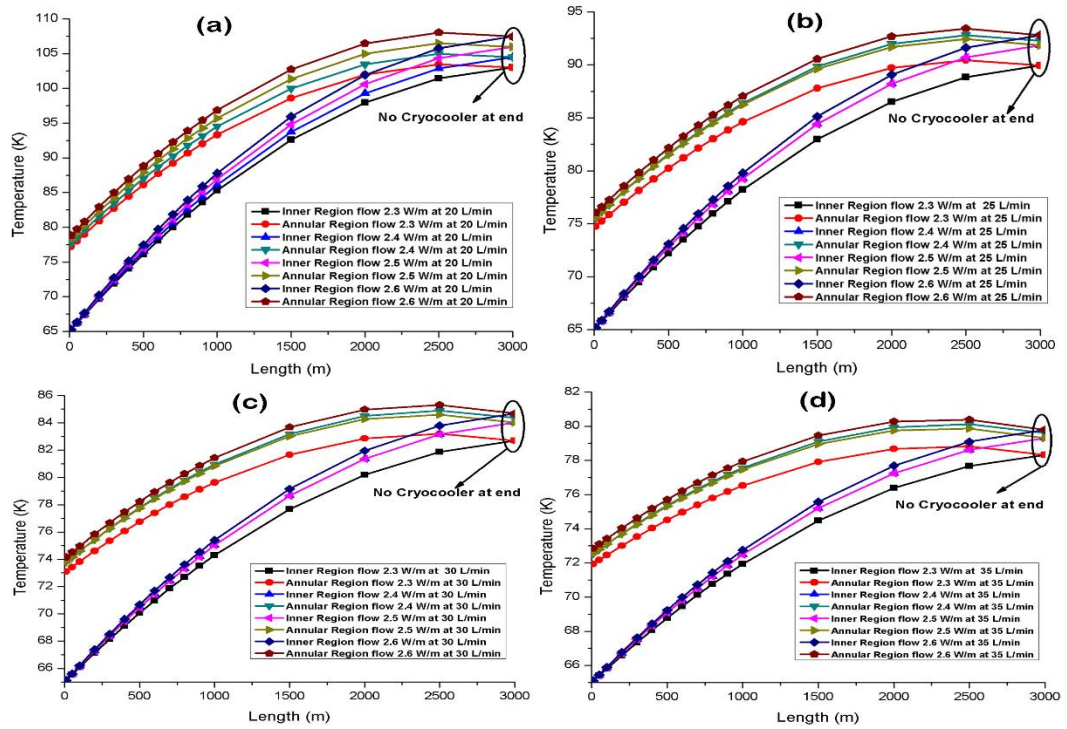


Figure 5.4 Temperature distribution along the cable at different heat loads with constant volumetric flow: a) at 20 L/min, b) at 25 L/min, c) at 30 L/min, d) at 35 L/min.

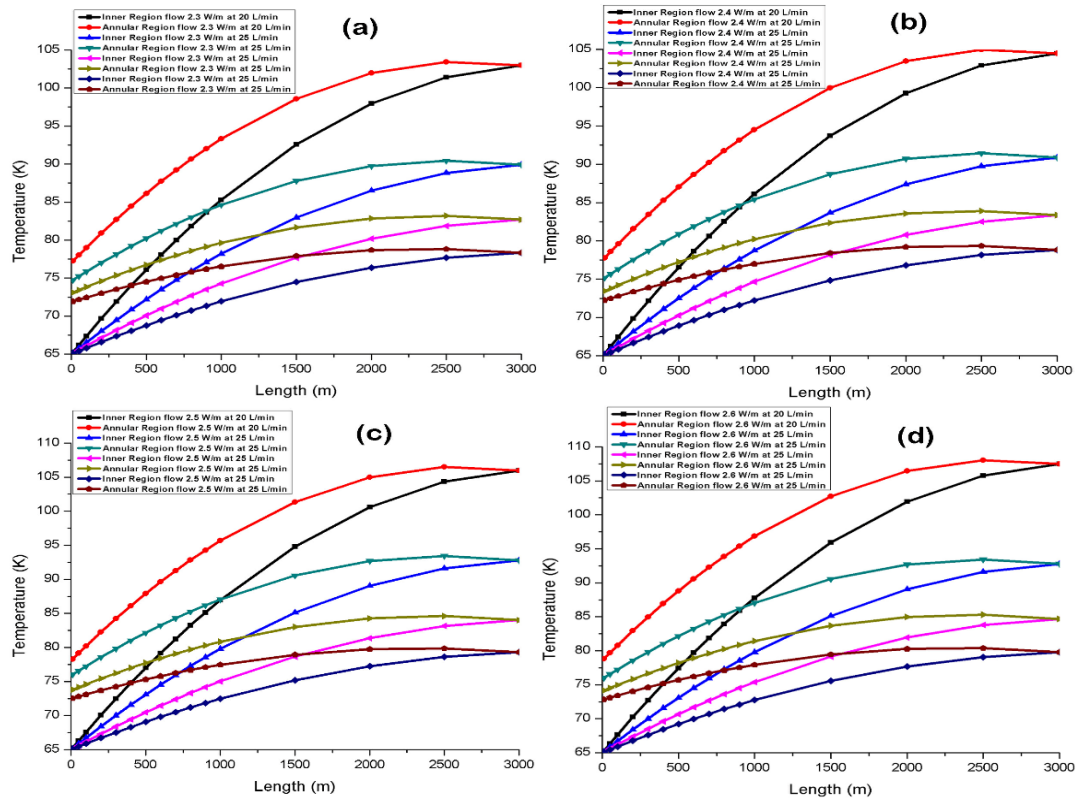


Figure 5.5 Temperature distribution along the cable at different volumetric flow with constant heat loads: a) at 2.3 W/m, b) at 2.4 W/m, c) at 2.5 W/m, d) at 2.6 W/m.

Table 5-1 Feasibility of HTS cable cooling with defined lengths

LD _{1c} /LD _{0c} (0.040/ 0.0775 m)	Cable length (m)	Mass flow rate (kg/s)	Maximum temperature (K) at 2.3 (W/m)	Maximum temperature (K) at 2.4 (W/m)	Maximum temperature (K) at 2.5 (W/m)	Maximum temperature (K) at 2.6 (W/m)	Pressure drop (bar)
	1500	0.286	75.85	76.27	76.69	77.10	2.8059
		0.358	72.47	72.75	73.03	73.31	4.3837
		0.43	70.53	70.74	70.95	71.16	6.3124
		0.501	69.363	69.5258	69.68	69.856	8.5912
	2000	0.286	83.13	83.84	84.55	85.26	3.7412
		0.358	77.23	77.70	78.174	78.64	5.8450
		0.43	73.91	74.24	74.57	74.91	8.4166
		0.501	71.87	72.12	72.38	72.63	11.4550
	2500	0.286	92.33	93.41	94.49	95.57	4.6766
0.358		83.22	83.93	84.64	85.34	7.3062	
0.43		78.129	78.62	79.12	79.63	10.5207	
0.501		75.03	75.40	75.78	76.15	14.3187	
3000	0.286	103.43	105	106.50	108.04	5.6119	
	0.358	90.435	91.43	92.44	93.42	8.7675	
	0.43	83.16	83.89	84.6	85.30	12.6249	
	0.501	78.81	79.33	79.86	80.38	17.1825	

The maximum possible length of counter cooled HTS cables depending upon the mass flow rates and heat fluxes have been investigated and compiled in the Table 5-1. In order to cool the defined cable length, the maximum temperature rise and pressure drop must be considered within the operating range (see Figure 3.2), (65K to 80K, 2bar to 14bar) of LN₂. Few combinations do not fall under the defined operating range of LN₂ to meet the design criteria of long length cable. The maximum possible length of HTS cable can be 2.5 km with existing parameters for effective cooling. The dark red boxes indicate the feasibility of such HTS cable lengths with those combinations.

5.2.4 Comparison of temperature profiles of LN₂ with SCN

Temperature distribution of liquid nitrogen (LN₂) and supercritical nitrogen (SCN) along the cable at various volumetric flow are compared in Figure 5.6 Comparison of temperature distribution of LN₂ and SCN along the cable at varying volumetric flow a) at 20L/min, b) at 25 L/min, c) at 30 L/min, d) at 35 L/min. It can be concluded from the results that difference between maximum temperature and inlet temperature, denoted by (δt) in the cable is significant lesser in case of SCN as compared to LN₂. The main

cause of decreased δt in case of SCN is due to five times higher isobaric specific heat compared to that of LN02. Moreover, it can also be seen from the results that in case of LN2 the maximum temperature in the cable is laying at the same location ($L=2500\text{m}$) at volumetric flow rates from 20 L/min to 30 L/min. However, the maximum temperature location is reduced to a length of 2000m at volumetric flow rate of 35L/min in case of SCN flow.

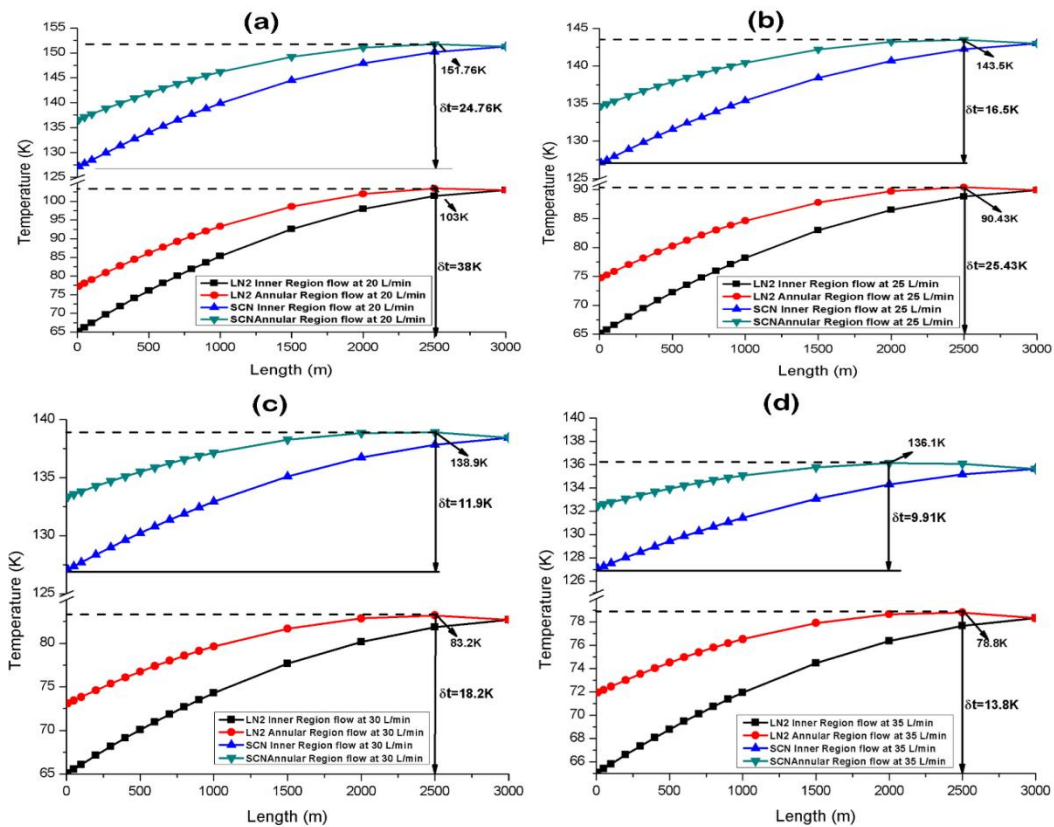


Figure 5.6 Comparison of temperature distribution of LN₂ and SCN along the cable at varying volumetric flow a) at 20L/min, b) at 25 L/min, c) at 30 L/min, d) at 35 L/min

5.3 Nusselt Numbers in HTS Cables

The effect of various corrugation topologies, heat flux and heat generation on heat transfer analysis in counter cooled HTS cable is presented in this section. Heat transfer analysis in the form of Nusselt number inside a counter cooled HTS cable is discussed. It is observed that heat transfer analysis in terms of Nusselt number affected significantly by the heat flux and heat generation unlike the hydraulic analysis.

5.3.1 Effect of Heat Flux on Nusselt Numbers

The combined effect of various corrugation topologies (rectangular, circular and triangular), heat flux at constant heat generation of 800W/m^3 on Nusselt number is presented in this section. Average Nusselt number at Reynolds number ranges from 30,000 to 60,000 for different corrugation topologies is presented in Figure 5.7, Figure 5.8 and Figure 5.9. It is noted that as Reynolds number increases, the Nusselt number for the various corrugation shapes also increases. Whereas, the heat flux reduces, the Nusselt number for the various corrugation shapes in the HTS cable increases. The highest Nusselt number values were presented by rectangular corrugation shaped HTS cable due to the presence of high recirculation and thin boundary layer. The maximum Nusselt number in the rectangular corrugation shaped HTS cable is found to be 206 at Reynolds number of 57500 and heat flux of 4W/m^2 .

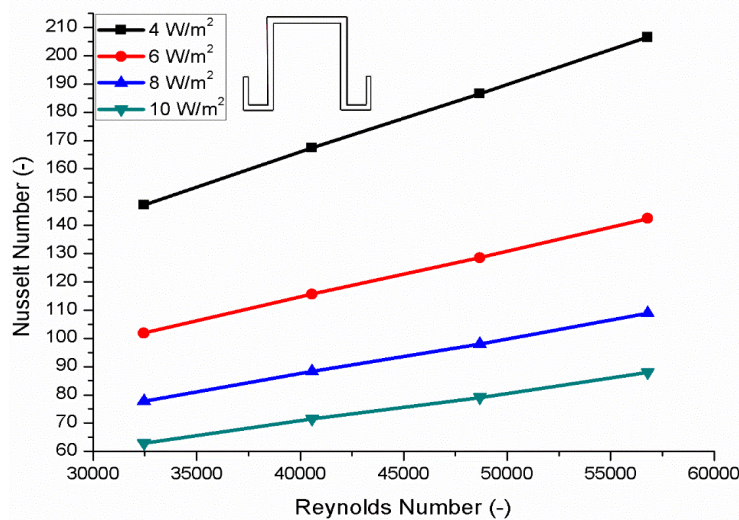


Figure 5.7 Effect of heat flux on Nusselt number at constant heat generation of 800 W/m^3 with rectangular corrugation

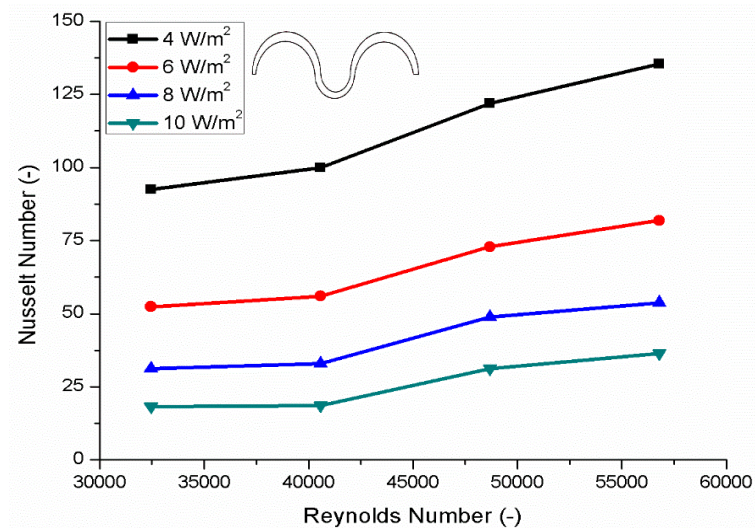


Figure 5.8 Effect of heat flux on Nusselt number at constant heat generation of 800 W/m³ with circular corrugation

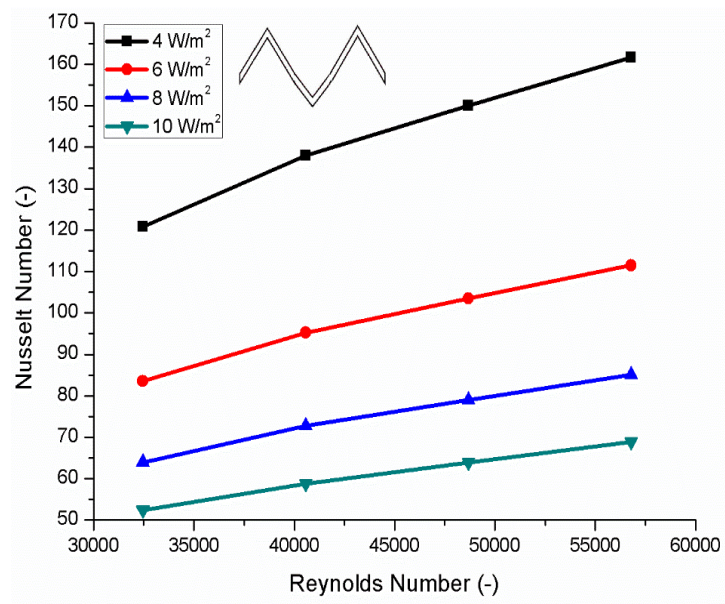


Figure 5.9 Effect of heat flux on Nusselt number at constant heat generation of 800 W/m³ with triangular corrugation

5.3.2 Effect of A.C Loss on Nusselt Numbers

The combined effect of various corrugation topologies (rectangular, circular and triangular) and heat generation at constant heat flux of 6W/m² on Nusselt number is dedicated in Figure 5.10, Figure 5.11 and Figure 5.12. The enhancement of heat transfer in rectangular corrugation shaped HTS cable is an evident from increase in the Nusselt number as shown in Figure 5.10. With increase in the Reynolds number, the Nusselt number also increases can be observed from the results. Similarly, the A.C. losses

increases, the average nusselt number for the various corrugation shapes HTS cable increases. Also, the highest Nusselt number of 250 is presented by rectangular corrugation shaped HTS cable at the A.C loss of 2.5 W/m with Reynolds number of 57500.

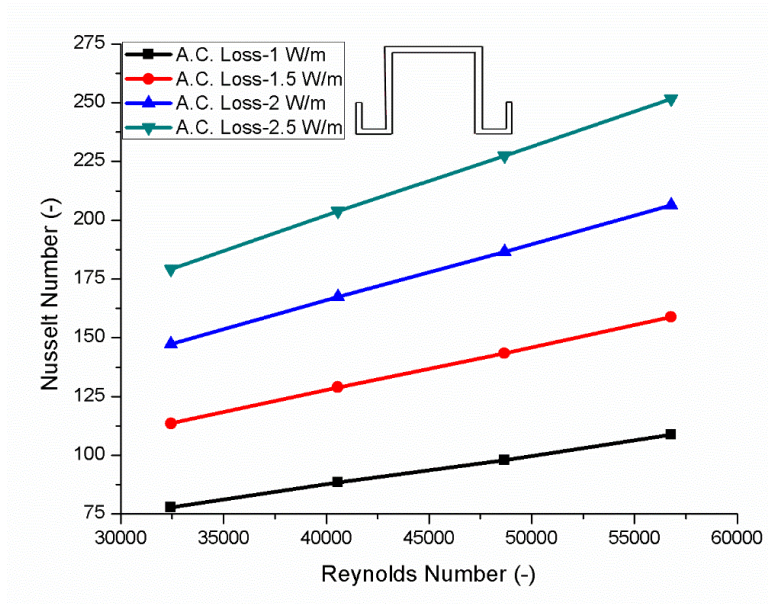


Figure 5.10 Effect of A.C loss on Nusselt number at constant heat flux of 6 W/m² with rectangular corrugation

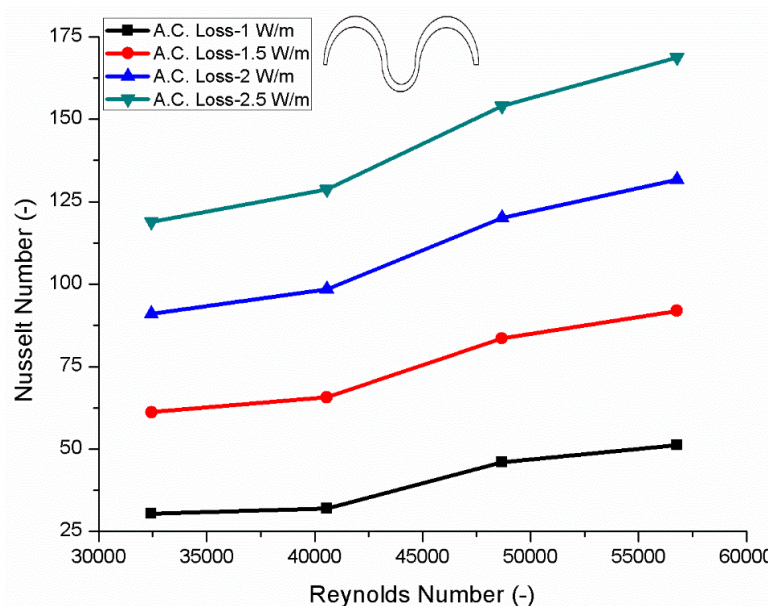


Figure 5.11 Effect of A.C loss on Nusselt number at constant heat flux of 6 W/m² with circular corrugation

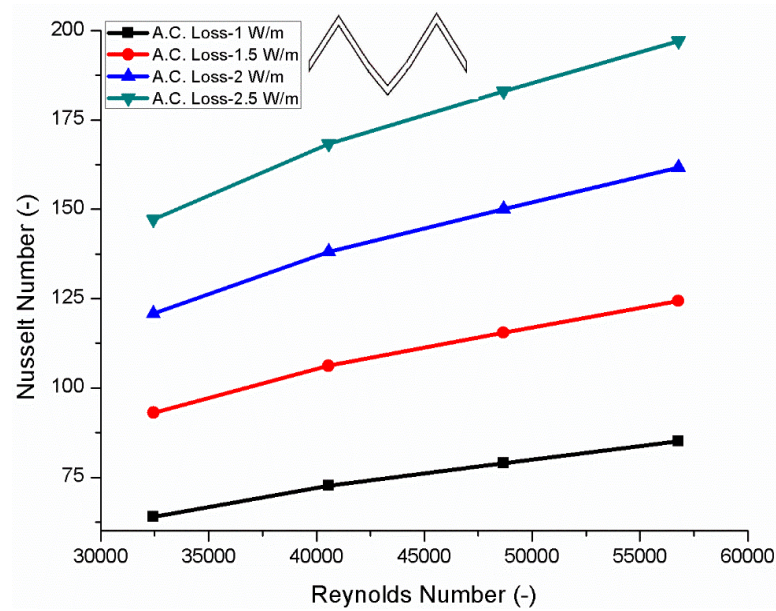


Figure 5.12 Effect of A.C loss on Nusselt number at constant heat flux of 6 W/m^2 with triangular corrugation

5.3.3 Effect of LN2 temperature on Nusselt Number

The effect of LN2 inlet temperature ranges from 65K to 70K on the Nusselt number in circular corrugation shape HTS cable is shown in Figure 5.13. The Nusselt number is obtained at constant heat flux of 4 W/m^2 and A.C loss of 2 W/m with Reynolds numbers range from 32500 to 57500. The average Nusselt number follows the increasing trend at different Reynolds number. It is also reported that the Nusselt number reduces significantly with increase in the LN2 inlet temperature in the HTS cable. Therefore, it can be concluded that the higher heat transfer takes place at LN2 inlet temperature of 66K and Reynolds number of 57500.

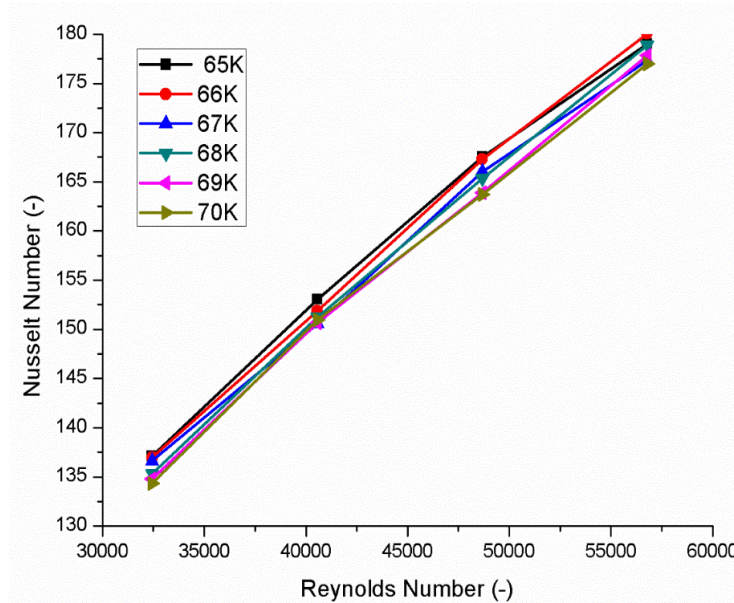


Figure 5.13 Effect of coolant inlet temperature on Nusselt number at heat flux of 4 W/m^2 and heat generation of 800 W/m^3

5.4 Cooling Capacity

The cooling capacity is the measure of LN2 ability in removal of heat resulting from heat-in-leaks, A.C losses and dielectric losses. The effect of various corrugation topologies, heat flux and heat generation on heat transfer analysis in counter cooled HTS cable is presented in this section. Heat transfer analysis in the form of cooling capacity is discussed for counter cooled HTS cable. Moreover, it is also observed that heat transfer analysis in terms of cooling capacity affected significantly by the heat flux and heat generation unlike the hydraulic analysis.

5.4.1 Effect of Heat Flux on Cooling Capacity

This section reveals the combined effect of various corrugation topologies (rectangular, circular and triangular), heat flux at constant heat generation of 800 W/m^3 on cooling capacity of HTS cable cooling system. It is observed from the Figure 5.14, Figure 5.15 and Figure 5.16 that with increase in the flow rates, the required cooling capacity of LN2 also increases and with maximum heat flux, the required cooling capacity will be higher. Moreover, the highest required cooling capacity were presented by rectangular corrugation shaped HTS cable. The highest cooling capacity in the rectangular corrugation shaped HTS cable cooling system is found to be 3.88 W at volumetric flow rate of 35 L/min and heat flux of 10 W/m^2 .

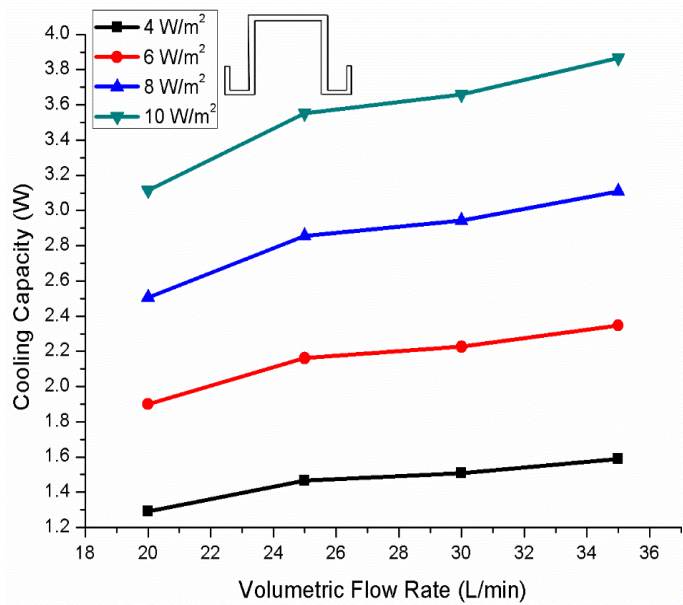


Figure 5.14 Effect of heat flux on cooling capacity at constant heat generation of 800 W/m^3 with rectangular corrugation

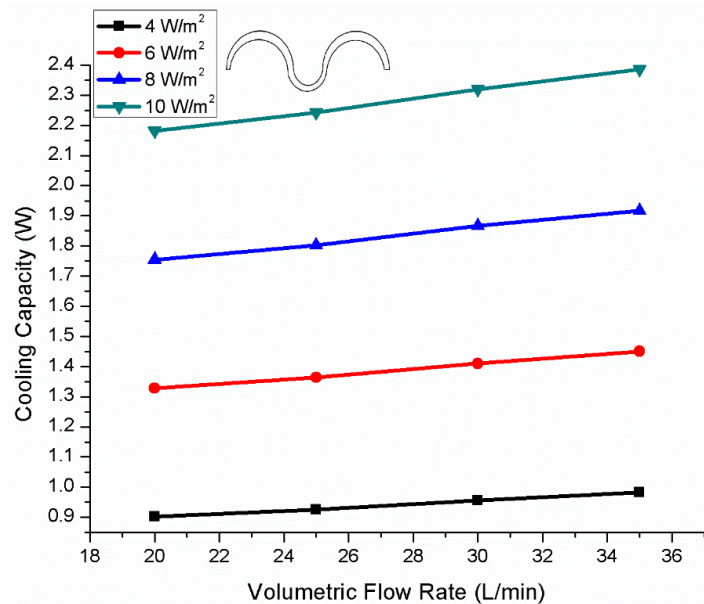


Figure 5.15 Effect of heat flux on cooling capacity at constant heat generation of 800 W/m^3 with circular corrugation

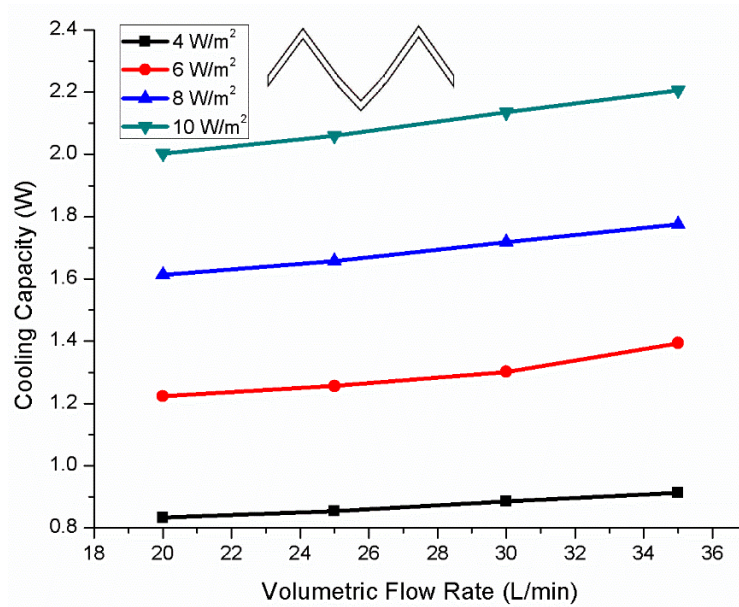


Figure 5.16 Effect of heat flux on cooling capacity at constant heat generation of 800 W/m³ with triangular corrugation

5.4.2 Effect of A.C Loss on Cooling Capacity

Figure 5.17, Figure 5.18 and Figure 5.19 dedicates the combined effect of various corrugation topologies (rectangular, circular and triangular) and heat generation at constant heat flux of 6W/m² on cooling capacity of HTS cable system. The results show that with increase in the A.C. loss the cooling capacity also increases and with high flow rates the required cooling capacity will be higher. The maximum required cooling capacity of LN2 is found to be 1.61 W in rectangular corrugation shape HTS cable at flow rate of 35L/min and A.C loss of 2.5 W/m. The results show that heat transfer analysis is significantly affected by the various heat fluxes and heat generations unlike the hydraulic analysis.

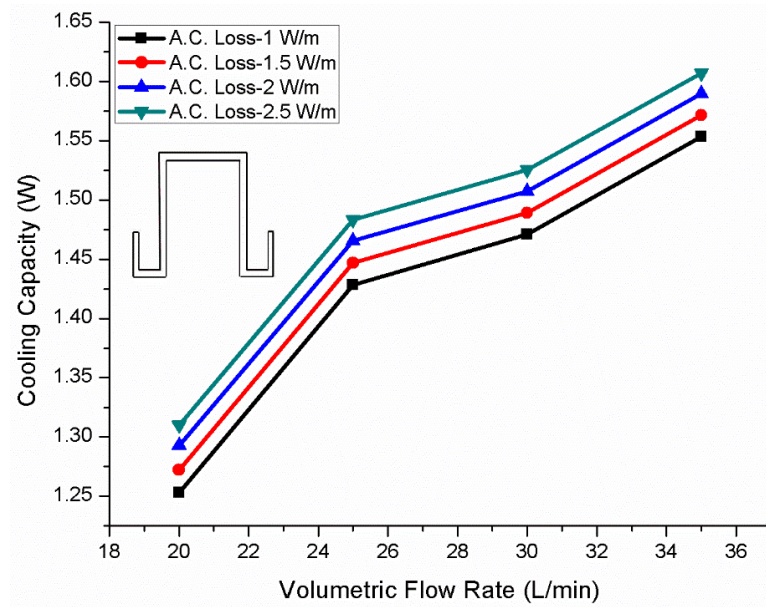


Figure 5.17 Effect of A.C loss on cooling capacity at constant heat flux of 6 W/m^2 with rectangular corrugation

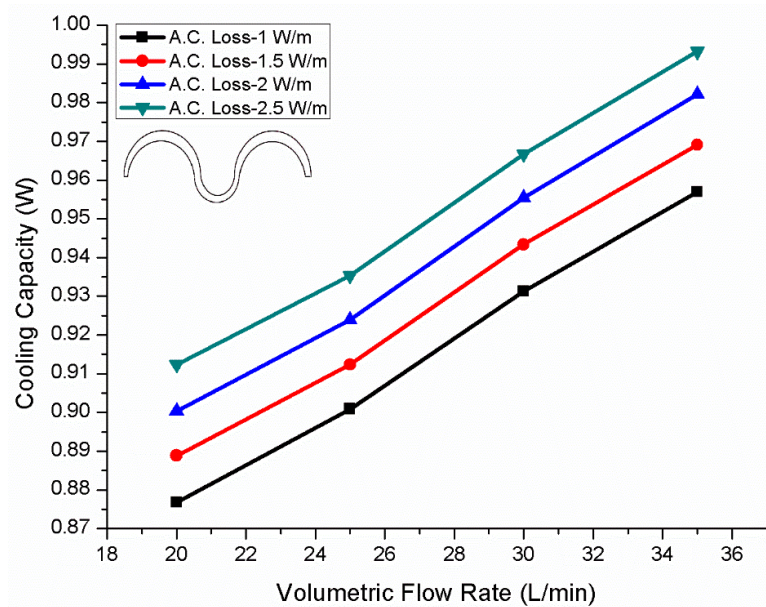


Figure 5.18 Effect of A.C loss on cooling capacity at constant heat flux of 6 W/m^2 with circular corrugation

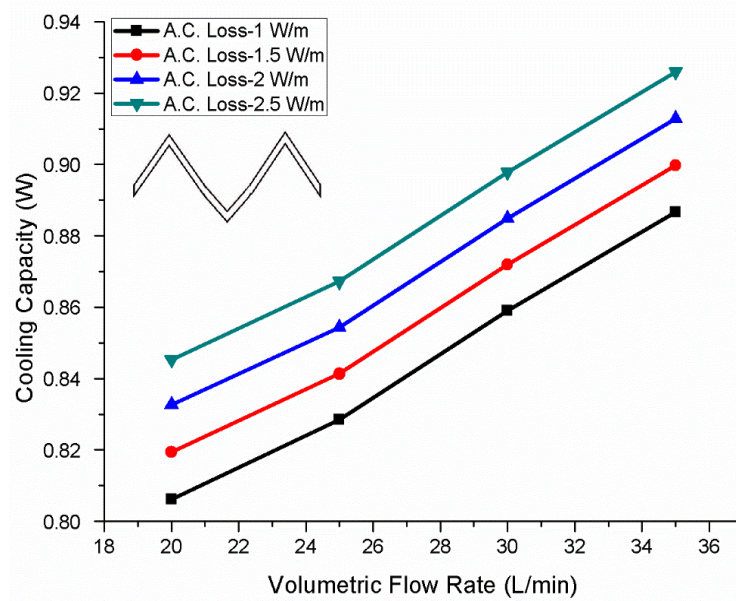


Figure 5.19 Effect of A.C loss on cooling capacity at constant heat flux of 6 W/m^2 with triangular corrugation

5.4.3 Effect of LN2 temperature on Cooling Capacity

Figure 5.20 illustrates the effect of LN2 inlet temperature ranges from 65K to 70K on the cooling capacity in circular corrugation shape HTS cable. The cooling capacity is obtained at a constant heat flux of 4 W/m^2 and A.C loss of 2 W/m . The cooling capacity of LN2 in the HTS cable increases with increase in the volumetric flow rate from 20L/min to 35L/min. It can be seen from the results that LN2 inlet temperature significantly affect the cooling capacity in the HTS cable. It is also reported that cooling capacity increases as the LN2 inlet temperature increases from 65K to 70K. The maximum required cooling capacity of LN2 is found to be 1.03W at inlet temperature of 70K and volumetric flow rate of 35L/min.

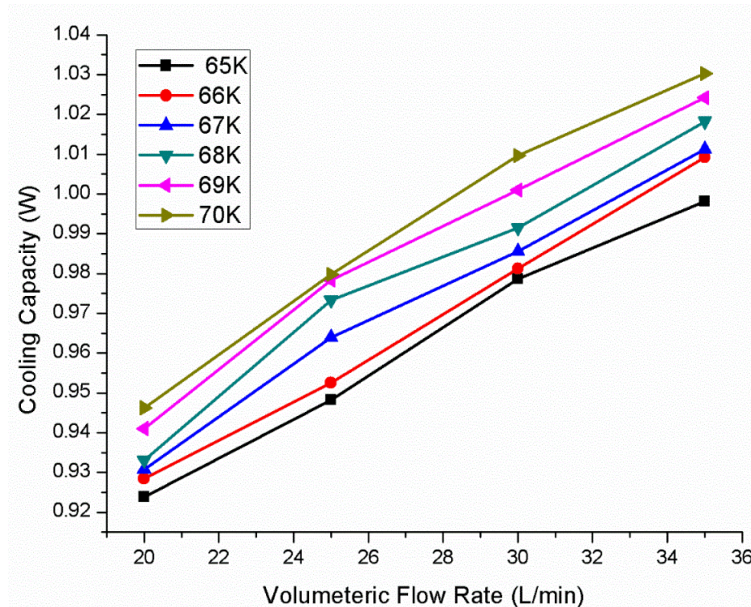


Figure 5.20 Effect of coolant inlet temperature on cooling capacity at heat flux of 4 W/m^2 and heat generation of 800 W/m^3

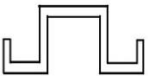


5.5 Summary and Conclusions

This chapter demonstrates the comparison of temperature difference between outlet and inlet of counter flow HTS cable using LN2 estimated by Dondapati et al. [102] and that estimated by Ivanov et al. [103]. The effect of various turbulence models available with CFD package software, heat fluxes, A.C losses (heat generation) and LN2 inlet temperature on Nusselt number and cooling capacity was also evaluated in this chapter. Moreover, the effect of flow rates and heat fluxes on the temperature distribution in liquid nitrogen along the HTS cable is also investigated with and without cryocooler at the end of the cable. In addition, heat transfer across the long length cold dielectric counter cooled High Temperature Superconducting (HTS) cables are significantly influenced by the different corrugation (rectangular, circular and triangular) topologies. Thus, temperature distribution of turbulent LN2 flow in counter cooled HTS cable with various corrugation topologies is also computationally investigated. Therefore, the effect of various heat-in-leak losses (heat flux) and A.C. losses (heat generation) on the thermal performance of LN2 was significantly affected.

A nonlinear temperature distribution is observed along the length of HTS cable. Liquid nitrogen with varying volumetric flow rates of 20-35L/min and total heat loss (A.C. loss and exterior heat load) of 2.3-2.6 W/m reveals interesting facts about cooling of cables with longer lengths. It is concluded from the results that lower heat loads and

high volumetric flow rate reduces the maximum temperature in the cable which further prevents the boiling of LN2. The maximum temperature attained within the operating range of the cable is found to be 79.63 K at volumetric flow rate of 30 L/min and a heat load of 2.6 W/m. The maximum pressure drop within the operating range of the cable is found to be 11.45 bar at a volumetric flow rate of 35 L/min with the cable length of 2.0 km. The maximum possible length of 2.5 km can be achieved at the flow rate of 30 L/min and with heat fluxes of 2.3-2.6 W/m within the defined operating range. Moreover, The Nusselt number obtained from the rectangular corrugation has increased which indicates the higher heat transfer rate than that of other two corrugation shapes as shown in Table 5-2. Consequently, the temperature difference between outlet and inlet for LN2 in the counter flow HTS cable of different corrugation topologies is lower than the other HTS cable system (single-way cooling). It was also observed that the LN2 inlet temperature from 65K to 70K significantly affects the thermal performance of HTS cable. One of the promising thermal characteristics such as Nusselt number reduces significantly with increase in the LN2 inlet temperature. However, the other thermal parameter such as cooling capacity of the entire cable system increases as the LN2 inlet temperature increases.

Table 5-2 Comparison of thermal characteristics with various corrugations

Corrugation	Effect of Heat Flux (W/m^2)		Effect of A.C loss (W/m)	
	Nusselt Number (-)	Cooling Capacity (W)	Nusselt Number (-)	Cooling Capacity (W)
	206	3.9	252	1.610
	135	2.4	169	0.995
	162	2.2	200	0.925

6 ENTROPY GENERATION IN HTS CABLE

In the previous chapter, thermal issues in HTS cable with turbulent flow of LN₂ are discussed. This chapter investigates the entropy generation in the various corrugation shaped HTS cables. Entropy generation addresses the thermodynamics, fluid mechanics and heat transfer issues simultaneously in an engineering system as shown in Figure 6.1. The lesser will be the entropy generation in a system, the higher will be the efficiency of that engineering system. Thereby, in order to estimate the loss of valuable energy (exergy), entropy generation distribution in the HTS cable is needed. Entropy generation occurs due to the friction in the flow, heat transfer between the finite temperature difference and mixing of the fluid flowing in the channel. Since no mixing in the present defined problem is considered. Therefore, an investigation of distribution of entropy generation due to heat transfer between the finite temperature difference which governs the thermal gradients in the HTS cable are performed using computer simulations. In addition, an investigation of distribution of entropy generation due to friction in the flow which governs the velocity gradients in the HTS cable using computer simulations has performed in this chapter. Moreover, the effect of heat flux and A.C loss on the total entropy generation in the various corrugation (rectangular, circular and triangular) shaped HTS cable is also discussed.

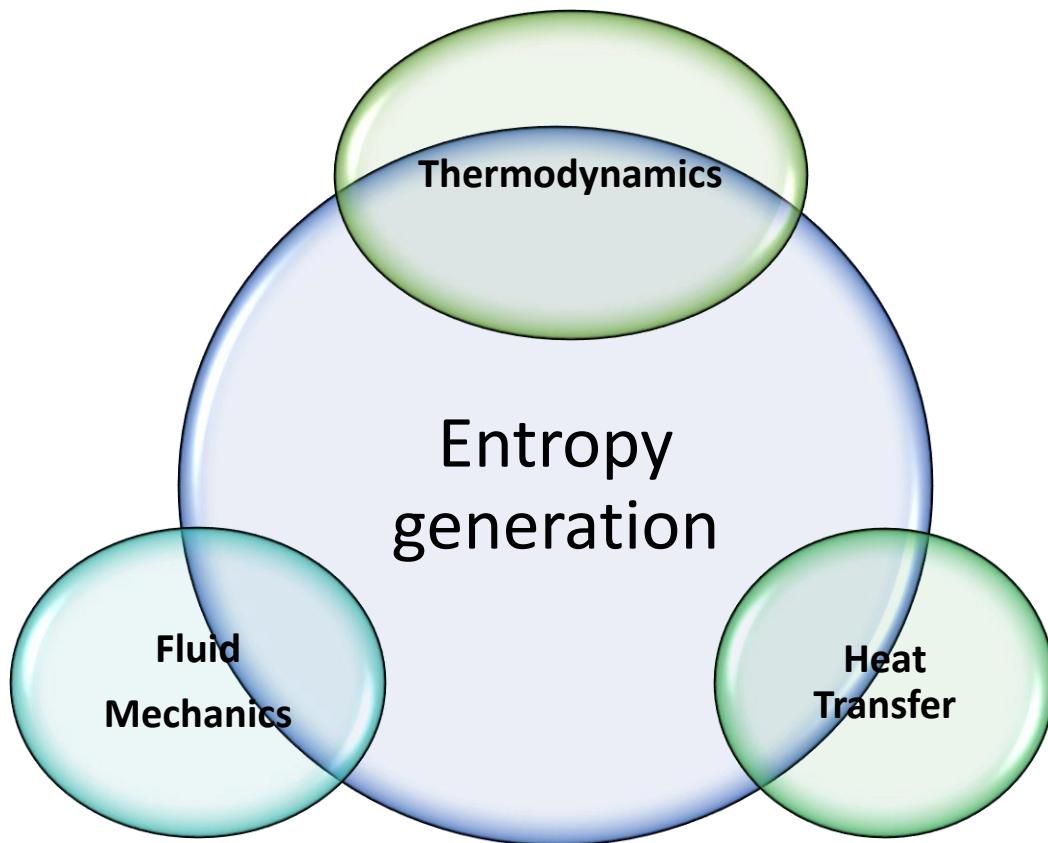


Figure 6.1 Entropy generation in a system consisting of thermodynamics, fluid mechanics and heat transfer

6.1 Effect of Heat flux on Entropy Generation

This section explores the combined effect of various corrugation topologies (rectangular, circular and triangular), heat fluxes of 4 W/m^2 - 10 W/m^2 at constant heat generation of 800 W/m^3 on the total entropy generation rate of HTS cable cooling system. Figure 6.2, Figure 6.3, Figure 6.4 and Figure 6.5 represents the effect of various heat fluxes such as 4 W/m^2 , 6 W/m^2 , 8 W/m^2 and 10 W/m^2 respectively. The results reveal that with increase in the volumetric flow rate, the entropy generation rate in the HTS cables with various corrugations also increase. Also, it is found that as heat flux increases, the total entropy rate will also be increasing for each corrugation topology. Finally, it is concluded from the computational investigation that the triangular corrugation shape HTS cable shows the lesser entropy generation rate as compared with that of other two corrugation (rectangular and circular) topologies. The minimum total entropy generation in the triangular corrugation shaped HTS cable is due to the lower temperature difference (see Figure 5.1). The highest entropy generation rates of 0.016

W/m^3-K , $0.0159 W/m^3-K$ and $0.0156 W/m^3-K$ at $35L/min$ is found for rectangular, circular and triangular corrugations respectively.

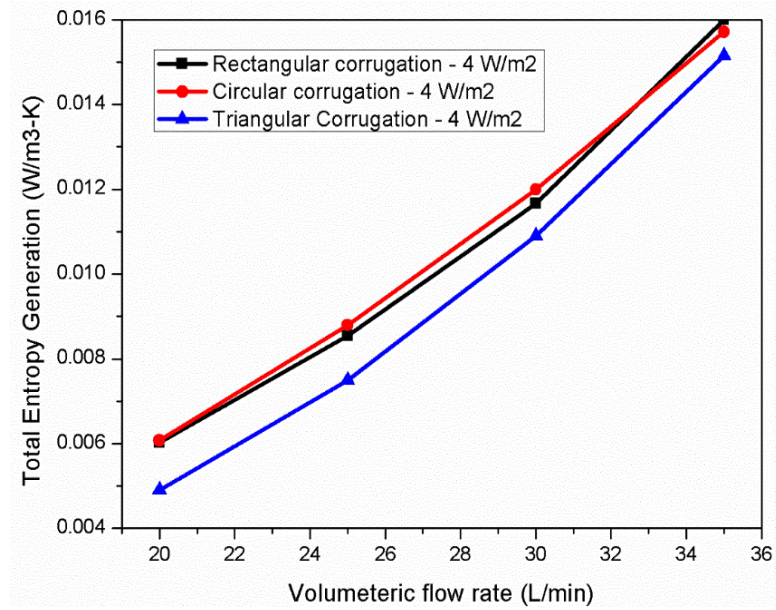


Figure 6.2 Effect of heat flux of $4 W/m^2$ on total entropy generation at constant heat generation of $800 W/m^3$ with all three corrugations (rectangular, circular and triangular)

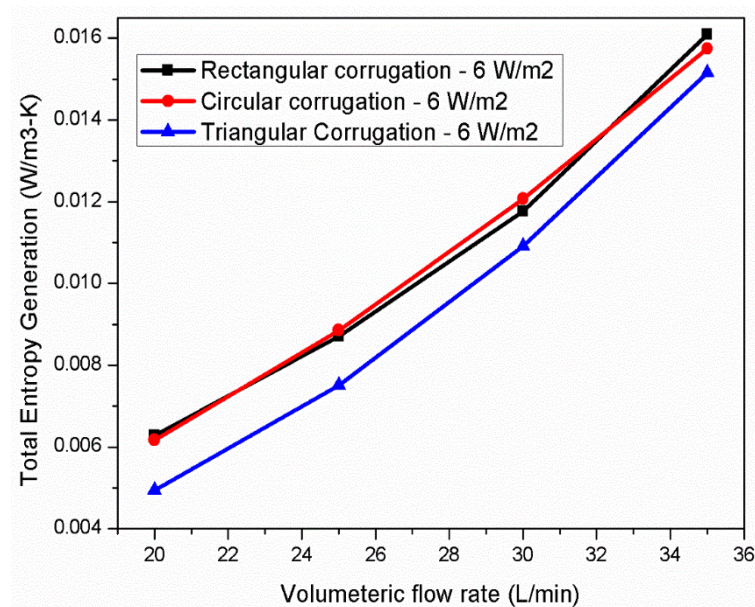


Figure 6.3 Effect of heat flux of $6 W/m^2$ on total entropy generation at constant heat generation of $800 W/m^3$ with all three corrugations (rectangular, circular and triangular)

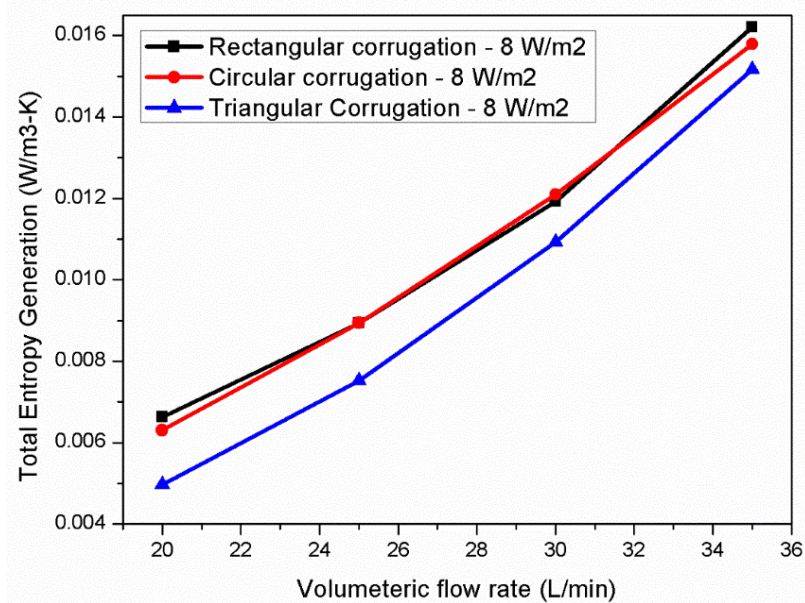


Figure 6.4 Effect of heat flux of 8 W/m² on total entropy generation at constant heat generation of 800 W/m³ with all three corrugations (rectangular, circular and triangular)

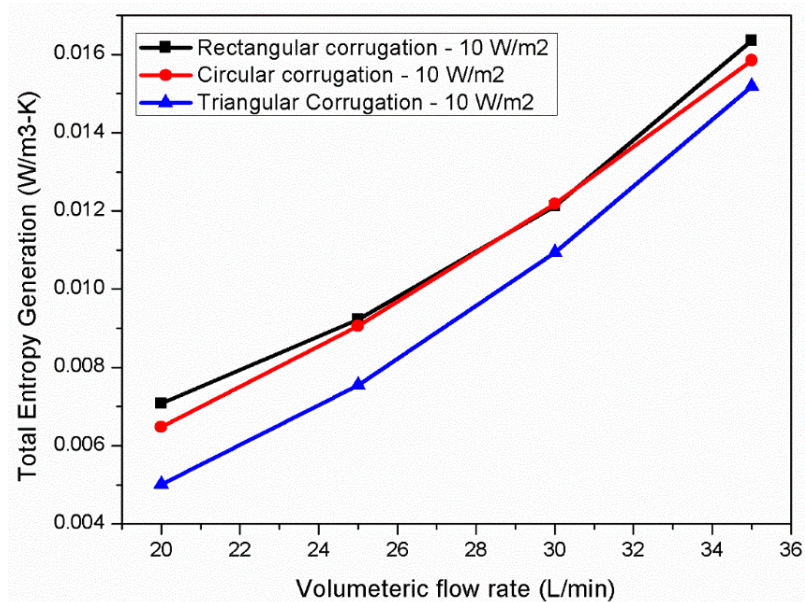


Figure 6.5 Effect of heat flux of 10 W/m² on total entropy generation at constant heat generation of 800 W/m³ with all three corrugations (rectangular, circular and triangular)

6.1.1 Entropy Generation due to Thermal Gradients

The entropy generation for a fluid having viscous and forced convection flow, is mainly due to the velocity and temperature gradients present in the fluid flowing in a channel. The entropy generation due to thermal gradients in the HTS cable with turbulent LN2 flow is presented in this section. Figure 6.6, Figure 6.7, Figure 6.8 and Figure 6.9 illustrate the effect of various heat fluxes ranges from 4 W/m^2 - 10 W/m^2 on the entropy generation due to thermal gradients with different corrugation (rectangular, circular and triangular) topologies. Moreover, the entropy generation due to the thermal gradients is found to be decreasing with increase in the volumetric flow rates. However, entropy generation due to the thermal gradients rises with increase in the heat flux at the outer walls of the HTS cable. It can also be clearly observed from the results that triangular corrugation shaped HTS cable has the lowest entropy generation as compared with that of circular and rectangular corrugations. The maximum entropy generation due to thermal gradients in triangular shaped HTS cable is found to be $0.00019 \text{ W/m}^3\text{K}$ at a heat flux of 4 W/m^2 . Finally, it is concluded from the results that the entropy generation due to temperature gradients is contributing less in the total entropy generation.

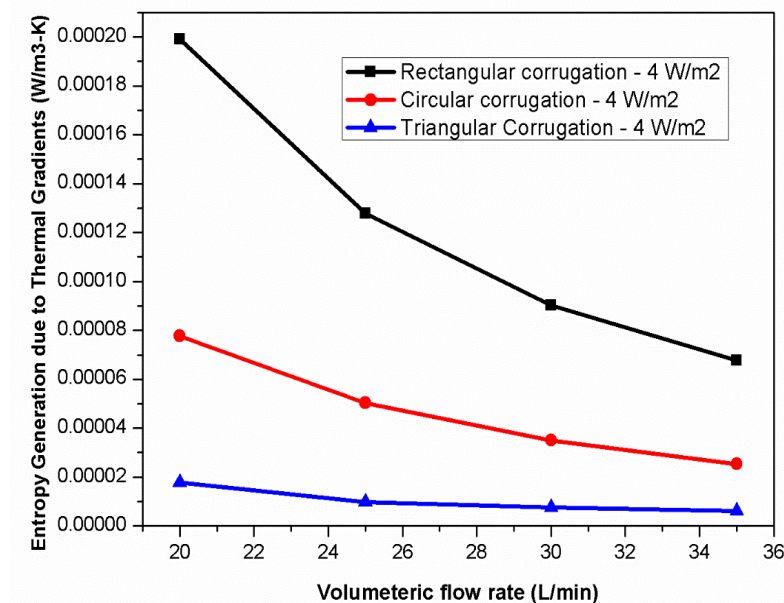


Figure 6.6 Effect of heat flux of 4 W/m^2 on entropy generation due to thermal gradients at constant heat generation of 800 W/m^3 with all three corrugations (rectangular, circular and triangular)

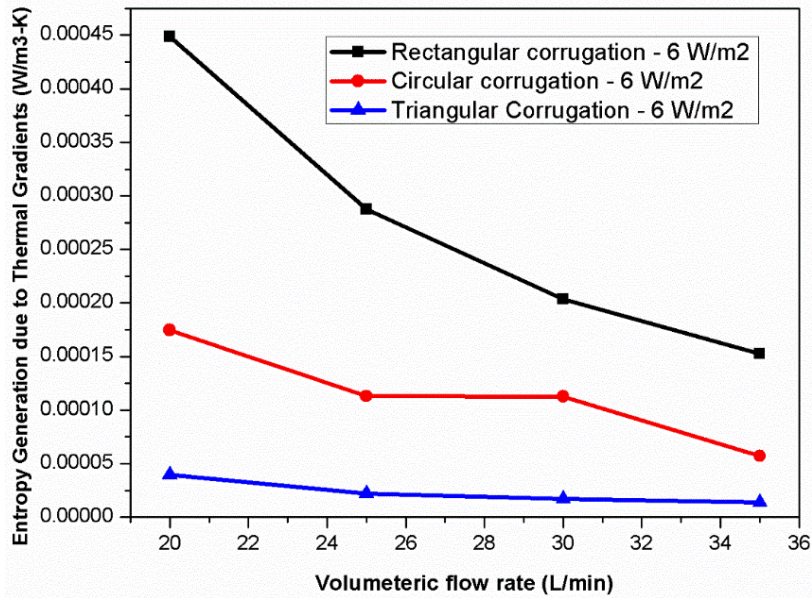


Figure 6.7 Effect of heat flux of 6 W/m² on entropy generation due to thermal gradients at constant heat generation of 800 W/m³ with all three corrugations (rectangular, circular and triangular)

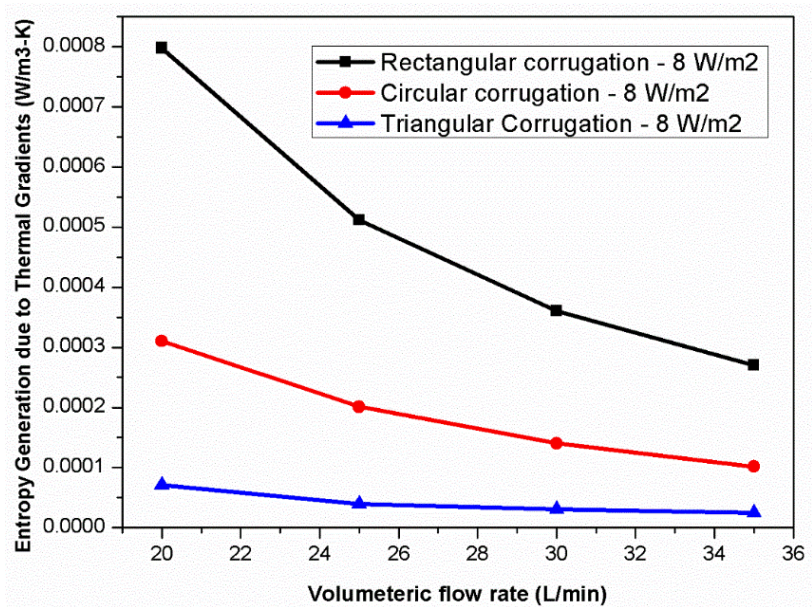


Figure 6.8 Effect of heat flux of 8 W/m² on entropy generation due to thermal gradients at constant heat generation of 800 W/m³ with all three corrugations (rectangular, circular and triangular)

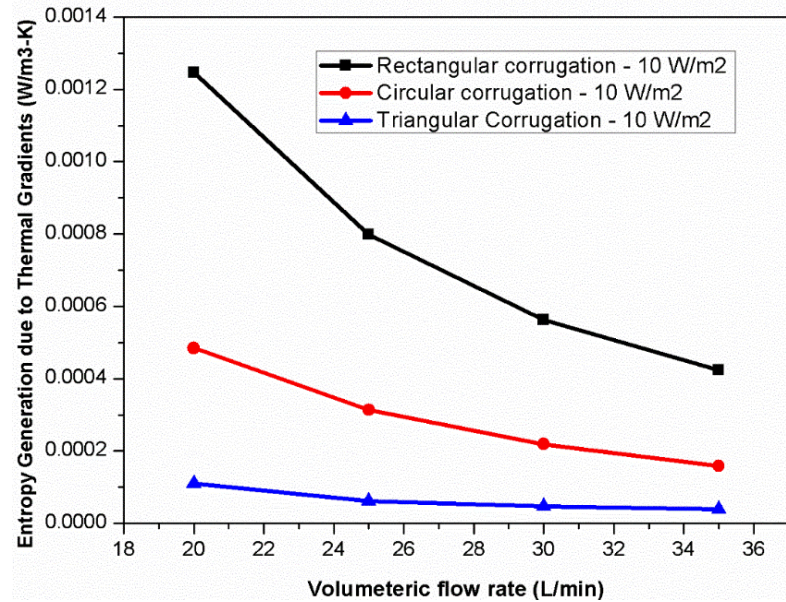


Figure 6.9 Effect of heat flux of 10 W/m² on entropy generation due to thermal gradients at constant heat generation of 800 W/m³ with all three corrugations (rectangular, circular and triangular)

6.1.2 Entropy Generation due to Velocity Gradients

The entropy generation due to velocity gradients is second most important contributing factor in enhancing the total entropy generation. The frictional losses between moving fluid and wall surface of the channel cause the velocity gradients which further leads to the total entropy generation. Figure 6.10, Figure 6.11, Figure 6.12 and Figure 6.13 depicts the effect of various heat fluxes ranges from 4 W/m² - 10 W/m² on the entropy generation due to velocity gradients with different corrugation (rectangular, circular and triangular) topologies. As can be seen from the results, the entropy generation due to velocity gradients increase with increase in the volumetric flow rate. However, no significant difference is observed in the entropy generation due to velocity gradients as the heat flux increases unlike the entropy generation due to temperature gradients. The lowest entropy generation due to velocity gradients is observed in the triangular corrugation shaped HTS cable. The maximum entropy generation due to velocity gradients in triangular shaped HTS cable is found to be 0.0013 W/m³-K at a volumetric flow rate of 35L/min. Finally, it can be concluded that the entropy generation due to velocity gradients is more dominating in enhancing the total entropy generation in HTS cable.

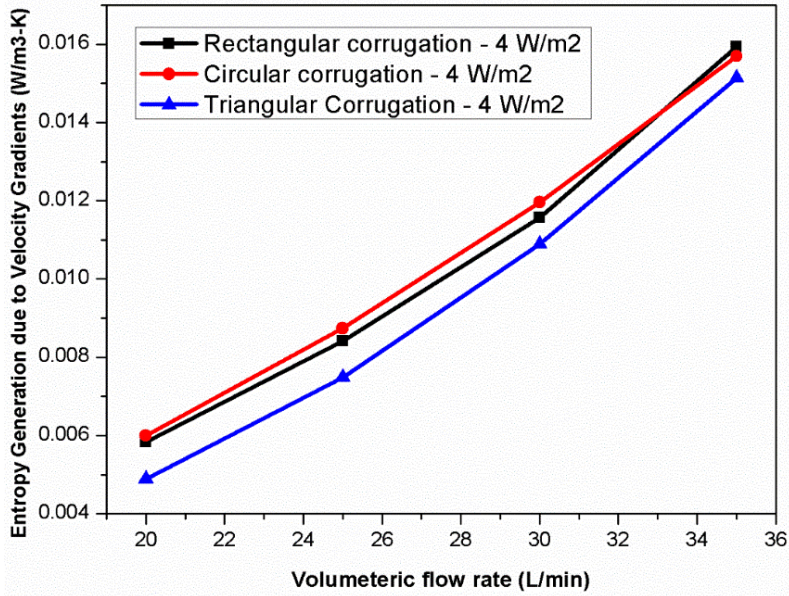


Figure 6.10 Effect of heat flux of 4 W/m² on entropy generation due to velocity gradients at constant heat generation of 800 W/m³ with all three corrugations (rectangular, circular and triangular)

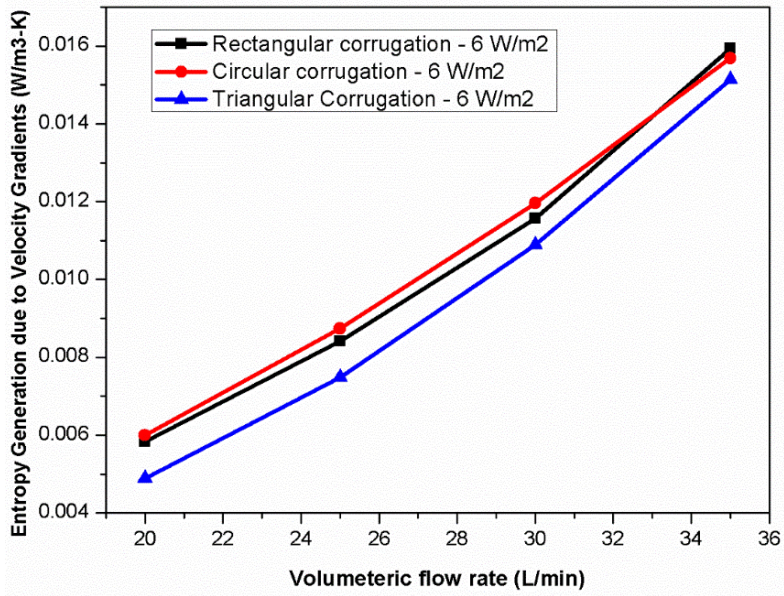


Figure 6.11 Effect of heat flux of 6 W/m² on entropy generation due to velocity gradients at constant heat generation of 800 W/m³ with all three corrugations (rectangular, circular and triangular)

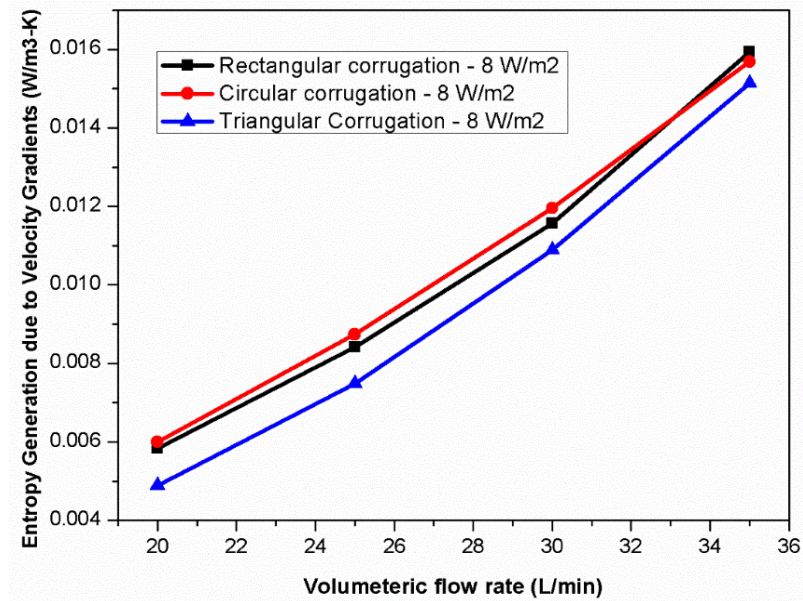


Figure 6.12 Effect of heat flux of 8 W/m² on entropy generation due to velocity gradients at constant heat generation of 800 W/m³ with all three corrugations (rectangular, circular and triangular)

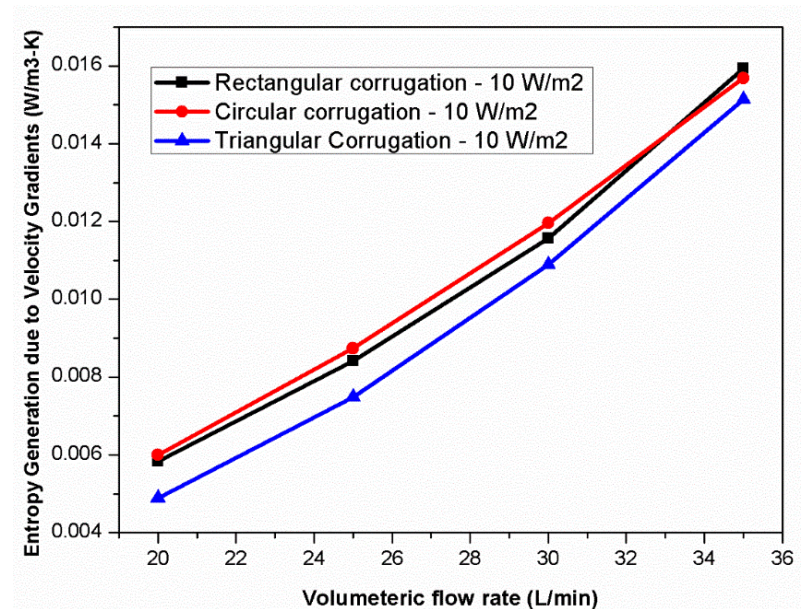


Figure 6.13 Effect of heat flux of 10 W/m² on entropy generation due to velocity gradients at constant heat generation of 800 W/m³ with all three corrugations (rectangular, circular and triangular)

6.2 Effect of A.C losses on Entropy Generation in the HTS Cable

This section includes the combined effect of various corrugation topologies (rectangular, circular and triangular), A.C losses of 1 W/m -2.5 W/m at constant heat flux of 6W/m² on the total entropy generation rate of HTS cable cooling system. Figure 6.14, Figure 6.15, Figure 6.16 and Figure 6.17 represents the effect of various A.C

losses such as 1 W/m, 1.5 W/m, 2 W/m and 2.5 W/m respectively. The results represent that with increase in the volumetric flow rate, the entropy generation rate in the HTS cables with various corrugations also increases. No significant difference is obtained with the effect of various losses on the total entropy generation in HTS cable. Moreover, the similar results of the total entropy generation are obtained from each of the A.C losses in HTS cable. Hence, it can be concluded from the computational investigation that the triangular corrugation shape HTS cable shows the lesser entropy generation rate as compared with that of other two corrugation (rectangular and circular) topologies. The highest entropy generation rates of 0.016 W/m³-K at 35L/min is found for all the corrugations such as rectangular, circular and triangular shaped HTS cable.

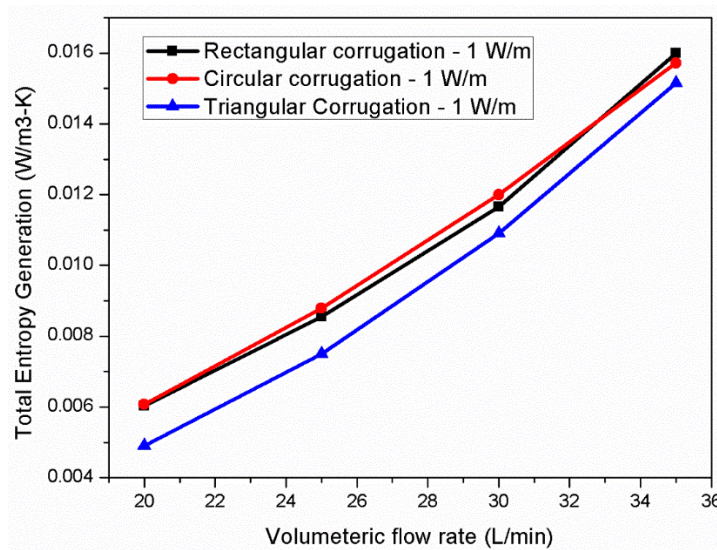


Figure 6.14 Effect of A.C loss of 1 W/m on total entropy generation at constant heat flux of 6 W/m² with all three corrugations (rectangular, circular and triangular)

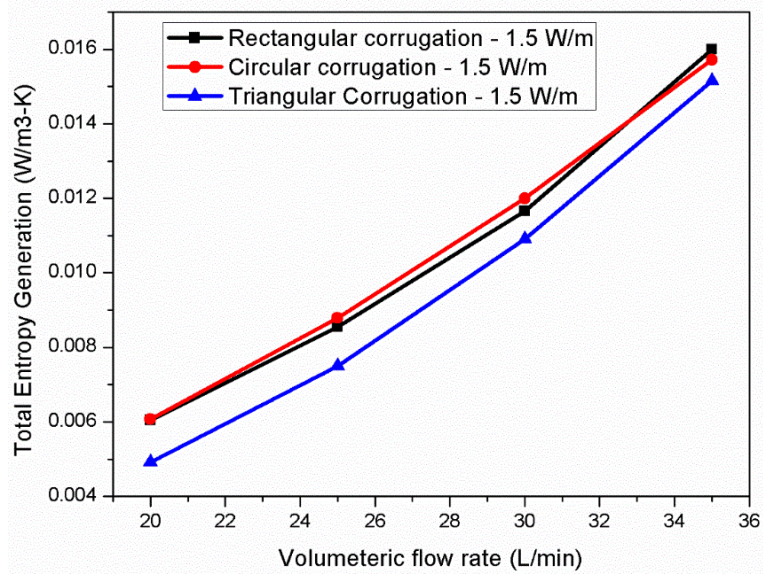


Figure 6.15 Effect of A.C loss of 1.5 W/m on total entropy generation at constant heat flux of 6 W/m² with all three corrugations (rectangular, circular and triangular)

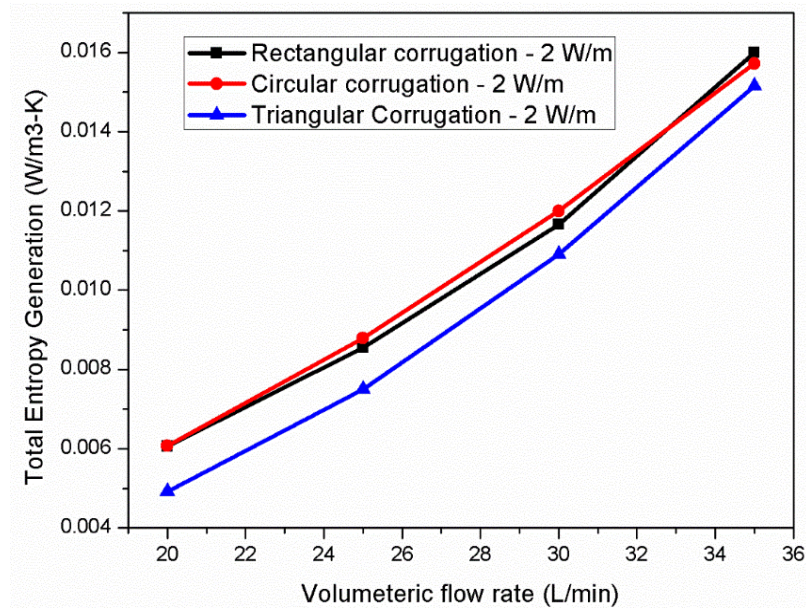


Figure 6.16 Effect of A.C loss of 2 W/m on total entropy generation at constant heat flux of 6 W/m² with all three corrugations (rectangular, circular and triangular)

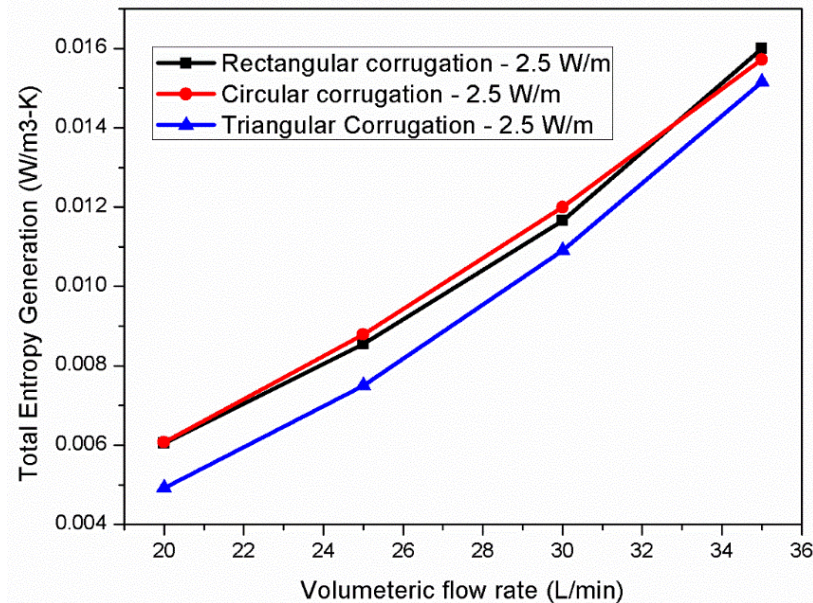


Figure 6.17 Effect of A.C loss of 2.5 W/m on total entropy generation at constant heat flux of 6 W/m² with all three corrugations (rectangular, circular and triangular)

6.2.1 Entropy Generation due to Thermal Gradients

The entropy generation due to thermal gradients in the HTS cable with turbulent LN₂ flow at various A.C losses is presented in this section. Figure 6.18, Figure 6.19, Figure 6.20 and Figure 6.21 illustrate the effect of various A.C losses ranges from 1W/m - 2.5W/m on the entropy generation due to thermal gradients with different corrugation (rectangular, circular and triangular) topologies. It is observed from the results that triangular corrugation shaped HTS cable has the lowest entropy generation as compared with that of circular and rectangular corrugations. The maximum entropy generation due to thermal gradients in triangular shaped HTS cable is found to be 0.00019 W/m³K at a constant heat flux of 4 W/m². The entropy generation due to thermal gradients at different A.C losses is found to be similar as entropy generation due to thermal gradients at heat flux of 4 W/m². Further no significant difference is obtained in the entropy generation due to thermal gradients at different A.C losses. Hence, it signifies that the A.C losses are less contributing in enhancing the entropy generation of HTS cable despite of heat flux.

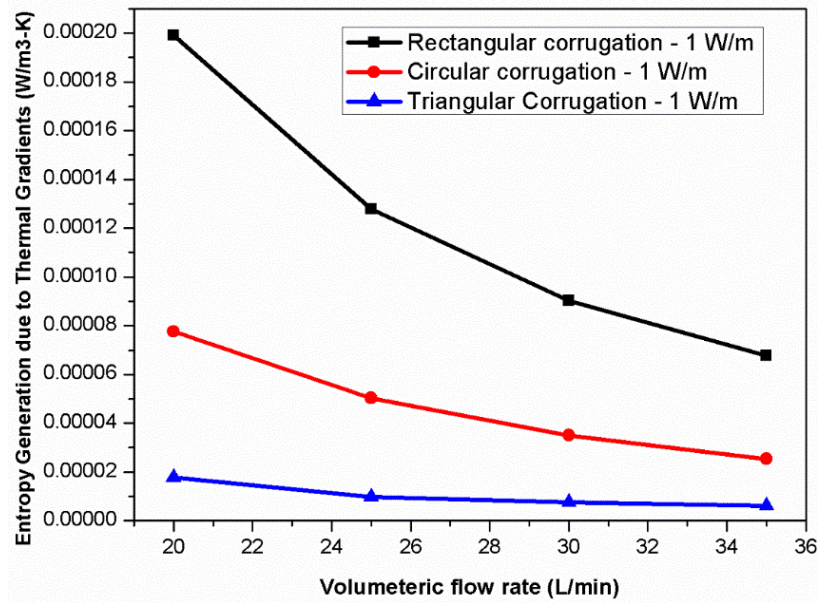


Figure 6.18 Effect of A.C loss of 1 W/m on entropy generation due to thermal gradients at constant heat flux of 6 W/m² with all three corrugations (rectangular, circular and triangular)

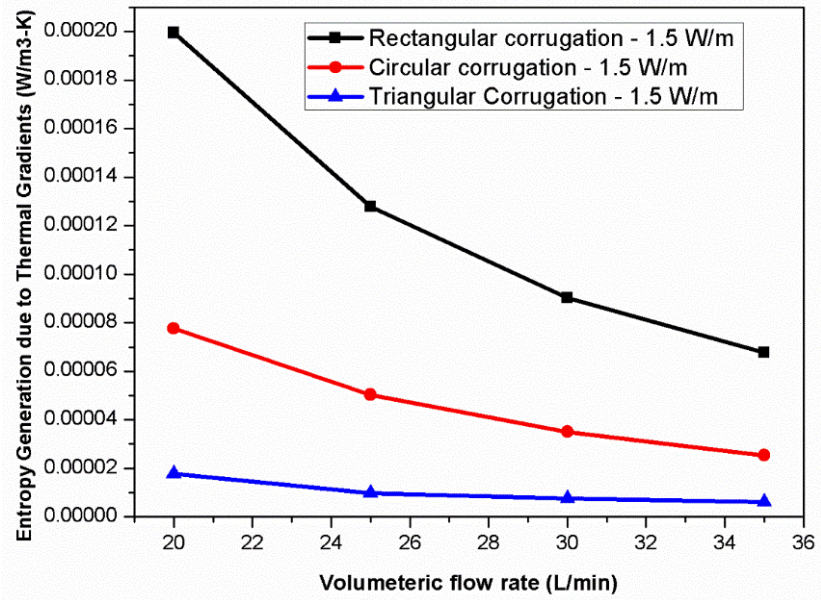


Figure 6.19 Effect of A.C loss of 1.5 W/m on entropy generation due to thermal gradients at constant heat flux of 6 W/m² with all three corrugations (rectangular, circular and triangular)

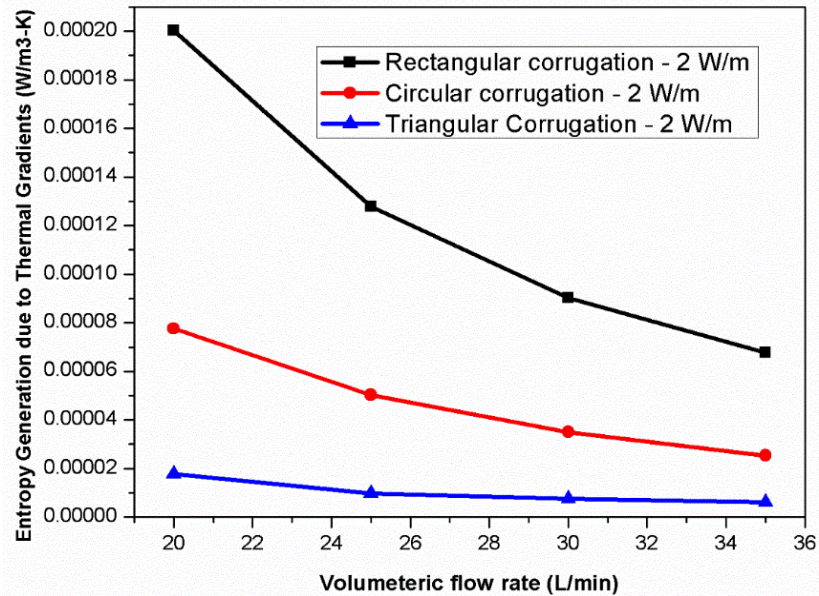


Figure 6.20 Effect of A.C loss of 2 W/m on entropy generation due to thermal gradients at constant heat flux of 6 W/m² with all three corrugations (rectangular, circular and triangular)

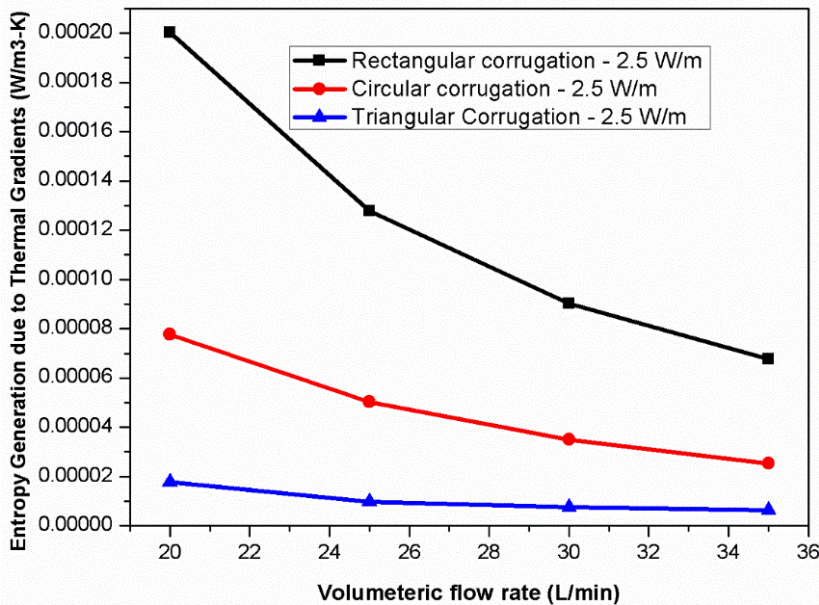


Figure 6.21 Effect of A.C loss of 2.5 W/m on entropy generation due to thermal gradients at constant heat flux of 6 W/m² with all three corrugations (rectangular, circular and triangular)

6.2.2 Entropy Generation due to Velocity Gradients

Figure 6.22, Figure 6.23, Figure 6.24 and Figure 6.25 shows the entropy generation due to velocity gradients at various A.C losses ranges from 1 W/m to 2.5 W/m with different corrugations. However, no significant difference is observed in the entropy generation due to velocity gradients as the A.C losses increase equivalent to the entropy generation due to velocity gradients at various heat fluxes. Hence, it can be observed from the

results that there is no significant effect of A.C losses and Heat fluxes on the entropy generation due to velocity gradients.

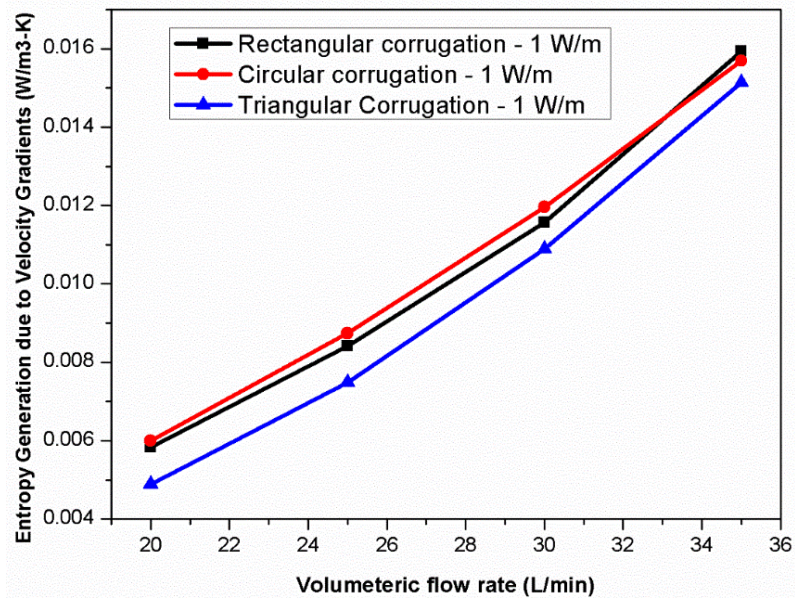


Figure 6.22 Effect of A.C loss of 1 W/m on entropy generation due to velocity gradients at constant heat flux of 6 W/m² with all three corrugations (rectangular, circular and triangular)

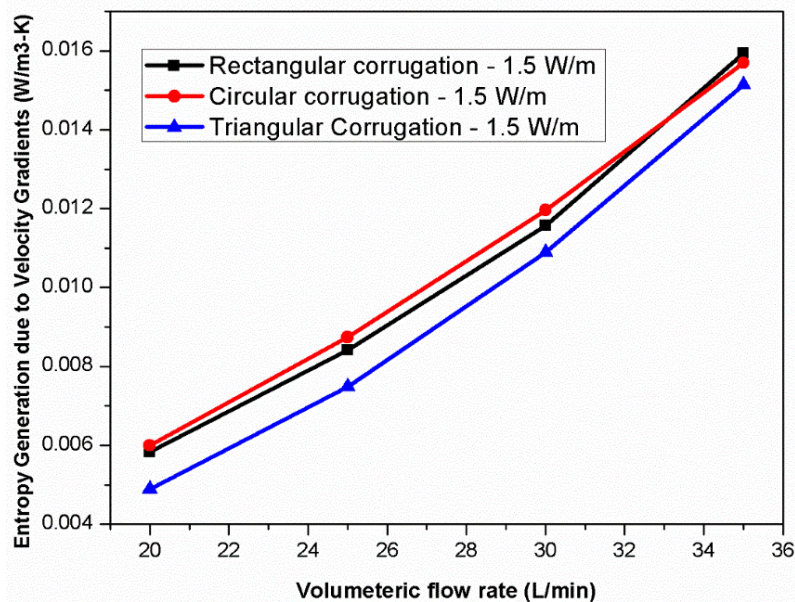


Figure 6.23 Effect of A.C loss of 1.5 W/m on entropy generation due to velocity gradients at constant heat flux of 6 W/m² with all three corrugations (rectangular, circular and triangular)

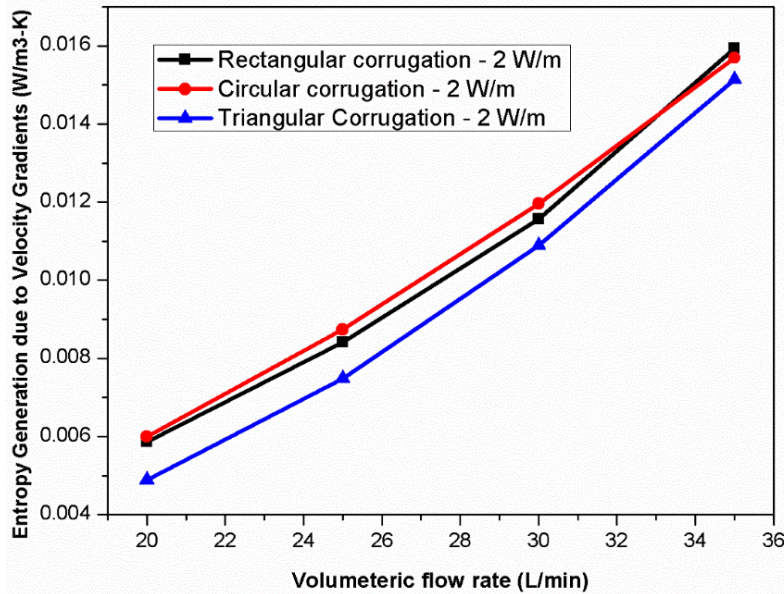


Figure 6.24 Effect of A.C loss of 2 W/m on entropy generation due to velocity gradients at constant heat flux of 6 W/m² with all three corrugations (rectangular, circular and triangular)

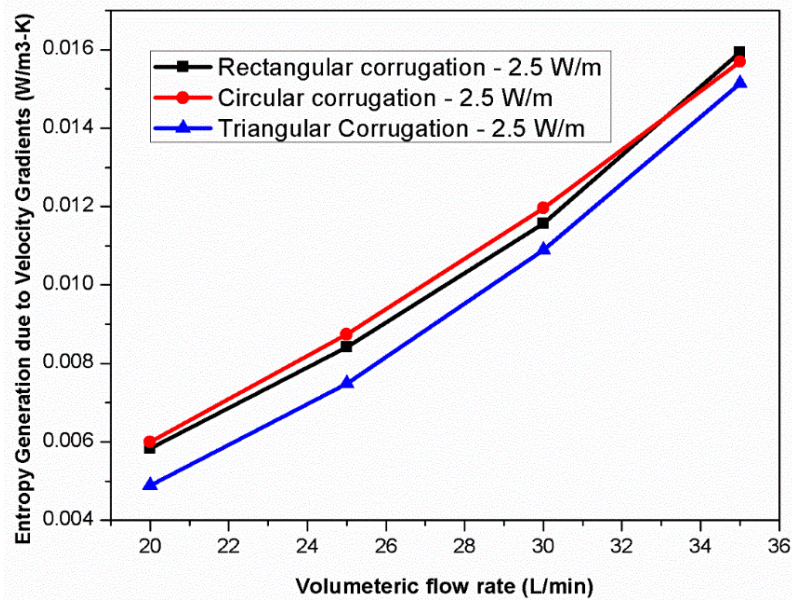


Figure 6.25 Effect of A.C loss of 2.5 W/m on entropy generation due to velocity gradients at constant heat flux of 6 W/m² with all three corrugations (rectangular, circular and triangular)

6.3 Summary and Conclusions

This section concludes the entropy generation phenomenon in the HTS cable with LN₂ turbulent flow. Moreover, the entropy generation due to velocity gradients and thermal gradients are also investigated computationally. In addition, the effect of various A.C losses, heat fluxes and corrugation topologies are considered for the analysis of entropy generation. The key findings of this chapter are as follows:

- It is found that as heat flux increases, the total entropy rate will also be increasing for each corrugation topology. Moreover, the entropy generation due to the thermal gradients also rises with increase in the heat flux at the outer walls of the HTS cable. However, no significant difference is observed in the entropy generation due to velocity gradients as the heat flux increases.
- No significant difference is obtained with the effect of various losses on the total entropy generation in HTS cable. Further no significant difference is obtained in the entropy generation due to thermal gradients at different A.C losses. In addition, no significant difference is observed in the entropy generation due to velocity gradients as the A.C losses increase equivalent to the entropy generation due to velocity gradients at various heat fluxes.
- It is also concluded from the results that there is no significant effect of A.C losses and heat fluxes on the entropy generation due to velocity gradients in the HTS cable. However, a significant effect A.C losses and heat fluxes on the entropy generation due to thermal gradients is seen.
- Hence, a significant effect of heat flux on total entropy generation is found whereas no such effect of A.C losses on total entropy generation is observed.

7 CONCLUSIONS AND FUTURE SCOPE

This chapter explores the conclusion and future recommendations based on the outcomes of the study and research objectives framed in the section 2.6. This thesis has presented and discussed the thermohydraulic studies and entropy generation in long length cold dielectric counter cooled High Temperature Superconducting (HTS) cables. The main intention of the analytical and computational thermohydraulic studies on HTS cable was to develop new skills, mathematical models and more understandings about design of HTS cable with long distance lengths. Contributions were made in the analytical approach of solving one-dimensional model using heat balance equations for temperature distributions in the HTS cable. Similarly, contributions in the computational approach of investigating thermohydraulic analysis in counter flow HTS cable.

7.1 Conclusions

The key findings of study can be summarized as follows:

- It is observed from the results that no significant difference between the effect of heat flux (heat-in-leaks) and the effect of heat generation (A.C losses) on the hydraulic performance of the HTS cable.
- A significant effect of LN2 inlet temperatures on hydraulic performance of the HTS cable is observed. The hydraulic parameters such as pressure drop, pumping power and friction factor are found to be decreasing, with increase in the LN2 inlet temperature.
- The thermal performance of the HTS cable is significantly affected by heat flux (heat-in-leaks) and heat generation (A.C losses). It is also found from the results that effect of heat flux (heat-in-leaks) contributes more than that of heat generation (A.C losses) in enhancing the temperature of the HTS cable.
- The effect of LN2 inlet temperature also affects the thermal performance of the HTS cable. The thermal characteristics such as Nusselt number reduces with increase in the LN2 inlet temperature and cooling capacity is observed to be increasing as LN2 inlet temperature increases.

- A nonlinear temperature distribution is observed along the length of HTS cable. The maximum possible length of 2.5 km can be achieved at the flow rate of 30 L/min and with heat fluxes of 2.3-2.6 W/m within the defined operating range.
- Hence, a significant effect of heat flux on total entropy generation is found whereas no such effect of A.C losses on total entropy generation is observed. Moreover, the velocity gradients are found to be dominating as that of thermal gradients in the total entropy generation.

7.2 Future Scope

The further improvements in research work presented in the thesis to enhance the cooling efficiency and design of HTS cable are as follows:

- Cooling strategies for stacked tapes in conduits (circular or rectangular) may be developed and associated hydraulic and thermal characteristics may be estimated.
- Solid cryogens are reported to be effective in cooling HTS magnets. Similarly, such investigations are necessary for HTS cables.
- Inclusion of nanoparticles in fluids is found to have enhanced thermophysical properties thereby aiding thermohydraulic characteristics. Such nano-cryogenic fluids may be implemented to further enhance the cooling of HTS cables.
- Entropy Generation Minimization (EGM) techniques can be used to optimize the mass flow rates for the computational thermohydraulic modeling of HTS cable.

REFERENCES

- [1] A. Malagoli, G. Grasso, M. Vignolo, A. Tumino, V. Braccini, C. Bernini, M. Tropeano, A. S. Siri, D. Nardelli, and M. Modica, “Long length MgB₂ conductors for industrial applications,” in *Advances in Science and Technology*, 2006, vol. 47, pp. 238–245.
- [2] S. S. Kalsi, *Applications of high temperature superconductors to electric power equipment*. Wiley, 2011.
- [3] R. Wesche, A. Anghel, B. Jakob, G. Pasztor, R. Schindler, and G. Vécsey, “Design of superconducting power cables,” *Cryogenics (Guildf.)*, vol. 39, no. 9, pp. 767–775, 1999.
- [4] J. A. Demko, J. W. Lue, M. J. Gouge, J. P. Stovall, U. Sinha, and R. L. Hughey, “Practical AC Loss and Thermal Considerations for HTS Power Transmission Cable Systems,” *IEEE Trans. Appl. Supercond.*, vol. 11, no. 1, pp. 1789–1792, 2001.
- [5] H. Noji, K. Haji, and T. Hamada, “AC loss analysis of 114 MVA high-T_c superconducting model cable,” *Phys. C Supercond.*, vol. 392–396, pp. 1134–1139, Oct. 2003.
- [6] M. Yagi, S. Tanaka, S. Mukoyama, M. Mimura, H. Kimura, S. Torii, S. Akita, and a. Kikuchi, “Measurement of ac losses of superconducting cable by calorimetric method and development of HTS conductor with low AC losses,” *IEEE Trans. Applied Supercond.*, vol. 13, no. 2, pp. 1902–1905, Jun. 2003.
- [7] H. Noji, K. Ikeda, K. Uto, and T. Hamada, “Numerical analysis of the AC loss in a high-TC superconducting cable measured by calorimetric method,” *Phys. C Supercond.*, vol. 425, no. 3–4, pp. 97–100, Sep. 2005.
- [8] H. Noji, “Numerical analysis of the AC losses of 500-m HTS power cable in Super-ACE project,” *Cryogenics (Guildf.)*, vol. 47, no. 2, pp. 94–100, Feb. 2007.
- [9] T. Famakinwa, Q. M. Chen, and S. Yamaguchi, “3D finite element analysis of eddy current losses of HTS tapes—Self field analysis,” *Phys. C Supercond.*,

- vol. 434, no. 1, pp. 71–78, Feb. 2006.
- [10] T. Famakinwa, Q. M. Chen, and S. Yamaguchi, “3D finite element analysis of eddy current loss of HTS tapes – External field analysis,” *Phys. C Supercond.*, vol. 459, no. 1–2, pp. 18–23, Aug. 2007.
- [11] J. Ogawa, H. Nakayama, S. Odaka, and O. Tsukamoto, “AC loss characteristics of YBCO conductors carrying transport currents in external AC magnetic fields,” *Cryogenics (Guildf.)*, vol. 45, no. 1, pp. 23–27, Jan. 2005.
- [12] H. M. Wen, L. Z. Lin, Y. B. Lin, Z. Y. Gao, S. T. Dai, and L. Shu, “AC losses measurement of 1 m long HTS cable,” *Phys. C Supercond.*, vol. 386, pp. 52–55, Apr. 2003.
- [13] J. W. Lue, J. A. Demko, L. Dresner, R. L. Hughey, U. Sinha, J. C. Tolbert, and S. K. Olsen, “AC Losses of Prototype HTS Transmission Cables,” 1998.
- [14] J. Oestergaard, J. Okholm, K. Lomholt, and O. Toennesen, “Energy losses of superconducting power transmission cables in the grid,” *IEEE Transactions on Applied Superconductivity*, vol. 11, no. 1, pp. 2375–2378, 2001.
- [15] K. Ryu, Y. H. Ma, Z. Y. Li, S. D. Hwang, and H. J. Song, “AC losses of the 5m BSCCO cables with shield,” *Phys. C Supercond.*, vol. 470, no. 20, pp. 1606–1610, Nov. 2010.
- [16] V. S. Vysotsky, K. A. Shutov, A. A. Nosov, N. V. Polyakova, S. S. Fetisov, V. V. Zubko, and V. E. Sytnikov, “AC loss of a model 5m 2G HTS power cable using wires with NiW substrates,” *J. Phys. Conf. Ser.*, vol. 234, 2010.
- [17] F. Grilli, S. Stavrev, B. Dutoit, and S. Spreafico, “Numerical Modeling of a HTS Cable,” *IEEE Trans. Appl. Supercond.*, vol. 13, no. 2, pp. 1886–1889, 2003.
- [18] J. Joo, S. Kim, K. J. Song, C. Park, R. Ko, H. Kim, and J. Hong, “Characteristics Measurements of HTS Tape with Parallel HTS Tapes,” *IEEE Trans. Appl. Supercond.*, vol. 16, no. 2, pp. 119–122, 2006.
- [19] S. Fukui, R. Kojima, J. Ogawa, M. Yamaguchi, T. Sato, and O. Tsukamoto,

- “Numerical Analysis of AC Loss Characteristics of Cable Conductor Assembled by HTS Tapes in Polygonal Arrangement,” *IEEE Trans. Appl. Supercond.*, vol. 16, no. 2, pp. 143–146, 2006.
- [20] A. K. M. Alamgir, C. Gu, and Z. Han, “Comparison of self-field effects between Bi-2223 / Ag tapes and pancake coils,” *Phys. C Supercond. its Appl.*, vol. 424, pp. 138–144, 2005.
- [21] D. E. Daney, M. P. Maley, H. J. Boenig, J. O. Willis, J. Y. Coulter, L. Gherardi, and G. Coletta, “Single-phase AC losses in prototype HTS conductors for superconducting power transmission lines,” *Phys. C Supercond.*, vol. 310, no. 1–4, pp. 236–239, Dec. 1998.
- [22] L. Y. Xiao, S. T. Dai, Y. B. Lin, Z. Y. Gao, F. Y. Zhang, X. Xu, and L. Z. Lin, “Development of HTS AC Power Transmission Cables,” *IEEE Trans. Appl. Supercond.*, vol. 17, no. 2, pp. 1652–1655, 2007.
- [23] D. Politano, M. Sjoström, G. Schnyder, and J. Rhyner, “Technical and economical assessment of HTS cables,” *IEEE Transactions on Applied Superconductivity*, vol. 11, no. 1, pp. 2477–2480, 2001.
- [24] C. Sumereeder, “Dielectric measurements on HTS insulation systems for electric power equipment,” *Phys. C Supercond. its Appl.*, vol. 386, pp. 411–414, 2003.
- [25] D. Koh, H. Yeom, and K. Lee, “Outgassing Test of High Temperature Superconducting (HTS) Power Cable Cryostat,” *IEEE Trans. Appl. Supercond.*, vol. 16, no. 2, pp. 1590–1593, 2006.
- [26] A. Kimura and K. Yasuda, “R & D of Superconductive Cable in Japan,” *IEEE Trans. Appl. Supercond.*, vol. 15, no. 2, pp. 1818–1822, 2005.
- [27] S. Mukoyama, M. Yagi, H. Hirano, Y. Yamada, T. Izumi, and Y. Shiohara, “Development of HTS power cable using YBCO coated conductor,” *Phys. C Supercond.*, vol. 445–448, pp. 1050–1053, Oct. 2006.
- [28] Z. Li, K. Ryu, S. Fukui, S. D. Hwang, and G. Cha, “AC Loss Measurement of a

- Short HTS Cable With Shield by Electrical Method,” *IEEE Trans. Appl. Supercond.*, vol. 21, no. 3, pp. 1005–1008, 2011.
- [29] S. Mukoyama, M. Yagi, N. Fujiwara, and H. Ichikawa, “Conceptual design of 275 kV class high-Tc superconducting cable,” *Phys. C Supercond. its Appl.*, vol. 470, no. 20, pp. 1563–1566, 2010.
- [30] V. V Zubko, A. A. Nosov, N. V Polyakova, S. S. Fetisov, and V. V Vysotsky, “Hysteresis Loss in Power Cables Made of 2G HTS Wires With NiW Alloy Substrate,” *IEEE Trans. Appl. Supercond.*, vol. 21, no. 3, pp. 988–990, 2011.
- [31] S. S. Fetisov, V. V. Zubko, A. A. Nosov, and V. S. Vysotsky, “Losses in Power Cables Made of 2G HTS Wires with Different Substrates,” *Phys. Procedia*, vol. 36, pp. 1319–1323, Jan. 2012.
- [32] M. Kalsia, R. S. Dondapati, and P. R. Usurumarti, “AC Losses and Dielectric Losses in High Temperature Superconducting (HTS) Power Cables for Smart Grid Applications : A Comprehensive Review,” *Int. J. Control theory Appl.*, vol. 9, no. 41, pp. 309–317, 2016.
- [33] O. Maruyama, T. Ohkuma, T. Masuda, M. Ohya, S. Mukoyama, and M. Yagi, “Development of REBCO HTS power cables,” *Phys. Procedia*, vol. 36, pp. 1153–1158, 2012.
- [34] M. D. Ainslie, T. J. Flack, and A. M. Campbell, “Calculating transport AC losses in stacks of high temperature superconductor coated conductors with magnetic substrates using FEM,” *Phys. C Supercond.*, vol. 472, no. 1, pp. 50–56, Jan. 2012.
- [35] and Y. Zhuonan Zhou, Jiahui Zhu, Huifeng Li, Ming Qiu, Zhenming Li, Kaizhong Ding, “Magnetic-Thermal Coupling Analysis of the Cold Dielectric High Temperature Superconducting Cable,” *IEEE Trans. Appl. Supercond.*, vol. 23, no. 3, pp. 3–6, 2013.
- [36] J. He, Y. Tang, B. Wei, J. Li, L. Ren, J. Shi, K. Wang, X. Li, Y. Xu, and S. Wang, “Thermal analysis of HTS power cable using 3-D FEM model,” *IEEE Trans. Appl. Supercond.*, vol. 23, no. 3, pp. 1–4, 2013.

- [37] G. Vyas, R. S. Dondapati, and P. R. Usurumarti, "Parametric Evaluation of AC Losses in 500 MVA/1.1 kA High Temperature Superconducting (HTS) Cable for Efficient Power Transmission: Self Field Analysis," *Model. Symp. (EMS), 2014 Eur.*, pp. 315–319, 2014.
- [38] S. Fuchino, N. Tamada, I. Ishii, and N. Higuchi, "Hydraulic characteristics in superconducting power transmission cables," vol. 354, pp. 4–7, 2001.
- [39] C. H. Lee, C. D. Kim, K. S. Kim, D. H. Kim, and I. S. Kim, "Performance of heat transfer and pressure drop in superconducting cable former," *Cryogenics (Guildf.)*, vol. 43, pp. 583–588, 2003.
- [40] D. K. D. Koh, H. Y. H. Yeom, Y. H. Y. Hong, and K. L. K. Lee, "Performance tests of high temperature superconducting power cable cooling system," *IEEE Trans. Appl. Supercond.*, vol. 14, no. 2, pp. 1746–1749, 2004.
- [41] A. Sasaki, M. Hamabe, T. Famakinwa, S. Yamaguchi, A. Radovinsky, and H. Okumura, "Cryogenic Fluid Dynamics for DC Superconducting Power Transmission Line," *IEEE Trans. Appl. Supercond.*, vol. 17, no. 2, pp. 1748–1751, 2007.
- [42] A. Sasaki, M. Hamabe, T. Famakinwa, S. Yamaguchi, and A. Radovinsky, "A NUMERICAL ANALYSIS IN LN2 CHANNEL FOR DC-SC POWER TRANSMISSION LINE," *AIP Conf. Proc.*, vol. 985, pp. 75–82, 2008.
- [43] Y. Ivanov, H. Watanabe, M. Hamabe, T. Kawahara, J. Sun, and S. Yamaguchi, "Design Study of LN2 Circulation in a Long SC Power Transmission Lines," *Phys. Procedia*, vol. 36, pp. 1372–1377, 2012.
- [44] Y. V. Ivanov, H. Watanabe, M. Hamabe, J. Sun, T. Kawahara, and S. Yamaguchi, "Circulation pump power for 200 m cable experiment," *Phys. C Supercond.*, vol. 471, no. 21–22, pp. 1308–1312, 2011.
- [45] A. Sasaki, Y. Ivanov, and S. Yamaguchi, "LN2 circulation in cryopipes of superconducting power transmission line," *Cryogenics (Guildf.)*, vol. 51, no. 9, pp. 471–476, Sep. 2011.

- [46] B. Zajackowski, A. J. M. Giesbers, M. Holtrust, E. Haenen, and R. den Heijer, “Feasibility of inline cooling in long distance HTS power line,” *Cryogenics (Guildf)*, vol. 51, no. 4, pp. 180–186, Apr. 2011.
- [47] R. S. Dondapati and V. V Rao, “Pressure Drop and Heat Transfer Analysis of Long Length Internally Cooled HTS Cables,” *Appl. Supercond. IEEE Trans.*, vol. 23, no. 3, pp. 2–5, 2013.
- [48] E. Shabagin, C. Heidt, S. Strauß, and S. Grohmann, “Modelling of 3D temperature profiles and pressure drop in concentric three-phase HTS power cables,” *Cryogenics (Guildf)*, vol. 81, pp. 24–32, 2017.
- [49] Z. Li, Y. Li, W. Liu, J. Zhu, and M. Qiu, “Comparison of Liquid Nitrogen Flow Resistance in Corrugated Pipe With Smooth Pipe for HTS Cable,” *IEEE Trans. Appl. Supercond.*, vol. 25, no. 3, 2015.
- [50] O. Maruyama and T. Mimura, “Fluid characteristic of liquid nitrogen flowing in HTS cable,” *J. Phys. Conf. Ser.*, vol. 1054, 2018.
- [51] Z. Q. Zuo, W. B. Jiang, Z. G. Yu, and Y. H. Huang, “Effect of inserted HTS power transmission cables on friction loss in corrugated pipes,” *IOP Conf. Ser. Mater. Sci. Eng.*, vol. 502, 2019.
- [52] C. Lee, D. Kim, S. Kim, D. Y. Won, and H. S. Yang, “Thermo-Hydraulic Analysis on Long Three-Phase Coaxial HTS Power Cable of Several Kilometers,” *IEEE Trans. Appl. Supercond.*, vol. 29, no. 2, pp. 1–5, 2019.
- [53] I. Das and V. V Rao, “Hydraulic analysis of liquid nitrogen flow through concentric annulus with corrugations for High Temperature Superconducting power cable,” *Cryogenics (Guildf)*, 2019.
- [54] S. Fuchino, M. Furuse, and N. Higuchi, “Longitudinal Temperature Distribution in Superconducting Power Cables with counter-Flow Cooling,” *IEEE Trans. Appl. Supercond.*, vol. 12, no. 1, pp. 1339–1342, 2002.
- [55] M. Furuse, S. Fuchino, and N. Higuchi, “Counter flow cooling characteristics with liquid nitrogen for superconducting power cables,” *Cryogenics (Guildf)*,

- vol. 42, pp. 405–409, 2002.
- [56] M. Furuse, S. Fuchino, and N. Higuchi, “Investigation of structure of superconducting power transmission cables with LN₂ counter-flow cooling,” *Phys. C Supercond.*, vol. 386, pp. 474–479, 2003.
- [57] J. A. Demko, J. W. Lue, M. J. Gouge, P. W. Fisher, D. Lindsay, and M. Roden, “Analysis of a Liquid Nitrogen-Cooled Tri-Axial High-Temperature Superconducting Cable System,” *Am. Inst. Phys.*, vol. 49, pp. 913–920, 2004.
- [58] A. Posada, Y. I. Kim, and V. Manousiouthakis, “On conduction-cooling of a high-temperature superconducting cable,” *Cryogenics (Guildf.)*, vol. 46, no. 6, pp. 458–467, Jun. 2006.
- [59] J. A. Demko and R. C. Duckworth, “Cooling Configuration Design Considerations for Long-Length HTS Cables,” *IEEE Trans. Appl. Supercond.*, vol. 19, no. 3, pp. 1752–1755, 2009.
- [60] Y. Ivanov, A. Radovinsky, A. Zhukovsky, A. Sasaki, H. Watanabe, T. Kawahara, M. Hamabe, and S. Yamaguchi, “Compact counter-flow cooling system with subcooled gravity-fed circulating liquid nitrogen,” *Phys. C Supercond.*, vol. 470, no. 20, pp. 1895–1898, 2010.
- [61] J. A. Souza, J. C. Ordonez, R. Hovsopian, and J. V. C. Vargas, “Thermal Modeling of Helium Cooled High-Temperature Superconducting DC Transmission Cable,” *IEEE Trans. Appl. Supercond.*, vol. 21, no. 3, pp. 947–952, 2011.
- [62] O. Maruyama, T. Ohkuma, T. Izumi, and Y. Shiohara, “Numerical Analysis of Heat Transfer and Fluid Characteristics of Flowing Liquid Nitrogen in HTS Cable,” *Phys. Procedia*, vol. 58, pp. 330–333, 2014.
- [63] H. Chang, K. Nam, and H. Suk, “Integrated design of cryogenic refrigerator and liquid-nitrogen circulation loop for HTS cable,” *Cryogenics (Guildf.)*, vol. 80, pp. 183–192, 2016.
- [64] S. Lee, H. Sung, M. Park, D. Won, J. Yoo, and H. S. Yang, “Analysis of the

- Temperature Characteristics of according to a Liquid Nitrogen Circulation Method for Real-Grid Application in Korea,” *Energies*, vol. 12, pp. 1–11, 2019.
- [65] A. Z. Sahin, “Irreversibilities in various duct geometries with constant wall heat flux and laminar flow,” *Energy*, vol. 23, no. 6, pp. 465–473, 1998.
- [66] A. Z. Sahin, “The effect of variable viscosity on the entropy generation and pumping power in a laminar fluid flow through a duct subjected to constant heat flux,” *Heat Mass Transf.*, vol. 35, pp. 499–506, 1999.
- [67] E. B. Ratts and A. G. Raut, “Entropy Generation Minimization of Fully Developed Internal Flow With Constant Heat Flux,” *J. Heat Transfer*, vol. 126, pp. 656–659, 2004.
- [68] T. H. Ko and K. Ting, “Entropy generation and thermodynamic optimization of fully developed laminar convection in a helical coil,” *Int. Commun. Heat Mass Transf.*, vol. 32, pp. 214–223, 2005.
- [69] R. S. Dondapati and V. V Rao, “Entropy generation minimization (EGM) to optimize mass flow rate in dual channel cable-in-conduit conductors (CICCs) used for fusion grade magnets,” *Fusion Eng. Des.*, vol. 89, no. 6, pp. 837–846, Jun. 2014.
- [70] F. M. White, *Fluid Mechanics*, Second Ed. Mc Graw Hill, 1986.
- [71] M. Kalsia and R. S. Dondapati, “Thermohydraulic Analysis of Cold Dielectric High Temperature Superconducting Cable with Counter-flow Cooling,” *Phys. C Supercond. its Appl.*, vol. 564, pp. 59–67, 2019.
- [72] S. M. Vanaki and H. A. Mohammed, “Numerical study of nanofluid forced convection flow in channels using different shaped transverse ribs,” *Int. Commun. Heat Mass Transf.*, vol. 67, pp. 176–188, 2015.
- [73] H. Stel, R. E. M. Morales, A. T. Franco, S. L. M. Junqueira, and R. H. Erthal, “Numerical and Experimental Analysis of Turbulent Flow in Corrugated Pipes,” *J. Fluids Eng.*, vol. 132, 2010.

- [74] A. Özden, H. Demir, Ş. Ö. Atay, F. Kanta, and A. Selim, “Numerical investigation of heat transfer and pressure drop in enhanced tubes,” *Int. Commun. Heat Mass Transf. J.*, vol. 38, pp. 1384–1391, 2011.
- [75] D. Zhang, H. Tao, Y. Xu, and Z. Sun, “Numerical Investigation on Flow and Heat Transfer Characteristics of Corrugated Tubes with Non-uniform Corrugation in Turbulent Flow,” *Chinese J. Chem. Eng.*, vol. 26, no. 3, pp. 437–444, 2017.
- [76] S. Eiamsa-ard and P. Promvonge, “Numerical study on heat transfer of turbulent channel flow over periodic grooves,” *Int. Commun. Heat Mass Transf.*, vol. 35, pp. 844–852, 2008.
- [77] R. Kiml, A. Magda, S. Mochizuki, and A. Murata, “Rib-induced secondary flow effects on local circumferential heat transfer distribution inside a circular rib-roughened tube,” *Int. J. Heat Mass Transf.*, vol. 47, pp. 1403–1412, 2004.
- [78] P. Orlandi, “Properties of d- and k-type roughness in a turbulent channel flow Properties of d- and k-type roughness in a turbulent channel flow,” *Phys. fluids*, vol. 19, no. 2007, 2019.
- [79] L. Xiao-wei, M. Ji-an, and L. Zhi-xin, “International Journal of Heat and Mass Transfer Roughness enhanced mechanism for turbulent convective heat transfer,” *Int. J. Heat Mass Transf.*, vol. 54, no. 9–10, pp. 1775–1781, 2011.
- [80] K. Bilen, M. Cetin, H. Gul, and T. Balta, “The investigation of groove geometry effect on heat transfer for internally grooved tubes,” *Appl. Therm. Eng.*, vol. 29, no. 4, pp. 761–769, 2009.
- [81] B. Launder, “The Numerical Computation of Turbulent Flow Computer Methods,” *Comput. Methods Appl. Mech. Eng.*, vol. 3, no. 2, pp. 269–289, 1974.
- [82] C. Thianpong, P. Eiamsa-ard, K. Wongcharee, and S. Eiamsa-ard, “Compound heat transfer enhancement of a dimpled tube with a twisted tape swirl generator,” *Int. Commun. Heat Mass Transf.*, vol. 36, no. 7, pp. 698–704, 2009.

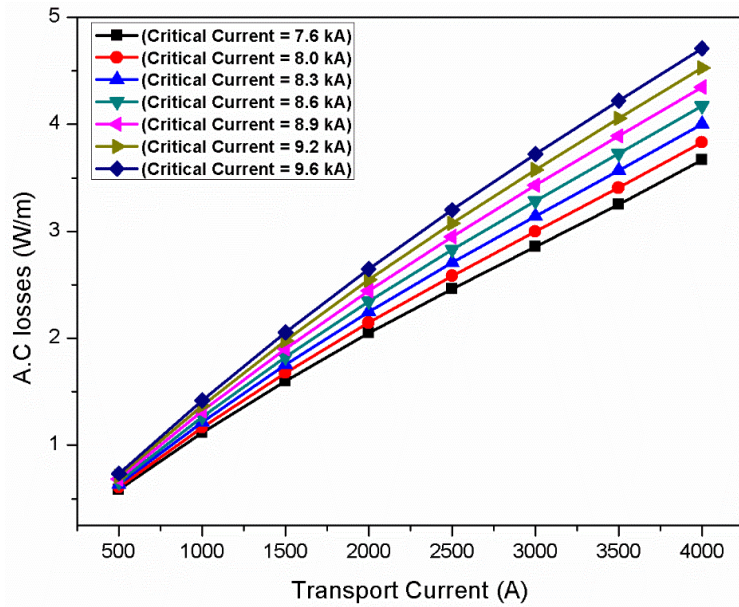
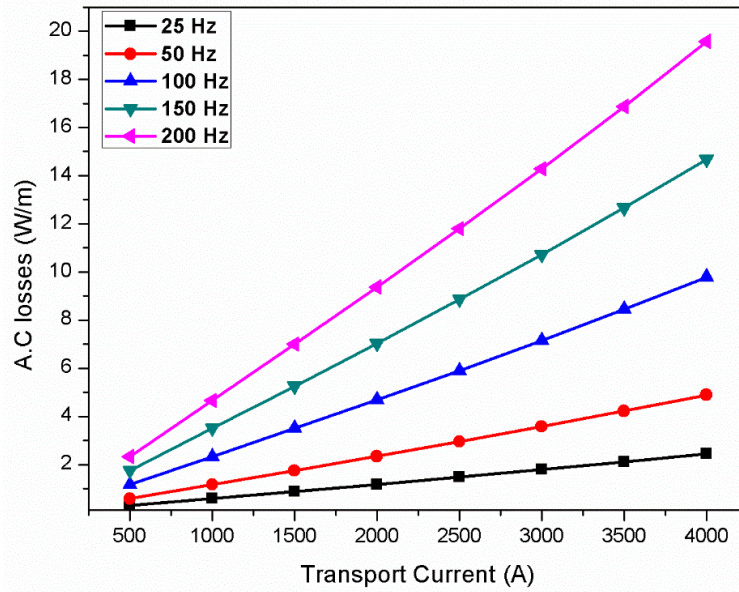
- [83] P. Naphon, M. Nuchjapo, and J. Kurujareon, "Tube side heat transfer coefficient and friction factor characteristics of horizontal tubes with helical rib," *Energy Convers. Manag.*, vol. 47, pp. 3031–3044, 2006.
- [84] S. Pethkool, S. Eiamsa-ard, S. Kwankaomeng, and P. Promvong, "Turbulent heat transfer enhancement in a heat exchanger using helically corrugated tube," *Int. Commun. Heat Mass Transf.*, vol. 38, no. 3, pp. 340–347, 2011.
- [85] A. Vatani and H. A. Mohammed, "Turbulent Nanofluid Flow Over Periodic Rib- Grooved Channels," *Eng. Appl. Comput. Fluid Mech.*, vol. 7, no. 3, pp. 369–381, 2014.
- [86] H. A. Mohammed, A. K. Abbas, and J. M. Sheriff, "Influence of geometrical parameters and forced convective heat transfer in transversely corrugated circular tubes," *Int. Commun. Heat Mass Transf.*, vol. 44, pp. 116–126, 2013.
- [87] O. Manca, S. Nardini, and D. Ricci, "Numerical analysis of water forced convection in channels with differently shaped transverse ribs," *J. Appl. Math.*, vol. 2011, 2011.
- [88] M. Ahsan, "Numerical analysis of friction factor for a fully developed turbulent flow using $k-\epsilon$ turbulence model with enhanced wall treatment," *Beni-Suef Univ. J. Basic Appl. Sci.*, vol. 3, no. 4, pp. 269–277, 2014.
- [89] A. Kaood, H. Eltahan, M. A. Yehia, and E. E. Khalil, "Numerical investigation of heat transfer and friction characteristics for turbulent flow in various corrugated tubes," *J. Power Energy*, vol. 233, pp. 1–19, 2018.
- [90] X. Chen, H. Han, K. Lee, B. Li, and Y. Zhang, "Turbulent heat transfer enhancement in a heat exchanger using asymmetrical outward convex corrugated tubes," *Nucl. Eng. Des.*, vol. 350, no. January, pp. 78–89, 2019.
- [91] S. Song, X. Yang, F. Xin, T. J. Lu, S. Song, X. Yang, F. Xin, and T. J. Lu, "Modeling of surface roughness effects on Stokes flow in circular pipes," *Phys. fluids*, vol. 30, no. 2, 2018.
- [92] M. Pisarenco, "Friction Factor Estimation for Turbulent Flows in Corrugated

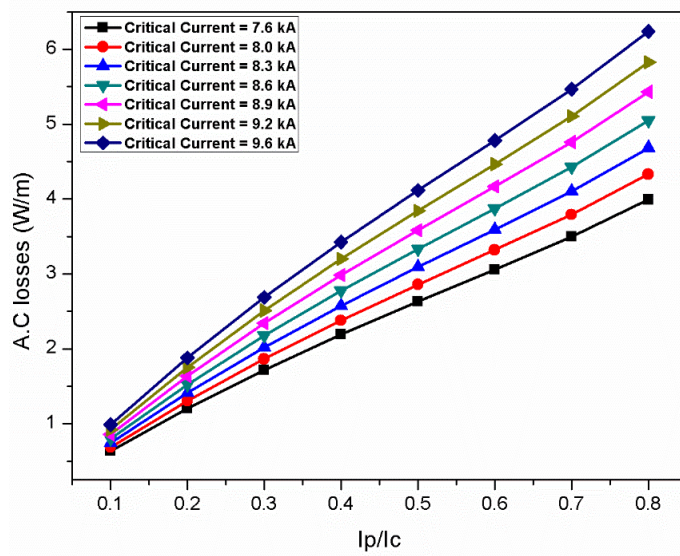
- Pipes with Rough Walls,” *J. Offshore Mech. Arct. Eng.*, vol. 133, no. February, pp. 1–9, 2011.
- [93] H. Benzenine and R. Saim, “Comparative study of the thermo-convective behavior of a turbulent flow in a rectangular duct in the presence of three planar baffles and / or corrugated (waved),” *J. Eng. Sci. Technol.*, vol. 13, no. 1, pp. 35–47, 2018.
- [94] V. Zimparov, “Enhancement of heat transfer by a combination of a single-start spirally corrugated tubes with a twisted tape,” *Exp. Therm. FLUID Sci.*, vol. 25, pp. 535–546, 2002.
- [95] L. Xiao-wei, M. Ji-an, and L. Zhi-xin, “Experimental study of single-phase pressure drop and heat transfer in a micro-fin tube,” *Exp. Therm. FLUID Sci.*, vol. 32, pp. 641–648, 2007.
- [96] D. L. Gee, “FORCED CONVECTION HEAT TRANSFER IN HELICALLY RIB-ROUGHENED TUBES,” *Int. J. Heat mass Transf.*, vol. 23, pp. 1127–1136, 1980.
- [97] R. L. Webb, E. R. G. Eckert, and R. J. Goldstein, “HEAT TRANSFER AND FRICTION IN TUBES WITH REPEATED-RIB ROUGHNESS,” *Int. J. Heat Mass Transf.*, vol. 14, pp. 601–617, 1971.
- [98] D. F. Dipprey and R. H. Sabersky, “Heat and Momentum Transfer in Smooth and Rough Tubes at Various Prandtl Numbers,” *Int. J. Heat mass Transf.*, vol. 6, pp. 329–353, 1963.
- [99] E. N. Sieder and G. E. Tate, “Heat Transfer and Pressure Drop of Liquids in Tubes,” *Ind. Eng. Chem.*, vol. 28, no. 12, pp. 1429–1435, 1936.
- [100] J. San and W. Huang, “Heat transfer enhancement of transverse ribs in circular tubes with consideration of entrance effect,” *Int. J. Heat Mass Transf.*, vol. 49, pp. 2965–2971, 2006.
- [101] “A review of non iterative friction factor correlations for the calculation of pressure drop in pipes,” *J. Sci. Technol. .*, vol. 4, no. 1, pp. 1–8, 2014.

- [102] R. S. Dondapati, J. Ravula, S. Thadela, and P. R. Usurumarti, “Analytical approximations for thermophysical properties of supercritical nitrogen (SCN) to be used in futuristic high temperature superconducting (HTS) cables,” *Phys. C Supercond. its Appl.*, vol. 519, pp. 53–59, 2015.
- [103] Y. Ivanov, H. Watanabe, M. Hamabe, T. Kawahara, and J. Sun, “Observation of the thermosiphon effect in the circulation of liquid nitrogen in HTS cable cooling system,” *Phys. Procedia*, vol. 27, pp. 368–371, 2012.

Appendix A

Estimation of A.C losses in the Counter Cooled HTS Cable





Initial Parameters

`%Ic (A) Critical current of HTS tape`

`%muo permeability in free space`

`%gamma ratio of peak current to the critical current`

`%QAC (W/m) AC losses in the HTS cable`

`%1-7 number represents the AC losses for various Ic`

```
>> i=1
```

```
Ic=300;
```

```
muo=4.00E-07;
```

```
for gamma=0.2:0.1:0.9
```

```
for QAC1=0:0.5:5
```

```
QAC1=[ ((240^2) * (muo/pi)) * ((1-gamma) * log(1-gamma) + (gamma-0.5*gamma^2)) ]
```

```
QAC2=[ ((250^2) * (muo/pi)) * ((1-gamma) * log(1-gamma) + (gamma-0.5*gamma^2)) ]
```

```
QAC3=[ ((260^2) * (muo/pi)) * ((1-gamma) * log(1-gamma) + (gamma-0.5*gamma^2)) ]
```

```
QAC4=[ ((270^2) * (muo/pi)) * ((1-gamma) * log(1-gamma) + (gamma-0.5*gamma^2)) ]
```

```
QAC5=[ ((280^2) * (muo/pi)) * ((1-gamma) * log(1-gamma) + (gamma-0.5*gamma^2)) ]
```

```
QAC6=[ ((290^2) * (muo/pi)) * ((1-gamma) * log(1-gamma) + (gamma-0.5*gamma^2)) ]
```

```
QAC7=[ ((300^2) * (muo/pi)) * ((1-gamma) * log(1-gamma) + (gamma-0.5*gamma^2)) ]
```

```
QAC1gamma(i)=QAC1;
```

```
QAC2gamma(i)=QAC2;
```

```
QAC3gamma(i)=QAC3;
```

```
QAC4gamma(i)=QAC4;
```

```
QAC5gamma(i)=QAC5;
```

```
QAC6gamma(i)=QAC6;
```

```
QAC7gamma(i)=QAC7;
```

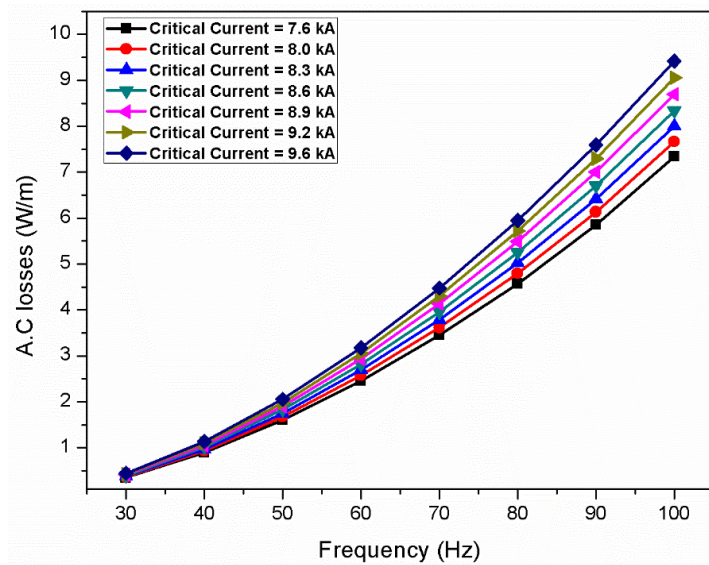
```
end
```

```
i=i+1
```

```
end
```

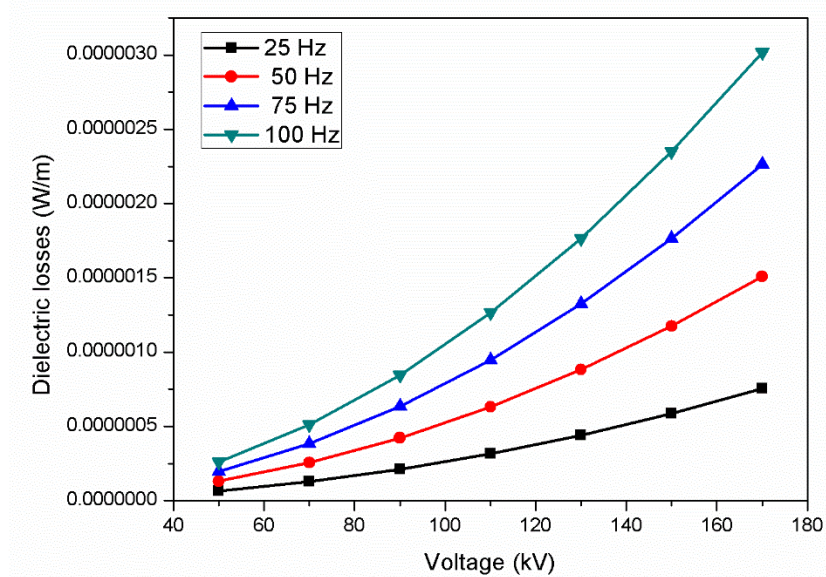
```
gamma=0.2:0.1:0.9
```

```
plot(gamma, QAC1gamma, gamma, QAC2gamma, gamma, QAC3gamma, gamma, QAC4gamma, gamma, QAC5gamma, gamma, QAC6gamma, gamma, QAC7gamma)
```



Appendix B

Estimation of Dielectric losses in the Counter Cooled HTS Cable



Initial parameters

```
% Pd- Dielectric losses
```

```
% Up- Ground to peak voltage
```

```
% eps- Dielectric constant of the insulation
```

```
% eps0- Permittivity of free space
```

```
% rod- outer radius of dielectric
```

```
% rid- inner radius of dielectric
```

```
% omega- angular power frequency
```

```
% x- phase to ground peak voltage
```

```
% tand- the loss angle
```

```
% Pdfif- Dielectric losses at frequency of 50 Hz
```

```
% Pdsev- Dielectric losses at frequency of 75 Hz
```

```
% Pdhun- Dielectric losses at frequency of 100 Hz
```

```
>> i=1
```

```
eps=2.3;
```

```
tand=0.00058;
```

```
rod=25;
```

```

rid=20;
epso=0.000000000000885;
for Up=50:20:170
for Pd=0:0.000001:0.00000005

Pd=[ (157.07*(Up)^2)*(eps*tand)*(pi*epso)/log(rod/rid)]
Pdfif=[ (314.15*(Up)^2)*(eps*tand)*(pi*epso)/log(rod/rid)]
Pdsev=[ (471.23*(Up)^2)*(eps*tand)*(pi*epso)/log(rod/rid)]
Pdhun=[ (628.31*(Up)^2)*(eps*tand)*(pi*epso)/log(rod/rid)]

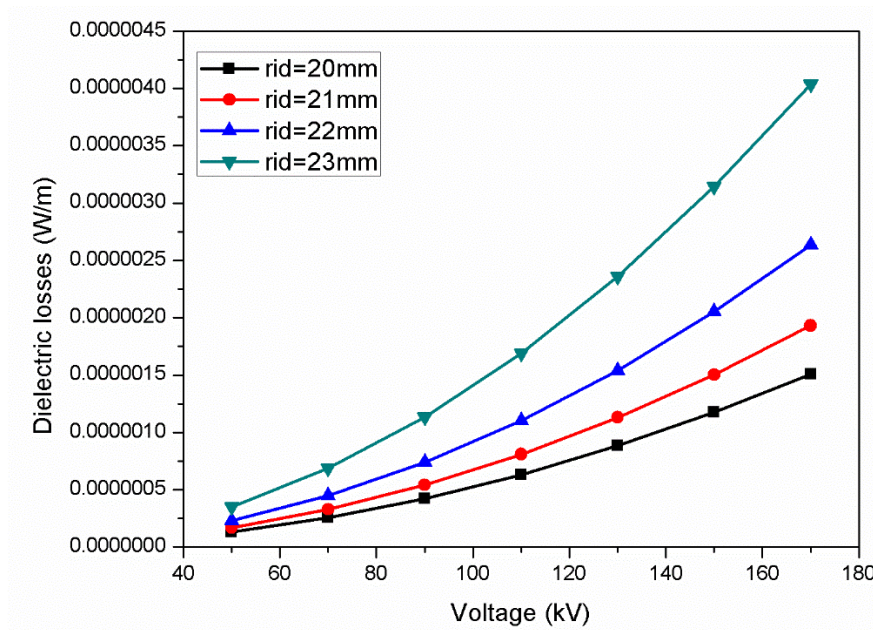
PdUp(i)=Pd;
PdfifUp(i)=Pdfif;
PdsevUp(i)=Pdsev;
PdhunUp(i)=Pdhun;

end

i=i+1
end

Up=50:20:170
plot (Up,PdUp,Up,PdfifUp,Up,PdsevUp,Up,PdhunUp)

```



```

Initial parameters
% Pd- Dielectric losses
% Up- Ground to peak voltage
% eps- Dielectric constant of the insulation
% eps0- Permittivity of free space
% rod- outer radius of dielectric
% rid- inner radius of dielectric
% omega- angular power frequency
% x- phase to ground peak voltage
% tand- the tan delta loss

% Pdfif- Dielectric losses at radius of 21 mm
% Pdsev- Dielectric losses at radius of 22 mm
% Pdhun- Dielectric losses at radius of 23 mm

>> i=1
eps=2.3;
tand=0.00058;
omega=314.15;
rod=25;

```



```

epso=0.00000000000885;
for Up=50:20:170
for Pd=0:0.000001:0.0000005

Pd=[ (omega*(Up)^2)*(eps*tand)*((pi*epso)/log(rod/20))]
Pdfif=[ (omega*(Up)^2)*(eps*tand)*((pi*epso)/log(rod/21))]
Pdsev=[ (omega*(Up)^2)*(eps*tand)*((pi*epso)/log(rod/22))]
Pdhun=[ (omega*(Up)^2)*(eps*tand)*((pi*epso)/log(rod/23))]

PdUp(i)=Pd;
PdfifUp(i)=Pdfif;
PdsevUp(i)=Pdsev;
PdhunUp(i)=Pdhun;

end
i=i+1
end
Up=50:20:170
plot (Up,PdUp,Up,PdfifUp,Up,PdsevUp,Up,PdhunUp)

```

Appendix C

Temperature Profiles in HTS Cable without cryocooler at the End

Initial parameters

K (W/m-k), overall linear thermal conductance between inner region and annular region

Q_{total} , summation of all the heat loads ($Q_{ac} + Q_e + q_x$)

Q_{ac} (W/m), heat loss per unit length produced by electrical dissipation

Q_e (W/m), heat loss per unit length from the ambient

q_x (W/m), amount of heat exchanged between both the flows

M (Kg/s), mass flow rate of coolant

C_p (j/kg-K), specific heat of the coolant

L (m), length of the HTS cable

T_o (K), inlet temperature of coolant

T_2 (K), Temperature of annular region flow

T_1 (K), Temperature of inner region flow

```
>> i=1
K=0.1738;
Qtotal=2.3;
MCp=573.773;
L=3000;
Qac=1.4;
To=65;
for x=10:10:3000
for T1=65:1:110
T1=[-
(pi*K*Qtotal*x^2)/(MCp)^2]+[(1/MCp)*((2*pi*K)*(Qtotal)*(L)/(MCp)+(Qac/2))*(x)+To]
T2=[-
(pi*K*Qtotal*x^2)/(MCp)^2]+[(1/MCp)*((2*pi*K)*(Qtotal)*(L)/(MCp)-(1.6))*(x)+To+((Qtotal/MCp)*L)]
T1x(i)=T1;
```

```
T2x(i)=T2;  
end  
i=i+1  
end  
x=10:10:3000  
plot(x,T1x,x,T2x)
```

Appendix D

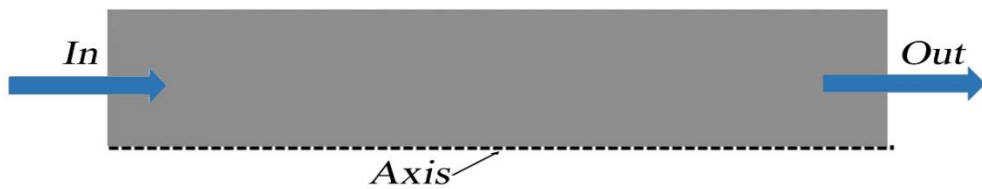
Temperature Profiles in HTS Cable with cryocooler at the End

```
>> i=1
K=0.1738;
Qtotal=2.4;
MCp=573.773;
Qf1=0.05;
Qac=1.4;
To=65;
for x=10:100:3000
for T1=65:1:110
T1=[-
(pi*K*Qtotal*x^2)/(MCp)^2]+[(1/MCp)*((2*pi*K)*(10.5485)+(Qac/2
)+(Qf1))*(x)+To]
T2=[-
(pi*K*Qtotal*x^2)/(MCp)^2]+[(1/MCp)*((2*pi*K)*(10.5485)+(Qac/2
)+(Qf1)-(Qtotal))*(x)+To+(10.5485)]
T1x(i)=T1;
T2x(i)=T2;
end
i=i+1
end
x=10:100:3000
plot(x,T1x,x,T2x)
```

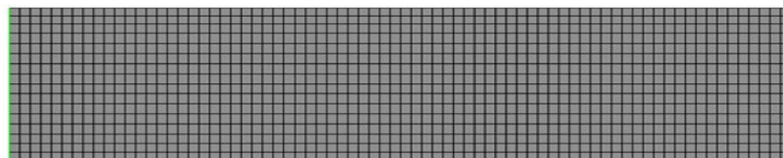

Appendix E

Performance of k- ϵ reliable turbulence model

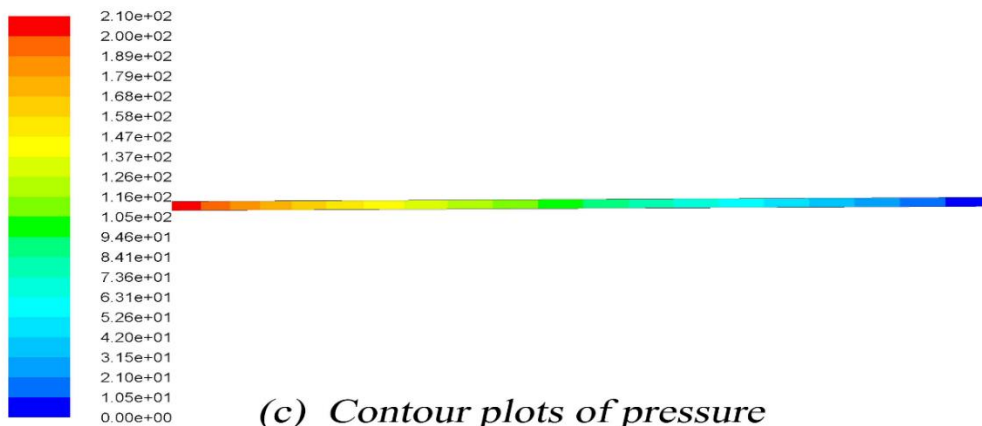
Parameters	Approach (2D Axisymmetric Computational Model)
Diameter of cylinder (mm)	14
Length of cylinder (mm)	500
Material Used	Liquid Nitrogen (LN2)
Density of LN2 (kg/m ³)	860
Viscosity of LN2 (Pa-s)	0.000282
Turbulence Model	k- ϵ reliable
Mass-flow inlet (kg/s)	0.1, 0.2, 0.3, 0.4, 0.5
Boundary Outlet	Outflow
Pressure Drop (Pa)	208.33, 696.4, 1443.50, 2428.35, 3637.58



(a) Computational model

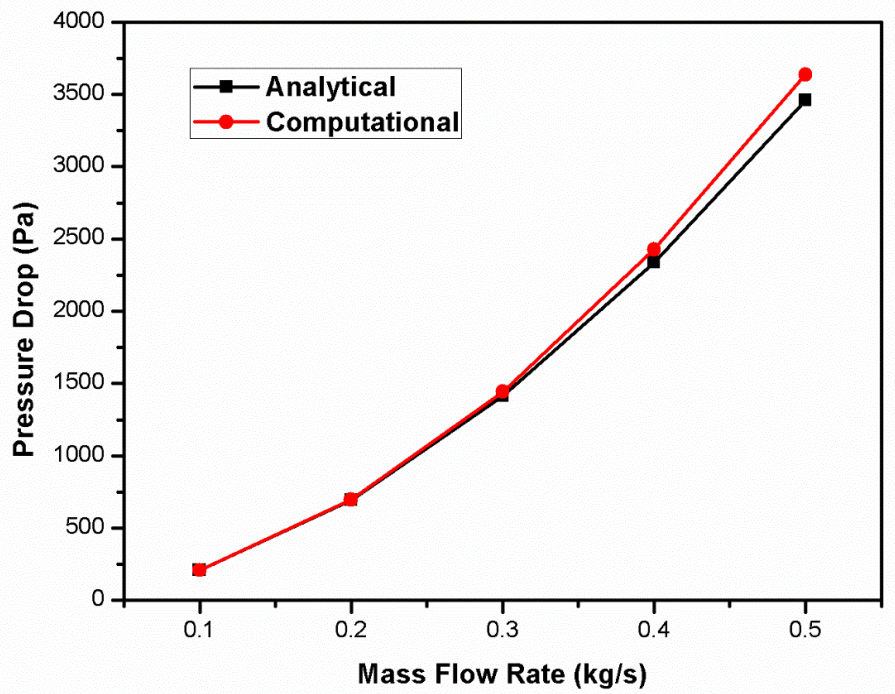


(b) Quad Mesh generated



(c) Contour plots of pressure

Parameters	Approach (Analytical)
Diameter of cylinder (mm)	14
Length of cylinder (mm)	500
Density of LN2 (kg/m ³)	860
Viscosity of LN2 (Pa-s)	0.000282
Mass-flow inlet (kg/s)	0.1, 0.2, 0.3, 0.4, 0.5
Friction factor (Blasius Formula)	$f=(100*Re)^{-0.25}$
Pressure Drop (Pa)	206.87, 695.5, 1414.00, 2339.35, 3456.90



List of Publications

1. **Mohit Kalsia**, Raja Sekhar Dondapati, “*Influence of Flow Rate and Heat Flux on the Temperature Distribution in Long Length Counter Flow Cooled Cold Dielectric HTS Cables*,” **Physica C: Superconductivity and its applications**, 1353549 (2019).
2. **Mohit Kalsia**, Raja Sekhar Dondapati, “*Influence of Corrugation Topology on Thermohydraulic Performance of Cold Dielectric Counter Cooled High Temperature Superconducting Cable*,” **Physica C: Superconductivity and its applications**, vol. 566, (2019).
3. **Mohit Kalsia**, Raja Sekhar Dondapati, “*Thermohydraulic Analysis of Cold Dielectric High Temperature Superconducting Cable with Counter-Flow Cooling*,” **Physica C: Superconductivity and its applications**, vol. 564, pp. 59–67 (2019).
4. **Mohit Kalsia**, Raja Sekhar Dondapati and Preeti Rao Usurumarti, “*Statistical correlations for thermophysical properties of Supercritical Argon (SCAR) used in cooling of futuristic High Temperature Superconducting (HTS) cables*,” **Physica C: Superconductivity and its applications**, vol. 536 pp. 30–34 (2017).
5. **Mohit Kalsia**, Raja Sekhar Dondapati and Preeti Rao Usurumarti, “*Conceptual Design of High Temperature Superconducting (HTS) Cables: A Review*,” **International Journal of Mechanical Engineering and Technology**, vol. 8, pp. 1180–1188 (2017).
6. Vikul Vasudev, **Mohit Kalsia**, Raja Sekhar Dondapati and Preeti Rao Usurumarti, “*Conceptual Design and Cooling Strategies of Current Lead for Superconducting Power Transmission Applications*,” **IEEE Region 10 Annual International Conference**, Proceedings/TENCON (2017).
7. **Mohit Kalsia**, Raja Sekhar Dondapati and Preeti Rao Usurumarti, “*AC Losses and Dielectric Losses in High Temperature Superconducting (HTS) Power Cables for Smart Grid Applications: A Comprehensive Review*,” **International journal of control theory and applications**, 9(41), pp. 309-317 (2016).



Influence of flow rate and heat flux on the temperature distribution in long length counter flow cooled cold dielectric HTS cables

Mohit Kalsia, Raja Sekhar Dondapati*

School of Mechanical Engineering, Lovely Professional University, Phagwara 144 401, India

ARTICLE INFO

Keywords

Counter flow cooling
Temperature profiles
Cold dielectric
HTS cable
Cryocooler

ABSTRACT

The technical advantages of using High Temperature Superconducting (HTS) cables have drawn the attention of most of the researchers around the world. However, the cooling design of these cables nevertheless remains a challenge for the researchers and manufacturers. Therefore, in the present work, an attempt has been made to ease the challenge of cooling of long length High Temperature Superconducting (HTS) cables. Counter flow cooling arrangements of liquid nitrogen (LN₂) have been proposed and analysed the longitudinal temperature distribution along the superconducting cable using heat balance equations. Also, in the present work the solution for the temperature distribution profiles of LN₂ in counter cooled HTS cable are also obtained assuming one dimensional (1-D) model. In particular, nonlinear axial temperature profiles of LN₂ in the counter cooled HTS cable are found. The single phase cold dielectric HTS cable with stainless steel corrugated pipes as flow paths are used for the analysis. Liquid nitrogen with varying volumetric flow rates of 20–35 L/min and total heat loss (A.C. loss and exterior heat load) of 2.3–2.6 W/m reveals interesting facts about cooling of cables with longer lengths. The defined cable length range at constant diameter (inner and annulus pipe) for the analysis was considered as 1.5–3 km. As a result, the maximum possible HTS cable length of 2.5 km can be achieved at the flow rate of 30 L/min and heat fluxes of 2.3–2.6 W/m within the defined operating range.

Nomenclature

HTS	High Temperature Superconductors
LN ₂	liquid nitrogen
1-D	one-dimensional
A.C	alternating current (W/m)
SCN	supercritical nitrogen
SCAR	supercritical argon
PPLP	polypropylene laminated paper
Q _e	exterior heat in flux (W/m)
L	cable length (m)
V	volumetric flow rate (L/min)
m	mass flow rate (kg/s)
C _p	average constant specific heat capacity (j/kg-k)
T ₀	operating temperature (K)
T ₁ , T ₂	temperatures of inner and annular region (K)
P	pressure (bar)
Q _{AC}	heat dissipation due to A.C loss (W/m)
q(x)	heat flow from the annular to inner region (W/m)
k	overall thermal conductance between annular to inner region
h ₁ , h ₂	heat transfer coefficients between corrugated walls and the LN ₂
λ	thermal conductivity of dielectric (W/mK)

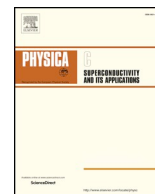
C ₁ , C ₂	constants in Eq. (8)
I.D _{I,C}	inner diameter of inner corrugated pipe
I.D _{O,C}	inner diameter of outer corrugated pipe

1. Introduction

The High Temperature Superconducting (HTS) cables, which may be cooled by abundantly available cryogenic fluid i.e., liquid nitrogen (LN₂), are able to transmit ten times more electrical power compared to conventional copper cables with tiny transmission losses. In the previous years, manufacturers and researchers worldwide have continually designed as well as experimented prototype HTS power cables. These experiments have proven the performance of HTS power cables, and indicated that the cables are actually prepared to be used in the networks. However, the cooling design of these cables nevertheless remains a challenge for the researchers. Therefore, various studies have described different cooling strategies which might be suitable for short length cables [1–6]. Also, various models such as analytical, numerical and experimental models were proposed to investigate the temperature profiles in the HTS cables with counter flow cooling technique for long transmission lines [7–11]. The primary benefit of counter cooling is much more effective use of cooling power, which reduces probably the highest temperature of the cable and space saving, by making provision for the coolant to go back within the cable it-

* Corresponding author.

E-mail address: drsekhar@ieee.org (R.S. Dondapati)



Influence of corrugation topology on thermohydraulic performance of cold dielectric counter cooled high temperature superconducting cable

Mohit Kalsia, Raja Sekhar Dondapati*

School of Mechanical Engineering, Lovely Professional University, Phagwara, 144401, India

ARTICLE INFO

Keywords:

Corrugation topology
Cold dielectric
Counter flow
HTS cable
Turbulent kinetic energy
Boundary layer separation

ABSTRACT

Fluid flow, pressure drop and heat transfer across the long length cold dielectric counter cooled High Temperature Superconducting (HTS) cables are significantly influenced by the different corrugation (rectangular, circular and triangular) topologies. Thus, in this present work, thermal and hydraulic characteristics of turbulent LN₂ flow in counter cooled HTS cable with various corrugation topologies are computationally investigated. The 2-D axisymmetric model of HTS cable with counter flow cooling system is considered by changing the corrugation shapes for Reynolds number ranging from 3.0×10^4 to 6.0×10^4 . Heat flux from ambient temperature on outer corrugated pipe and heat generation from A.C. losses in the HTS tapes are also considered in the present simulations. In addition, distribution of the velocity, temperature and turbulent kinetic energy (TKE) of liquid nitrogen (LN₂) in the HTS cable with various corrugations are estimated using computational fluid dynamics (CFD) technique. Finite volume method is adapted to solve the governing equations (continuity, momentum and energy) using Semi-Implicit Pressure Linked Equations (SIMPLE) scheme with $k - \epsilon$ turbulence model and enhanced wall treatment. The results reveal that the corrugation topologies (rectangular, circular and triangular) have significant effect on heat transfer and pressure drop. The corrugated pipes with different topologies exhibit different friction factors due to the variations in the contact of wall surfaces with the LN₂. Moreover, the calculated friction factors for all the three corrugation topologies are compared with the experimental results available in the literature. Further, the results of temperature difference between outlet and inlet temperatures of LN₂ are validated with the available experimental measurements. Finally, it was concluded that the effect of heat flux and AC Losses on cooling capacity and heat transfer is found to be significant as compared that on friction factor and pumping power.

1. Introduction

High temperature superconducting (HTS) power cables have been developing as a solution of increasing power demand due to their advantages of lower losses, large transmission capability, light weight and smaller diameter with higher ampacity. The HTS cables exhibit various kind of losses such as AC losses in the superconductor, dielectric losses in dielectric material, the heat influx through the cryogenic enclosure wall from ambient temperature and pressure losses in LN₂ flowing through corrugated pipes. In order to encounter such losses in the HTS cable, thermal and hydraulic analysis of LN₂ is necessary. After years of research, the HTS cables have been acknowledged to be installed in the grids for large scale power transmission. However, the efficient cooling system and flow system in HTS cable is still one of the major issues for the researcher and manufacturers. Therefore, several studies on cooling mechanism (thermal) and flow system (hydraulic) in corrugated pipe

HTS cables have been carried out and published so far. Kottonau et al. [1] has analyzed the pressure drop and heat transfer for four various cooling concepts in three phase concentric HTS cable. The HTS cable may also have other different cooling arrangements such as single flow cooling and counter flow cooling systems. When LN₂ flows through either inner or annular flexible corrugated pipe to reduce the temperature rise in HTS cable, termed as single flow cooling system. The thermohydraulic analysis of HTS cable using single flow cooling system is described by [2–10]. The influence of corrugation pitch and depth on pressure drop and heat transfer in warm dielectric HTS cable with single flow cooling systems using computer simulations have been investigated by Lee et al. [4] and Dondapati et al. [6]. Whereas, the thermal and fluid characteristics of LN₂ in annular channel in the HTS cable have been investigated by Sasaki et al. [7] and Maruyama et al. [5]. However, there are few reports on the thermohydraulic behavior of the non-cryogenic fluid flowing through corrugated pipes with single

* Corresponding author.

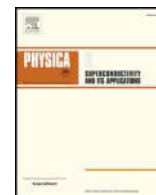
E-mail address: drsekhar@ieee.org (R.S. Dondapati).

<https://doi.org/10.1016/j.physc.2019.1353525>

Received 4 July 2019; Received in revised form 19 August 2019; Accepted 5 September 2019

Available online 05 September 2019

0921-4534/ © 2019 Elsevier B.V. All rights reserved.



Thermohydraulic analysis of cold dielectric high temperature superconducting cable with counter-flow cooling

Mohit Kalsia, Raja Sekhar Dondapati*

School of Mechanical Engineering, Lovely Professional University, Phagwara 144 401, India

ARTICLE INFO

Keywords:

Cold dielectric
HTS cables
Counter flow
Thermohydraulics

ABSTRACT

High temperature superconducting (HTS) cables cooled with liquid nitrogen (LN_2) have been found to be most promising alternative to conventional cables for meeting the ever-rising energy demand across the world. The heat accommodated by the LN_2 flowing in HTS cable has various major sources such as AC loss in the superconductor, dielectric loss in dielectric material, and heat influx through the cryogenic enclosure wall from ambient temperature. Thus, in order to operate long length HTS cables, the thermal and hydraulic analysis of LN_2 flowing in the HTS cable is essential. However, the LN_2 flow is more complex when flowing through stainless steel corrugated pipes with counter-flow cooling arrangement. In the present work, counter-flow cooling system is considered for the analysis to reduce the highest temperature attained in the HTS cable. Moreover, the influence of various heat fluxes and heat generations on the pressure drop and heat transfer is carried out using computational fluid dynamics (CFD) approach. The two-equation turbulence model k-epsilon ($k-\epsilon$) is used to analyze the thermohydraulic behavior of LN_2 , where the thermophysical properties of LN_2 are considered to be temperature dependent. The obtained pressure drop is compared with the experimental data of a parallel flow HTS system, fabricated in NEDO project. Consequently, the friction factor for counter flow HTS system is found to be quite larger than the parallel flow HTS system.

1. Introduction

The ever-rising demand for power across the world has led many researchers and scientists to look out for alternate techniques which can meet the power demand efficiently. Over the decades, the development of High Temperature Superconductors (HTS) has been progressing significantly and opened new opportunities for power industries. The HTS cables are one of the most promising and attractive applications with advantages of size and larger transmission capabilities compared to conventional copper cables. After years of research, the HTS cables are found suitable to be deployed in power grids with various configurations and dedicated cooling systems. The feasibility studies with respect to HTS cables such as cost analysis, physical construction and installation with appropriate safety procedures and benefits comparison with conventional cables are carried out by Zhang et al. [1]. However, the efficiency of HTS cable cooling systems remains one of the challenges for power grids. Therefore, many researchers have described their own HTS cooling systems experimentally, numerically/analytically and computationally with single flow cooling system and counter flow cooling system. In single flow cooling system [2–6], LN_2 flows through either inner or annular flexible corrugated pipe parallel to each

other to reduce the temperature rise in HTS cable with different physical parameters such as diameter, number of tapes and length of cable. Lee et al. [2] and Dondapati et al. [4, 7] have investigated the effect of corrugation pitch and depth on pressure drop and heat transfer in warm dielectric HTS cable with single flow cooling systems using computer simulations. Whereas, Sasaki et al. [5] and Maruyama et al. [6] have computationally investigated the thermal and fluid characteristics of LN_2 in annular channel in the HTS cable. Moreover, few statistical correlations for thermophysical properties of supercritical fluids such as supercritical nitrogen (SCN) and supercritical argon (SCAR) were also suggested as feasible coolants for the thermohydraulic analysis of Hg based superconducting cables [8,9]. On the other hand, counter flow cooling system [10–19] has its own advantage of compact size due to elimination of separate LN_2 return pipe and efficient cooling of HTS cables. Fuchino et al. [19] has analytically examined the cooling of HTS cables with counter-flow of LN_2 along with the effect of thermal conductance of cable dielectric. Although, Zajaczkowski et al. [18] has also analytically proposed the concept of inline cooling system with counter flow to achieve the cables of infinite length, where an infinite long HTS cable is divided into several sections consist of cryo-cooler. In case of inline cooling the cryogen in the inner corrugated pipe can either pass

* Corresponding author.

E-mail address: drsekhar@ieee.org (R.S. Dondapati).

<https://doi.org/10.1016/j.physc.2019.06.006>

Received 28 December 2018; Received in revised form 28 March 2019; Accepted 20 June 2019

Available online 21 June 2019

0921-4534/ © 2019 Elsevier B.V. All rights reserved.



Contents lists available at ScienceDirect

Physica C: Superconductivity and its applications

journal homepage: www.elsevier.com/locate/physc

Statistical correlations for thermophysical properties of Supercritical Argon (SCAR) used in cooling of futuristic High Temperature Superconducting (HTS) cables



Mohit Kalsia^a, Raja Sekhar Dondapati^{a,*}, Preeti Rao Usurumarti^b

^aSchool of Mechanical Engineering, Lovely Professional University, Phagwara, 144 401, India

^bDepartment of Mechanical Engineering, PVK Institute of Technology, Anantpur, 515 001, India

ARTICLE INFO

Article history:

Received 3 April 2017

Accepted 19 April 2017

Available online 20 April 2017

Keywords:

Supercritical Argon

HTS cable

Correlations

ABSTRACT

High Temperature Superconducting (HTS) cables are emerging as an alternative to conventional cables in efficient power transmission. However, these HTS cables require cooling below the critical temperature of superconductors used to transmit larger currents. With the invention of high temperature superconductors whose critical temperatures are up to 134 K (Hg based), it is a great challenge to identify a suitable coolant which can carry away the heating load on the superconductors. In order to accomplish such challenge, an attempt has been made in the present work to propose supercritical Argon (SCAR) as the alternative to cool the HTS cables. Further, a statistical correlation has been developed for the thermophysical properties such as density, viscosity, specific heat and thermal conductivity of SCAR. In addition, the accuracy of developed correlations is established with the help of few statistical parameters and validated with standard database available in the literature. These temperature dependent accurate correlations are useful in predicting the pressure drop and heat transfer behaviour in HTS cables using numerical or computational techniques. In recent times, with the sophistication of computer technology, solving of various complex transport equations along with the turbulence models became popular and hence the developed correlations would benefit the technological community. It is observed that, a decrease in pressure, density and viscosity are found to be decreasing whereas the thermal conductivity and specific heat increase significantly. It can be concluded that higher heat transfer rate and lower pumping power can be achieved with SCAR as coolant in the HTS cables.

© 2017 Elsevier B.V. All rights reserved.

1. Introduction

High Temperature Superconducting (HTS) cables are identified as one of the solutions for large scale power transmission with higher efficiency due to their low electrical resistance at cryogenic temperatures. Hence, these high performing HTS cables need attention with regard to design, manufacturing and analysis for safe operation. The design issues of HTS cable were discussed by Wesche et al. [20], Cho [2], Ohya et al. [14] and Yagi et al. [21]. Whereas, manufacturing and development methodologies were reported by Cho et al. [3] and Mizuno et al. [13]. Further, pressure drop and heat transfer in HTS cables was computationally investigated by Dondapati and Rao [6], Vyas et al. [19] and Kalsia et al. [9] with Liquid Nitrogen (LN₂) as coolant. Moreover, Maruyama et al. [12] have discussed about the numerical analysis of heat transfer characteristics against heat generation and fluid characteristics

such as pressure drop in HTS cable. However, as the use of LN₂ causes multiphase flow phenomenon hindering the effective heat transfer, the use of single phase coolants such as supercritical fluids could be an alternative solution. The use of these supercritical fluids for the construction of superconducting magnets was already reported by Dondapati and Rao [5], Raja Sekhar and Rao [16] and Dondapati and Rao [7]. It was reported, through CFD analysis, the pressure drop and heat transfer of supercritical helium coolant in dual channel cable in conduit conductor (CICC) used in fusion grade magnets can be enhanced. Moreover, it is reported that the use of supercritical nitrogen (SCN) in HTS cables enhances heat transfer [4]. Also, experimental and numerical investigations of the fluid flow and heat transfer characteristics of the supercritical nitrogen in the mini-tube were discussed by Zhang et al. [22]. In addition, reduction of pressure losses by introducing different shapes of cryo-pipe in HTS cables using CFD analysis was discussed by Sasaki et al. [17].

In order to safely operate these HTS cables must be cooled below its critical temperature with efficient cooling methodologies.

* Corresponding author.

E-mail address: drsekhar@ieee.org (R.S. Dondapati).



CONCEPTUAL DESIGN OF HIGH TEMPERATURE SUPERCONDUCTING (HTS) CABLES: A REVIEW

Mohit Kalsia

Research Scholar, School of Mechanical Engineering,
Lovely Professional University, Punjab, India.

Raja Sekhar Dondapati

Associate Professor, School of Mechanical Engineering,
Lovely Professional University, Punjab, India.

Preeti Rao Usurumarti

Assistant Professor, School of Mechanical Engineering,
PVK Institute of Technology, Anantapur, India.

ABSTRACT

High temperature superconducting (HTS) cables for power transmission applications are gaining prominence as the efficiency of transmission is higher as compared to that of conventional cables. Various issues such as mechanical, thermal and electrical issues related to the design of HTS cables are to be understood in order to reduce losses, manufacturing and maintenance costs. In the present review, these issues related to the design of high temperature superconducting (HTS) cable are discussed. AC losses due to various parameters are understood and revisited. AC losses measurement techniques are reviewed in order to understand and compare the accuracy of measurement. Mechanical losses due to bending, buckling and fracture were reviewed. All the losses in the cable will deposit the heat in the HTS cables. Hence cooling strategies adapted to cool these cables in order to avoid quenching, damaging of cables and of terminations is also presented.

Key words: AC Loss, HTS cables, Mechanical Stress.

Cite this Article: Mohit Kalsia, Raja Sekhar Dondapati and Preeti Rao Usurumarti, Conceptual Design of High Temperature Superconducting (HTS) Cables: A Review. *International Journal of Mechanical Engineering and Technology*, 8(7), 2017, pp. 1180–1188.

<http://www.iaeme.com/IJMET/issues.asp?JType=IJMET&VType=8&IType=7>

Conceptual Design and Cooling Strategies of Current Lead for Superconducting Power Transmission Applications

Vikul Vasudev
School of Mechanical Engineering
Lovely Professional University
Jalandhar, India
vikul.vasudev93@gmail.com

Raja Sekhar Dondapati
School of Mechanical Engineering
Lovely Professional University
Jalandhar, India
drsekhar@iecee.org

Mohit Kalsia
School of Mechanical Engineering
Lovely Professional University
Jalandhar, India
kalsiamohit.007@gmail.com

Preeti Rao Usurumarti
Department of Mechanical Engineering
PVK Institute of Technology
Anantapur, India
preeti.iitkgp@gmail.com

Abstract— The superconducting power transmission applications requires current lead for transferring electric current from room temperature to the cryogenic environment. The current lead being made from a normal conductor requires special cooling as high density current is passed from it. In this paper, a generalized conceptual design of the current leads for all the superconducting applications is presented. This design of the current lead is derived from the past designs used in superconducting applications. A heat balance equation that governs the quenching of the lead is derived considering all the modes of heat infiltration into the lead. The whole lead has been divided into different parts so that each aspect can be emphasized upon to achieve maximum current carrying capacity with minimum cooling load. The cooling strategies adopted for maintaining the cryogenic environment inside the lead with minimum cooling load on the refrigerator are also discussed.

Keywords—Current leads; HTS material; cooling strategies; helium bath

I. INTRODUCTION

Current lead is the component that connects the superconductor at cryogenic temperature to the power source at room temperature. Current leads are made up of a normal conducting material at the room temperature end, so Copper or Brass is used generally for this purpose due to their high electrical conductivity. Electric current in the units of kilo Amperes flows through the current leads, so there is a high risk of metal failure due to Joules heating in the Copper element. Proper cooling strategies should be adopted to maintain the temperature of these leads in order to avoid generation of any additional cooling load in the Cryocooler. Basically two techniques are used to cool the current leads; one is using the single or double staged cryocooler and other is

convective cooling using Helium bath at cold end also known as Vapor Cooled Current Leads. In the process of cooling the current leads, the sole purpose is to prevent the heat leakage into the cold end, because that will result in higher cooling load. During practical current lead operation, thermal energy enters the system via three sources. The first and the most dominant cause for heat infiltration is the conductive heat transfer from the warm end at room temperature. This exposure of current leads to the heat source is uncontrollable and accounts for the maximum cooling load requirements. The second cause is the heat generated within the conductor element due to Joule's heating effect otherwise known as I^2R losses. Third cause of heat infiltration is the heat radiated from the surroundings which is negligible because it can be controlled by using proper insulation techniques.

Vapour cooling technique for current leads was presented by Chen [1] in 1979. Since then, many researchers have been working on fabricating the correct design for the leads. Research in this field has given rise to the trend of using the binary current leads containing a normal conductor and a superconducting element together. Since the cold end is maintained at almost 4 Kelvin, High Temperature Superconducting (HTS) material is used as the temperature there is below the Transition temperature (T_c) of the superconductor. Fusion energy reactors built since T-7 Tokamak in 1977, Tore Supra in 1987, Wendelstein 7-X in 2007 to the largest energy project in the world ITER currently under development, all of them require current leads to power up their superconducting magnets. The HTS cables used for power transmission at large distances, like the Long Island Power Corporation and the Albany cable project also require current leads for each of the three phases. Similarly, superconducting magnets used in MRI scanning machines

AC Losses and Dielectric Losses in High Temperature Superconducting (HTS) Power Cables for Smart Grid Applications: A Comprehensive Review

Mohit Kalsia*, Raja Sekhar Dondapati** and Preeti Rao Usurumarti***

ABSTRACT

High Temperature Superconducting (HTS) cables are being used for effective power transmission and distribution as the losses in these HTS cables are less compared to those in conventional power cables. HTS cable constitutes of BSCCO-2233 or YBCO-123 with critical temperatures 110K at zero Tesla and 90K at zero Tesla respectively are highly opted due to larger handling current carrying capacity. During the operation of HTS cable, receives heat flux from the ambient, AC losses through the superconducting tape, dielectric losses from dielectric material, heat-in-leaks from the current leads.

Hence, it is essential to estimate the losses during the operation of HTS cable. Hence, in the present work, a method of estimating the AC losses during transmission and distribution is presented. Electric probe method and Calorimetric thermal methods are frequently used to measure AC losses. The dielectrical losses are increased due to raise in temperature from the heat fluxes. In this paper, different AC losses and dielectric losses are estimated and methods available in the literature to measure these losses are reviewed.

Keywords: HTS cables; AC losses; Dielectric losses; Calorimeter and Electrical methods ; Dielectric materials.

1. INTRODUCTION

High temperature superconducting (HTS) cables are emerging as substitute to next generation power transmission and distribution in power grid applications. These cables not only handle larger currents but also compact and have low losses as compared with conventional cables. Superconductors have zero electrical resistance and conducts electricity with no losses. However, when the alternating current is transmitted through the superconductors, different losses such as AC losses and dielectric losses are [1], [2] encountered. Hence, in designing the HTS cable the factors to be considered are presented in the following sections.

1.1. AC Losses

AC losses comprises of hysteresis losses [1]–[5] in superconducting tapes, eddy current losses [6] in sheath material and coupling losses[5], [6] between the mutlifilaments of HTS tapes. AC losses due to Self field are investigated in detail by Vyas et al [7] and found that the AC losses depend on the transport current. Further, the method of measuring these AC losses by calorimetric method [8], [9], electrical circuit method [9], [10] and contactless electrical measurement [11] are reported in the literature. Moreover, it was reported that the AC losses can be minimized by changing the gaps between the superconducting tapes [12] and reduction in AC losses up to 1.8/W/m/phase is achieved at 5kA [13].

* School of Mechanical Engineering Lovely Professional University, Phagwara, Punjab, India, Email: kalsiamohit.007@gmail.com

** School of Mechanical Engineering Lovely Professional University, Phagwara, Punjab, India, Email: drsekhar@ieee.org

*** Department of Mechanical Engineering PVK Institute of Technology Ananthapur, Andhra Pradesh, India, Email: preeti.iitkgp@gmail.com